Speciation analysis in renewable feedstocks and petroleum heavy oil fractions

Victor Garcia-Montoto

▶ **To cite this version:**

Victor Garcia-Montoto. Speciation analysis in renewable feedstocks and petroleum heavy oil fractions. Analytical chemistry. Université de Pau et des Pays de l'Adour, 2020. English. NNT : 2020PAUU3009 . tel-03007872

HAL Id: tel-03007872
https://theses.hal.science/tel-03007872

Submitted on 16 Nov 2020

HAL is a multi-disciplinary open access archive for the deposit and dissemination of scientific research documents, whether they are published or not. The documents may come from teaching and research institutions in France or abroad, or from public or private research centers.

L'archive ouverte pluridisciplinaire **HAL**, est destinée au dépôt et à la diffusion de documents scientifiques de niveau recherche, publiés ou non, émanant des établissements d'enseignement et de recherche français ou étrangers, des laboratoires publics ou privés.

THÈSE

UNIVERSITE DE PAU ET DES PAYS DE L'ADOUR

École doctorale des Sciences Exactes et leurs Applications

Présentée et soutenue le 21 Septembre 2020

par **Victor GARCIA MONTOTO**

pour obtenir le grade de docteur
de l'Université de Pau et des Pays de l'Adour
Spécialité : Chimie Analytique

SPECIATION ANALYSIS IN RENEWABLE FEEDSTOCKS AND PETROLEUM HEAVY OIL FRACTIONS

MEMBRES DU JURY

RAPPORTEURS

• Jorge RUIZ ENCINAR	Professeur / Université de Oviedo
• Pierre GIUSTI	HDR / TOTAL Raffinage Chimie

EXAMINATEURS

• Florence PANNIER	Professeure / Université de Pau et des Pays de l'Adour
• Lucie CONIGLIO	Maitre de conférences / Université de Lorraine

DIRECTEURS

• Brice BOUYSSIERE	Professeur / Université de Pau et des Pays de l'Adour
• Jan H. CHRISTENSEN	Professeur / Université de Copenhague

UNIVERSITÉ DE PAU ET DES PAYS DE L'ADOUR

PREFACE

This PhD thesis, subjected to the PhD Cotutelle Agreement signed between the University of Pau and Adour Countries in France and the University of Copenhagen in Denmark has been carried out at the Institut des Sciences Analytiques et Physico-Chimique pour l'Environnement et les Matériaux (IPREM) from the University of Pau and Adour Countries and at the Department of Plant and Environmental Sciences (PLEN) from the University of Copenhagen. Throughout this three-year project, a close collaboration was shared with the Danish company Haldor Topsoe.

This PhD thesis was financed by the Environmental & Energy Solutions project, carried out by the University of Pau and Adour Countries in collaboration with the CNRS.

First of all, I would like to express my sincere gratitude to my two advisors: Prof. Brice Bouyssiere and Prof. Jan H. Christensen for their continuous support and guidance throughout the last three years. I would also like to thank Sylvain Verdier (Haldor Topsoe) for his great collaborations and the support and encouragement he gave me.

I would like to thank my former teachers of Analytical Chemistry, Prof. Jorge Ruiz Encinar and Prof. Florence Pannier, as well as Dr. Pierre Giusti and Dr. Lucie Coniglio for accepting being part of the thesis committee.

I would like to thank the support that I received from the professors at both the University of Pau and University of Copenhagen. Without their support I would not have been able to achieve the goals I proposed to myself: Nikoline Juul Nielsen, Linus Malmquist, Giorgio Tomasi, Peter Christensen, Jette Petersen (KU) and Christine Gleyzes (UT2A).

I want to thank my fellow labmates and colleagues for all the help they have provided to me and the good moments we have shared during our free time: Vicmary Vargas, Remi Moulian, Aurore Mere, Ntau Mafisa and Fang Zheng (UPPA); Heng Li, Pablo Denti and Josephine Lubeck (KU) and Yuan Xu and Thomas Stehrer, my great colleagues during the longest eight days of my life, sampling, processing and analysing sediments in the Arctic Station from Qeqertarsuaq, in Greenland.

I will never forget all the friends I have made during the last three years. Among all the fantastic people I have met, I would like to thank my Spanish group of friends (Javier, Little Sergio, Miguel, Laura, Nuria, Luis, Carlos, Emilio and many others); my Catalan group of friends (Roger, Annia, Marta, Miquel, Toni and Joan), my Russian group of Friends (Marty, Meri, Sophie, Koen, Teresa and Rali), my flatmate Theo and my old friends for the great moments I have shared with all of them.

I would like to thank my family for their patience and their continuous support and advice, and to Yin Xu for all those unforgettable moments that we have shared in the several countries we have visited together.

ABSTRACT

This thesis incorporates the application of several analytical methodologies to the speciation analysis of renewable feedstocks and petroleum heavy oil fractions. Separation techniques such as gel permeation chromatography (GPC) and supercritical fluid chromatography (SFC) have been combined with the elemental detection that inductively coupled plasma mass spectrometry (ICP-MS) provides to obtain a fingerprint of those species of interest, based on their hydrodynamic volume, present in samples with complex matrices. However, the combination of these separation techniques with ICP-MS was not an easy task.

With the purpose of providing to the analytical chemistry platform with novel approaches for the speciation analysis of complex samples, two novel tools have been devised during this three-year's project: (1) a cheap alternative to the current total consumption nebulisers, produced via 3D-printing and whose capillary has been built in PEEK, has been developed and validated for the analysis of trace elements in organic matrices via GPC-ICP-MS and (2) a novel interface has been designed and optimised for the trace element analysis via SFC-ICP-MS. Although very promising results have been obtained, further experiments must be carried out with these two methodologies to obtain a better understanding of the inorganic species present in renewable feedstocks and bio-oils.

The size distribution of sulfur, nickel and vanadium species in atmospheric residue fractions has been obtained via GPC-ICP-HRMS analyses to track and understand their evolution during two important industrial processes that are destined to convert these heavy oils into transportation fuels: hydrodemetallization and hydrodesulfurization. Furthermore, the phosphorus-, sodium-, iron-, magnesium- and sulfur-containing species' size distributions in lignocellulosic fast pyrolysis oils and fatty acid feedstocks have been also obtained, demonstrating that high-molecular aggregates are formed within these complex samples when they are stored.

Alternative methodologies for the analysis of renewable feedstocks have been tested. The use of electrothermal vaporisation coupled to inductively coupled plasma optical emission spectroscopy (ETV-ICP-OES) has provided with highly promising results. A methodology

that does not require the use of freon-R12 gas has been optimised and validated for the total analysis of eight trace elements in complex samples. Besides, the distribution of the species containing trace elements such as P, Na, Mg and Al among others, based on their vaporisation temperatures, has been obtained.

RESUME

Ce manuscrit de thèse intègre l'application de plusieurs méthodologies analytiques à l'analyse de spéciation des matières premières renouvelables et des fractions de pétrole lourd. Des techniques de séparation telles que la chromatographie par perméation de gel (GPC) et la chromatographie en phase liquide supercritique (SFC) ont été combinées avec la détection élémentaire fournie par la spectrométrie de masse haute résolution à plasma à couplage inductif (ICP-MS), afin d'obtenir une empreinte digitale de ces espèces d'intérêt, basé sur leur volume hydrodynamique, présent dans les échantillons à matrices complexes.

La combinaison de ces techniques de séparation avec l'ICP-MS n'a pas été une tâche facile. Cependant, afin de fournir à la plate-forme de chimie analytique de nouvelles solutions pour l'analyse de spéciation d'échantillons complexes (1), une alternative bon marché aux nébuliseurs à consommation totale actuelle, produite via l'impression 3D et dont le capillaire a été construit en PEEK, a été développé et validé pour l'analyse des éléments trace dans les matrices organiques via GPC-ICP-MS et (2) une nouvelle interface a été conçue et optimisée pour l'analyse des éléments trace via SFC-ICP-MS. Bien que des résultats très prometteurs aient été obtenus, de nouvelles expérimentations doivent être menées avec ces deux méthodologies afin de mieux comprendre les espèces inorganiques présentes dans les matières premières renouvelables et les bio-huiles.

La distribution en taille des espèces de soufre, de nickel et de vanadium dans les fractions de résidus atmosphériques a été obtenue via des analyses GPC-ICP-HRMS afin de suivre et de comprendre leur évolution au cours de deux processus industriels importants destinés à convertir ces fractions de pétrole lourd en carburants de transport: l'hydrodémétallisation et l'hydrodésulfuration. En outre, les distributions de tailles des espèces contenant du phosphore, du sodium, du fer, du magnésium et du soufre dans les huiles de pyrolyse lignocellulosique et les charges d'acide gras ont également été obtenues, démontrant que des agrégats de haut poids moléculaire se forment dans ces échantillons complexes lorsqu'ils sont stockés.

Des méthodologies alternatives pour l'analyse des matières premières renouvelables ont été testées. L'utilisation de la vaporisation électrothermique couplée à la spectroscopie

d'émission optique à plasma à couplage inductif (ETV-ICP-MS) a fourni des résultats très prometteurs. Une méthodologie qui ne nécessite pas l'utilisation de gaz fréon-R12 a été optimisée et validée pour l'analyse totale de huit éléments trace dans des échantillons complexes. De plus, la répartition des espèces contenant des éléments trace tels que P, Na, Mg et Al entre autres, en fonction de leurs températures de vaporisation, a été obtenue.

ABSTRAKT

Denne PhD afhandling anvender forskellige analytiske metoder til specieringsanalyse af vedvarende råmaterialer og petroleumstunge oliefraktioner. I afhandlingen anvendes separationsteknikker som gel permeations kromatografi (GPC) og superkritisk væskekromatografi (SFC) i kombination med detektion af elementer somved induktiv koblet plasma-højopløsningsmassespektrometri (ICP-MS). Metoderne anvendes til at måle det kemiske fingeraftryk af specier i komplekse matricer , baseret på speciernes hydrodynamiske volumen. Kombinationen af kromatografiske separationsteknikker med ICP-MS var ikke en let opgave.

For at opnå en forbedre analyse af komplekse matricer blev der udviklet en række nye forbedrede metoder til specifikationsanalysen af komplekse prøver: (1) en billig alternativ til den nuværende "total consumption nebuliser" blev udviklet og valideret til sporstof anlayse i organiske matricer via GPC-ICP-MS. Den nye nebuliser blev produceret ved 3D print af PEEK materiale; (2) et nyt interface blev designet og optimeret til sporelementanalyse ved SFC-ICP-MS. Selvom der er opnået meget lovende resultater, skal yderligere eksperimenter udføres med disse to metoder for at opnå en bedre forståelse af specierne som er tilstede i vedvarende råmaterialer og bioolier.

Størrelsesfordelingen af svovl-, nikkel- og vanadiumspecier i atmosfæriske restfraktioner er opnået via GPC-ICP-HRMS-analyser for at spore og forstå deres udvikling under to vigtige industrielle processer, der er designet til at omdanne ukonventionelle olier til transportbrændstof: hydrodemetallization og afsvovling.

Endvidere er størrelsesfordelingen af forfor-, natrium-, jern-, magnesium- og svovlholdige specier målt i lignocellulosiske pyrolyseolier og fedtsyreholdige-råmaterialer. Disse resultater viser, at der dannes højmolekylære aggregater i disse komplekse prøver, når de opbevares ved normale forhold.

Alternative metoder til analyse af vedvarende råmaterialer er blevet testet. Der blev opnået lovende resultater ved anvendelsen af elektrotermisk fordampning koblet til induktivt koblet plasmaoptisk emissionsspektroskopi (ETV-ICP-OES). En ETV-ICP-OES

metode som ikke kræver anvendelse af freon-12-gas, er blevet optimeret og valideret til analyse af summen af otte sporstoffer i komplekse prøver. Metoden blev anvendt til analyse af sammensætningen af P, Na, Mg og Al specier baseret bl.a. på deres fordampningstemperaturer.

CONTENTS

Preface ... **2**
Abstract ... **4**
Résumé ... **6**
Abstrakt ... **8**
List of abbreviations ... **13**
List of tables ... **17**
List of figures ... **18**
List of publications ... **21**
Introduction ... **23**
Aims and objectives ... 23
Outline of the thesis ... 25
Chapter 1: From Biomass to Bio-oil. Production and composition ... **28**
1.1. Definitions of Biomass and Bio-oil ... 28
1.2. Classification of bio-oils ... 29
1.3. Renewable feedstocks ... 30
1.3.1. Lignocellulosic biomass ... 30
1.3.2. Sugars and starch. ... 33
1.3.3. Oils and fats ... 34
1.3.4. Municipal waste ... 34
1.4. Bio-Oil from pyrolysis: Production and composition ... 35
1.4.1. Pyrolysis and fast pyrolysis ... 35
1.4.2. General composition of Pyrolysis Oil ... 36
1.4.3. Main impurities present in Pyrolysis Oils ... 37
1.4.3.1. Char ... 37
1.4.3.2. Oxygenated compounds ... 37
1.4.3.3. Inorganic species ... 38
1.5. Biodiesel and renewable diesel ... 40
1.5.1. Biodiesel production and general properties ... 40
1.5.2. General composition of biodiesel ... 41
1.5.3. Renewable diesel ... 42
1.5.4. Main impurities in Biodiesel, Renewable Diesel and their feedstocks ... 43
1.6. Bio Oils refining: Hydrodeoxygenation (HDO) ... 47
1.6.1. Reactions ... 48

1.6.2. Catalysts....49
1.6.3. Catalyst deactivation....50
Chapter 2: Analytical methods....53
2.1. Chromatographic techniques....53
2.1.1. Principles of Chromatography....53
2.1.2. Gel Permeation Chromatography (GPC)....59
2.1.3. Supercritical Fluid Chromatography (SFC)....62
2.2. Detection....65
2.2.1. Inductively Coupled Plasma Mass Spectrometry (ICP-MS)....65
2.2.2. Inductively coupled plasma – optical emission spectroscopy (ICP-OES). 73
Chapter 3: Novel analytical tools for the speciation analysis of bio-oils: A 3D-Printed total consumption nebuliser....76
3.1. Methodology....76
3.2. 3D-printed total consumption microflow nebuliser development for trace element analysis in organic matrices *via* inductively coupled plasma mass spectrometry 79
3.3. Discussion and perspectives....85
Chapter 4: Novel SFC-ICP-MS hyphenation for the speciation analysis of complex matrices....87
4.1. Previous SFC-ICP-MS interfaces....87
4.2. Hyphenating supercritical fluid chromatography – inductively coupled plasma mass spectrometry: Interface development and analysis of unconventional oils 90
Chapter 5. ETV-ICP-OES for the analysis of bio-oils....113
5.1. Introduction....113
5.2. Materials and methods....116
5.2.1. Instrumentation....116
5.2.2. Samples and reagents....117
5.2.3. Procedure 118
5.3. Results and discussion 119
5.3.1. ETV-ICP-OES Optimisation....119
5.2.2. Method validation. 125
5.3.3. Speciation analysis of fast pyrolysis oils via ETV-ICP-OES....126
5.4. Conclusion 132
Chapter 6: Importance of GPC-ICP-HRMS on the speciation analysis of complex matrices....134
6.1. Crude oil composition and its derivates....135

6.2. Understanding the removal of V, Ni and S in crude oil atmospheric residue hydrodemetallization and hydrodesulfurization 137
Chapter 7: GPC-ICP-MS speciation analysis in bio-oils 145
7.1. Current trends on inorganic speciation and total analysis of bio-oils.....145
7.1.1. Total analysis 145
7.1.1.1. Biodiesel, bioethanol and their feedstocks 146
7.1.2. Speciation Analysis 148
7.1.2.1. Biodiesel, bioethanol and their feedstocks 149
7.1.2.2. Pyrolysis Oils.....150
7.2. Speciation analysis of trace elements in renewable feedstocks via GPC-ICP-HR MS 153
7.2.1. Samples, methodology and instrumentation.....153
7.2.2. Methodology and calibration of the columns.....156
7.2.3. Analysis of S, Na, Fe and Mg in fast pyrolysis oils 158
7.2.4. Phosphorus speciation analysis of fatty-acid based feedstocks and fast pyrolysis biocrudes via gel permeation chromatography inductively coupled plasma high resolution mass spectrometry.....170
Concluding remarks and perspectives 190
Bibliography..... 194
Annexes 213
Poster presented at the 48th International Symposium on High-Performance Liquid Phase Separations and Related Techniques.....213
Simplification of heavy matrices by liquid-liquid extraction: Part I – How to separate LMW, MMW and HMW compounds in maltene fractions of V, Ni and S compounds.215
Simplification of heavy matrices by liquid-solid extraction: Part II – How to separate LMW, MMW and HMW compounds in asphaltene fractions for V, Ni and S compounds. 222
Spatial and temporal trends of Polycyclic Aromatic Hydrocarbon (PAH) contamination in sediments from different locations in western Greenland. 231

LIST OF ABBREVIATIONS

AAS - Atomic Absorption spectroscopy

AC - Alternating Current

AES - Atomic Emission Spectrometry

AR - Atmospheric Residue

BEH - Ethylene Bridged Hybrid

BHT - Butylated Hydroxytoluene

C18 - Octadecyl Silane

CO - Crude Oil

DC - Direct Current

DCM - Dichloromethane

DF - Dilution Factor

DL – Detection Limit

EDTA - Ethylenediaminetetraacetic acid

ESI -Electrospray Ionization

ETV - Electrothermal Vaporization

FT - Fourier Transform

FT-ICR-MS - Fourier Transform Ion Cyclotron Resonance Mass Spectrometry

FT-IR - Fourier Transform Infrared Spectroscopy

GC - Gas Chromatography

GF - Graphite Furnace

GPC - Gel Permeation Chromatography

HCO - Heavy Cycle Oil

HDC - Hydrodynamic Chromatography

HDM - Hydrodemetalation

HDO - Hydrodeoxygenation

HDS - Hydrodesulfurization

HDT – Hydrotreating

HMW - High Molecular Weight

HPLC - High-Pressure Liquid Chromatography / High-Performance Liquid Chromatography

HPL - Hydratable Phospholipid

HR - High Resolution

ICP - Inductively Coupled Plasma

ICR -Ion Cyclotron Resonance

IPREM - Institut des Sciences Analytiques et Physico-Chimique pour l'Environnement et les Matériaux

IR – InfraRed

KU - Københavns Universitet

LC - Liquid Chromatography

LMW - Low Molecular Weight

LOD - Limit of Detection

LOQ - Limit of Quantification

LR - Low Resolution

MeOH - Methanol

MMW - Medium Molecular Weight

MR - Medium Resolution

MS - Mass Spectrometry

NHPL - Non-Hydratable Phospholipid

NIST – National Institute of Standards and Technology

NMR - Nuclear Magnetic Resonance

NP - Normal Phase

PAC - Polycyclic Aromatic Compounds

PAH - Polycyclic Aromatic Hydrocarbon

PL - Phospholipid

PMT - Photomultiplier Tube

ppm - parts per million

ppb - parts per billion

PS - Polystyrene

RI - Refractive Index

RP - Reversed Phase

RSD - Relative Standard Deviation

RTI – Research Triangle Institute (U.S. Company)

SEC - Size Exclusion Chromatography

SRM – Standard Reference Material

TGA - Thermogravimetric Analysis

THF – Tetrahydrofuran

TIC - Total Ion Chromatogram

TLC - Thin Layer Chromatography

TMS - Trimethyl Silane

TOF - Time of Flight

UV - Ultraviolet

VD - Vacuum Distillates

VGO - Vacuum Gas Oil

VR - Vacuum Residues

XANES - X-ray absorption near edge structure

LIST OF TABLES

Table 1. Overview of the main reactions occurring during HDO.[50] 49
Table 5. ICP-OES parameters used for all the analysis carried out via ETV-ICP-OES. 117
Table 6. R^2 coefficient for each analysed wavelength. 125
Table 7. Concentrations in mg kg^{-1}, R^2 and detection limits in mg kg^{-1} determined for the SRM 1085b via ETV-ICP-OES. 126
Table 2. Main techniques used for the speciation analysis of pyrolysis oils.[123] 151
Table 3. Sample name, type of feedstock and total concentration in ppm of P, S, Na, Fe and Mg 154
Table 4. Definition of the molecular weight interval for the different fractions obtained via GPC-ICP-MS. 158

LIST OF FIGURES

Figure 1. Outline of the objectives covered in this thesis. 25
Figure 2. Chemical structure of cellulose. 31
Figure 3. Schematic structure of Cellulose, Hemicellulose and Lignin fibres in the cell wall.[14] 32
Figure 4. Schematic representation of some lignocellulosic fast pyrolysis products.[14] 33
Figure 5. Alcoholic fermentation diagram. 33
Figure 6. Main routes for the production of bio-oils from triglycerides.[16] 34
Figure 7. General fast pyrolysis of biomass diagram.[21] 35
Figure 8. Typical oxygenated hydrocarbons in pyrolysis oils.[19] 38
Figure 9. Transesterification process for the production of biodiesel.[36] 40
Figure 10. Schematic diagram of an industrial biodiesel production process.[37] 41
Figure 11. Reaction pathway for the production of n-alkanes from triglycerides[40]. 42
Figure 12. Structure of the most common phospholipids in animal fats and vegetable oils.[42] 44
Figure 13. Representation of the different paths of various molecules in a packed chromatographic column.[59] 55
Figure 14. General variation of H versus mobile phase velocity. (Van Deemter Equation). 57
Figure 15. Applications of HPLC[57]. 58
Figure 16. Van Deemter plot for HPLC. 59
Figure 17. GPC separation mechanism.[61] 60
Figure 18. Example of a GPC chromatogram with RI detection for a mixture of four different polystyrenes.[61] 61
Figure 19. CO_2 P-T diagram[62] 63
Figure 20. Block diagram of a SFC ACQUITY UPC² System.[64] 64
Figure 21. Van Deemter plots for SFC and HPLC separations in a C_{18} column.[57] 65
Figure 22. Main components of an ICP-MS instrument. 66
Figure 23. Schematic diagram of a concentric glass nebuliser.[66] 67
Figure 24. Quadrupole mass filter.[80] 69
Figure 25. Double Focusing Magnetic Sector mass analyser diagram.[81] 71
Figure 26. Faraday Cup Diagram.[81] 72
Figure 27. Schematic diagram of an Electron Multiplier detector. 72
Figure 31. Main components of an ICP-OES. 73
Figure 32. ICP OES and Rowland circle components.[66] 74
Figure 33. Photomultiplier tube components diagram. 75
Figure 35. GPC-ICP-MS / UV-Vis diagram of the set up used during this work. [82] 76
Figure 36. Diagram of the modified DS-5 total consumption nebulizer.[72] 77
Figure 37. SFC-ICP-MS interface proposed by Carey et al. 88
Figure 38. SFC ICP MS chromatogram at m/z = 52 for a mixture of two Cr compounds. 88
Figure 39. Experimental setup of an electrothermal vaporiser (Adapted from Asfaw et al.[89]). 114
Figure 40. ETV-ICP-OES set up. 116
Figure 41. Temperature ramp design for the optimisation of the ETV-ICP-OES parameters. 120

Figure 42. Corrected intensities for each wavelength and normalised vs. reaction gas flow. 121
Figure 43. Relative standard deviation (n = 3) of each wavelength vs. reaction gas flow. 121
Figure 44. Corrected intensities for each wavelength and normalised vs. carrier gas flow. 122
Figure 45. Relative standard deviation (n = 3) of each wavelength vs. carrier gas flow.122
Figure 46. Corrected intensities for each wavelength and normalised vs. bypass gas flow. 123
Figure 47. Relative standard deviation (n = 3) of each wavelength vs. bypass gas flow.123
Figure 48. Regression curves obtained for three elements: Ag 338.289 nm (blue), Al 167.078 nm (orange) and K 766.491 (grey). 124
Figure 49. Temperature program for the speciation analysis of trace elements in fast pyrolysis oils via ETV-ICP-OES. 127
Figure 50. ETV-ICP-OES transient signal for P species in different fast pyrolysis oil samples.....128
Figure 51. ETV-ICP-OES transient signal for Na, Cr, Mn and Ca species in different fast pyrolysis oil samples. 130
Figure 52. ETV-ICP-OES transient signal K, Mg, Al and Zn species in different fast pyrolysis oil samples. 132
Figure 53. Schematic representation of the crude oil distillation cuts.[73] 135
Figure 54. (A) Determination of Co, Ni and V in a certified reference material by three different methods. (B) Determination of Cu, Fe and Mn in four different samples by GF AAS and ETV-ICP-MS[109]. 147
Figure 55. Evolution of the concentration of Na and Mg along the bioethanol production process[121]. 150
Figure 56. Speciation of heavy metals in pyrolysis oil from sewage sludge 152
Figure 57. Results of the analyses of P, S, Na, Mg and Fe (in ppm) for the different laboratories that participated in the round-robin study directed by Haldor Topsoe. [104,131] 155
Figure 58. GPC calibration using 10 polystyrene standards dissolved in three different solutions and detected by a UV-VIS detector.....156
Figure 59. GPC calibration curve. 157
Figure 60. Sulfur (^{32}S) size distribution via GPC-ICP-HRMS for pyrolysis oils produced from red oak, milorganite and a 50:50 blend of both. 160
Figure 61. Sulfur (^{32}S) size distribution via GPC-ICP-HRMS for pyrolysis oils produced from milorganite, a blend of milorganite and loblolly pine wood and a commercial fast pyrolysis oil sample.....160
Figure 62. Distribution of the S-containing species for the five samples analysed via GPC-ICP-HRMS. 161
Figure 63. Sodium (^{23}Na) size distribution via GPC-ICP-HRMS for pyrolysis oils produced from red oak, milorganite and a 50:50 blend of both. 162
Figure 64. Sodium (^{23}Na) size distribution via GPC-ICP-HRMS for pyrolysis oils produced from milorganite, a blend of milorganite and loblolly pine wood and a commercial fast pyrolysis oil sample.....163
Figure 65. Distribution of the Na-containing species for the five samples analysed via GPC-ICP-HRMS. 164

Figure 66. Iron (^{56}Fe) size distribution via GPC-ICP-HRMS for pyrolysis oils produced from red oak, milorganite and a 50:50 blend of both. 165
Figure 67. Iron (^{56}Fe) size distribution via GPC-ICP-HRMS for pyrolysis oils produced from milorganite, a blend of milorganite and loblolly pine wood and a commercial fast pyrolysis oil sample.....166
Figure 68. Distribution of the Fe-containing species for the five samples analysed via GPC-ICP-HRMS. 167
Figure 69. Magnesium (^{24}Mg) size distribution via GPC-ICP-HRMS for pyrolysis oils produced from red oak, milorganite and a 50:50 blend of both. 168
Figure 70. Magnesium (^{24}Mg) size distribution via GPC-ICP-HRMS for pyrolysis oils produced from milorganite, a blend of milorganite and loblolly pine wood and a commercial fast pyrolysis oil sample.....168
Figure 71. Distribution of the Fe-containing species for the five samples analysed via GPC-ICP-HRMS. 170

LIST OF PUBLICATIONS

Peer-reviewed publications

- **Article 1:** Garcia-Montoto, V.; Mallet, S.; Arnaudguilhem C.; Christensen, J. H. and Bouyssiere, B. 3D-printed total consumption microflow nebuliser development for trace element analysis in organic matrices via inductively coupled plasma mass spectrometry. *J. Anal. At. Spectrom*., 2020, **35**, 1552-1557. 10.1039/D0JA00182A

- **Article 2:** Garcia-Montoto, V.; Verdier, S.; Maroun, Z.; Egeberg, R.; Tiedje, J. L.; Sandersen, S.; Zeuten, P. and Bouyssiere, B. Understanding the removal of V, Ni and S in crude oil atmospheric residue hydrodemetallization and hydrodesulfurization. Fuel Processing Technology, 2020, **201**, 106341. 10.1016/j.fuproc.2020.106341

- **Article 3:** Garcia-Montoto, V.; Denti, P.; Malmquist, L.; Verdier, S.; Bouyssiere, B. and Christensen, J. H. Hyphenating supercritical fluid chromatography and inductively coupled plasma mass spectrometry: A proof of concept. J. Anal. At. Spectrom., 2020, Accepted Manuscript. 10.1039/D0JA00376J

- **Article 4:** Gascon, G.; Negrin, J.; Garcia-Montoto, V.; Acevedo, S.; Lienemann C. P. and Bouyssiere, B. Simplification of Heavy Matrices by Liquid–Liquid Extraction: Part I—How to Separate LMW, MMW, and HMW Compounds in Maltene Fractions of V, Ni, and S Compounds. *Energy Fuels,* 2019, **33**, 3, 1922–1927. 10.1021/acs.energyfuels.8b03974

- **Article 5:** Gascon, G.; Negrin, J.; Garcia-Montoto, V.; Acevedo, S.; Lienemann C. P. and Bouyssiere, B. Simplification of Heavy Matrices by Liquid–Solid Extraction: Part II—How to Separate the LMW, MMW, and HMW Compounds in Asphaltene Fractions for V, Ni, and S Compounds. *Energy Fuels,* 2019, **33**, 9, 8110–8117. 10.1021/acs.energyfuels.9b01511

Manuscripts in the process of being peer-reviewed and published

- **Manuscript 1:** Garcia-Montoto, V.; Verdier, S.; Dayton, D.; Mante, O.; Arnauldguilhem, C.; Christensen J.H.; Bouyssiere, B. Phosphorus speciation analysis of fatty-acid based feedstocks and fast pyrolysis biocrudes via gel permeation chromatography inductively coupled plasma high resolution mass spectrometry. **(To be submitted to RSC Green Chemistry).**

- **Manuscript 2:** Garcia-Montoto, V.; Stehrer, T.; Xu, Y.; Juul-Nielsen, N.; Christensen, P.; Christensen J.H. Spatial and temporal trends of Polycyclic Aromatic Hydrocarbon (PAH) contamination in sediments from different locations in western Greenland. **(Manuscript written at the Arctic Station of Qeqertarsuaq, Greenland).**

INTRODUCTION

The production of renewable feedstocks and designed to obtain high-quality transportation fuels is growing considerably due to the upcoming shortage of fossil fuel products. Furthermore, the RED II legislation (Renewable Energy Directive for 2021–2030 in the European Union) has set a series of measures and obligations that will guarantee that at least 14% of the transportation fuel has been produced from renewable feedstocks by 2030.

The use of petroleum heavy oil fractions, such as atmospheric residues, and bio-oils, to produce high-quality transportation fuels, has increased rapidly during the last decade. However, the presence of heteroatoms and other metals within these petroleum heavy oil fractions oils is causing several problems, such as the emission of poisonous compounds to the atmosphere and the catalyst poisoning during the hydrotreating processes among others. Thus, understanding the nature of these trace elements and their speciation is essential to improve the production yields and the quality of those energy sources produced from renewable feedstocks and petroleum heavy oil fractions.

These elements, such as P, Fe, Mg, S and other trace elements present in renewable feedstocks; and V, Ni and S compounds, present at hundred ppm levels in crude oil and its heavy fractions, must be removed from the feedstocks in order to be processed and converted into transportation fuels.

Aims and objectives

Few analytical methodologies have been developed for the speciation analysis of those trace-element-containing species in crude oils and petroleum heavy oil fractions. However, in the present day, the development of such methodologies for the speciation analysis of bio-oils and renewable feedstocks have not been developed yet.

Thus, in this thesis, the development and validation of a set of novel tools and methodologies designed for the speciation analysis of bio-oils and renewable feedstocks are investigated. The work that is discussed in this thesis can be broken down into several objectives (O):

- **O1 (instrumental development)**: To introduce, develop and validate novel analytical tools for the speciation analysis of bio-oils and renewable feedstocks. This objective has been divided into three sub-objectives:

    - **O1a**: Development of a new total consumption nebuliser, produced through 3D-printing, that lowers the instrumental costs and allows the hyphenation of ICP-MS with LC. In addition, the hypothesis that suggest that this nebuliser would facilitate the speciation analysis of those species that might have interactions with the fused silica that was built in previous total consumption nebuliser versions has been tested.

    - **O1b**: Development and validation of an SFC-ICP-MS interface that will contribute to the improvement of the chromatographic resolution of the inorganic speciation analysis in complex samples.

    - **O1c**: To develop and validate a Freon-12-free methodology based on the coupling of ETV and ICP-OES for the inorganic speciation analysis of complex matrices based on their vaporisation temperatures.

- **O2 (instrumental applications)**: To obtain a better understanding of the composition and chemical structure of the hetero-atomic composition of bio-oils, renewable feedstocks and petroleum heavy oil fractions. This objective has been divided into two sub-objectives:

    - **O2a:** To adapt an existing GPC-ICP-MS methodology for the speciation analysis of atmospheric residue hydrodemetallization and hydrodesulfurization fractions.

    - **O2b:** To adapt an existing GPC-ICP-MS methodology for the speciation analysis of several hetero-atomic containing compounds in renewable feedstocks.

Objectives **O1a**, **O1b** and **O1c** are covered in Chapters 3, 4 and 5, respectively, of this thesis; and the objectives **O2a** and **O2b** are covered in Chapters 6 and 7, respectively. This distribution is illustrated in Figure 1.

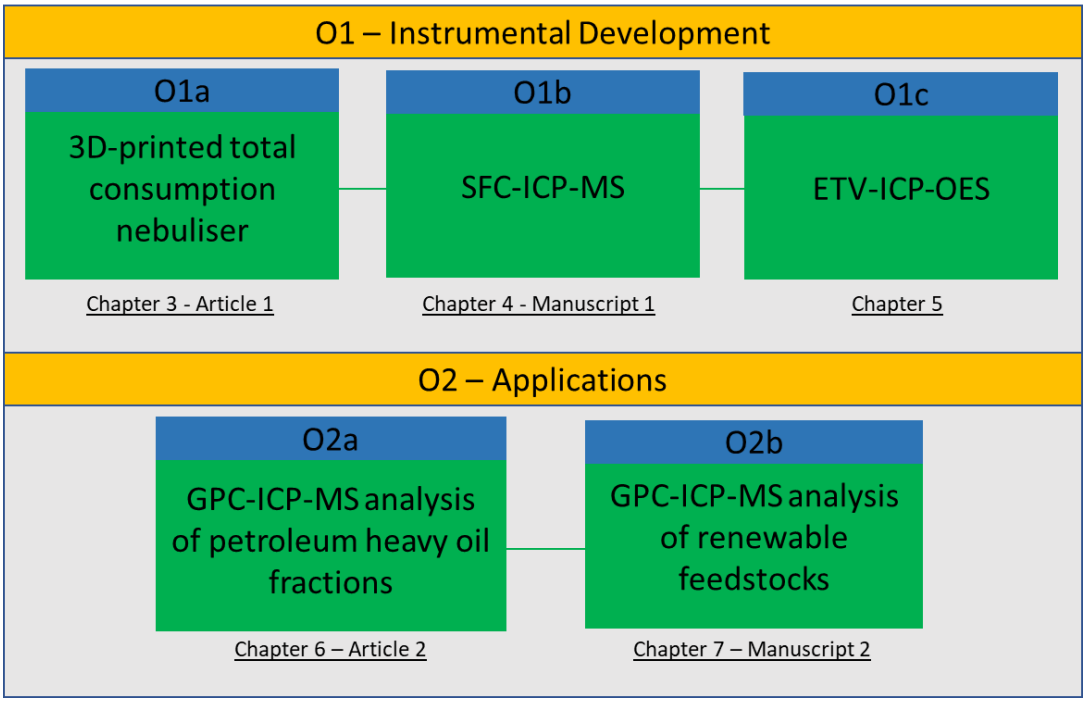

Figure 1. Outline of the objectives covered in this thesis.

Outline of the thesis

This PhD thesis has been divided into seven chapters. In the first two chapters a short literature review is presented, discussing (1) the production and composition of different bio-oils and renewable feedstocks and (2) the fundaments of the analytical methodologies that were used in this three-year project.

In the third chapter of this PhD thesis, the development and validation of a total consumption nebuliser that was made through 3D-printing technology is presented. This new nebuliser, which was built with a PEEK capillary, can connect either the outlet of a chromatographic column or a pump, allowing both chromatographic and total analyses of complex samples. The replacement of the fused silica capillary that was used in previous total consumption micronebulisers eliminates both the interactions and potential

permanent retention that some elements might have with it and will allow the speciation analysis of other trace elements as well, like silicon in bio-oils and renewable feedstocks.

In the fourth chapter, a novel interface for the hyphenation of SFC and ICP-MS has been presented. Supercritical fluid chromatography can provide to the separation of complex matrices with a very high number of theoretical plates. However, hyphenating SFC with an elemental detection like ICP-MS had not been yet carried out for modern SFC instrumentation. Thus, an interface that allows the hyphenation between SFC, using CO_2 and MeOH as the mobile phase, with ICP-MS has been developed. This chapter contains the preliminary results of the first use of this novel interface for both total and speciation analyses of renewable feedstocks and unconventional oils.

Chapter five discusses the development and application of an ETV-ICP-OES methodology that allows the speciation analysis of trace elements in complex matrices based on their vaporisation point. An optimisation of the gas flows, including the use of the alternative reaction gas SF_6, has been carried out and the method has been validated for the total analysis of eight trace elements by analysing the NIST SRM 1085b. Finally, the distribution of several trace element species in fast pyrolysis oils, based on their vaporisation temperature, has been obtained. Monomodal, bimodal and multimodal distributions have been observed among the different heteroatom-containing species present within such complex samples.

In the sixth chapter a GPC-ICP-HRMS methodology has been applied to the speciation analysis of the vanadium, nickel and sulfur species that are present in the atmospheric residue that is hydrotreated to obtain transportation fuels. The results that are presented within this chapter describe how the high molecular weight species containing sulfur, vanadium and nickel have been removed differently than the rest of lower molecular weight compounds during the hydrodesulfurization and hydrodemetalation processes. In addition, the loss of activity of the catalyst showed how it is more noticed on the hydrotreating of the high molecular weight compounds.

The appendix of this thesis contains one poster and other manuscripts that were either published or redacted during this three-year project. In two of these manuscripts, which were published in the journal ACS Energy & Fuels, the application of the GPC-ICP-HRMS method presented in this thesis is carried out to obtain a better understanding of the crude oil hetero-atomic species composition. The last manuscript, which is slightly out of the scope of this thesis, was redacted at the University of Copenhagen after having carried out several GC-MS experiments in an arctic station in Greenland, with the purpose of understanding the PAH pollution trends in the sediments of such pristine environment.

CHAPTER 1: FROM BIOMASS TO BIO-OIL. PRODUCTION AND COMPOSITION

1.1. Definitions of Biomass and Bio-oil

Biomass is defined by the IUPAC as the material produced by the growth of microorganisms, plants of animals,[1] but it can also be considered as the biodegradable fraction of products, waste and residues from biological origin from agriculture (including vegetal and animal substances), as well as the biodegradable fraction of industrial and municipal waste among other products.[2]

Biomass has been used as a source of energy all over the world for thousands of years until nowadays.[3] In 2017, the use of waste biomass and its derivates provided about 5% of the total primary energy use in the United States, becoming the most widely used renewable energy source at that time.[4]

The use of natural biomass as energy resource possesses numerous advantages. It consists of a renewable source and it is also CO_2 neutral[5,6] as all the CO_2 produced during combustion will be equal to the CO_2 naturally collected from the atmosphere during its formation by photosynthesis.

The use of industrial and municipal waste biomass cannot be considered a renewable source, but it still constitutes an important alternative to fossil fuels. It could also suppose an important improvement in general waste management strategies.

Bio-oils (also known as biofuels or agrofuels) are those solid, liquid or gaseous fuels that have been produced from biomass. They could also be defined as those fuels that are produced from organic matter rather than fossil fuels. With the application of different chemical processes, it is possible to produce bio-oil from biomass, which constitutes a potential alternative source of energy to fossil fuels.

1.2. Classification of bio-oils

Depending on the type of biomass feedstocks used to produce bio-oils, they can be classified into different groups:

- Primary bio-oils: Direct combustion of natural and unprocessed biomass such as wood, pellets, animal waste and crop residues among others. Normally used to supply heating or electricity production needs.[7]

- Secondary bio-oils: They are produced by processing biomass and consist of chemically modified primary bio-oils. Depending on the process and the material used, secondary bio-oils are classified into three subgroups:

  - First-generation bio-oils: They are generally produced from edible crops such as sugars, grains or seeds. Bioethanol, which is produced by fermentation of the sugars and starch present in crops (wheat, corn, potato, etc.) and biodiesel, which is produced from different vegetable oils (rapeseed, soybeans, animal fats, etc.) by transesterification processes are clear examples of first-generation bio-oils.
    Production of first-generation of bio-oils requires an outsize amount of land, initially used to produce food, which would be exclusively dedicated to feedstock. Chisti et al. showed that even for palm crops, which have one of the most abundant yields, the 24% of the United States of America's total cropland would be required to meet only 50% of their transport fuel needs.[8]

  - Second-generation bio-oils: They are produced by processing the non-edible residues from lignocellulosic biomass (trees, grass, etc.) and municipal waste (tyres, plastics, etc.). Lignocellulosic biomass feedstocks have a high content of cellulose, hemicellulose and lignin, which could be considered as an important source of carbon. However, their high content in oxygen and other inorganic elements require hydrodeoxygenation processes and catalysis upgrading that will be explained in section 1.6 of this manuscript. These feedstocks have a lower cost than the first-generation ones, but the conversion process to transportation fuels will be quite expensive until numerous improvements are deployed and applied.

- Third-generation bio-oils: They derive from microalgae, which possess high lipid productivity. These lipids are produced in the form of triacylglycerols, which are ideal for the production of bio-oil.[9] Besides, microalgae biomass production can produce a large number of proteins and carbohydrates in short times under normal conditions by assimilating CO_2 and sunlight and by consuming about 1.83 kg of CO_2 per kilogram of dry algal biomass.[7,10]

  One of the main advantages of third-generation bio-oils is explained by Chisti et al.[8] Their work illustrates the competence of microalgae yields by comparing them with the first-generation feedstock production: Only between 1 and 3% of the United States' total cropping area would be required to meet the 50% of their transport fuel needs if it were dedicated to producing microalgae biomass.

1.3. Renewable feedstocks

The major biomass feedstocks that are used to produce bio-oils and other renewable transportation fuels can be divided into groups, being these: Lignocellulosic biomass, sugars and starches, oils and fats, and industrial and municipal wastes. This review will focus on those whose samples will be analysed and studied during this work.

1.3.1. Lignocellulosic biomass

Lignocellulosic biomass is the most abundant renewable feedstock on the Earth, and it consists of a very rich source of carbon. It involves all the agricultural residues, both animal and vegetal and energy crops, among others. The components with the highest interest as chemical feedstocks are cellulose, hemicellulose and lignin. Their abundances vary according to the type of feedstock but generally are within the range of 38 – 50 % for cellulose; 23 – 32 % for hemicellulose and 15 – 25 % for lignin.[11]

- Cellulose: Consists of an organic polymer with the formula $(C_6H_{10}O_5)_n$ and it is the most abundant compound in the cell wall of the plant cells. Its structure consists of a straight-chain formed by the condensation of D-glucose monomers through ß(1→4)-glycosidic bonds, which are detailed in Figure 2.

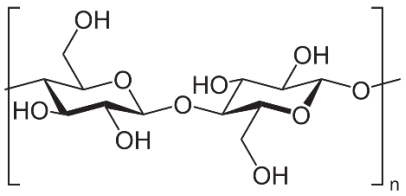

Figure 2. Chemical structure of cellulose.

- Hemicellulose: Consists of a group of polysaccharides that are present in most of the plants and vegetables. Their main role is to harden and strengthening the cell walls and their structure is formed by different monosaccharides linked through ß(1→4)-glycosidic bonds that shape a long branched chain. Even though it might seem simple to break these glycosidic bonds to obtain glucose molecules, it is a difficult process. The difference between hemicellulose and cellulose is that the former normally consists of shorter chains, shaping a branched polymer with different sugar monomers.

- Lignin: Complex heteropolymer present in the cell walls in wood and bark that provides rigidity and strength to the plant. It possesses hydrophobic properties that make this polymer a key component in water transportation within the plants. Knowing the actual molecular weight of this polymer is a challenge and numerous methods have been carried out to determine this value.[12] It is characterized by its abundant aromatic groups and the numerous structures they can form. Its structure is formed by the dehydrogenate polymerization of three molecules classified as "monolignols". They are the p-coumaryl, p-coniferyl and synapyl alcohols.[13]

  The structure of a lignin-carbohydrate complex is shown in Figure 3. It is possible to observe the high presence of oxygen within the carbon-rich structure. This high carbon content could be employed as a source of energy.

These three major components are distributed in the cell walls shaping a complex structure where all they are connected through hydrogen bonds (mainly with cellulose) and covalent bonds.[14] At the same time, cellulose polymers are gathering to form

microfibers, while lignin and hemicellulose polymers are inserted in the inner space, as it can be observed from Figure 3. Schematic structure of Cellulose, Hemicellulose and Lignin fibres in the cell wall.[14]

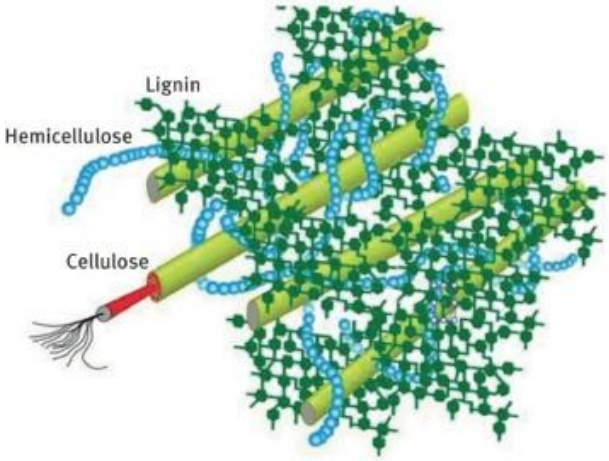

Figure 3. Schematic structure of Cellulose, Hemicellulose and Lignin fibres in the cell wall.[14]

During the first fast pyrolysis stages, the cellulose structure is degraded due to the rupturing of the ß(1→4)-glycosidic bonds. Furans and levoglucosan (which is used as a chemical tracer for biomass burning in atmospheric analyses) among numerous glucose-based compounds, gases, char and H_2O are released from this process.

Hemicellulose structure, due to the presence of different monomers and its branched structure, follows a different degradation process: each monosaccharide is degraded to different products including char and gases. For instance, the xylan degradation can lead to the formation of various anhydrosugars and other sub-products such as acetic acid.[14]

Lignin structure, which is more complex, follows a completely different path. While the glycosidic bonds are degraded as for glucose and hemicellulose, the cleavage of ether bonds leads to the formation of new products. Re-polymerization and side-chain conversion

reactions also take place, resulting in a wider range of products, including the formation of char, water and gas.

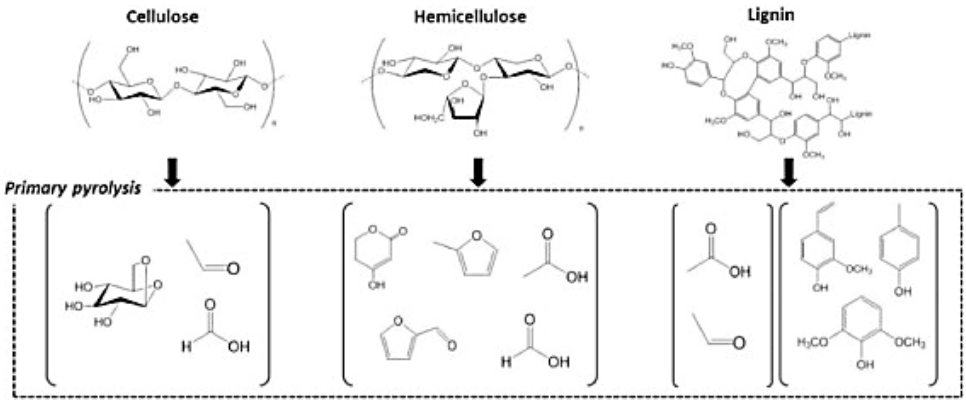

Figure 4. Schematic representation of some lignocellulosic fast pyrolysis products.[14]

1.3.2. Sugars and starch.

Different varieties of crops are harvested to produce first-generation bio-oils. These crops contain materials such as sugar cane, wheat or fruits that are rich in sugars, and also rice, corn and potatoes, which are rich in starch.

Sugars, which consist of soluble carbohydrates, are easily converted into ethanol through a biological process called alcoholic fermentation, that also produces carbon dioxide as a by-product, whose simplified reaction scheme is shown in Figure 5. [15]

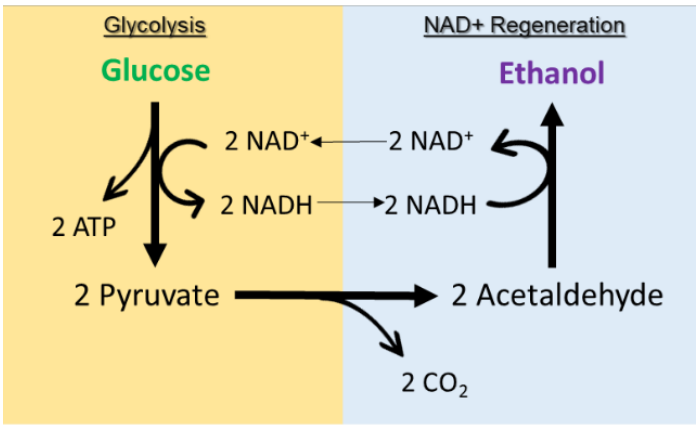

Figure 5. Alcoholic fermentation diagram.

Starch, however, is a polymer formed by the glycosidic bond union of glucose monomers. These glucose monomers can be extracted and, subsequently, through a fermentation process, they are transformed in bio-ethanol.

1.3.3. Oils and fats

Raw materials such as vegetable oils (palm oil, soybean oil, etc.) and several animal fat wastes such as tallow originating from pork, lamb, etc. can be used as a feedstock for biodiesel production. These materials contain a high concentration of triacylglycerides that after a transesterification process become fatty acid alkyl esters, which are the main component of biodiesel. [16]

They can also be treated with H_2 through a catalytic reaction to obtain a paraffin-based and completely deoxygenated fuel, also known as green diesel.

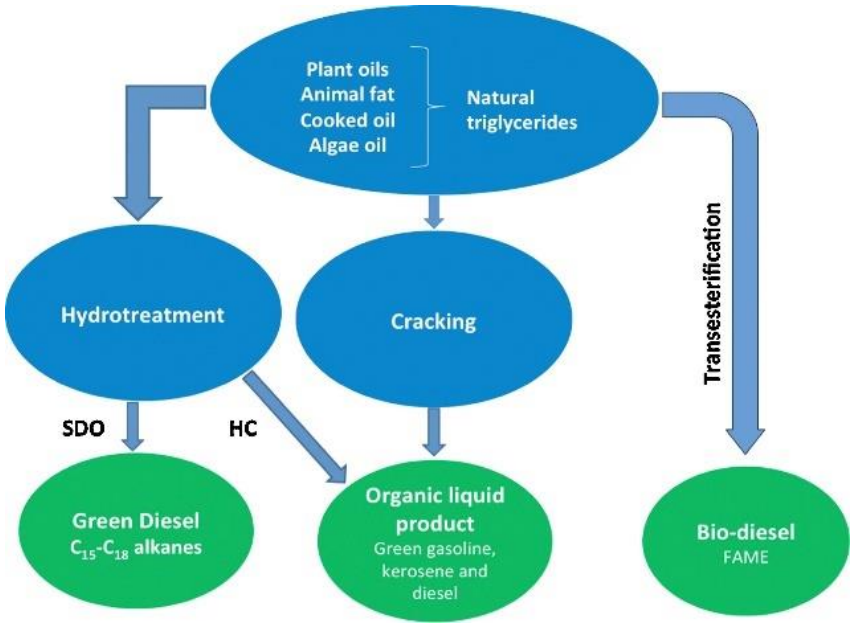

Figure 6. Main routes for the production of bio-oils from triglycerides.[16]

1.3.4. Municipal waste

Municipal wastes varying from sewage sludge to scrap tyres mean an important source of materials that can be used for the production of bio-oils. As the use of edible feedstocks to

generate bio-oils cause several ethical issues due to the lack of food in certain parts of the world, the use of non-edible materials such as wastes becomes a useful alternative. [17,18]

One of the most problematic waste materials in terms of storage and disposal, due to their long durability and non-biodegradability, is the scrap tyres. Thus, new methods for recycling scrap tyres have been developed during the last years.[18]

The main components of this feedstock are rubber, which consists mainly of organic polymers, and carbon black, a sub-product of petroleum. Thus, pyrolysis of tyres degrades the rubber polymers into smaller gaseous compounds that are condensed and used as bio-oils. Other sub-products such as char and gas that can be used in the energy industry are obtained by this method.

1.4. Bio-Oil from pyrolysis: Production and composition

1.4.1. Pyrolysis and fast pyrolysis

The rapid heating of biomass at temperatures between 400 and 800 °C in absence of oxygen results in a decomposition of its organic matter into three products whose proportion could vary depending on the process parameters and/or the biomass feedstock: char (also known as bio-char),[19] permanent gases and organic vapours that can be condensed, resulting in a liquid that is known as bio-oil.[20] In Figure 7 a diagram showing the different processes carried out to produce fast pyrolysis oils is detailed.

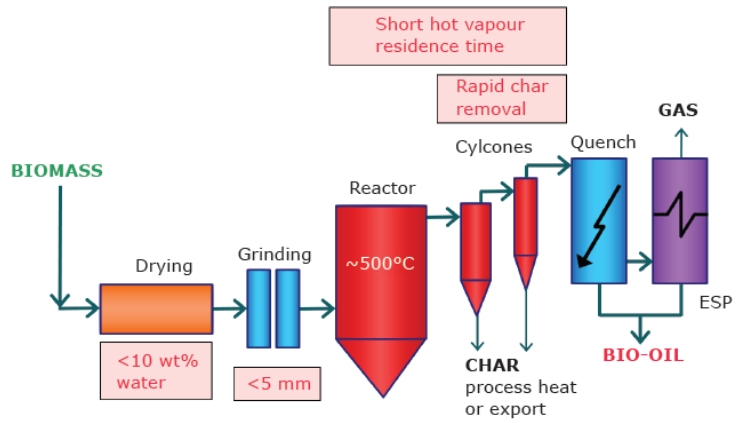

Figure 7. General fast pyrolysis of biomass diagram.[21]

While the use of high temperatures and long residence times during pyrolysis leads to gas formation, the use of low temperatures and long residence times leads to the formation of char. The optimum conditions for the production of bio-oils are medium temperatures with short residence times, which means high heating rates.[22] These conditions are applied in the process called "Fast Pyrolysis", which consists of one of the most important processes in the production of bio-oils.

Fast pyrolysis tolerates the use of any form of biomass. Nearly 100 different biomass types (agricultural wastes, energy crops, solid wastes, etc.) have been tested by many laboratories. Bio-oil is the main product, with yields up to 75 wt. %, together with char and gas.[23]

1.4.2. General composition of Pyrolysis Oil

Fast pyrolysis oil consists of a dense, sticky and dark brown coloured liquid. It possesses a strong smoky odour and normally, due to the feedstock moisture and the water produced during the whole process and storage, it presents two different phases (aqueous and organic).

GC-MS analyses of the aqueous phase were performed by Zhang et al.[24] This work shows its high concentration of water-soluble compounds such as acetic acid, hydroxyacetone and phenols among others. Therefore, this aqueous phase cannot be used as a fuel, but it is interesting as it could be a source of water-soluble chemicals.

Even though the major constituents of bio-oil can vary from each biomass feedstock, the organic phase generally possesses a high content in carbon and oxygen, mainly in the form of oxygenated hydrocarbons. These could be classified in these groups: acids, sugars, alcohols, ketones, aldehydes, phenols and derivates, furans and other mixed oxygenated compounds.[25] Besides, it is possible to find some fractions of lignin that could reach the 5000 Dalton.

1.4.3. Main impurities present in Pyrolysis Oils

1.4.3.1. Char

Char is a carbon-rich solid residue that is produced after pyrolysis of biomass with high content in carbon and it is considered as one of the main sources of inorganic compounds, especially phosphorus, silicon, sodium, calcium and potassium containing species.[26]

It acts as a vapour cracking catalyst, so it should be eliminated. To do so, cyclones and hot vapour filtration are the most common methods used.[23] Collecting the char residue is important, as it can be used as a low-grade fuel due to its high content in carbon and as a soil additive.

1.4.3.2. Oxygenated compounds

The oxygen content of these bio-oils is usually 35 - 40 wt. % which provides to the bio-oil with lower heating power, higher viscosity and corrosiveness:[21,27]

- Water is one of the main important oxygenated compounds (up to 25 wt % depending on the feedstock) present in raw pyrolysis oils and it cannot be separated.[25]

- The presence of carboxylic acids in bio-oils reduce the pH (2 – 3) and make them more corrosive for the handling equipment and storage vessels.[19]

- The presence of oxygenated compounds can promote etherification and esterification reactions whose main product is water, which reduces the bio-oil heating value. Besides, the condensation and polymerization reactions increase the average molecular weight of the bio-oil, which is directly linked with the increase of viscosity.[28] Figure 8 shows some of the typical oxygenated hydrocarbons found in pyrolysis oil: These compounds can be either monofunctional like phenol and benzaldehyde, or multifunctional such as 2-hydroxy-3-methoxybenzoic acid.

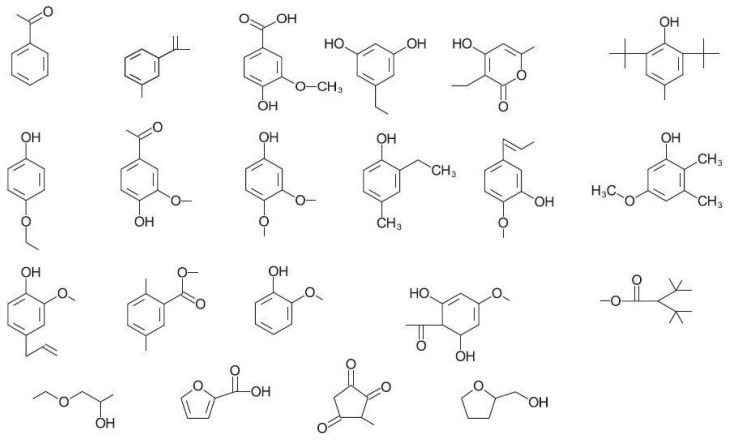

Figure 8. Typical oxygenated hydrocarbons in pyrolysis oils.[19]

Thus, upgrading processes of pyrolysis oils must be carried out with the purpose of removing the high oxygen content and transforming this low-energetic renewable feedstock into high-quality transportation fuels.

1.4.3.3. Inorganic species

The presence of numerous inorganic elements causes numerous issues in engines, pipes and other equipment such as slagging, fouling and ash related problems. They also reduce the heating value of the pyrolysis oil and could cause environmental pollution due to the emission of some of these compounds.

One of the main sources of these inorganic compounds in pyrolysis oil due to their higher presence is char. Agblevor et al.[26] studied the alkali composition of pyrolysis oils and showed that about 100% of potassium in the initial feedstock is provided by char. Other elements, such as Calcium and Phosphorus could have different origins including char as well.

The main elemental inorganic constituents of pyrolysis oil are the following ones:[29]

- Potassium: It is one of the most abundant metals present in plants and their nutrients as it is present in the cell-wall components and lignin. Nowakowski et al.[30] studied the effect of potassium on lignin pyrolysis and confirmed its high influence on the increase of char yield during pyrolysis.

- Calcium: Fifth most abundant element in earth crust, very important nutrient in plants and essential element in the cell walls, hence its presence in bio-oils such as lignocellulose and vegetable oils. It has been found that this element can form hard deposits in gas turbines airfoils, causing loss of performance and being difficult to be removed.[31]

- Sulfur: Depending on the type of biomass that has been employed to produce bio-oils, sulfur can be present with different abundances. Pyrolysis oils from crops, which are rich in proteins, contains a high concentration of sulfur, as this element is present in amino acids such as methionine and cysteine.[32] Other types of biomass sources, such as tyres, could contain a much higher concentration of sulfur due to the vulcanisation process carried out to harden the rubber they are made from, which consists in heating this material with sulfur compounds. Among the different sulphur species in tyres pyrolysis oils, some sulphur PAHs have been already identified.[33]

  As one of the main impurities in crude oil, sulfur compounds are already well known since they cause corrosion in numerous alloys, catalyst poisoning and they are the cause of the emission of toxic gases to the atmosphere. Research into the speciation analysis of the different compounds containing sulfur in crude oil and its derivates have been performed thoroughly during the last years, focusing on achieving a better understanding of the characteristics of these species and thus adapt different desulfurization processes to obtain better results.

- Phosphorus: This element is present with a high abundance in biomass, as it consists of an essential nutrient for the growth of numerous organisms. This element can be found in fatty acids, phospholipids and sterols among other abundant biomolecules. Like potassium, it has negative effects on the pyrolysis oil stability since an increase of the pyrolysis oil viscosity caused by polymerisation reactions has been observed. In addition, its presence also increases the char yield during the pyrolysis process, which could cause future problems in engines and equipment.[34] Phosphorus speciation analyses in ash have been carried out in

different types of pyrolysis oils and it was found that it forms different phosphates with calcium, potassium and iron.[35]

- Other trace elements, which are very abundant in the earth's crust, and, therefore, present in soils where the organic matter used as feedstock is grown, are amongst others, silicon, aluminium, magnesium and sodium.

1.5. Biodiesel and renewable diesel

1.5.1. Biodiesel production and general properties

As it has been briefly mentioned before, biodiesel consists mainly in the product of the transesterification reaction of the different triacylglycerides present in either animal or vegetal lipid-based feedstocks such as soybean oil or tallow fat with an alcohol in the presence of a catalyst. A general pathway for the production of biodiesel is presented in Figure 9:

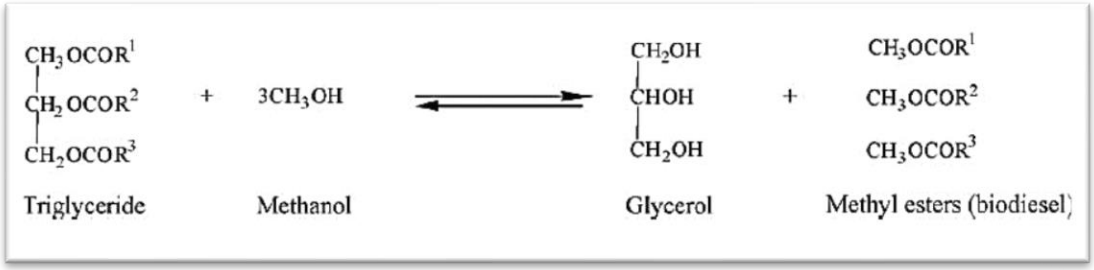

Figure 9. Transesterification process for the production of biodiesel.[36]

Biodiesel is far different from petroleum diesel, and some of its advantages are summarized below:[37]

- Derived from a renewable source.
- High biodegradability.
- Lower emission of toxic gases (except for NO_X).
- Higher flashpoint.
- Excellent lubricity.

Nowadays, biodiesel is blended with petroleum diesel and used in diesel engines, due to its high viscosity. However, this blending is advantageous as the higher lubricity of the biodiesel improves the protection of the fuel injection systems in engines.

The industrial transesterification process takes place in a reactor where an alcohol, generally methanol, a catalyst that could be either acid or basic, and the fatty feedstocks are mixed under agitation for around 1h and at 60 ˚C.[37] Once the reaction has been carried out, glycerol is removed from the products in a settling tank or a centrifuge and the methyl esters are neutralized and purified.

Figure 10 depicts a schematic diagram of the industrial process for the production of biodiesel in feedstocks like soybean oil.

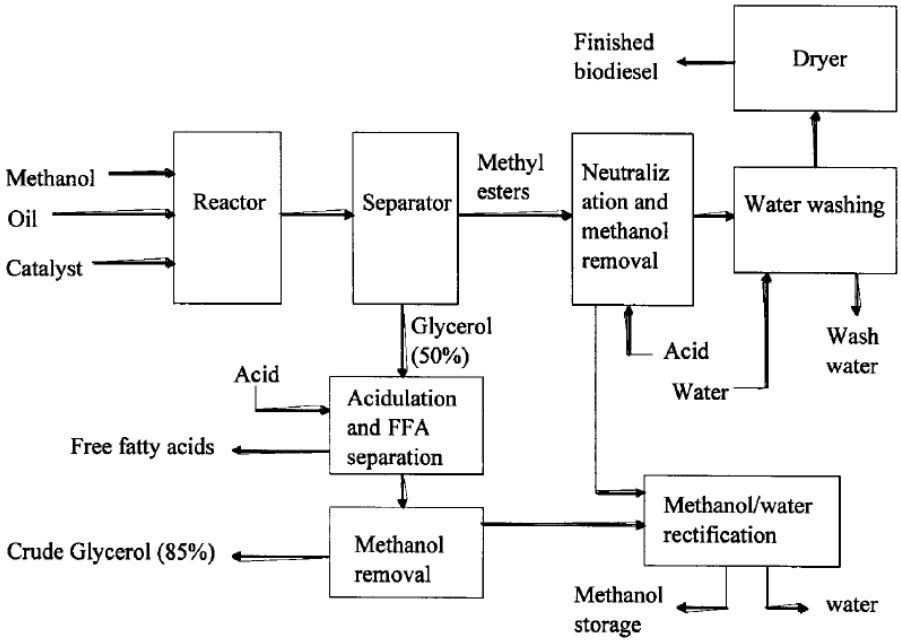

Figure 10. Schematic diagram of an industrial biodiesel production process.[37]

1.5.2. General composition of biodiesel

When the transesterification process is over, a mixture of different fatty acid methyl esters (FAME) is the main component of the products. These FAMEs are different for each

feedstock that is used to produce them. Hoekman et al.[38] studied the general composition of biodiesel produced from twelve different feedstocks.

Oleic, Palmitic and Stearic acid methyl esters are the principal species present in biodiesel produced from tallow, which is one of the feedstocks that will be analysed in this research project. FAMEs, whose carbon chains length vary from 6 up to 24 carbons and up to 4 instaurations, have been found for these types of feedstock.

However, Linoleic, Oleic and Palmitic were the principal FAMEs found in Soybean Oil, which is the other of the feedstocks analysed during this project.

1.5.3. Renewable diesel

Produced from feedstocks such as animal fats and vegetable oils, whose potential diesel-type molecules, independently of either the seed type or the animal, are the triglycerides. These triglycerides can react under hydroprocessing conditions to form different n-alkanes whose number of carbons is within the diesel length depending on the pathway followed during the process.

This process is carried out in a reactor at conditions above 300°C and 45 bar and with a hydrogen-to-oil ratio of 500 nL/L and the reaction pathway carried out along the process is described in Figure 11, where the triglycerides present in the feedstocks react with the hydrogen in the presence of a catalyst saturating the double bonds within the triglycerides.[39]

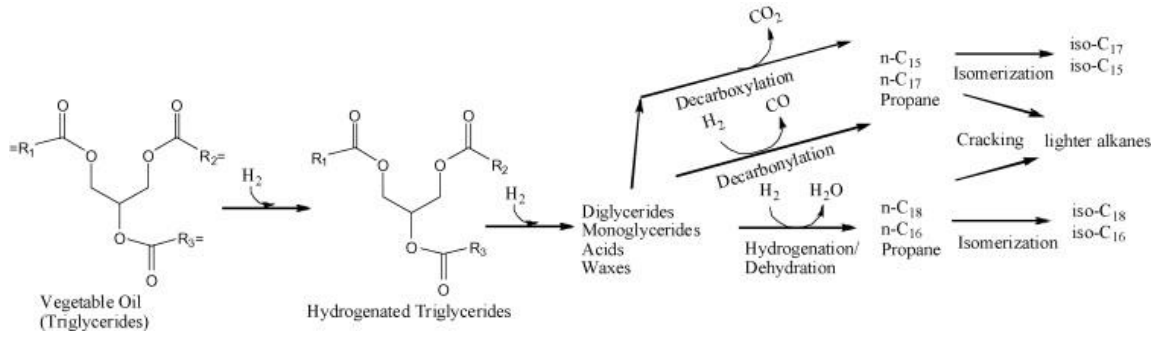

Figure 11. Reaction pathway for the production of n-alkanes from triglycerides[40].

This first pathway is followed by a second reaction where the triglycerides are completely broken producing either H_2O and propane (hydrogenation pathway) or CO_2 and propane instead (decarboxylation pathway) as subproducts, added to the correspondent n-alkanes whose length is equal to each triglyceride length minus one.

One of the key factors in this process is the catalyst selection, since it must be able to handle the excess of CO produced within the reactor that inhibits the desulphurization process, among other factors that might reduce drastically the life of the catalyst and worsen the properties and composition of the process products.

1.5.4. Main impurities in Biodiesel, Renewable Diesel and their feedstocks

Not only can the type of FAMEs present in biodiesel or the n-alkanes within the green diesel vary depending on the feedstock. The nature of the impurities in these bio-oils can also have a high variation depending on the raw materials that have been used as a feedstock.

1.5.4.1. Phosphorus

As one of the main components of all the cell membranes, phospholipids are one of the main sources of phosphorus contamination. This contamination has been suggested by Van Gerpen et al.[41] as a source of catalyst destruction during the transesterification process causing an important yield reduction: 50 ppm of phosphorus in a vegetable oil feedstock could reduce the yield up to a 5%.

Phospholipids, which are the major constituent of the lipid bilayer, are a class of lipids that are present in all the types of cell membranes. Their basic structure is constituted by a diacylglycerol backbone with a phosphate ester-linked to the third carbon of a glycerol molecule. Depending on the compound that is attached to the phosphate group of the phospholipid, different structures can be formed. The main compounds that are linked to this phosphate group are the choline, ethanolamine, serine and inositol. When they are part of the skeleton of the phospholipids, they modify their physical and chemical behaviour.

The structure of the most common phospholipids is detailed in Figure 12 and their chemical behaviour differences can be predicted from their structure, especially when paying attention to the different phosphate groups and the compound that is linked to them, which characterises the phospholipid.[42]

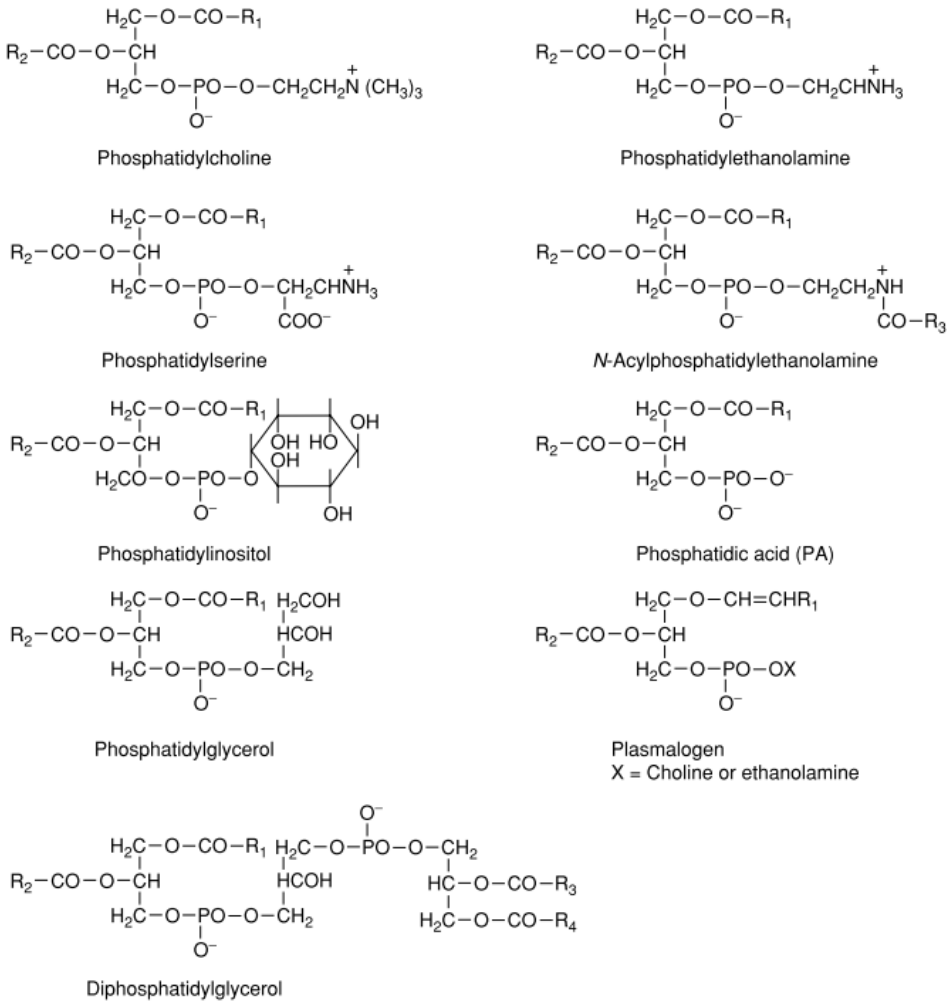

Figure 12. Structure of the most common phospholipids in animal fats and vegetable oils.[42]

From all the existing phospholipids, there are five of them that have been found as major components in nature: phosphatidylcholine (PC), phosphatidylinositol (PI), phosphatidylserine (PS), phosphatidic acid (PA) and phosphatidylethanolamine (PE). These major components are divided into two groups concerning their interaction with water: hydratable (HPLs) and non-hydratable (NHPLs) phospholipids.

The fatty acid chains that constitute the backbone of the phospholipids commonly have a length that varies from C_4 to C_{26}, with saturations that vary from one to six double bonds, located in different parts of the acyl group. Depending on the source of these phospholipids, such as vegetable or animal origins, the length and saturation rates of these compounds might vary.

Another issue that these compounds cause concerning the production of either biodiesel or renewable diesel is the formation of gums. The phospholipids possess a strong emulsifying action that can reduce the catalysts' life during the transesterification processes. Besides, other metallic species might be attached to these phosphatides leading to the formation of oxidant compounds such as aldehydes and ketones, amongst others, and ultimately degrade the biodiesel produced.[43,44] Thus, a process known as "degumming" must be carried out to refine the vegetable oils and animal fats before they are used. This process consists of the removal of the maximum number of phospholipids via different phases.

Depending on the nature of the phospholipids present in a fatty acid feedstock, different degumming techniques can be used to obtain an optimal elimination of the phosphorus species within the sample in a faster way.

One of these methods is the water degumming, in which water is used to hydrate the HPLs. These hydrates, which are insoluble in oils due to their aggregation rates, form oil-insoluble particles that can be eliminated by simple centrifugation. Regarding soybean oil, the HPLs fraction already means more than 50% of the phosphorus content.[44]

Other chemical degumming methods have been reviewed by Sharma et al.[44] and Sengar et al.[43] who have studied the degumming process for soybean and rice bran oil samples respectively. A general overview is given below:

- Water degumming, which was already explained above, consists of the elimination of the hydratable fraction of the phospholipids present in fatty acid feedstocks. It also allows the recovery of lecithin, a mixture of phospholipids and other compounds, which can be used as an additive in the food industry.

- Chemical degumming groups all the different methods where the addition of a chemical reagent is carried out. The use of acids, such as citric acid and phosphoric acid help in the decomposition of numerous PL complexes with Na and Mg ions, amongst others, being ultimately eliminated by centrifugation. Other reagents, such as EDTA, a chelating reactive, or electrolyte solutions are also used for the removal of NHPLs.

- Enzymatic degumming. Considered as one of the best processes currently available to reduce the phosphorus content up to less than 5 ppm in rice bran oil, converts the NHPLs to HPLs, which are ultimately removed by centrifugation. Phospholipase, in an acidic medium, is the most commonly used enzyme.

- Membrane degumming. The fundament of this process is based on both the molecular sizes of the phospholipid molecules, which are approximately 1.0 – 1.5 nm and their molecular weights. Furthermore, these PLs can form micelles whose size can reach up to 200 nm of size and 20 kDa of weight. Thus, making these oil samples passing through a series of membranes with a determined pore size, depending on the sample, will allow the elimination of these undesirable species. Amongst all the types of membranes, ceramic (Al2O3, TiO2, etc.) and polymeric (PVDF, PI, PES) membranes are currently in use. They have a high efficiency, but they are expensive and require larger amounts of time rather than other degumming methods.

1.5.4.2. Other inorganic species.

- Sulfur: This element is present in all type of living cells, hence its high abundance in both vegetable and animal feedstocks. Apart from the bad effect that sulfur emissions could have in the environment, these compounds have been found that can cause catalyst deactivation during the hydrodeoxygenation process of vegetable oils.[45]

- Silicon: Different species of this element are commonly present in biodiesel samples due to its presence as silicon oxide in feedstock crops. Their presence can cause damage to the engines, and the oxides formed during combustion can form slag deposits and corrosive compounds.[46,47]

- Iron: Haemoglobin for animal feedstocks and poor storage conditions of vegetable feedstocks could be the main sources of iron contamination. Besides, iron species have been found to cause great damage in engines during their combustion.[47]

- Magnesium, calcium, sodium and potassium: Their concentration in the biodiesel could vary depending on the type of feedstock employed. Together with K, the presence of Mg and Na could cause solid deposit in engines. [30,31]

1.6. Bio Oils refining: Hydrodeoxygenation (HDO)

Some renewable feedstocks, such as fast pyrolysis oil, can be burned directly in some static applications such as boilers, furnaces, engines and turbines.[48] However, as it has been mentioned before, the high content in water and oxygenated compounds reduces the pyrolysis oil's heating value. In addition, the low pH, instability and the presence of char and other impurities could cause solid deposits and corrosion on engines and pipes.

Thus, transforming the crude bio-oil into a hydrocarbon fuel with high heating value, stability and low content of impurities requires an upgrading process.

Solvent addition, vacuum distillation and filtration are some of the physical upgrading processes that have been reviewed by Mostafazadeh et al.[49] However, the catalytical upgrading processes of bio-oils possess greater importance since the greatest improvements are achieved with these processes.

Catalytical processes designed for petroleum refining have been known and improved throughout the years. As it has been mentioned before, raw pyrolysis oils have a much higher oxygen content that must be lowered to transform these raw materials into stable products with high commercial value, efficient heating and low corrosion rates that will

allow them being used as liquid transportation fuels with a high content of hydrocarbons. Besides, due to the much lower concentration of other elements such as S, it is clear that applying the same catalytical upgrading methods as those for fossil feeds (containing less than 0.1% oxygen) is not efficient.

Hydrodeoxygenation is one of the most used pathways to upgrade bio-oils to meet these criteria. Other catalytical methods, such as Hydrodemetallization and Hydrodesulfurization, will be reviewed briefly in the publication enclosed within the Chapter 4 of this manuscript on their application to the conversion of crude oil atmospheric residues into transportation fuels.

1.6.1. Reactions

In this catalytical process, among all reactions that may occur for a given catalyst at certain conditions, the oxygen present in the bio-oil is removed as the water product of a hydrogenolysis reaction in the presence of a catalyst. Table 1 shows an overview of the different reactions generally occurring during HDO and their most common used acronyms.[50] These reactions occur depending on the choice of the catalyst and its selectivity towards the different reactions they are involved in.

Table 1. Overview of the main reactions occurring during HDO.[50]

Reaction name	Reaction
Decarboxylation (DCO)	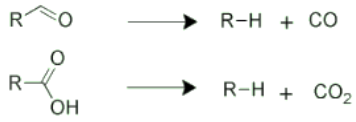
Hydrodeoxygenation (HDO)	
Hydrogenation (HYD)	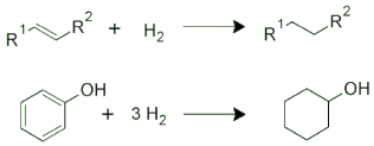
Direct deoxygenation (DDO)	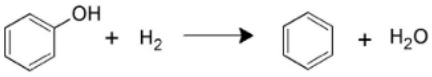
Cracking (CRA)	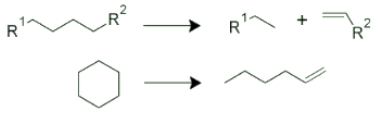
Hydrocracking (HCR)	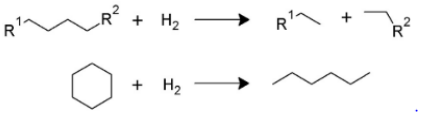
Demethylation (DME)	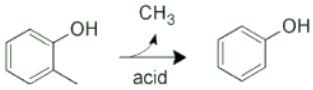
Demethoxylation (DMO)	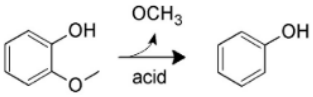
Methyl transfer (MT)	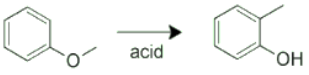

1.6.2. Catalysts

The main groups of HDO catalysts can be summarized in sulphides, oxides, transition metals. The type of catalyst, added to other operating conditions such as temperature, residence time and hydrogen pressure, is crucial to obtain a high-value fuel.

- Sulphides, such as Co-/NiMoS and Re_2S among others, have been widely used in bio-oil (HDO) and crude oil upgrading. One of their advantages is the tolerance to

the sulphur present in these feeds. However, H_2S must be added continuously to keep the catalyst within its sulphide form during HDO. A co-processing hydrodeoxygenation and hydrodesulfurization has been reported from Sepulveda et al.[51] In this research work, the H_2S resulting from the HDS process acts as a sulfiding agent and extends the lifetime of the catalyst.

- Oxides, such as Mo, W, Ni and V oxides among others, require lower H_2 pressure.[52]

- Reduced transition metals, such as Pt, Pd, Ru and Rh, which are commonly used in organometallic chemistry have higher activity in reactions such as hydrogenation (HYD) and hydrodeoxygenation (HDO). However, in contrast to sulphides, they are not tolerant of sulphur, whose presence within the feed could cause catalyst poisoning. [53]

1.6.3. Catalyst deactivation

The catalyst's loss of activity over time is a problem which might cost large amounts of money to the industry. Although catalyst deactivation cannot be avoided over time, this degradation can be slowed down, and catalysts' lives can be extended.

Catalyst deactivation could be caused by different factors. Chemical deactivation is the most common, but other mechanisms such as fouling, consisting of the deposition of species on the catalyst surface and pores, or thermal degradation, causing thermally induced loss of activity/selectivity.[53]

- Water: In pyrolysis oil HDO, water is the main catalyst poison towards a broad group of catalysts.[50] Since it is formed during fast pyrolysis of biomass and HDO, it can saturate the active sites of both oxide and sulphide catalysts and also decrease some of the transition metal catalyst's activity. For instance, Laurent et al.[54] concluded that under hydrotreating conditions, water causes the loss of two-thirds of the initial activity of a NiMoS catalyst in less than 60 hours. Hence the importance of physical upgrading of pyrolysis oil and water removal before catalyst upgrading.

- Carbon deposition: Polymerisation condensation reactions could occur at the catalytic surface, leading to a deposition of carbon that blocks the active sites and causes lower activity and selectivity rates. Even though the carbon formation depends on the feed composition, it might be controlled by adjusting the process conditions, such as temperature and H_2 pressure.[50]

- Inorganic species:

    - Chlorine: Organically bound chlorine has been found that causes a considerable loss of activity in catalysts such as Ni-MoS_2/ZrO_2.[55].

    - Potassium: For the same type of catalyst (Ni-MoS_2/ZrO_2), its impregnation with KNO_3 caused a decrease of the degree of oxygenation up to 85% showing that this loss of activity could be caused by the occupation of some the vacancy sites of the catalyst by potassium.[55]

    - Phosphorus: This element is the cause of several problems during the catalytical process. It has been reported that the presence of phosphorus compounds, normally present as phospholipids within these matrices, cause the deactivation of the catalyst: the phospholipids are decomposed into phosphoric acid, that acts as an oligomerization/polimerization catalyst, promoting the deposition of high-molecular-weight oligomers on the catalyst surface. In addition, the presence phosphorus increased the concentration of oxygenated compounds (fatty acids and fatty esters) at the end of the catalytical process.[56]

CHAPTER 2: ANALYTICAL METHODS

In this chapter, a short review of the analytical techniques that have been used during this three-year PhD is given. With the purpose of organizing the structure of this chapter, the analytical techniques have been divided into two subgroups: those concerning the separation of the analytes and those concerning the detection.

2.1. Chromatographic techniques.

Complex matrices such as bio-oils and their feedstocks that have been analysed throughout this project require a high-efficiency separation of the species that form them. With the purpose of achieving this high-efficiency separation, several techniques have been used throughout this three-year project.

Chromatography is a separation method used for the first time in the early 1900s by Mikhail Tswett, who used to separate vegetal pigments such as chlorophyll and xanthophyll by using a glass column filled with fine particles of $CaCO_3$. Within the column coloured bands corresponding to the different components of these pigments appeared, hence the name of "chromatography".

Since then, the use of chromatography has grown exponentially until nowadays as it has become one of the standard methods for chemical separation. [57]

2.1.1. Principles of Chromatography

In Tswett's set up, the vegetal pigments were dissolved in a liquid that carried them through the column while they were interacting with the fine particles that defined the column filling. The carrying liquid is called "mobile phase" while the material within the column has been called "stationary phase".[57]

The different interactions between the molecules of a mixture that has been dissolved in the mobile phase and the molecules of both mobile and stationary phases will cause a retention of certain molecules with higher affinity versus those molecules that have either

less or no interactions at all. Thus, molecules that have been retained due to their higher affinity will be eluted later.

Since the separation is a result of the equilibrium between two immiscible phases, there exists a relation between the amount of solute in the stationary phase (s) and the amount of solute in the mobile phase (s). Thus, for a given solute, the retention factor (k) has been defined as the quantity of solute in the stationary phase divided by the quantity of solute in the mobile phase, and since the amount of solute in a solution is equal to its concentration (C) times the volume of solution (V), the retention factor can be expressed as:

$$k = \frac{C_s V_s}{C_m V_m} \qquad \text{Equation 1}$$

The retention time (t_R) is then defined for a given solute as the time passed from the injection of the sample until the detection of this compound. By rearranging Equation 1, the retention factor (k) can be experimentally determined by the following equation:

$$k = \frac{t_R - t_0}{t_0} \qquad \text{Equation 2}$$

being t_0 defined as the column "dead-time" which consists of the retention time of the solvent peak which does not interact with the stationary phase. Equation 2 allows the experimental calculation of the retention factor for each peak in a chromatogram, being an important parameter that evaluates the performance of the separation of a certain solute.

Another important term that evaluates the separation of two chromatographic peaks is the chromatographic resolution (R_S) which can be expressed as:

$$R_s = \frac{\sqrt{N}}{4}(\alpha - 1)\left(\frac{k}{1+k}\right) \qquad \text{Equation 3}$$

Being α a term expressing the selectivity of the column and N the column plate number, which is a concept that measures the efficiency of the column separation, consisting of the ability of a column to provide narrow peaks for a certain solute. The larger the value of N, the better is the separation and the narrower are the peaks obtained.

The value of N is dependent on the width of a peak (W) and its retention time (t_R). However, the width of a peak is affected by multiple factors that will determine the quality of separation. By understanding these factors, it will be possible to select the optimal chromatographic conditions and columns to obtain the best results possible. [57,58]

- *Eddy diffusion* (A) is one of the factors that contribute to peak broadening. Since the stationary phase within a chromatographic column is not perfectly ordered, the molecules of the mobile phase will follow different paths before reaching the end of the column.

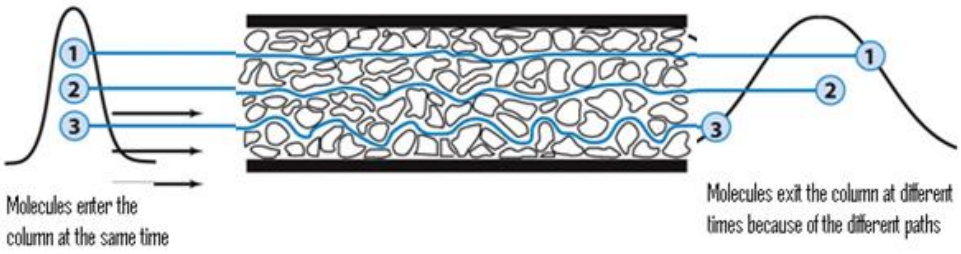

Figure 13. Representation of the different paths of various molecules in a packed chromatographic column.[59]

- *Longitudinal diffusion* (B) of the analytes along the column is the second factor contributing to the peak broadening and it is inversely proportional to the mobile phase linear velocity. Since some of the molecules move faster than the others within the mobile phase, the effect will be higher the lower the flow is.

- *Mobile phase mass transfer* (C) is the last factor contributing to peak broadening. During elution, analyte molecules are interacting with the stationary phase in an equilibrium. Since this process is not equal for all the analyte molecules as it is dependent on the particle size and porosity and viscosity and velocity of the flow among other factors, some analyses will spend longer time into a particle pore than others. During this time, other molecules will have moved further along the column and this fact will be reflected in the chromatogram as a broader peak.

If these three factors are put together and considering that the height equivalent to a theoretical plate (H) is the number of theoretical plates (N) divided between the length of the column (L), the following equation is obtained:

$$H = A + \frac{B}{u} + Cu$$

Equation 4

where A, B and C are the three factors previously described and u the mobile phase velocity. [57,58]

Equation 4 is known as the "Van Deemter Equation" and if the height equivalent to a theoretical plate (H) is plotted versus the mobile phase velocity (u) the graph shown in Figure 14 is obtained:

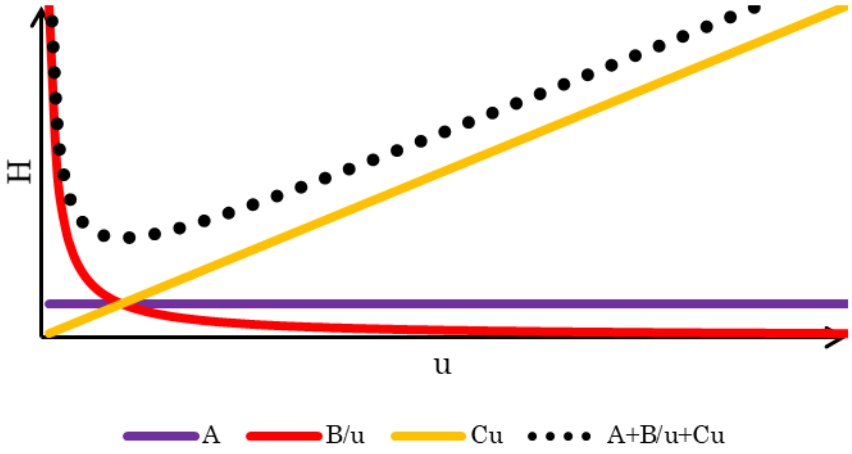

Figure 14. General variation of H versus mobile phase velocity. (Van Deemter Equation).

In the graph shown in Figure 14, the dotted line represents the variation of the height equivalent to a theoretical plate (H) versus the mobile phase velocity (u) including the three factors causing the peak broadening. It is possible to observe how for a certain mobile phase velocity there is a minimum of theoretical plate height. This velocity will be the optimal flow rate for a chromatographic separation. If the flow is lower, the *longitudinal diffusion* term (B/u) will cause an increase of H, leading to a worse separation efficacy and loss of resolution. The same would happen if the flow is higher: the *mobile phase mass transfer* (C) term will contribute to the peak broadening.

This relation between both terms H and u varies significantly among the different chromatographic methods. A general classification of these methods based on the physical state of the mobile phase is established:

- *Gas Chromatography* (GC) is a separation technique where the components of a vaporised sample carried by a gaseous mobile phase interact with the solid stationary phase of a column. However, in order to vaporise the analytes, they are heated in an oven at high temperatures. Excessive heating rates would make it unsuitable for molecules with a high molecular weight such as some of the samples analysed during this PhD.

- *Liquid Chromatography* (LC) is a separation technique where the components of a sample are carried out by a liquid mobile phase and interact with a liquid or solid stationary phase within a column or a plate. When column liquid chromatography separations are carried out, the columns are normally packed with quite small stationary phase particles (2 – 10 μm), which increases the efficacy due to a decrease of the *Eddy diffusion* factor (A). However, the size of the stationary phase particles requires high pressures to achieve the elution of the mobile phase. This chromatography method of separation with high pressure is called as HPLC (High-Performance Liquid Chromatography).

  Depending on the physical properties of the mobile phase in HPLC such as polarity and molecular weight, Liquid Chromatography can be further divided. The different types of HPLC are depicted in Figure 15. Applications of HPLC57. Gel Permeation Chromatography is one of the types of HPLC used in this project and its principles will be detailed in this chapter.

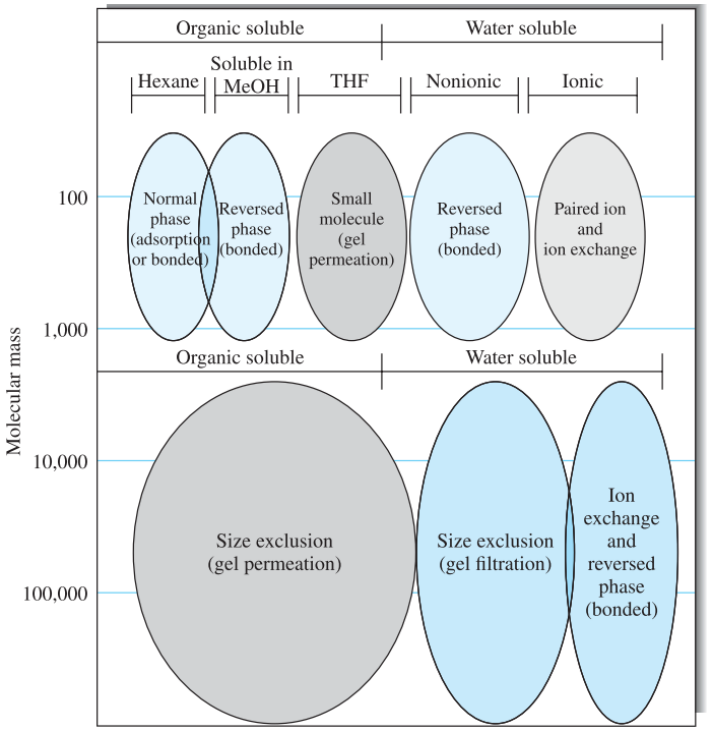

Figure 15. Applications of HPLC[57].

As mentioned before, the A term (*Eddy diffusion*) is reduced due to the packing within the columns. Besides, the *longitudinal diffusion* term (B/u) is not significative in HPLC unless the mobile phase flow rates are extremely low. Thus, the optimal flow rate is slower than in other separations such as GC, and the van Deemter plot would resemble as it is depicted in Figure 16, achieving much higher efficiency separations with higher resolutions. [57,58]

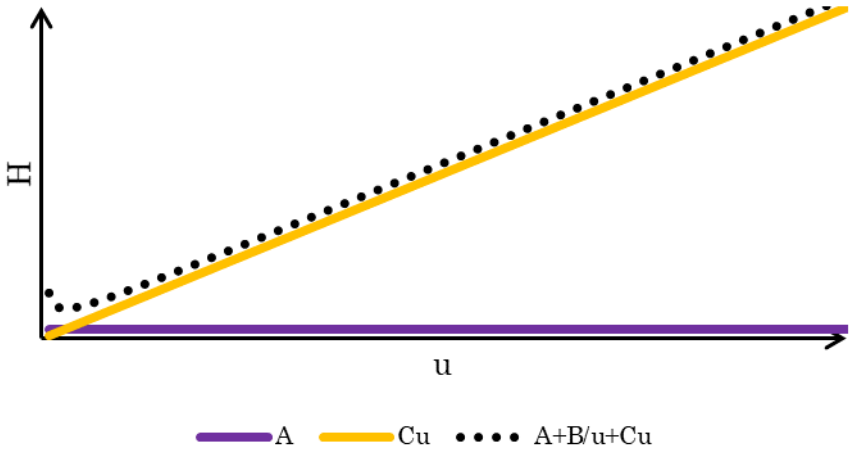

Figure 16. Van Deemter plot for HPLC.

- *Supercritical Fluid Chromatography* (SFC) is a separation technique where the mobile phase is composed mainly of supercritical carbon dioxide and other coeluents such as methanol or ethanol among others. One of the advantages of this separation method is that it combines some of the advantages of both *Gas Chromatography* and *Liquid Chromatography*.

2.1.2. Gel Permeation Chromatography (GPC)

Size-exclusion chromatography (SEC), also called *Gel Permeation Chromatography* (GPC) when an organic solvent is used as mobile phase, is one of the LC applications for the separation of molecules according to their hydrodynamic volumes. [60]

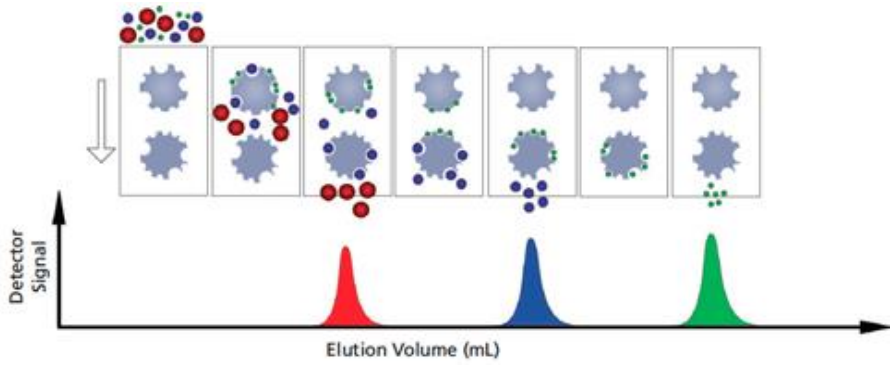

Figure 17. GPC separation mechanism.[61]

To achieve an effective separation, GPC column packings consist of small polymer particles containing pores (~ 5 µm) where the analyte molecules can be trapped and removed momentarily from the mobile phase, causing, therefore, retention. The residence time within the particles varies with the size of pore and the hydrodynamic volume of the molecule as it is described in Figure 17. Thus, molecules with larger diameters than the size of the pores are excluded and do not suffer retention and will be eluted together at the exclusion volume of the system whereas the molecules whose diameters are smaller than the pore size will penetrate within the pores.

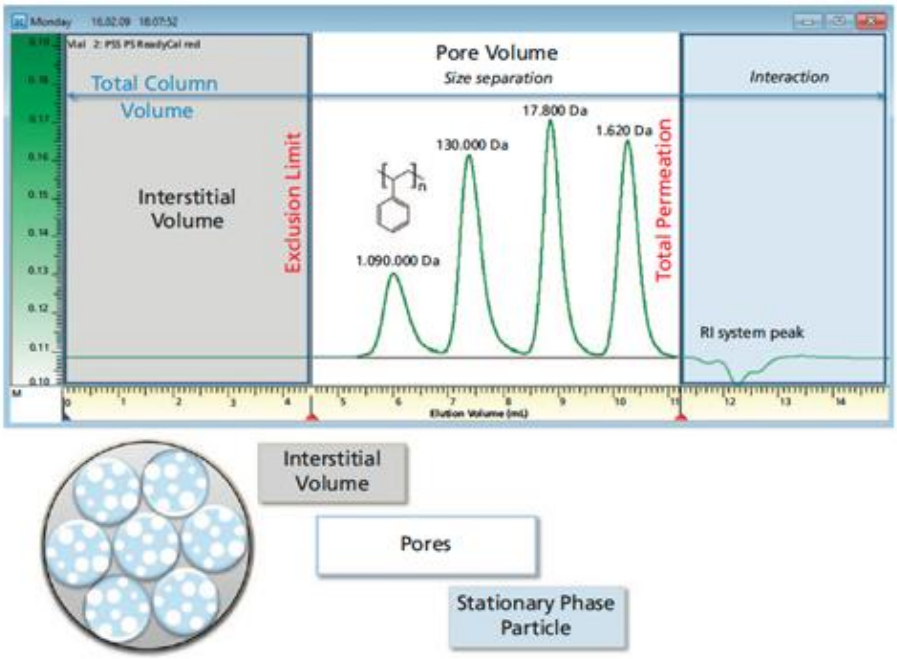

Figure 18. Example of a GPC chromatogram with RI detection for a mixture of four different polystyrenes.[61]

It is important to point out that neither chemical nor physical interactions take place between the analytes and the stationary phase. Hence, theoretically, there is an upper limit to retention time: no analytes are retained longer than the column total permeation time. Figure 18 explains visually the structure of a GPC chromatogram and it is possible to observe three different regions: [60]

- *The interstitial volume* consists of the time that takes the mobile phase to reach the detector. If the mobile phase contained molecules whose size is much bigger than the pore diameter (*exclusion limit*), a peak would be observed at the end of this region.

- *Pore volume* consists of the region where the analytes reach the detector, corresponding the first peaks to the bigger size molecules and the opposite for the small peaks.

- *Total permeation volume* is the time when no more peaks are expected theoretically, as all the solute molecules have penetrated the pores completely, since no

interactions between the analytes and the mobile phase are expected. When the molecules with a significative smaller size in respect to the pore size are eluted, since they are very small, they elute all together in a single band labelled *D*.

With the purpose of understanding why the peaks are wider in this type of chromatography, it is necessary to pay attention to Equation 4 again. In *gel permeation chromatography*, the resolution of the peaks is strongly conditioned by the peak broadening, and this factor is controlled mainly by the *mass transfer* term (C), since the longitudinal effect (B) is generally insignificant: analyte molecules tend to have high hydrodynamic volumes and, therefore, very small diffusion coefficients.[60]

However, when the analyte molecules have smaller hydrodynamic volume, a theory based on the coupling concept of both eddy and lateral diffusion terms has been formulated. This theory establishes that the molecules do not only follow their path within the column, but they can also travel between different paths through the column packing columns. This coupling results in a reduced band broadening respect to *eddy diffusion* term (A) by itself.[60]

Other factors such as the column conditions, kinetic factors and experimental parameters such as temperature, solvent viscosity and sample concentration among others contribute as well to the peak broadening in *gel permeation chromatography*.[60]

2.1.3. Supercritical Fluid Chromatography (SFC)

Supercritical fluid chromatography, as it has been introduced above, is a hybrid of liquid chromatography (LC) and gas chromatography (GC), since the mobile phase, in this case, is a fluid in supercritical conditions.

Carbon dioxide (CO_2) is one of the most common substances used as a mobile phase in SFC since it consists of an abundant and inexpensive gas as well as non-toxic.

When both the temperature and pressure of a substance such as CO_2 are above its critical point (Figure 19), this substance becomes a supercritical fluid. [57]

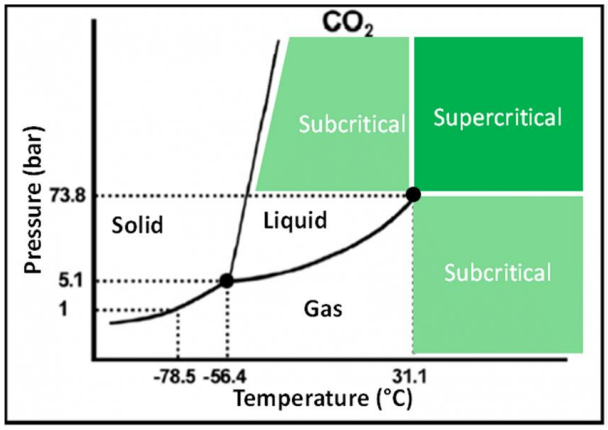

Figure 19. CO_2 P-T diagram[62].

This new physical state provides with new properties to the CO_2. One of the main important ones is the behaviour as a gas, but with a density more likely to a liquid. This property is related to its ability to dissolve large non-volatile molecules such as PAHs and large alkanes among others. Besides, in order to recover these solutes, the only step required is the evaporation of the CO_2 under laboratory conditions.[57]

The state-of-the-art instrumentation used in SFC is quite similar to the instruments used for HPLC, being some of the most important differences the restrictors used to keep the pressure conditions within the chromatographic system and the oven where the columns are subjected to temperature control. These two elements are essential to keep the supercritical conditions.

Whereas CO_2 is the main component of the mobile phase since it is an excellent solvent for a broad variety of nonpolar organic molecules, organic modifiers can be added to the mobile phase flow to improve the solubility of some molecules and avoid the precipitation of the analytes within the system. Modifiers such as methanol or ethanol among others are commonly used and their composition within the mobile phase can sometimes reach 100% of the flow, always depending on the stationary phases that are being used and the target analytes.[63]

Figure 20 explains schematically the main components of a SFC instrument: Two pumps compress the mobile phase fluids up to critical conditions and it is then that they are mixed and sent towards the column through the injector, where the sample joins the

chromatographic system and passes through the column/s that have been heated previously within the column manager. Once the mobile phase exits the columns, it is sent to a detector, which may be a photodiode array, incorporated in numerous commercial instruments. Another detection method that is commonly used for SFC is the Mass Spectrometry. In order to avoid the precipitation of the analytes through the tubing towards the mass spectrometer, a make-up solvent can be pumped within the mobile phase before injection.

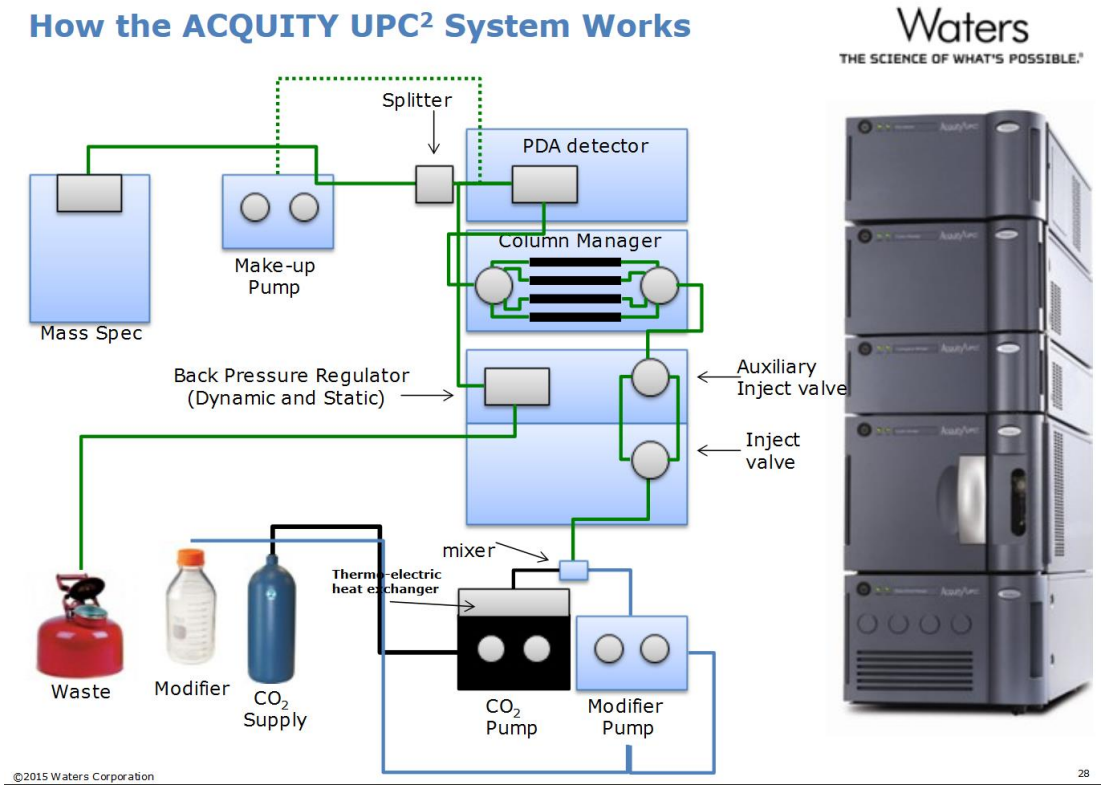

Figure 20. Block diagram of a SFC ACQUITY UPC² System.[64]

In SFC there exists a huge variety of stationary phases, ranging from very polar (silica gel) to C18, being originally all of them designed for HPLC columns. The length and particle size of these columns may vary depending on the purposes of each analysis.

Regarding the performance characteristics of this type of chromatography, the advantages of using SFC have been studied by D. Gere who compared the Van Deemter plots of two separations carried out with a 5- µm octadecyl (C_{18}) with both, SFC and LC elution.[65]

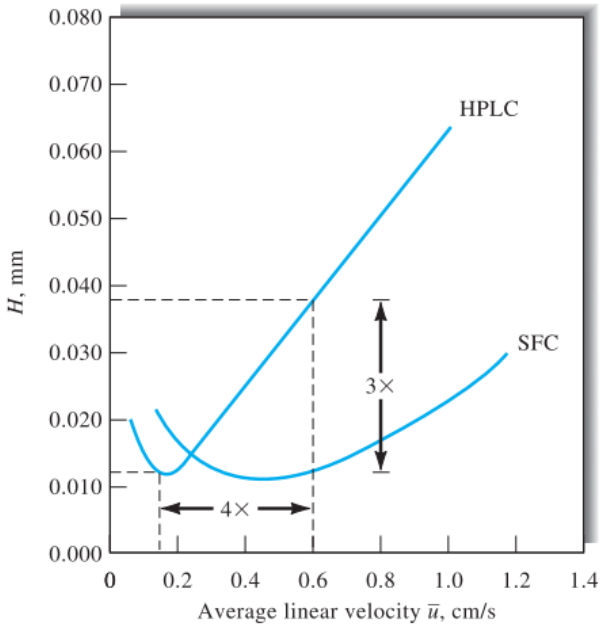

Figure 21. Van Deemter plots for SFC and HPLC separations in a C_{18} column.[57]

The plot of both curves can be observed in Figure 21 showing a significantly better performance for the analyses carried out with supercritical fluids: with SFC, at a mobile phase velocity of 0.6 cm/s (four times the HPLC's linear velocity) the column yields a plate height equivalent to three times less large than for HPLC. This fact can be reflected in a reduction of analyses while keeping the separation efficiency for SFC in respect to HPLC.

2.2. Detection

In the previous sections, an explanation about the methods used to perform the molecular separations which lead to the speciation analysis has been done. In this section, the description of different methods used for the obtention of the data will be carried out as well as their combination with the methods already introduced.

2.2.1. Inductively Coupled Plasma Mass Spectrometry (ICP-MS)

Inductively Coupled Plasma Mass Spectrometry (ICP-MS) is a method based on the detection of the isotopes present in a sample based on their mass/charge (m/z) and their

corresponding measured intensities. Before reaching the detector, the sample has been atomised and ionised within an argon plasma that achieves temperatures as high as 10,000 K.

Figure 22 presents the main components of an ICP-MS instrument and their role will be described below:

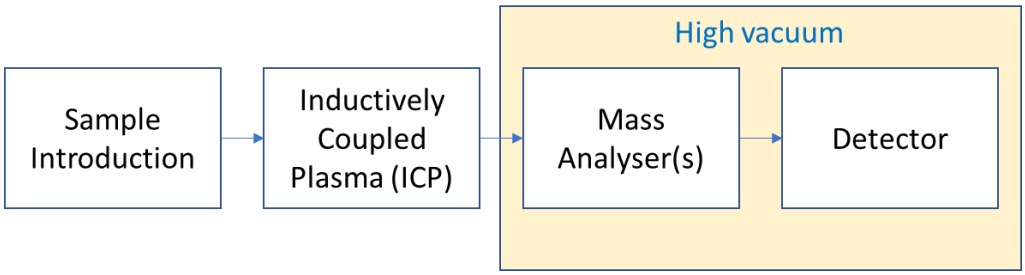

Figure 22. Main components of an ICP-MS instrument.

2.2.1.1. Sample introduction – Total consumption micronebulisers

The sample introduction is one of the most critical processes during ICP-MS analyses. When the sample is a liquid, a nebuliser has to be used for these purposes. This nebuliser creates an aerosol where the sample is finely divided into small drops that are carried by a gas flow towards the plasma, where the sample is atomized and ionised.

The most common means of sample introduction in ICP techniques are the concentric glass nebulisers, whose fundamental parts are presented in Figure 23. At the tip of these nebulisers, a high-speed gas causes the aspiration of the liquid flow within the capillary that this gas surrounds by the Bernoulli effect. The aerosol is generated as the gas breaks up the liquid flow towards the plasma into fine droplets of different sizes.[66] Generally, a spray chamber is used to filter the sample aerosol and to allow only those droplets with an appropriate size to reach the plasma.

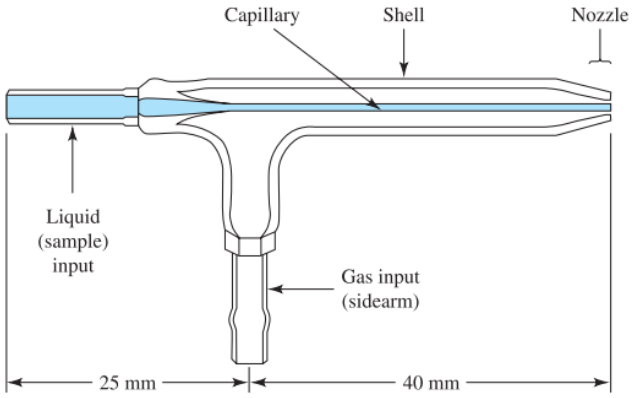

Figure 23. Schematic diagram of a concentric glass nebuliser.[66]

Since all the samples within this work are liquids that must be dissolved in organic solvents, they have been dissolved in THF. The introduction of organic solvents into ICP-MS is a challenging task since an excess of organic solvent can cause the extinction of the plasma, the formation of carbon deposits on the cone surfaces and an increase of the isotopic interferences during the ICP-MS analyses. Thus, the limitation of the amount of solvent that arrives to the plasma was achieved by using a total consumption microflow nebuliser that allows very low-flow ICP-MS sample injections.

Schaumloffel et al.[67] developed a sheathless interface equipped with a total consumption nebuliser that operated at flow rates in the range 0.5 – 7.5 µL min^{-1} to hyphenate HPLC and ICP-MS. This nebuliser was designed from a previous micro-nebuliser that was designed for coupling capillary electrophoresis to ICP-MS.[68] The use of a spray chamber was no longer required and very low peak broadenings and low detection limits where achieved. With this total consumption nebuliser model, they managed to develop a method for the analysis of small amounts of uranium and plutonium in contaminated samples and another method for the analysis of selenium in protein tryptic digests. [69,70] of micro- and nano-LC with ICP-MS.[71]

Giusti et al.[72] succeeded in increasing the total consumption nebuliser capillary causing the elimination of clogging, pressure instability and memory effects that the previous version possessed. With this new version, an insight of the trace element composition in crude oil samples was accomplish in numerous works. [73–76] In the Chapter 3 of this PhD

thesis, the hyphenation of HPLC and ICP-MS with this total consumption nebuliser is discussed.

Total consumption nebulisers are currently used for numerous HPLC-ICP-MS applications such as the detection of As species in urine and Hg and Pb species in fish liver, among others.[77] In addition, new designs are still being carried out with respect to this type of nebulisers to improve the quality of the analysis of numerous samples via ICP-MS such as the development of a low-cost demountable nanoflow nebuliser to couple nano-HPLC with ICP-MS.[78]

In this work, the development and optimisation of a 3D-printed total consumption nebuliser, based on the one that was developed by Giusti et al.[72], are described for the introduction of bio-oil samples dissolved in THF to reduce the interferences provided by the silica capillary commonly used in crude oil speciation analyses.

Another method of sample introduction for ICP-MS might be Electrothermal Vaporisation, which will be deeply described in Chapter 5.

2.2.1.2. Inductively Coupled Plasma (ICP)

A very intense and white plasma formed by ions and electrons is generated within a torch consisting of three concentric quartz tubes through which an argon gas flow streams to shape the plasma and cool down the quartz. When the sample as an aerosol reaches the plasma, its molecules are desolvated, atomised and ionised.

Although some elements can be ionized to higher charged states, the majority of the elements of the sample are ionized to singly charged positive ions with an ionization efficiency close to 100%.[79]

Once the ionisation has been produced in the plasma, the ions pass through an interface based on two platinum cones (sample cone and skimmer cone) that separates the mass analyser, which is working in a very high vacuum, from the plasma, which works at atmospheric conditions. Within this interface, the positive ions are separated from electrons and molecular species by a negative voltage. Then, they are accelerated and focused by magnetic ion lenses onto the entrance of the mass analyser.[66]

2.2.1.3. Mass analysers in ICP-MS

The function of a mass analyser is to separate the ions produced in the plasma according to their mass-to-charge ratio (m/z). There are several types of mass analysers providing different properties, such as different mass ranges, analysis speed, transmission, mass accuracy and resolution.

Among the wide variety of mass analysers used in mass spectrometry, in this work two of them will be described: quadrupole and magnetic sector.

2.2.1.3.1. Quadrupole

The quadrupole is a compact, less expensive and rugged instrument that allows the transmission of ions with certain m/z values, acting as a mass filter.

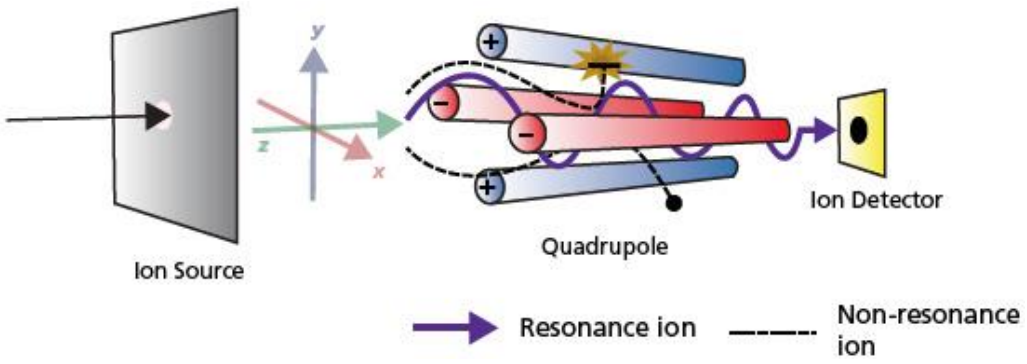

Figure 24. Quadrupole mass filter.[80]

As it is shown in Figure 24 a quadrupole is formed by four parallel cylindrical rods acting as electrodes, being each opposite pair of rods connected electrically in such a way that one pair is connected to the positive pole of a variable dc source and the other pair to the negative one. At the same time, 180° out of phase ac voltages are applied to each pair of rods. This combination of ac and dc voltages will allow only those ions having a certain m/z value to pass through the quadrupole, whereas the rest of the ions will strike the rods and will be converted to neutral molecules.

A quadrupole can operate in two modes: *Scan mode*, in which the voltages increase simultaneously with time, and m/z ratios varying from 0 up to 4000 can be obtained within a few milliseconds; and *Selected Ion Monitoring (SIM)*, in which only the ions with the m/z values within the specified range pass through the quadrupole.

One of the quadrupole properties is its high efficiency to focus the trajectory of ions. However, the mass range is quite narrow, and ions with an m/z value higher than 4000 are poorly focused. Thus, based on the quadrupole principle, *ion guides* such as hexapoles and octapoles have been designed by adding one and two extra pair of rods respectively to a quadrupole, increasing, therefore, the mass range for simultaneous transmission of ions.

2.2.1.3.2. Double Focusing Magnetic Sector mass analysers

Whereas the quadrupole uses a combination of both alternating and direct potentials to separate the different ions originated in the ICP, the magnetic sector mass analyser applies a magnetic field that deflects the trajectories of the ions as they pass through.

At a given magnetic field intensity (B), two ions with the same mass (m), charge (q) and velocity will be deflected following a circular trajectory with a characteristic radius (r) defined by the following equation,

$$r = \frac{\sqrt{2mE_k}}{qB} \qquad \text{Equation 5}$$

being E_k their kinetic energy, which consists of the only factor affecting the dispersion of both ions. In order to avoid the dispersion of two ions with the same m/z value, an electrostatic field is applied employing an electric sector analyser, which focuses ions of the same mass onto the same point in space, which in this case it consists of a slit towards the detector.

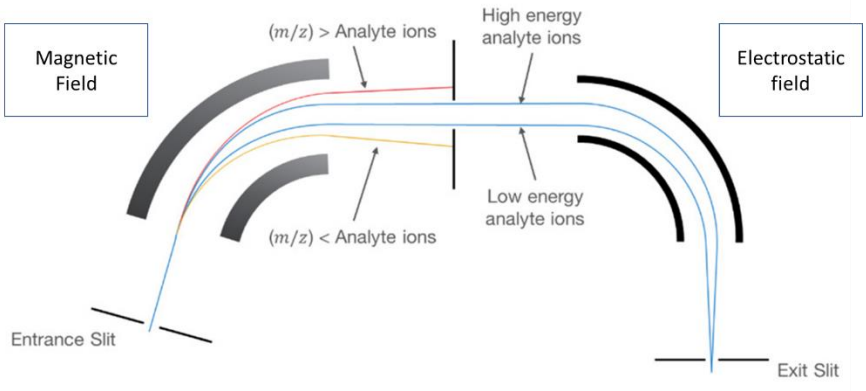

Figure 25. Double Focusing Magnetic Sector mass analyser diagram.[81]

This *double-focusing* configuration, by coupling both magnetic and electrostatic fields and whose basis are schematically depicted in Figure 25, provides with a high mass resolution potential allowing to solve a wide variety of polyatomic interferences.

2.2.1.4. Detector

Once the ions have been selected as a function of their m/z values by either the quadrupole or the double magnetic sector analysers, they reach the detector where they are transformed into a signal.

There exist several types of detectors, but in this section, only two types will be described:

- *Faraday cup*: As it is shown in Figure 26, it consists of a cylinder with a small orifice and connected to the ground via a resistor. When the ions reach the inner part of the cylinder, they are neutralised by either donating or accepting electrons from the cylinder walls, becoming neutralised. This transfer of electrons generates a signal, that can be detected.

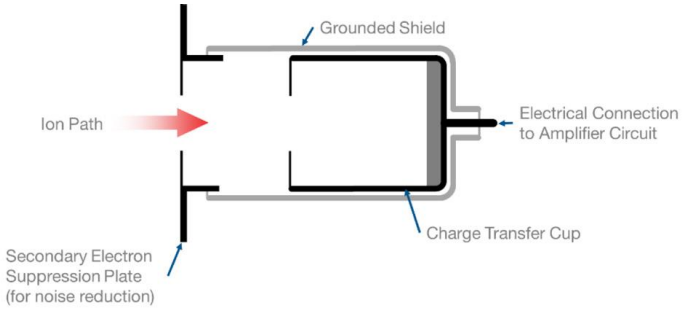

Figure 26. Faraday Cup Diagram.[81]

However, despite their high precision and robustness, this type of detectors has very low sensitivity and slow response time.

- *Electron multipliers*: This device is composed of a series of dynodes that collect and convert positive ions into an electrical signal. Figure 27 shows a schematic diagram of an electron multiplier. When the ion beam strikes the first dynode, it generates a burst of electrons that are attracted to the next dynode, hitting it, being attracted to the following dynode and so forth, due to the decreasing negative potentials where these dynodes are held in. The cascade of electrons created along these dynodes will provide an electric current high enough that provides with a current gain of up to 10^7.

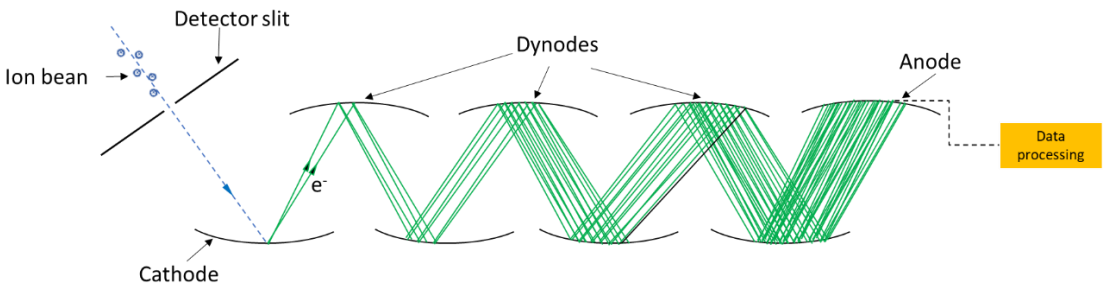

Figure 27. Schematic diagram of an Electron Multiplier detector.

Compared to the Faraday Cup, this detector provides with faster response and higher sensitivity, and they are ideal to be placed behind the exit slit of a magnetic

sector mass spectrometer since the ions reaching the detector possess enough kinetic energy to eject electrons from the first dynode of the device.[66]

Some instruments, such as the Thermo Element XR used in this work, use the Electron Multiplier detector, which normally provides a linear response in a range over 10^9, and then, by combining it with a Faraday Cup, the linear response is increased up to 10^{12}.

2.2.2. Inductively coupled plasma – optical emission spectroscopy (ICP-OES).

Inductively coupled plasma – optical emission spectrometry is an analytical technique used for the detection of chemical elements based on their corresponding emission wavelengths generated within a plasma. [66]

The majority of the main components of an ICP-OES are similar to the components of an ICP-MS (Figure 28): The sample introduction and the excitation of the elements present in a sample consist of the same principle: *Sample introduction* (Section 0) and *Inductively Coupled Plasma* (Section 0).

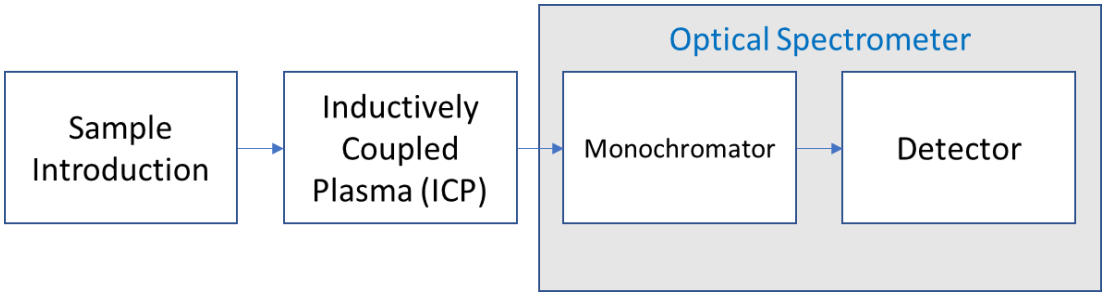

Figure 28. Main components of an ICP-OES.

However, since this method is based on the detection of emission wavelengths and not ions, the mass analyser is replaced by an optical device that transmits a desired wavelength from the plasma, were several wavelengths are emitted from its core.

In ICP-OES, the wavelength originated in the plasma can be measured radially, perpendicular to its axis or axially (being this arrangement used in ICP-MS). In Figure 29, the main components of an ICP-OES with axial configuration are described.

The radiation generated in the plasma is focused through lenses towards a slit located before the monochromator, or, in some advanced instruments, polychromator, whose functions consist of separating the radiation into its different wavelengths in order to be able to detect and quantify the ones corresponding to the elements that are measured.

Separating these wavelengths can be carried out simultaneously with a polychromator whose main component is known as a *Rowland circle* whose grating surface (where the radiation wavelengths disperse) is located along a circumference in such a way that shapes a concave diffraction grating. [66]

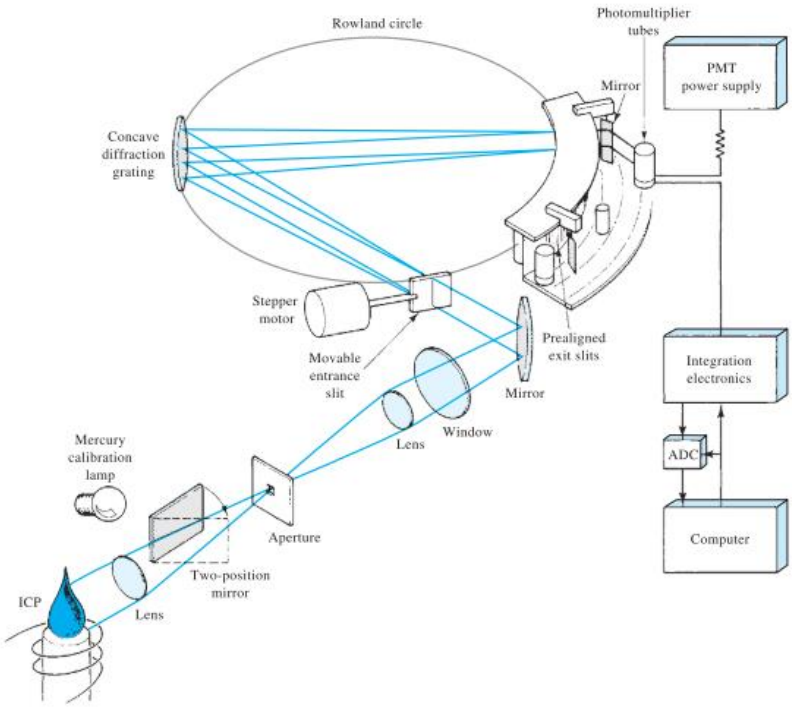

Figure 29. ICP OES and Rowland circle components.[66]

When the radiation hits this diffraction grating, numerous wavelengths will be directed to the detector, located on the opposite side of the circumference, where this radiation will be transformed into an electric signal.

The most common detector in optical emission spectrometry is the *photomultiplier tube* (PMT) whose fundament resembles the *electron multipliers* used in mass spectrometry, and whose components are showed in Figure 30.

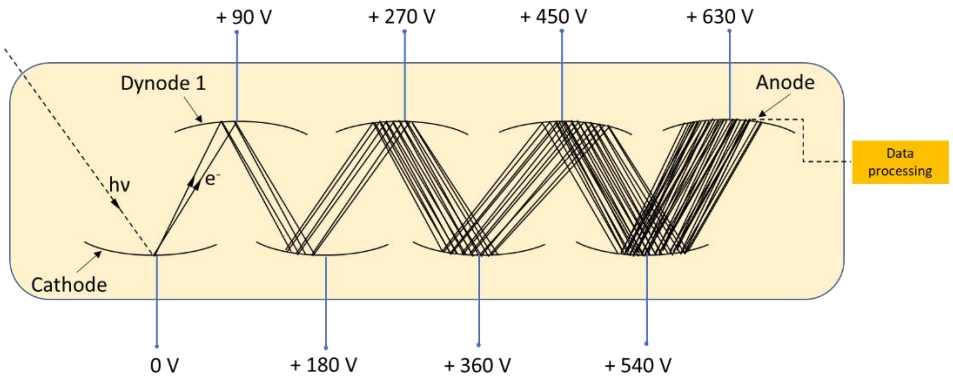

Figure 30. Photomultiplier tube components diagram.

This plasma source spectroscopy provides with the lowest detection limits among all the emission spectroscopy techniques. Besides, the lack of mass interferences such as the ones occurring in ICP-MS that do not allow the detection of other ions with the same mass, make this detection method ideal for the speciation analysis of several elements.

CHAPTER 3: NOVEL ANALYTICAL TOOLS FOR THE SPECIATION ANALYSIS OF BIO-OILS: A 3D-PRINTED TOTAL CONSUMPTION NEBULISER

In this chapter, a novel alternative of a total consumption nebuliser, built through the use of the 3D-printing technology, is presented and validated in order to fulfil one of the main sub-objectives of this thesis (**O1a**). This alternative nebuliser, which does not have a built-in fused silica capillary that might cause interferences and permanent retention for the analysis of certain species (Si, K, etc.), can be produced in a very short time. The optimisation and validation steps of this new total consumption nebuliser are detailed in the **Article 1**, which has been attached to this chapter.

3.1. Methodology

The coupling of two of the techniques explained in Chapter 2, GPC and ICP-MS, which also allows carrying out a simultaneous analysis between GPC-ICP-MS and GPC-UV/Vis, is described in Figure 31 and consisted of one of the most used instrumental setups throughout this thesis project.

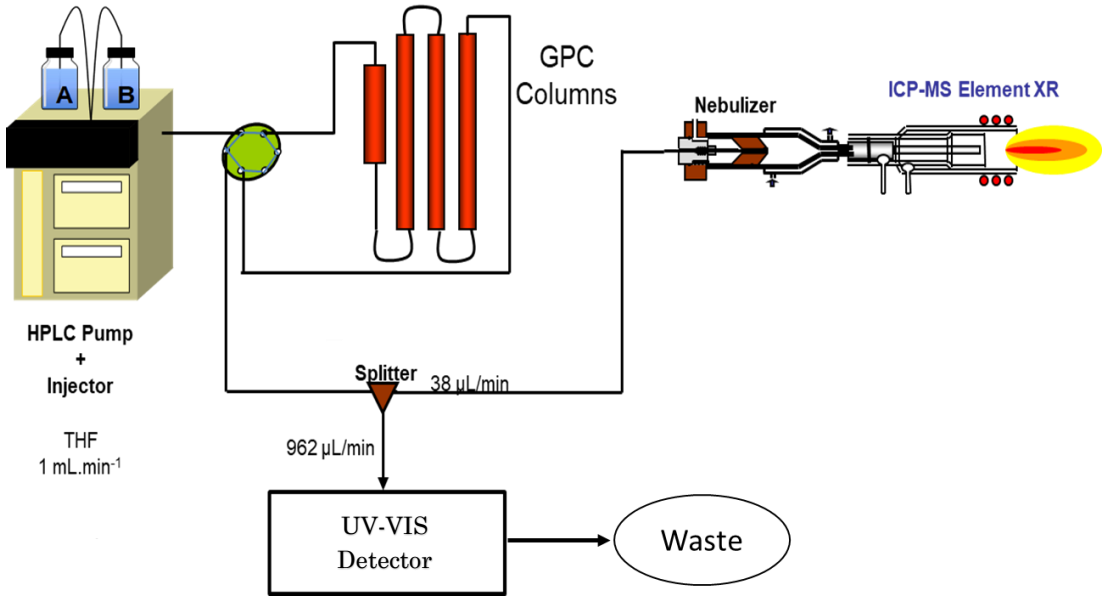

Figure 31. GPC-ICP-MS / UV-Vis diagram of the set up used during this work. [82]

A constant flow of 1 mL min^{-1} of THF stabilised with BHT is delivered from the HPLC pump and it is used as mobile phase for the chromatographic separation, which is carried out using three Waters styrene-divinylbenzene GPC columns: an HR4 column (particle size of 5 µm with an exclusion limit of 600,000 Da of polystyrene equivalent), an HR2 column (particle size of 5 µm with an exclusion limit of 20,000 Da) and an HR0.5 column (particle size of 5 µm and an exclusion limit of 1,000 Da of polystyrene equivalent). Besides, to prevent any damages to these columns, a Styragel guard column (4.6 mm i.d. and 30 mm length) was also fitted between the columns and the pumping system.

Once the separation has been completed, a splitter is used to deliver a low amount of mobile phase towards the ICP, since an excess of THF might extinguish the plasma. With a split rate of approximately 20:1, most of the mobile phase is splitted towards a Dionex UV-Vis detector which can record up to six different wavelengths.

The splitted low flow is delivered towards the plasma within a fused-silica capillary belonging to a modified DS-5 microflow total consumption nebulizer (CETAC, Omaha, NE), described in Figure 32 and mounted with a laboratory-made single pass jacketed glass spray chamber heated up to 60 °C by a water/glycol mixture using an RTE–111 thermostat (Neslab, Thermo Fisher Scientific) to provide energy to the organic matrix with heat in order to increase the sensitivity of the plasma ionization process.[72,76]

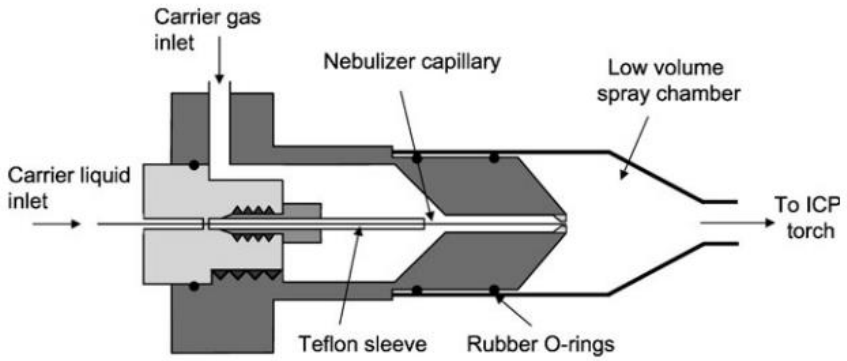

Figure 32. Diagram of the modified DS-5 total consumption nebulizer.[72]

This modified DS-5 nebulizer was coupled to a Scientific Element XR double-focusing sector field ICP-MS, equipped with a quartz injector (1.0 mm inner diameter (i.d.)), a Pt sampler cone (1.1 mm orifice diameter) and a Pt skimmer cone (0.8 mm orifice diameter).

An O_2 gas flow of 0.08 mL/min was delivered into the plasma to avoid carbon deposition on the cones' surfaces due to the introduction of organic matrices in the plasma. Both the instrument and mass calibration settings were optimized daily at resolutions of 300 (low resolution) and 4000. These optimizations were carried out using a tuning solution containing 1.0 ng g-1 of Ag, Al, B, Ba, Ca, Cd, Co, Cr, Cu, Fe, In, K, Li, Mg, Mn, Mo, Na, Ni, P, Pb, Sc, Si, Sn, Ti, V, Zn and Y in THF. A mass offset was also applied to compensate for the mass drift coming from the sector field magnet.

Numerous works have been carried out using this modified DS-5 nebulizer for the inorganic speciation in petroleum derivates.[75,76,83–85] However, to carry out speciation analysis in bio-oils, the size distribution of different elements, such as Si, K and Na amongst others, will be studied. The presence of Si within the fused-silica capillary carrying the mobile phase towards the nebulizer might interfere with the future target analytes. Hence, in this chapter, this hypothesis is tested and a new interface is introduced after having been optimised and validated for its use on the speciation analysis of complex samples via GPC-ICP-MS.

3.2. 3D-printed total consumption microflow nebuliser development for trace element analysis in organic matrices *via* inductively coupled plasma mass spectrometry

JAAS

ROYAL SOCIETY OF CHEMISTRY

TECHNICAL NOTE

View Article Online
View Journal

Check for updates

Cite this: DOI: 10.1039/d0ja00182a

3D-printed total consumption microflow nebuliser development for trace element analysis in organic matrices *via* inductively coupled plasma mass spectrometry

Victor Garcia-Montoto,[ab] Sylvain Mallet,[c] Carine Arnaudguilhem,[a] Jan H. Christensen[b] and Brice Bouyssiere *[a]

A new total consumption micronebuliser for ICP-MS was developed and optimised in this work. This nebuliser, V64-01, which was built through 3D printing, contains a larger internal diameter than other total consumption micronebulisers, a silicon-free capillary that perfectly tolerates a flow up to 65 μL min^{-1} THF, and the chances of incurring obstructions or clogging during a prolonged period of analysis are reduced. In addition, its production costs are minimal. To validate this nebuliser, its most important parameters were optimised (carrier gas and liquid flow rates), and the quantitative analysis of an SRM sample was carried out successfully. Calibration curves with great linearities (r^2 > 0.999) and detection limits between 0.84 and 2.85 ng g^{-1} were obtained for the analysis of 10 elements. In addition, GPC-ICP-MS chromatograms of the size distribution of V and Ni species in a reference crude oil sample were obtained, showing the same profile as with the previous nebulisers but also suggesting that, for some species of V and Ni in crude oil, permanent retention might have occurred within the fused silica capillary that connects the DS-5 total consumption micronebuliser with the HPLC system. This new 3D-printed total consumption nebuliser possesses the potential to become a good consumable that will allow for total and speciation analysis of numerous trace elements, such as Si, that, until now, due to either interactions with silica or interferences, were not possible to analyse.

Received 20th April 2020
Accepted 17th June 2020

DOI: 10.1039/d0ja00182a

rsc.li/jaas

Published on 17 June 2020. Downloaded by 674607 on 6/23/2020 12:34:00 PM.

Introduction

Analysis of trace element organic matrices such as crude oil, biomass or petrochemicals, is a subject that has increased in popularity within the last decade, and this interest will grow in the future. As an example, it is expected that the use of biomass as a feedstock to produce new sources of energy will rise, especially with the production of renewable transportation fuels, which will increase up to 20% by the year 2040.[1,2] These biomass feedstocks contain several elements, such as phosphorus, potassium, sodium, magnesium, iron, *etc.*, that might cause damage to engines, corrosion, and catalyst deactivation during their conversion to transportation fuels, among other issues.[3–5] Thus, total and speciation analysis of these elements in such complex organic matrices is a new challenge from an analytical point of view.

In total and speciation analysis, ICP-MS is the technique of choice, but for organic matrices, the introduction system of the ICP-MS system should be optimised in order to avoid segregation between the volatility of the analysed compounds and to maintain the stability of the plasma when organic samples are introduced (plasma flow rate, carbon deposition on the sampling cone, *etc.*).[6] The modified DS-5 nebuliser provided remarkable stability and high tolerance to strong organic solvents, such as tetrahydrofuran (THF) and xylene.[7] The modified DS-5 nebuliser has been developed and used in several studies where samples with complex matrices, such as crude oil atmospheric residues or asphaltene fractions, were analysed.[8–12] In the work by Caumette *et al.*,[10] the sample introduction was carried out with a DS-5 'total consumption micronebuliser' modified to have a relatively large internal diameter of the capillary (75 μm i.d.) and heated to reach better detection limits than those of conventional nebulisers.

Some techniques, such as the coupling of gel permeation chromatography (GPC) with inductively coupled plasma mass spectrometry (ICP-MS) that was investigated by Caumette *et al.*,[13,14] provided a fingerprint of the molecular weight distribution of the V, Ni and S species within crude oil and petroleum residue matrices.

[a]*Universite de Pau et des Pays de l'Adour, E2S UPPA, CNRS, Institut des Sciences Analytiques et de Physico-Chimie Pour l'Environnement et les Materiaux (IPREM), UMR5254, Helioparc, 64053 Pau, France. E-mail: brice.bouyssiere@univ-pau.fr*
[b]*Department of Plant and Environmental Sciences, University of Copenhagen, Thorvaldsensvej, 40, Frederiksberg C, Denmark*
[c]*Symalab, Technopôle Helioparc, 2, Avenue du President Pierre Angot, 64000, Pau, France*

Published on 17 June 2020. Downloaded by 674607 on 6/23/2020 12:34:00 PM.

However, despite its numerous applications and long-term stability, it is suspected that physical interactions might take place within the built-in-fused silica capillary that carries the mobile phase towards the plasma. It is for this reason that other interactions might occur when sample matrices contain Na, K and P, among others, and especially, Si compounds. Additionally, fused silica capillaries can be responsible for a high Si back-ground during analysis.

Thus, the objective of this work was to develop a nebuliser that allows the hyphenation between GPC and ICP-MS that complies with all of the advantages (long-term stability, total consumption and tolerance against THF) that the DS-5 version possesses and improve it by (1) modifying the internal diameter, which is larger in this new version, and (2) replacing the fused-silica capillary with PEEK tubing, which may reduce surface interactions with the analytes. We also expected the long-term stability of the nebuliser to increase, since, within this tubing, there will be lower chances of blockages or carryover, and production costs will decrease, as its manufacturing consists of 3D printing.

Hence, in order to validate this new 'total consumption micronebuliser' before studying its performance while hyphenating GPC and ICP-MS, two main experiments were designed: (1) the optimisation of the three main parameters that affect the efficiency of the nebulisation process in ICP-MS analyses was carried out: the carrier gas flow rate, the temperature of the spray chamber and the mobile phase flow, and (2) the quantitative analysis of the SRM 1085b. These experiments, that have been carried out in a "direct analysis mode", have not only validated this new ICP-MS consumable and allowed for the study of its behaviour, but they have also shown its potential as a cheap alternative to introducing organic matrices in ICP-MS for quantification analysis.

Experimental section

3D-printed total consumption micronebuliser

The design of this 3D-printed nebuliser, named V64-01, was based on the modified total consumption nebuliser developed by Giusti *et al.*,[7] improved some of the features of the original DS-5 nebuliser (CETAC, Omaha, NE), such as an increase in the internal diameter of the inner capillary. The internal diameters for the DS-5 and the modified DS-5 nebulisers were 50 and 70 μm, respectively, and the internal diameter of the capillary in V64-01 was 150 μm. In addition, this capillary was no longer made of fused silica, which might cause adsorption of analytes in the mobile phase and was instead made of PEEK tubing.

The V64-01 nebuliser was manufactured by SymaLab (Pau, France) through a 3D-printing technology known as stereolithography. The printing time was 14 hours with an accuracy of 50 μm. Three resins were tested as material for the construction of the nebuliser, EPOXY-PP, EPOXY-NM and EPOXY-HT, where, after the test, EPOXY-HT was the only resin that tolerated THF. EPOXY-HT was, furthermore, stable up to 250 °C.

The PEEK capillary (360 μm × 150 μm) was purchased from Cluzeau Labo (Sainte-Foy-La-Grande, France). It was fixed by stereolithography to the nebuliser, as shown in Fig. 1, so that the carrier gas flow can collide with the liquid flow coming from the PEEK tubing at its highest speed due to the constricted section of the gas inlet next to the orifice. This collision pulverizes the liquid flow and transports the droplets through the heated spray chamber towards the plasma.

Five different versions of this nebuliser were tested, obtaining different optimal carrier gas flows. This difference might be caused by accuracy issues. However, no other significant changes were observed.

Instrumentation

All analyses were carried out with a Thermo Scientific Element XR double-focusing sector field ICP-MS instrument (Thermo Fisher, Germany) equipped with a quartz injector (1.0 mm inner diameter), a Pt sampler cone (1.1 mm orifice diameter) and a Pt skimmer cone (0.8 mm orifice diameter). A gas flow of 0.08 L min^{-1} O_2 was added to the argon gas flow to avoid carbon deposition on the cones. This flow, which is 13 times lower than the carrier gas flow, has not been optimised, since its only function consists of avoiding the formation of carbon on the interface cones. Hence, this low flow rate has been selected in order to (1) avoid the deposition of carbon on the cones and (2) not increase the formation of those oxide ions within the plasma that might cause undesirable interferences that would difficult the analysis of certain species.

The instrument worked at a resolution of 300 for the analysis of ^{23}Na, ^{27}Al, ^{51}V, ^{60}Ni, ^{63}Cu, ^{66}Zn, ^{107}Ag and ^{118}Sn and at a resolution of 4000 to access spectrally interfered isotopes of ^{31}P and ^{56}Fe, applying, in this case, a mass offset to compensate for the mass drift coming from the sector field magnet.[14] The instrument was optimised daily by using a tuning solution containing 10 ng g^{-1} Ag, Al, B, Ba, Ca, Cd, Co, Cr, Cu, Fe, In, K, Li, Mg, Mn, Mo, Na, Ni, P, Pb, Sc, Si, Sn, Ti, V, Zn and Y in THF. The same solution has been used for the evaluation of all the parameters are studied in this work. Table 1 shows the ICP-HRMS working conditions.

The mass spectrometer was fitted with the V64-01 nebuliser mounted with a laboratory-made jacketed spray chamber heated up to 65 °C by a water/glycol mixture and controlled with

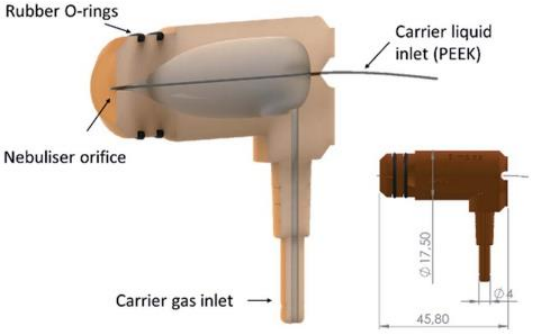

Fig. 1 Design of the V64-01 nebulizer. In the bottom-right part of the figure, the nebulizer dimensions are showed.

This journal is © The Royal Society of Chemistry 2020

Published on 17 June 2020. Downloaded by 674607 on 6/23/2020 12:34:00 PM.

Table 1 ICP-HRMS experimental conditions

ICP-HRMS experimental conditions	
RF power [W]	1500
Plasma gas flow rate [L min^{-1}]	16
Auxiliary gas flow rate [L min^{-1}]	0.90
Carrier gas flow rate [L min^{-1}]	1.080
O_2 gas flow rate [L min^{-1}]	0.080
Mobile phase flow rate (postsplit) [μL min^{-1}]	39
Extraction lens [V]	−2000.0
Focus lens [V]	−1400.0
X-deflection lens [V]	−0.20
Y-deflection lens [V]	0.40
Shape lens [V]	135.0

a Neslab RTE-111 temperature-controlled bath circulator (Thermo Fisher Scientific, Waltham, MA).

The carrier solution for the flow injection analyses (FIA) was delivered using an UltiMate 3000 microflow pump, an UltiMate 3000 autosampler and a low port-to-port dead volume micro-injection valve that were part of an HPLC UltiMate 3000 system (Dionex, Amsterdam, The Netherlands).

Chromatographic separation was performed using three Waters (Waters Corporation, Milford, MA) styrene-divinylbenzene gel permeation columns connected in series (7.8 mm i.d. × 300 mm length): HR4 (particle size, 5 μm; exclusion limit, 600 000 Da of polystyrene equivalent), HR2 (particle size, 5 μm; exclusion limit, 20 000 Da) and HR0.5 (particle size, 5 μm; exclusion limit, 1000 Da). A Styragel guard column (4.6 mm i.d. × 30 mm length) was fitted between the columns and the pumping system.

Samples and reagents

THF, Multisolvent GPC-grade, ACS-grade, and stabilised with 250 ppm of butylated hydroxytoluene (BHT) to prevent the formation of peroxides, and a mixture of xylene isomers, of Multisolvent ACS grade, were both purchased from Scharlab (Spain). The THF was used as mobile phase solvent for both chromatographic and flow injection analyses, whereas the xylene was used for the preparation of all solutions and dilutions of samples.

A Conostan (SCP Science, USA) multielement oil-based standard solution (S-21) containing 100 μg g^{-1} Ag, Al, B, Ba, Ca, Cd, Cr, Cu, Fe, Mg, Mn, Mo, Na Ni, P, Pb, Si, Sn, Ti, V and Zn was used to prepare standard addition samples for validation of the method.

The standard reference material, SRM 1085b, purchased from NIST (National Institute for Standards and Technology, Gaithersburg, MD, USA), and a laboratory internal oil reference (Middle East vacuum residue) were used for method validation. V=O tetraphenyl porphyrins (TPPs) were obtained from Sigma Aldrich (Germany).

Procedure

The quantitative analysis of SRM 1085b was carried out with the standard addition procedure. An aliquot of 0.15 g of the SRM was first diluted in 15 g of xylene. Then, 1.5 g of the resulting solution was diluted again in 15 g of xylene prior to analysis. The Conostan multielement solution (S-21) was diluted in xylene and added to aliquots of the twice-diluted sample so that solutions containing 0, 10, 20, 40, 80, and 160 ng g^{-1} were ready to be analysed. Injections of 5 μL in a mobile phase flow of 60 μL min^{-1} were performed in triplicate, and a FIA chromatogram was obtained.

The internal crude oil standard was diluted 50 times in THF. Twenty microliters were injected to obtain the size distribution chromatogram at a flow rate of 1 mL min^{-1}.

The chromatograms obtained for the Ni species were smoothed by using the Savitzky–Golay algorithm[15] in MATLAB 2018b, whereas the rest of the data treatment was performed in Microsoft Excel.

Results and discussion

Nebuliser parameter optimisation

As mentioned above, the three main parameters that affect the efficiency of the nebulisation are the carrier gas flow rate, the temperature of the spray chamber and the mobile phase flow. The effects of these parameters on the sensitivity for the three elements Li, In and U were investigated. Fig. 2 shows the effect of the carrier gas flow rate on the performance of the nebulisation process. Carrier gas flow rates between 0.8 and 1.3 L min^{-1} were tested. The optimal flow rate provided consistently high sensitivity (intensity) for all tested elements. Sensitivity was highest for Li and In at the highest gas flow rates of 1.2–1.3 L min^{-1}, but at these flow rates, the intensities for U dropped considerably, possibly due to its higher ionization potential and shorter time within the ionization source. In terms of sensitivity, Li normally provides intensities that are 10 times lower than those corresponding to U and In, since at lower gas flow rates Li atoms spend a longer time within the plasma, leading to the formation of double charged Li ions that are not be detected. Thus, the signal values have been

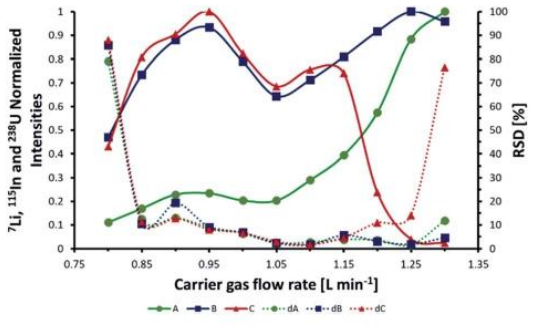

Fig. 2 Effect of the nebuliser carrier gas flow rates on the sensitivity of the ICP-MS. The three solid lines (A: lithium; B: indium; and C: uranium) describe the intensities obtained, whereas the dashed lines represent the relative standard deviation of the intensity measurements.

Published on 17 June 2020. Downloaded by 6/74607 on 6/23/2020 12:34:00 PM.

normalised in order to be compared between them and observe how their values increase with the increasing gas flow rate.

Therefore, the optimal carrier gas flow rate was considered to be 1.080 L min^{-1} since it provided a relatively high intensity for the three tuning ions with a low relative standard deviation.

In contrast to the modified DS-5 nebuliser, where the intensities drop constantly while reducing the carrier gas flow, in the V64-01 nebuliser, a minimum gas flow rate at which the nebulisation no longer occurred was observed, and droplets appeared on the area surrounding the nebuliser's orifice and the tip of the PEEK capillary. This observation might be caused by two factors that were not present in the previous nebuliser versions: (1) the increased internal diameter of the capillary, which carries a higher volume of mobile phase, and (2) the lack of energy from the gas to overcome the intermolecular forces between the mobile phase and the polymer surfaces around the nebuliser's orifice. Therefore, gas flow rates below 0.8 mL min^{-1} were not tested.

Because of all of these reasons, the choice of the optimal flow rate had to compromise the Li and In sensitivity to obtain an optimal sensitivity of the U ions.

Fig. 3 shows the effect of the spray chamber temperature on the signal intensities of Li, In and U, showing how heating the spray before it reached the plasma increased the sensitivity. This observation was in agreement with previous results in the open literature.[10]

The effect of temperatures ranging from 25 to 75 °C was studied. However, it seemed that the choice of the temperature was not one of the most critical parameters, since the highest intensities were obtained within a range of temperatures from 45 to 65 °C. However, a critical point that can be observed at 55 °C might have been caused by an error of either the measurements or the heating system, since the previous results show that a plateau is reached once the temperatures have reached 45 °C. Therefore, the selected temperature for all analyses was 65 °C, which provided the highest intensities with the highest reproducibility (lowest RSD%).

Fig. 4 shows that the sensitivity for Li, In and U were all directly proportional to the liquid flow rate. There was a stable

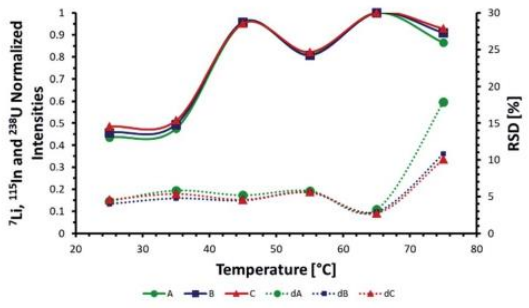

Fig. 3 Effect of the heated spray chamber temperatures on the sensitivity of the ICP-MS. The three solid lines (A: lithium; B: indium; and C: uranium) describe the intensities obtained, whereas the dashed lines represent the relative standard deviation for the intensity measurements.

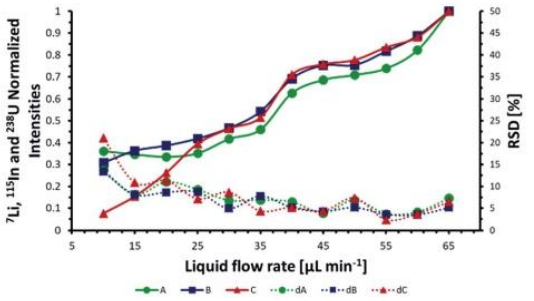

Fig. 4 Effect of the nebuliser liquid flow rates on the sensitivity of the ICP-MS. The three solid lines (A: lithium; B: indium; and C: uranium) describe the intensities obtained, whereas the dashed lines represent the relative standard deviation for the intensity measurements.

zone where the sensitivity was higher than >80% of the maximum sensitivity obtained (between 40 and 65 µL min^{-1}). However, above 65 µL min^{-1}, the reflected power of the plasma increased, which decreased the plasma stability due to the higher amounts of organic solvent in the plasma. Hence, we decided that the optimal flow rate was close to 60 µL min^{-1}.

Quantitative analysis

The analytical setup was validated by the analysis of SRM 1085b. The results from the analysis are summarized in Table 2. Detection limits at the ppb level were found for all elements analysed in this work, and calibration curves with good linearity were obtained. However, despite having acceptable low uncertainties and RSDs, the average error of the measurements increased with respect to the certified values, probably due to the high dilution that was chosen for performing the sample analysis (104 times diluted). This average error, which was not higher than 6%, and the good detection limits at the parts per billion level (0.99–2.85 ppb) could be used as an indicator of the proper function of this V64-01 3D-printed total consumption micronebuliser.

Speciation analysis

The GPC-ICP-MS chromatogram obtained when analysing the speciation of vanadium in both an internal oil reference (IOR) and one vanadium porphyrin are shown in Fig. 5. For both nebulisers, the same profile was observed for the vanadium porphyrin samples. This demonstrated that the V64-01 nebuliser did not affect the resolution of the separation compared to the DS-5 nebuliser. Concerning the IOR sample, the results for vanadium and nickel were similar to those obtained in previous results in the open literature.[16] However, with the V64-01 nebuliser, the signal was higher within the region of the medium-molecular-weight aggregates (24–27 min.) than that observed with the modified DS-5 nebuliser. Furthermore, the lower signal observed for the modified DS-5 nebuliser was not compensated by a higher signal in any other region of the chromatogram.

Thus, these results indicate a possible permanent retention of V species within the fused silica capillary of the DS-5

 This journal is © The Royal Society of Chemistry 2020

View Article Online
Technical Note JAAS

Published on 17 June 2020. Downloaded by 674607 on 6/23/2020 12:34:00 PM.

Table 2 Concentrations (in mg kg^{-1}) determined in the reference material; precision of the measurements, R^2 and detection limits (in ng kg^{-1})[a]

Element	Certified value	Measured concentration	RSD (%)	R^2	DL (ng g^{-1})
Na	305.2 ± 7.0	299 ± 21	3.5	0.999	2.85
Al	300.4 ± 9.3	298 ± 15	2.5	0.999	1.73
V	297.8 ± 6.8	298 ± 18	3.0	0.999	1.40
Ni	295.9 ± 7.4	303 ± 22	3.6	0.999	2.55
Cu	295.6 ± 8.5	302 ± 12	2.0	0.999	0.84
Zn	296.8 ± 6.8	303 ± 21	3.4	0.999	2.37
Ag	304.6 ± 8.9	303 ± 16	2.6	0.999	1.82
Sn	294	300 ± 20	3.3	0.999	2.30
P	299.9 ± 7.2	296.0 ± 9.5	4.5	0.999	1.07
Fe	301.2 ± 5.0	289.1 ± 8.8	4.7	0.999	0.99

[a] Both the certified and the measured values are expressed as the mass of analyte found ± an expanded uncertainty, equal to $U = k^*u_c$, where $k = 2$ (95% confidence) and u_c is the standard deviation of the measurement.

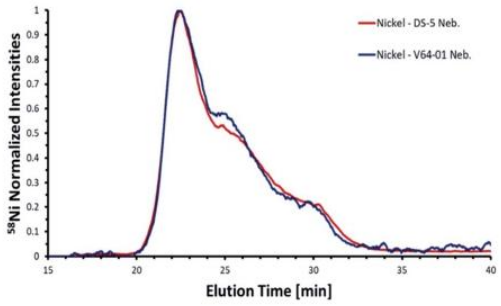

Fig. 5 GPC-ICP-HRMS chromatograms of the nickel species in the IOR sample. The red lines correspond to the old version of the nebuliser (DS-5), whereas the blue lines correspond to the 3D-printed nebuliser.

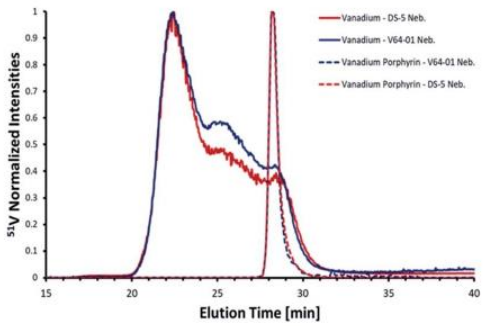

Fig. 6 GPC-ICP-HRMS chromatograms of the vanadium species in the IOR sample (solid lines) and a vanadium porphyrin (dashed lines). The red lines correspond to the old version of the nebuliser (DS-5), whereas the blue lines correspond to the 3D-printed nebuliser.

nebuliser: for the high-molecular-weight area (20–24 min), no significant changes were observed. However, within the region of low- (27–30 min) and medium-molecular-weight species (24–27 min), a decrease in the area of these peaks was observed with respect to the high-molecular-weight area (20–24 min). This fact can be checked considering the integration areas of the respective peak regions. Whereas the region corresponding to the medium and low-molecular weight species represents respectively the 37.3% and 17.4% of the total peak areas when using the V64-01 nebuliser, a different distribution is observed when using the DS-5 nebuliser: 32.1% and 15.3% respectively. These disproportionate peak area distributions could be an indicator that these compounds might be retained within the silica capillary.

Fig. 6 shows the GPC-ICP-MS chromatogram of Ni species in the IOR sample. The GPC-ICP-MS fingerprints for the medium- and low-molecular-weight species (24–35 min) are different for the two nebulisers, which also indicates that certain Ni species might have been retained in the DS-5 silica capillary. The peak areas corresponding to these regions are 37.3% and 17.4%, corresponding to the low- and medium-molecular weight obtained while using the V64.01 nebuliser while the areas obtained while using the DS-5 nebuliser were slightly lower: 35.5% and 16.5%.

These data agree with the hypothesis of permanent analyte retention occurring within the silica capillary and not within the PEEK tubing.

Conclusions

In this work, it was demonstrated that the use of 3D printing technology to produce low-cost and high-quality laboratory consumables is feasible and trustworthy. Consumables, such as V64-01, with high stability and proper functioning, could even improve the features of quartz or other consumables that are more expensive. In addition, the use of PEEK tubing as an internal capillary in this new total consumption micronebuliser could perfectly tolerate very strong organic solvents, such as THF.

Further analyses must be carried out to implement robust speciation analysis methods with this novel nebuliser. The speciation analysis of samples by HPLC-ICP-MS, such as that of biocrude and biolubricant samples containing numerous species of K, P and Si, among others, could be more straightforward with the use of the different features described in this work.

Published on 17 June 2020. Downloaded by 674607 on 6/23/2020 12:34:00 PM.

Conflicts of interest

There are no conflicts to declare.

Acknowledgements

The authors would like to thank Marvin Guivert and Nathan Camy for their help during the design and optimisation of this new nebulizer. The authors would also like to thank C. Martin, G. Berryman, W. Champion and J. Buckland for their help during the entire duration of this project. The financial support of the Conseil Regional d'Aquitaine (20071303002PFM) and the Fonds Europeén de Developpement Economique et Regional (FEDER) (31486/08011464) is acknowledged.

References

1 P. Azadi, R. Malina, S. R. H. Barrett and M. Kraft, *Renewable Sustainable Energy Rev.*, 2017, **76**, 1479–1484.
2 The European Parliament and the Council of the European Union, Official Journal of the European Union.
3 S. W. Banks, D. J. Nowakowski and A. Bridgwater, *Energy Fuels*, 2016, **30**, 8009–8018.
4 J. van Gerpen, *Fuel Process. Technol.*, 2005, **86**, 1097–1107.
5 D. Kubička and J. Horáček, *Appl. Catal., A*, 2011, **394**, 9–17.
6 R. Sánchez, J. L. Todolí, C.-P. Lienemann and J.-M. Mermet, *Spectrochim. Acta, Part B*, 2013, **88**, 104–126.
7 P. Giusti, Y. Nuevo Ordonez, C. Philippe Lienemann, D. Schaumloffel, B. Bouyssiere and R. Lobinski, *J. Anal. At. Spectrom.*, 2007, **22**, 88.
8 A. Desprez, B. Bouyssiere, C. Arnaudguilhem, G. Krier, L. Vernex-Loset and P. Giusti, *Energy Fuels*, 2014, **28**, 3730–3737.
9 V. Garcia-Montoto, S. Verdier, Z. Maroun, R. Egeberg, J. L. Tiedje, S. Sandersen, P. Zeuthen and B. Bouyssiere, *Fuel Process. Technol.*, 2020, **201**, 106341.
10 G. Caumette, C. P. Lienemann, I. Merdrignac, H. Paucot, B. Bouyssiere and R. Lobinski, *Talanta*, 2009, **80**, 1039–1043.
11 G. Gascon, J. Negrin, V. Garcia-Montoto, S. Acevedo, C. P. Lienemann and B. Bouyssiere, *Energy Fuels*, 2019, **33**, 1922–1927.
12 G. Gascon, J. Negrín, V. G. Montoto, S. Acevedo, C.-P. Lienemann and B. Bouyssiere, *Energy Fuels*, 2019, **33**, 8110–8117.
13 G. Caumette, C.-P. Lienemann, I. Merdrignac, B. Bouyssiere and R. Lobinski, *J. Anal. At. Spectrom.*, 2009, **24**, 263–276.
14 G. Caumette, C. P. Lienemann, I. Merdrignac, B. Bouyssiere and R. Lobinski, *J. Anal. At. Spectrom.*, 2010, **25**, 1123–1129.
15 A. Savitzky and M. J. E. Golay, *Anal. Chem.*, 1964, **36**, 1627–1639.
16 S. Gutierrez Sama, A. Desprez, G. Krier, C.-P. Lienemann, J. Barbier, R. Lobinski, C. Barrere-Mangote, P. Giusti and B. Bouyssiere, *Energy Fuels*, 2016, **30**, 6907–6912.

This journal is © The Royal Society of Chemistry 2020

3.3. Discussion and perspectives

In this work, the use of the 3D-printing has proven its usefulness to produce high-quality laboratory consumables and a new total consumption nebuliser has been validated through the total analysis of several trace elements in a reference standard provided by NIST. Concerning the speciation analysis results, several differences can be observed and some suggestions for future analyses with this consumable would be useful.

In the Figure 6 of Article 1, two chromatograms showing the size distribution of an internal oil reference are showed. Each of the chromatograms was obtained by using a different total consumption nebuliser. A difference on the areas that correspond to the retention times between 24 and 30 minutes can be observed: a decrease in the area of these peaks with respect to the high-molecular weight area (20-24 min) is observed for the chromatogram obtained with the modified DS-5 nebuliser. Although these data agree with the hypothesis of having a permanent analyte retention within the DS-5 fused silica capillary, further experiments should be carried out in future analyses to contrast this hypothesis. Collecting the eluted fractions and measuring their total concentration of V and Ni could be one of the approaches. However, further experiments could be used, such as a washing-up of the silica capillary with acetonitrile in order to release any potential species that might be trapped within its structure and repeat the experiments afterwards to check whether the same results are obtained. By carrying out these experiments, the hypothesis that has been considered during this work could be contrasted and validated.

Other future analysis should also focus on the speciation analysis of Si. The high presence of Si-containing compounds in the previous total consumption nebulisers avoided the obtention of useful Si speciation data. However, with the PEEK tubing that links this new total consumption nebuliser with the HPLC column outlet, no interferences are expected and an insight on the speciation of silicon in complex samples such as bio-oils and renewable feedstocks would be obtained.

CHAPTER 4: NOVEL SFC-ICP-MS HYPHENATION FOR THE SPECIATION ANALYSIS OF COMPLEX MATRICES

4.1. Previous SFC-ICP-MS interfaces

The coupling of Supercritical Fluid Chromatography with Inductively Coupled Plasma Mass Spectrometry possesses the potential of providing a huge number of theoretical plates to the separation of analytes from numerous families combined with the selectivity of ICP-MS detectors.

Coupling SFC and ICP-MS might be considered as an easy task, since the outlet of the SFC, once it is out of the restrictor, is in a gas state. However, when the mobile phase, which is held at high pressures, passes through the restrictor end, due to the free expansion of the gas that occurs, a significant decrease of temperature on this gas can be appreciated.

This effect is known as Thompson-Joule effect and can cause numerous issues when trying to couple the supercritical fluid chromatographs other detection techniques since the temperatures can reach very low values.[86]

Hyphenation of SFC with other techniques has been widely researched, but in this case, as one of the main objectives of this thesis, this section will focus on the SFC-ICP-MS hyphenation.

In the 1990s, Carey et al.[87] developed an interface capable of coupling both instruments. The interface that they developed consisted of a tee union where heated argon was introduced as the carrier gas of the plasma. However, the end of the restrictor was located near the end of the torch's injector and the gas-free expansion was produced a few centimetres from the plasma source. Thus, the role of the heated argon was to compensate this decrease of temperatures, so that the outlet of the restrictor would not have such low temperatures, and the plasma energy can be employed on ionising the components of the mobile phase.

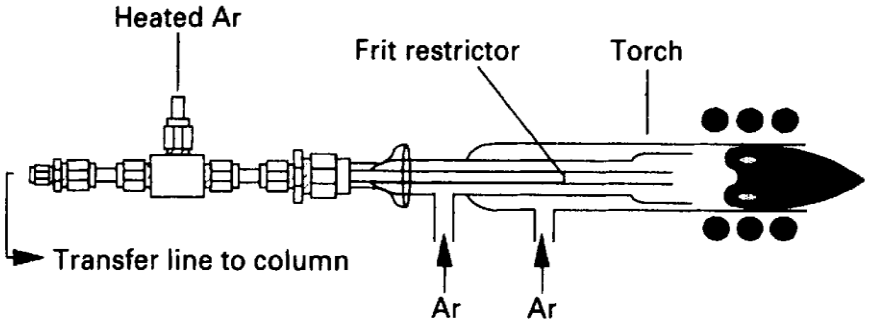

Figure 33. SFC-ICP-MS interface proposed by Carey et al.

Figure 34 shows one of the SFC-ICP-MS chromatograms obtained by Carey et al. with this interface. A 10 ng mixture of two chromium organometallic compounds was injected while using a nitrous oxide mobile phase. They achieved detection limits at the picogram level and high reproducibility levels, which can explain the high intensities of both peaks and their high separation's resolution.

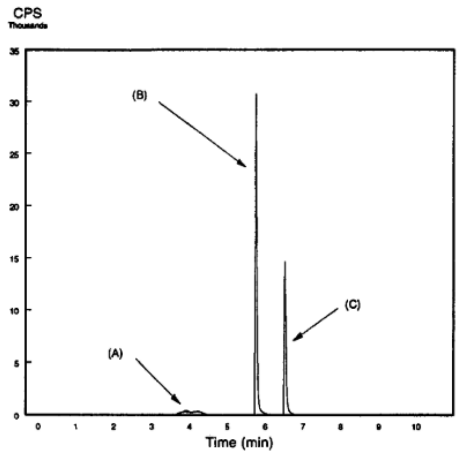

Figure 34. SFC ICP MS chromatogram at m/z = 52 for a mixture of two Cr compounds.

Other interface prototypes were also used for achieving this hyphenation, following the same principle of adding heat to the outlet of the restrictor to assure ionisation efficiency and avoiding the plasma switching off.[88]

However, all these interfaces were designed for capillary SFC, which is carried out in gas chromatography ovens and it is not adapted to the modern instrumentation, detailed in the Chapter 2.

Modern SFC, also known as convergence chromatography, does not only use one single carrier gas. The combination of different solvents and gases allows setting gradient programs that improve the chromatographic separation and increases the number of theoretical plates. However, adding an extra solvent when using these types of interface would cause the immediate extinction of the plasma, since an aerosol would probably be formed at the outlet of the restrictor and the droplets, of any size, would be injected directly into the plasma.

Thus, as the main objective of this thesis (**O1b**), an interface that allows the coupling of SFC and ICP-MS has been developed. The optimisation procedure and the results obtained are presented in the following article (**Article 3**), published in the RSC Journal of Analytical Atomic Spectrometry in October 2020.

4.2. Hyphenating supercritical fluid chromatography – inductively coupled plasma mass spectrometry: Interface development and analysis of unconventional oils

JAAS

ROYAL SOCIETY OF CHEMISTRY

TECHNICAL NOTE

Hyphenating supercritical fluid chromatography and inductively coupled plasma mass spectrometry: a proof of concept†

Cite this: DOI: 10.1039/d0ja00376j

Victor Garcia-Montoto, *[ab] Pablo Denti,[a] Linus M. V. Malmquist,[a] Sylvain Verdier,[c] Brice Bouyssiere *[b] and Jan Christensen[a]

Received 17th August 2020
Accepted 1st October 2020

DOI: 10.1039/d0ja00376j

rsc.li/jaas

The speciation analysis of complex mixtures of chemicals requires an efficient separation method and supercritical fluid chromatography (SFC) is one such technique that has been used for these purposes. Hyphenation of SFC to inductively coupled plasma mass spectrometry (ICP-MS) can provide elemental speciation information. However, the hyphenation of modern SFC instrumentation to ICP-MS has not yet been tested. The aim of this study was to develop a novel interface to hyphenate ICP-MS and modern HPLC-like SFC systems that enable the use of organic solvent gradients and packed columns. For this, an optimization of the most important parameters, such as SFC back pressure, gas temperature and position of the interface within the whole set up, was carried out, and quantitative analyses in flow injection analysis (FIA) mode of two biolubricants and one pyrolysis oil were accomplished, reaching DLs at the ppb level with the tested mobile phase compositions. In addition, in order to test the performance of this novel interface with real samples, chromatographic separation experiments of one pyrolysis oil and one coal tar using a 2-picolylamine column were carried out, confirming the stability of this new interface and its potential to become a powerful speciation technique in the future.

Introduction

Hyphenated systems based on the coupling of a chromatographic technique with element-specific detection, such as inductively coupled plasma-mass spectrometry (ICP-MS), are the recommended analytical tools for the elemental speciation analysis of complex samples, such as crude oils and petroleum products.[1,2]

The use of supercritical fluid chromatography (SFC) combined with molecular mass spectrometric detection (ESI-MS) has already shown its high efficiency for the separation, detection and identification of oxygenated compounds in highly complex samples like pyrolysis oil.[3] A further, interesting development would be the coupling of SFC to both ICP-MS and ESI-MS to obtain selective elemental detection while retaining the capability of performing molecular structure elucidation.

From a theoretical viewpoint, coupling SFC with ICP-MS should be straightforward since the mobile phase is already in a gaseous state and neither the nebulization process nor the selection of the finest droplets in a spray chamber is needed. However, pressure differences between the SFC system and the ICP-MS can cause a decrease in the temperature of the mobile phase, known as the Joule–Thomson effect,[4] which, in turn, may block the sample line. In addition, methanol can be added to SFC as a mobile phase modifier to increase the elution strength. In this case, sample transfer to the ICP-MS and ICP-MS parameters need to be optimized to minimize the negative effects of the organic solvent in the plasma, causing instability and, eventually, shutting it off.

In the 1990s, Carey *et al.*[5,6] developed an interface that allowed for selective elemental detection in capillary SFC by using a GC column. Carey and co-workers used a capillary column with supercritical CO_2 as the mobile phase in a GC-like system. However, such a system did not support the use of an organic solvent in a gradient, as in the case of modern HPLC-like SFC systems with packed columns. SFC systems with packed column separation allow for the analysis of compounds with a larger range of physicochemical properties (*e.g.*, polarity and volatility) through the use of different mobile phase compositions with different additives, improving both column performance and peak resolution, which is advantageous for the analysis of complex samples, such as unconventional oils.[7,8]

In this study, we present a novel interface for the hyphenation of HPLC-like SFC systems and ICP-MS, since, in the present time, there is not any available commercial interface

[a]Department of Plant and Environmental Sciences, University of Copenhagen, Thorvaldesensvej 40, 1871 Frederiksberg C, Denmark
[b]Universite de Pau et des Pays de l'Adour, E2S UPPA, CNRS, Institut des Sciences Analytiques et de Physico-chimie pour l'Environnement et les Materiaux (IPREM), UMR5254, 64000 Pau, France. E-mail: brice.bouyssiere@univ-pau.fr; victor.garcia-montoto@univ-pau.fr
[c]Haldor Topsoe A/S, Haldor Topsøes allé 1, 2800 Kgs. Lyngby, Denmark

† Electronic supplementary information (ESI) available. See DOI: 10.1039/d0ja00376j

This journal is © The Royal Society of Chemistry 2020

allowing this hyphenation. A proof of concept was established showing that the hyphenation of both techniques is feasible and useful for the analysis of complex chemical mixtures, such as crude oil, unconventional oils, fast pyrolysis oils and renewable feedstocks such as vegetable oils.

Experimental section

Samples and reagents

Single-element standards for ICP-MS were obtained from SCP Science (Quebec, Canada): Mg (10 000 μg mL^{-1} in 7% HNO_3), Na and Zn (10 000 μg mL^{-1} in 4% HNO_3) and Al, Cr, Mn and Pb (1000 μg mL^{-1} in 4% HNO_3). A solution containing 1 mg L^{-1} Na, Cr and Pb (standard mix) was prepared by diluting their respective standards in ACS reagent-grade (>99.0%) tetrahydrofuran (THF, stabilized with 250 ppm BHT) purchased from Sigma Aldrich (Germany). This solution was added at concentrations of 0.05, 0.1, 0.2, 0.4 and 0.8 ppm to the different samples described below to determine their composition by the standard addition method.

Standard solutions containing Na, Cr, Mn and Pb at concentrations of 0.01, 0.05, 0.1, 0.5, 01 and 10 mg L^{-1} for each element were prepared by diluting their respective standards in THF.

Crystalline carbonyl(chloro)bis(triphenylphosphine)rhodium(I) ($C_{37}H_{30}ClOP_2Rh$) and chromium (3+) tris[(2Z)-4-oxo-4-phenyl-2-buten-2-olate] ($C_{30}H_{27}CrO_6$, 99.80% purity) were purchased from Alfa Aesar (Kandel, Germany). A solution containing each of these compounds at 1 mg L^{-1} was prepared by dilution in THF, and 1 μL was injected to evaluate the performance of the interface.

Carbon dioxide (50 L with a dip tube, purity of 4.5), argon gas, and oxygen : argon gas (20 : 80) were obtained from AGA (Copenhagen, Denmark). Both LC-MS-grade methanol (MeOH) and LC-MS-grade formic acid (FA) were purchased from Sigma Aldrich (St. Louis, MO, USA).

The sample set consisted of five unconventional oils provided by Haldor Topsoe (Lyngby, Denmark). Two biolubricants and one pyrolysis oil obtained from tires had a known elemental composition. The remaining two samples, a pyrolysis oil produced from milorganite fertilizer and a coal tar, had an unknown elemental composition and were chosen for speciation analysis. All samples were diluted (by a factor of 10) in THF, and a sample volume of 2 μL, both for the sample and the corresponding blank, was injected into the SFC. For each sample, one chromatogram was obtained, following by blank injections in order to be sure that other analytes were retained in the columns.

SFC instrumentation

The SFC system used in this work consisted of an Acquity UPC^2 equipped with a Torus 2-picolylamine column (3.0 mm × 100 mm, 1.7 μm), both of which were purchased from Waters Corporation (Milford, MA, USA). The outlet from the SFC system was connected to a double T-piece splitter connected to the system's automated back pressure regulator (ABPR).

Both the column and mobile phase gradient program selected in this work were those suggested by Lübeck *et al.*[3] for the analysis of pyrolysis oil samples with SFC-ESI-MS. Since the proportions of eluent and co-eluent should not vary significantly in order to preserve the separation rates achieved by Lübeck *et al.*, two main changes were made to improve the compatibility with ICP-MS and facilitate hyphenation: (1) ethanol was replaced with methanol as a mobile phase modifier to reduce the amount of carbon injected into the plasma, and (2) the mobile phase rate was reduced by half to ensure plasma stability since the maximum mobile phase flow used in this work was half the value used by Lübeck *et al.* (from 1.5 to 0.75 mL min^{-1}).[3] Consequently, the gradient time was increased by two to obtain the same separation conditions.

The SFC analyses were run at a sample flow rate of 0.75 mL min^{-1} with carbon dioxide and methanol (0.1% formic acid) used as solvents A and B, respectively. Two different methods were used for (a) the analysis of the solution of metal-containing standard compounds and (b) the speciation analysis of unconventional oils. Run parameters are listed in Tables S1 and S2.†

Finally, in order to obtain the calibration curves intended for the calculation of DLs and for the quantitative multielement analysis, the injection of the standards was carried out under Flow Injection Analysis (FIA) conditions, using the same instrumentation with the exception of the column, with the argon gas temperature set to 40 °C and a back pressure of 120 bar. The calibration method used for the quantification of the one bio-oil and two biolubricants was carried out by using the standard additions method.

SFC-ICP-MS interface

A schematic diagram of the custom-made SFC-ICP-MS interface is shown in Fig. 1. The interface is a modified version of the design proposed by Carey *et al.*[5] in 1992. However, in our interface, a restrictor capillary (transfer line) connects one of the SFC double T-piece splitter openings to a quartz mini-cyclonic spray chamber (Meinhard, USA), enabling the use of a liquid mobile phase modifier, such as methanol. The use of large proportions of methanol in the mobile phase without a spray

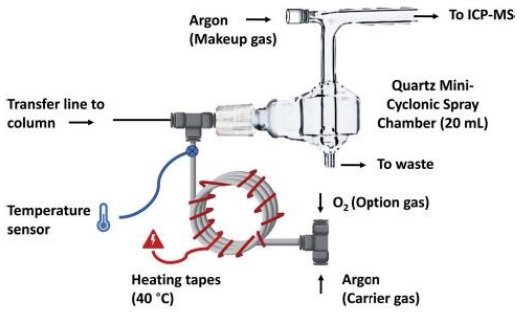

Fig. 1 Schematic representation of the custom-made SFC-ICP-MS interface used in this work.

This journal is © The Royal Society of Chemistry 2020

chamber would make the plasma so unstable that it would switch off during analysis: a previous prototype of this interface did not include the spray chamber and its performance was acceptable when working with a CO_2 mobile phase. However, the addition of small percentages of MeOH was causing the extinction of the plasma, probably caused by the MeOH droplets size exiting the transfer line. Therefore, in this interface, when the mobile phase containing methanol reached the end of the transfer line, at the entrance of a cyclonic spray chamber, it condensed and formed droplets due to the free expansion caused by the decompression of the gases at the end of the tube. Thus, only the smallest droplets were transferred to the plasma.

As shown in Fig. 1, the carrier gas (Ar) and the option gas (O_2) enter the spray chamber *via* a 1/8 and 2 × 1/4 inch tee union. Both gases were heated up to ~40 °C in a stainless-steel coil (6 m × 1/8 inches o.d.) wrapped with a fiberglass wraparound heating tape purchased from Omega (United Kingdom). The temperature of the coil was controlled by a custom-made thermostat that measured the temperature of the coil just at its very end, where it was connected to the tee union. The restrictor was placed across the tee union and held inside the spray chamber *via* an ezylok connector tubing adaptor. A more detailed diagram of the interface is showed in Fig. S1.† Fig. S2† shows the set-up aspect during analysis. The hot gas provided energy to avoid a decrease in temperature due to the expansion of CO_2 at the end of the restrictor tube, which would cause the formation of dry ice with consequent clogging of the tube. As part of the interface, an argon makeup flow entering at the top of the spray chamber contributed to stabilizing the plasma.

ICP-MS instrumentation

All measurements were carried out using an Agilent 7900 ICP-MS equipped with the sample introduction interface described above, a tapered quartz torch (1.5 mm internal diameter) and an octopole reaction system. The settings are summarized in Table S3† and were obtained after performing a tune analysis with a solution of 10.0 μg mL^{-1} Na, Cr and Pb in MeOH. The tuning solution was introduced in the interface through the second entrance of the double T-splitter at a speed of 250 μL min^{-1}.

The three samples whose quantification was carried out in this work had been previously analysed by an external laboratory within the company Haldor Topsoe. The analysis was carried out using an Agilent 7500ce ICP-MS using the procedures described in ASTM D8110-17.

Data analysis of the results obtained in this work was carried out using MATLAB and Microsoft Excel. The SFC-ICP-MS chromatograms were smoothed using the Saviztky–Golay algorithm,[9] with a polynomial of order 3 and a frame of 9 points.

Results and discussion

Back-pressure configuration

A high pressure is a mandatory requirement in SFC (Fig. S3†).[10] Hence, an automated back-pressure regulator (ABPR) was used to keep a constant and high back pressure within the instrument. In the Acquity UPC^2 system, the ABPR was placed after the columns in one of the two openings of the double T-splitter.

Different experiments were carried out to evaluate the influence of the ABPR position and to find the optimal instrumental setup for SFC-ICP-MS hyphenation.

Injections of 1 μL of a 1 mg L^{-1} mix of two metal-containing organic compounds were performed keeping the pressure of the system at 105 bar and according to the three configurations shown in Fig. 2.

As shown in Fig. 3, the use of a T-splitter is highly recommended when using the ABPR. It turned out that the ABPR itself possesses a large dead volume, which led to peak broadening. The lowest peak width was achieved when the back pressure regulator and the T-splitter were combined. However, for this configuration, the sensitivity of the signal obtained with the T-splitter was 10–20% of that obtained without the T-splitter. This was mostly due to the mobile phase being split, which reduced the sample flow reaching the ICP-MS. However, the signal-to-noise ratio increased significantly, since the background noise increase is negligible when compared to the peak increase.

Considering the peak obtained for the Cr standard injection, the peak width varied from 1.08 min in the A configuration to 0.23 and 0.08 min in the B and C configurations, respectively. Furthermore, the signal-to-noise ratio varied from 9.9 × 10^2 in the A configuration to 5.4 × 10^3 and 2.0 × 10^4 in the B and C configurations, respectively. Regarding the Rh standard, the solubility of this complex in supercritical CO_2 plays an important role, justifying the use of the C configuration. In C, the supercritical conditions were maintained within the whole system, and the compound reached the interface with almost

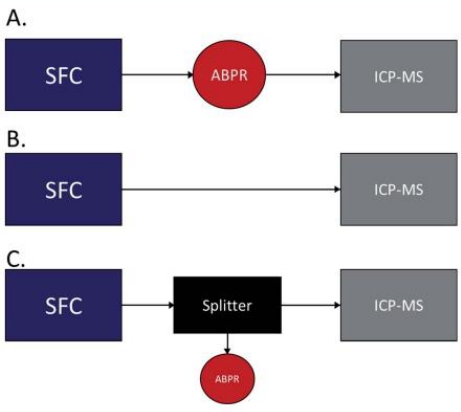

Fig. 2 Schematic representation of the three configurations of the SFC-ICP-MS interface: (A) SFC-ICP-MS + ABPR. The outlet of the column was connected directly to the ICP-MS interface after passing through the ABPR; (B) SFC-ICP-MS without ABPR. The outlet of the column was connected directly to the ICP-MS interface without passing through the ABPR; (C) SFC-ICP-MS + Split + ABPR. In this case, a double T-splitter was positioned after the column outlet. The ABPR was placed in one of the openings of the double T-piece splitter, in particular, that leading to waste.

This journal is © The Royal Society of Chemistry 2020

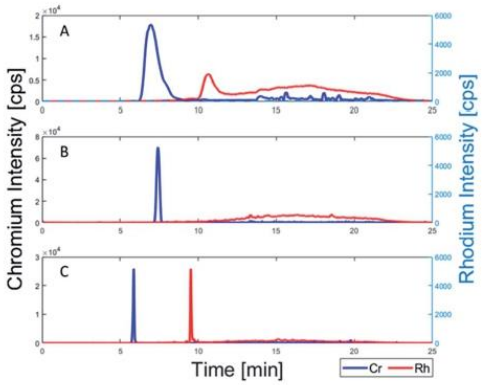

Fig. 3 Chromatograms corresponding to the analysis of two metal-containing organic compounds according to the three SFC-ICP-MS configurations. (A) ABPR without splitter. (B) No ABPR. (C) Splitter + ABPR.

no dispersion and with a very low peak width. However, in A, where the supercritical conditions were not maintained beyond the ABPR, the peak was much wider and had a long tail. Finally, in B, the Rh peak was not detected. Tailing of the Rh peak in A and no peak detection in B seemed to indicate a decrease in the elution strength of CO_2 in the absence of supercritical conditions. Thus, considering the solubility factor and the relatively low t_R for each peak in the C configuration, along with the highest signal-to-noise ratio values, the authors chose to carry out the rest of the work combining the T-splitter with the ABPR.

The next step was to optimize the pressure within the chromatographic system. A compromise had to be made since, (a) at high pressures, the plasma turned off when using methanol, probably due to a lack of energy in the plasma to vaporize and ionize high amounts of MeOH, and (b) low pressures would not guarantee supercritical conditions during the separation process, since the mixture of CO_2 and MeOH causes an increase in the critical points of their respective pure components.[10] Thus, the plasma stability was evaluated by setting the back pressure regulator to different pressure values. At a pressure of 120 bar, the plasma was found to be relatively stable. This fact was checked by reading the ICP reflected power measured, which was minimum. In addition, setting the column temperature to 60 °C ensured supercritical conditions during the separation of up to 20% MeOH in the mobile phase, according to the literature.[11,12]

Carrier gas temperature optimisation

Cooling produced by CO_2 expansion at the end of the restrictor capillary would cause the formation of dry ice, clogging the sample line. Thus, heat needed to be applied at the end of the capillary to provide enough energy to the mobile phase and avoid either its condensation or solidification. To this end, a tuning solution with three ions (Na, Cr, and Pb) was analysed in flow injection analysis (FIA) mode under different gas temperatures to determine the influence of the gas temperature on the sensitivity of the instrument. The effect of temperatures ranging from 30 to 70 °C was evaluated, and the results are reported in Fig. 4.

Higher temperatures could not be tested due to an increasing instability of the plasma, probably caused by higher amounts of methanol entering the plasma at increased temperatures. When the methanol in the mobile phase was 5% or higher, a spray appeared inside the spray chamber due to the condensation of methanol after gas expansion at the tip of the restrictor capillary. Part of the methanol in this spray drained out of the spray chamber into the waste. Thus, a higher carrier gas temperature caused a decrease in the amount of solvent condensation and therefore increased the flow of methanol going into the plasma, decreasing its power and stability.

Fig. 4 shows the normalized areas corresponding to the peaks of Na, Cr, and Pb standards acquired in FIA mode at different temperatures with 15% MeOH in the carrier flow, while Fig. S4† shows the FIA diagram for the same standards. Higher concentrations of MeOH would cause instability in the plasma at high temperatures, whereas some clogging might be caused at the end of the restrictor capillary by the dry ice formed when the carrier gas temperatures are lower and the concentration of MeOH in the mobile phase is lower. The Pb sensitivity increased the most (a factor of 5 from a normalized area of 0.2 to 1.0), followed by Cr, which increased by a factor of 2 (0.5 to 1.0), whereas the Na sensitivity seemed to be independent of temperature. One hypothesis that could explain this fact is that the analytes might have been carried over in a different proportion by the eluents in terms on their solubility in MeOH. However, measuring the concentration of these three elements by collecting and quantifying the drain of the spray chamber could not be performed. Still, this observation, which was in agreement with previous results,[13] could have been a consequence of the energy that the plasma possesses to ionize the sample after having carried out the vaporization and atomization processes of the analytes: the higher the carrier gas temperature is, the more effective the ionization in the plasma will be since less energy from the plasma will be used in processes that do not include the ionization of the analytes.

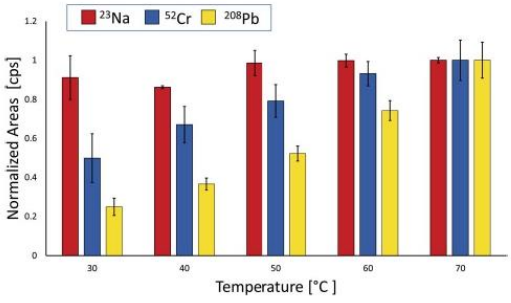

Fig. 4 Normalized areas for three elements—Na, Cr and Pb—plotted in a bar chart *vs.* the different carrier gas temperatures. The error bars represent the standard deviation of the area for three replicates.

This journal is © The Royal Society of Chemistry 2020

Indeed, the difference among the peak areas of these three elements agrees with their ionization potentials: the energy that is required to ionize Pb (715.6 KJ mol^{-1}) is much higher than that of Cr and Na (652.9 and 495.8 KJ mol^{-1}, respectively). This hypothesis agrees with the evolution of the corresponding signal-to-noise ratios: when the temperature was 30 °C, the *S*/*N* ratios for Na, Cr and Pb were respectively 236, 22 and 123. At 70 °C, their respective *S*/*N* ratios were (241, 37 and 487).

However, long-term stability was considered as important as sensitivity. Temperatures above 40 °C would yield higher sensitivity but would also lead to relatively less stable plasma than that at lower temperatures, as was observed during the experiments. In contrast, temperatures lower than 40 °C eventually clogged the restrictor capillary due to freezing of CO_2 when the percentage of methanol was below 5%. Therefore, 40 °C was considered the best optimal temperature for stability and sensitivity, and this temperature was selected for the rest of the development work.

Detection limit (DL) with different mobile phase compositions

The analysis of complex mixtures of chemicals requires the use of strong eluents since the use of CO_2 alone might not provide enough elution strength to elute the most polar species from the SFC column. The use of MeOH as a modifier was therefore tested. To understand the behaviour of the interface when the concentration of MeOH in the mobile phase changed, calibration curves were generated for four elements of interest that are commonly present in bio-oil samples. The DLs of the technique were calculated for three mobile phase compositions.

Fig. 5 shows the FIA peaks corresponding to the injection of the 1 mg L^{-1} standard solution of Na, Cr, Mn and Pb for the three mobile phase compositions that were used to determine the respective calibration curves. The results clearly showed how both the signal-to-noise ratio and the peak width improved with a higher presence of MeOH in the mobile phase, confirming that MeOH increases the elution strength for these standards during chromatographic separation. While for Cr, Mn and Pb, the highest *S*/*N* values were obtained for 30% of MeOH (267, 1514 and 2704 respectively), a different trend was observed for Na: the highest signal-to-noise ratio was 150 when the percentage of MeOH was 15%, and decreased up to 35 when the MeOH reached 30%. Fig. 5 also shows that the increase in MeOH did not negatively affect the detection of species with SFC-ICP-MS, as might be expected. In fact, increasing the amount of MeOH. In the mobile phase increased the sensitivity of the detection of some elements, such as Pb and other elements, that cannot be dissolved in solutions with a low proportion of MeOH. Nevertheless, these standards were used as a reference, and they might not be representative of all the species likely to be found in complex samples.

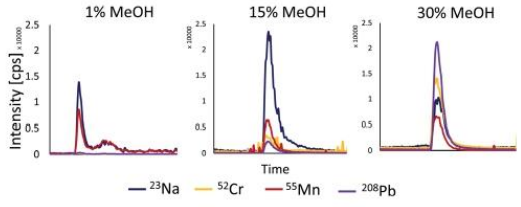

Fig. 5 Injections corresponding to 1 µL of a 1 mg L^{-1} solution at 1, 15 and 30% MeOH in the mobile phase.

The DLs for each element were calculated from the corresponding calibration curves, and the results are reported in Table 1. It appeared that an increasing percentage of MeOH from 1 to 30% in the mobile phase increased the sensitivity of the system, especially when increasing the proportion from 1 to 15% MeOH. This could be explained by the MeOH elution strength for polar compounds, as is the case for the compounds present in the solution. However, increasing the MeOH content from 15 to 30% caused an increase in the DLs, probably due to dilution effects: the excess of MeOH in the plasma that needs to be ionized is using the energy that, otherwise, would have been used on the ionization processes of the analytes. Thus, since the ionization power of the plasma is lower due to the presence of MeOH, lower analyte ions are reaching the detector, and therefore, the sensitivity decreases.

In complex samples, the matrix, the solubility of the analytes and, ultimately, the elution strength of the mobile phase will play important roles in defining the DLs. However, the calculation of the DLs *via* an external calibration curve obtained by FIA experiments helped increase the understanding of the performance of the system and the parameters influencing it. In addition, these LDs are in agreement with the concentration of trace elements detectable by ICP MS and present in the complex matrices targeted by this application.

Quantitative FIA of samples

To determine the accuracy of the SFC-ICP-MS method, the authors chose to carry out a quantitative multielement analysis of one bio-oil and two biolubricant samples. Since some of the analytes had already been analysed by the provider of the samples *via* ICP-MS, the known concentrations were used as a reference for the validation of the quantification performed in the present work, and they are shown in Table 2. Fig. S5† shows a typical SFC-ICP-MS flow injection analysis data following the standard addition methods. In this case, for three analytes in a bio-oil. Each of the peaks obtained in the FIAgram, for each element, represented the whole concentration of one element in the sample, since no chromatographic separation took place.

Comparing the slopes of the calibration curves corresponding to the elements that were analysed in the different samples

Table 1 DLs, in mg L^{-1}, obtained from the calibration curves for Na, Cr, Mn, and Pb with different mobile phase compositions

% MeOH	^{23}Na	^{52}Cr	^{55}Mn	^{208}Pb
1	0.88	0.77	0.80	0.66
15	0.43	0.19	0.19	0.40
30	1.01	0.48	0.51	0.67

Table 2 Results, in mg L^{-1}, of the quantitative analysis of different elements in three samples *via* flow injection analysis

	Element	SFC-ICP-MS (this study)	ICP-MS (external lab)
Bio-oil 1	Al	<0.09	0.04 ± 0.01
	Zn	2.8 ± 0.3	2.2 ± 0.5
	Cr	0.12 ± 0.01	n.m.*
Biolub. 1	Na	0.6 ± 0.5	0.8 ± 0.2
	Al	<0.08	<0.02
	Mg	4.6 ± 0.5	4.7 ± 0.9
	Cr	0.11 ± 0.08	n.m.*
Biolub. 2	Na	3.8 ± 0.2	3.8 ± 0.8
	Zn	1.6 ± 0.7	2.8 ± 0.6

and those generated for the previous DL study (Table S-4†), it was evident that for the analysis of a bio-oil sample the plasma ionisation power decreased due to the presence of other components in the matrix.[14]

SFC-ICP-MS analysis of unconventional oils

Fig. 6 and S7† show the SFC-ICP-MS selected ion chromatograms (SIC) for Na, Mg, and Al for both the pyrolysis oil and the coal tar samples. The SICs show that numerous compounds eluted within the first five minutes of the analysis. It was interesting that the Mg and Al peaks co-eluted, indicating that both elements are present in the same early-eluting species in the SFC-ICP-MS SICs. The acidity of the samples, added to the formation of methylcarbonic acid due to the reaction of MeOH with supercritical CO_2 might be the cause of the obtention of these Na, Mg and Al early peaks.[15] These species, that might coexist in the sample as salts, would not interact as efficiently with the protonated stationary phase (2-PIC) causing the detection of these early peaks at the beginning of the chromatogram.

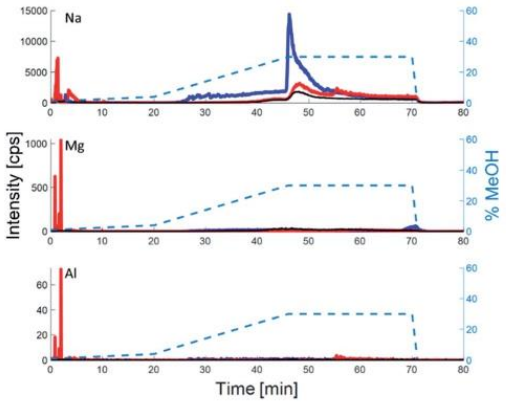

Fig. 6 SFC-ICP-MS SICs of Na, Mg and Al in the analysis of pyrolysis oil produced from milorganite fertilizer (blue), coal tar (red) and the corresponding blank (THF).

When the SFC gradient reached 30% MeOH, Na species appeared in the form of relatively broad peaks. In the pyrolysis oil, which was prepared from a fertilize, the high presence of Na species might be caused by their interaction with the pyrolysis oil matrix, rich in phosphorus species, such as phospholipids, which might have polymerized or suffer reactions such as hydroxylation during the pyrolysis process, increasing their polarity and trapping other ionic species such as sodium. With respect to the coal tar, the data suggest that these sodium species might be interacting with the asphaltenes or the naphthenic acids present in coal tar.

Fig. 6 shows the complete SFC-ICP-MS SIC, whereas Fig. S6† is a close-up version of the first 5 min of separation. This figure demonstrates that the concentrations of the elements in the early-eluting peaks were much higher in the coal tar than in the pyrolysis oil, as was expected due to the presence of these elements in coal tar, while Na also had a high intensity in the later-eluting peaks of the pyrolysis oil.[16]

Other elements detected in the coal tar are shown in the SFC-ICP-MS SICs in Fig. S7 and S8,† where two peak clusters were observed at the beginning of the chromatogram (1–5 min). The detection of these elements in the coal tar agreed with the inorganic composition of this dark and dense liquid confirmed in the literature[16] and confirmed the proper functioning of the interface. However, further investigations of this kind of sample may benefit from the use of different columns with a wider range of polarity interactions to achieve fully resolved and higher-quality chromatograms.

As it was mentioned before, there exists a significant difference between each analyte's DL along the different gradient configurations. Since the aim of this work was to provide with a proof-of-concept, these differences on the response factor of the instrument at different gradient values were not considered. Thus, for a more accurate analysis, the authors suggest that the use of an internal standard added constantly towards the spray chamber *via* a secondary pump would correct the measured intensities during the whole separation, providing with more trustable results. This internal standard could consist on an isotopically enriched solution that contains the element of interest.[17] Other approaches correcting this issue might be reached by delivering a post-column counter gradient in order to obtain a single detector response throughout the whole analysis.[18]

Conclusions

A proof of concept has been shown confirming that an interface that hyphenates these two techniques is achievable and does not require a high disbursement of money.

This interface allows for the analytical platform to be used for elemental speciation analysis of unconventional oil samples and other samples with complex matrices, such as environmental and biological samples.

The chromatographic results also indicate that further analyses need to be carried out to improve and optimize this hyphenated method. Further works should focus on improving the plasma stability for either higher mobile phase flows and

 This journal is © The Royal Society of Chemistry 2020

pressures, sensitivity or chromatographic separation, investigating the use of different column materials with other mobile phase compositions and gradients. With these improvements, SFC-ICP-MS possesses the potential to become a very powerful speciation technique for the analysis of complex samples, such as unconventional oils.

Conflicts of interest

There are no conflicts to declare.

Acknowledgements

We would like to thank Josephine Lubeck for her invaluable guidance and help with her very useful advice on SFC instrumentation.

References

1 G. Gascon, J. Negrin, V. Garcia-Montoto, S. Acevedo, C.-P. Lienemann and B. Bouyssiere, Simplification of Heavy Matrices by Liquid–Liquid Extraction: Part I—How to Separate LMW, MMW, and HMW Compounds in Maltene Fractions of V, Ni, and S Compounds, *Energy Fuels*, 2019, **33**, 1922–1927.

2 G. Gascon, J. Negrín, V. G. Montoto, S. Acevedo, C.-P. Lienemann and B. Bouyssiere, Simplification of Heavy Matrices by Liquid–Solid Extraction: Part II—How to Separate the LMW, MMW, and HMW Compounds in Asphaltene Fractions for V, Ni, and S Compounds, *Energy Fuels*, 2019, **33**, 8110–8117.

3 J. S. Lübeck, G. Tomasi, K. G. Poulsen, O. D. Mante, D. C. Dayton, S. Verdier and J. H. Christensen, Nontarget Analysis of Oxygenates in Catalytic Fast Pyrolysis Biocrudes by Supercritical Fluid Chromatography High-Resolution Mass Spectrometry, *Energy Fuels*, 2019, **33**, 296–306.

4 J. D. Pinkston and T. L. Chester, Putting Opposites Guidelines for Successful SFC/MS, *Anal. Chem.*, 1995, **67**, 650A–656A.

5 J. M. Carey, N. P. Vela and J. A. Caruso, Multi-Element Detection for Supercritical Fluid Chromatography by Inductively Coupled Plasma Mass Spectrometry, *J. Anal. At. Spectrom.*, 1992, **7**, 1173–1181.

6 J. M. Carey, N. P. Vela and J. A. Caruso, Chromium Determination by Supercritical Fluid Chromatography with Inductively Coupled Plasma Mass Spectrometric and Flame Ionization Detection, *J. Chromatogr. A*, 1994, **662**, 329–340.

7 C. R. Yonker and R. D. Smith, Study of Retention Processes in Capillary Supercritical Fluid Chromatography with Binary Fluid Mobile Phases, *J. Chromatogr. A*, 1986, **361**, 25–32.

8 C. West, J. Melin, H. Ansouri and M. Mengue Metogo, Unravelling the Effects of Mobile Phase Additives in Supercritical Fluid Chromatography. Part I: Polarity and Acidity of the Mobile Phase, *J. Chromatogr. A*, 2017, **1492**, 136–143.

9 A. Savitzky and M. J. E. Golay, Smoothing and Differentiation of Data by Simplified Least Squares Procedures, *Anal. Chem.*, 1964, **36**, 1627–1639.

10 T. S. Reighard, S. T. Lee and S. V. Olesik, Determination of Methanol/CO2 and Acetonitrile/CO2 Vapor-Liquid Phase Equilibria Using a Variable-Volume View Cell, *Fluid Phase Equilib.*, 1996, **123**, 215–230.

11 S. H. Page, S. R. Goates and M. L. Lee, Methanol/CO2 Phase Behavior in Supercritical Fluid Chromatography and Extraction, *J. Supercrit. Fluids*, 1991, **4**, 109–117.

12 P. S. Wells, S. Zhou and J. F. Parcher, Peer Reviewed: Unified Chromatography with CO2-Based Binary Mobile Phases, *Anal. Chem.*, 2003, **75**, 18 A–24 A.

13 G. Caumette, C.-P. Lienemann, I. Merdrignac, H. Paucot, B. Bouyssiere and R. Lobinski, Sensitivity Improvement in ICP MS Analysis of Fuels and Light Petroleum Matrices Using a Microflow Nebulizer and Heated Spray Chamber Sample Introduction, *Talanta*, 2009, **80**, 1039–1043.

14 B. Bouyssiere, F. Baco, L. Savary, H. Garraud, D. L. Gallup and R. Lobinski, Investigation of Speciation of Arsenic in Gas Condensates by Capillary Gas Chromatography with ICP-MS Detection, *J. Anal. At. Spectrom.*, 2001, **16**, 1329–1332.

15 L. Novakova, A. Perrenoud, I. Francois, C. West, E. Lesellier and D. Guillarme, Modern analytical supercritical fluid chromatography using columns packed with sub-2 μm particles: A tutorial, *Anal. Chim. Acta*, 2014, **824**, 18–35.

16 J. Du, W. Deng, C. Li, Z. Zhang, T. Yang, X. Cao, F. Du and Q. Sun, Multi-Metal Catalysts for Slurry-Phase Hydrocracking of Coal-Tar Vacuum Residue: Impact of Inherent Inorganic Minerals, *Fuel*, 2018, **215**, 370–377.

17 B. Klencsar, S. W. Li, L. Balcaen and F. Vanhaecke, High-performance liquid chromatography coupled to inductively coupled plasma – Mass spectrometry (HPLC-ICP-MS) for quantitative metabolite profiling of non-metal drugs, *Trends Anal. Chem.*, 2018, **104**, 118–134.

18 T. Gorecki, F. Lynen, R. Szucs and P. Sandra, Universal Response in Liquid Chromatography Using Charged Aerosol Detection, *Anal. Chem.*, 2006, **78**, 3186–3192.

SUPPORTING INFORMATION FOR

Supercritical fluid chromatography–inductively coupled plasma mass spectrometry (SFC-ICP-MS) hyphenation for the speciation analysis of unconventional oils

Victor Garcia-Montoto[a,b*], Pablo Denti[a], Linus M. V. Malmquist[a], Sylvain Verdier[c], Brice Bouyssiere[b*], Jan H. Christensen[a]

[a] Department of Plant and Environmental Sciences, University of Copenhagen, Thorvaldesensvej 40, 1871 Frederiksberg C, Denmark

[b] CNRS/Univ Pau & Adour Countries/E2S UPPA, Institut des Sciences Analytiques et de Physico-chimie pour l'Environnement et les Materiaux (IPREM), UMR5254, 64000 Pau, France

[c] Haldor Topsoe A/S, Haldor Topsøes allé 1, 2800 Kgs. Lyngby, Denmark

Caption to tables:

Table S1. Fast chromatographic method for the analysis of the two metal-containing compounds.

Table S2. SFC method for the speciation analysis of unconventional oils.

Table S3. ICP MS tune parameters used for all the analyses carried out in this work.

Table S4. Slopes corresponding to the standard addition calibration curves for the quantification of Zn, Cr and Al in a bio oil and two bio lubricants.

Caption to Figures:

Figure S1. Detailed schematic representation of the SFC-ICP-MS interface.

Figure S2. Photo of the interface set up during analysis.

Figure S3. P-T-X diagram of CO_2 and MeOH. For the conditions used in this work.

Figure S4. Injection of 1µL of a standard mix containing Na, Cr and Pb in FIA mode at temperatures from 30°C to 70°C.

Figure S5. Flow injection analysis via standard additions method results for the analysis of ^{27}Al, ^{63}Cu and ^{66}Zn in a pyrolysis oil sample.

Figure S6. Magnified section of the first 10 minutes of the SFC-ICP-MS SICs for the analysis of pyrolysis oil produced from milorganite fertilizer (blue), coal tar (red) and the corresponding blank (THF).

Figure S7. SFC-ICP-MS SICs for Mn, Fe and Cu in a coal tar (red) and the corresponding blank (black).

Figure S8. Extended SFC-ICP-MS SICs for Mn, Fe and Cu in a coal tar (red) and the corresponding blank (black).

Table S1. Fast chromatographic method for the analysis of the two metal-containing compounds.

Parameter	**Value**
Run time	25 min
Mobile phase (A:B)	CO_2:MeOH (0.1% FA)
Flow Rate	0.75 mL/min
Gradient (A:B)	Initial: 99:1 5 min: 96:4 (0.2% B / min) 25 min: 70:30 (1.3% B / min) 25.1 min: 99:1
Injection Volume	1.0 μL
Injection Solvent	THF
Column	2-PIC (3.0 x 100 mm, 1.7 μm)
Column Temperature	60 °C
ABPR	105 Bar

Table S2. SFC method for the speciation analysis of unconventional oils.

Parameter	**Value**
Run time	80 min
Mobile phase (A:B)	CO_2:MeOH (0.1% FA)
Flow Rate	0.75 mL/min
Gradient	Initial: 99:1
	20 min: 96:4 (0.2% B / min)
	46 min: 70:30 (1% B / min)
	70 min: 70:30
	70.2 min: 99:1
Injection Volume	2.0 μL
Injection Solvent	THF
Column	2-PIC (3.0 x 100 mm, 1.7 μm)
Column Temperature	60 °C
ABPR	120 Bar

Table S3. ICP MS tune parameters used for all the analyses carried out in this work

Parameter	Value
Plasma Parameters	
RF Power	1600 W
RF Matching	2.15 V
Sample Depth	18.0 mm
Carrier Gas (Ar)	1.00 L/min
Option Gas (O_2)	0.50 L/ min
Makeup Gas (Ar)	0.80 L/min
Lenses Parameters	
Extract 1	0.0 V
Extract 2	-110.0 V
Omega Bias	-100 V
Omega Lens	3.2 V
Cell Entrance	-40 V
Cell Exit	-60 V
Deflect	-0.6 V
Plate Bias	-60 V
Cell Parameters	
He Flow	4.0 mL/min
Octopole Bias	-18.0 V
Octopole RF	180 V
Energy Discrimination	5.0 V

Table S4. Slopes corresponding to the standard addition calibration curves for the quantification of Zn, Cr and Al in a bio oil and two bio lubricants

Element	Slope (DL Calculation)	Slope (Bio Oil)	Slope (Bio Lub 1)	Slope (Bio Lub 2)
Zn	10186	93	380	50
Cr	265509	23805	14114	n.m.*
Al	8781	1510	1388	n.m.*

* Cr and Al have not been measured in Bio Lub 2.

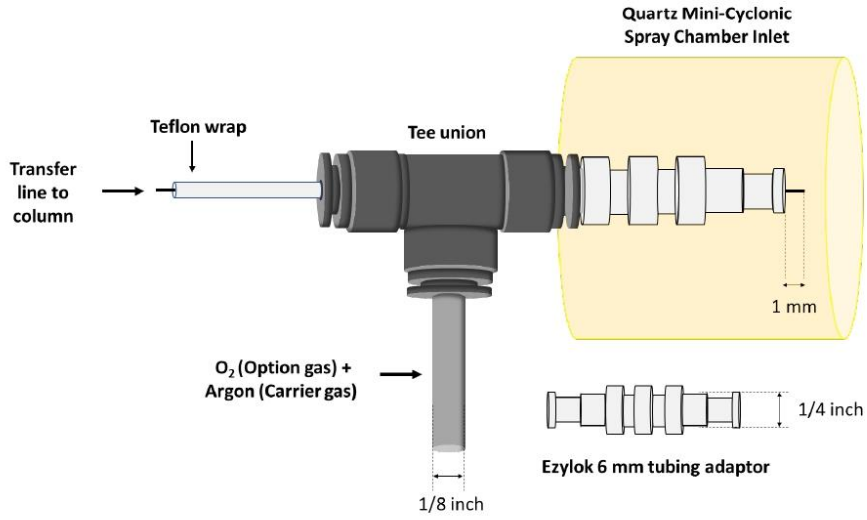

Figure S1. Detailed schematic representation of the SFC-ICP-MS interface.

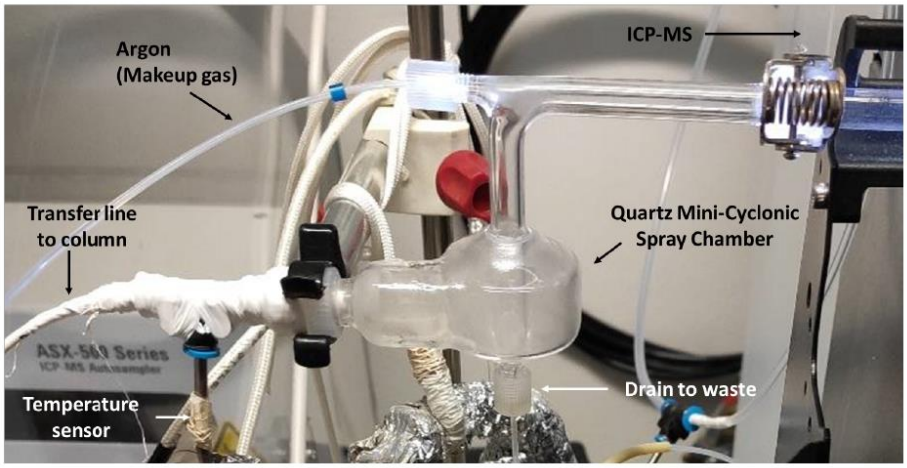

Figure S2. Photo of the interface set up during analysis.

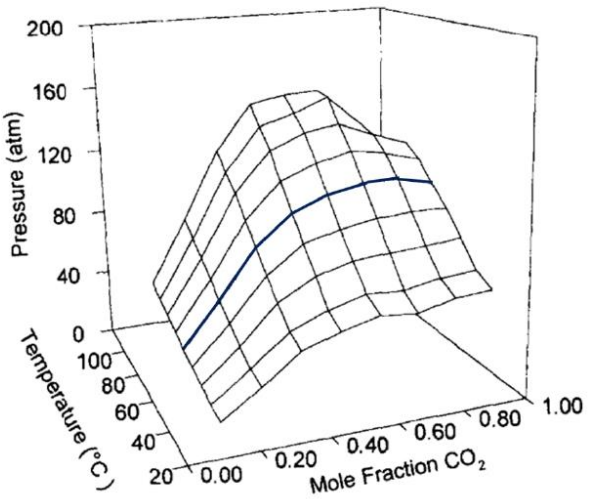

Figure S1. P-T-X diagram of CO_2 and MeOH. For the conditions used in this work, supercritical conditions (above the plane) are achieved at least until a 20% of MeOH[16].

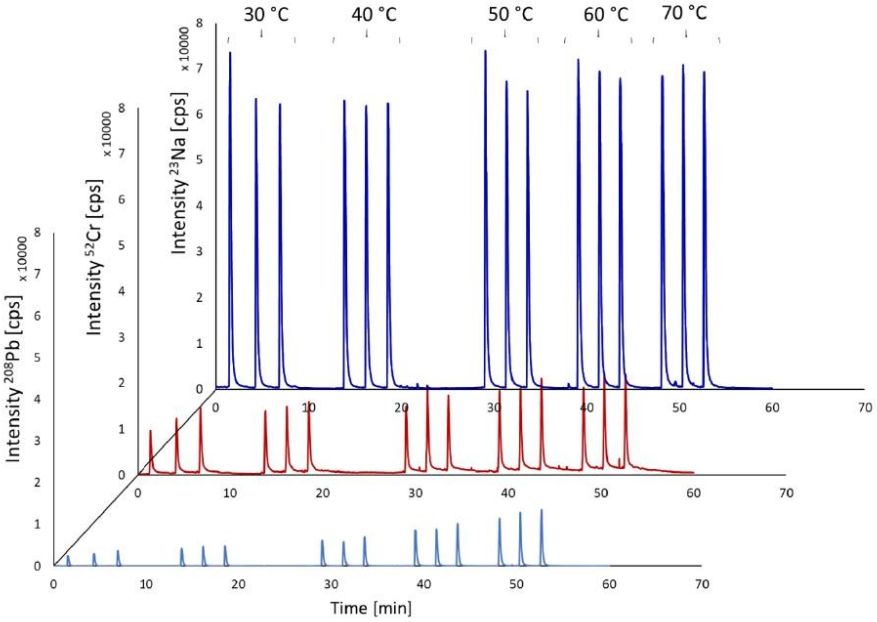

Figure S4. Injection of 1μL of a standard mix containing Na, Cr and Pb in FIA mode at temperatures from 30°C to 70°C.

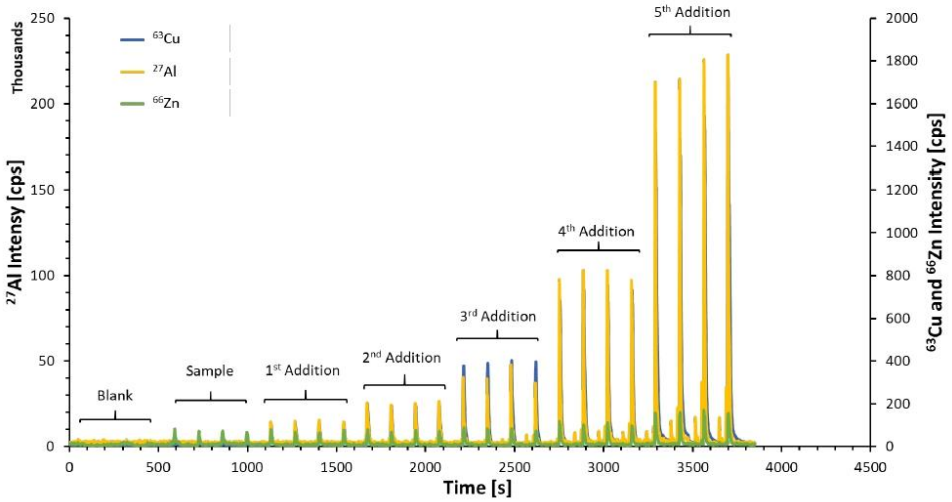

Figure S5. Flow injection analysis via standard additions method results for the analysis of ^{27}Al, ^{63}Cu and ^{66}Zn in a pyrolysis oil sample.

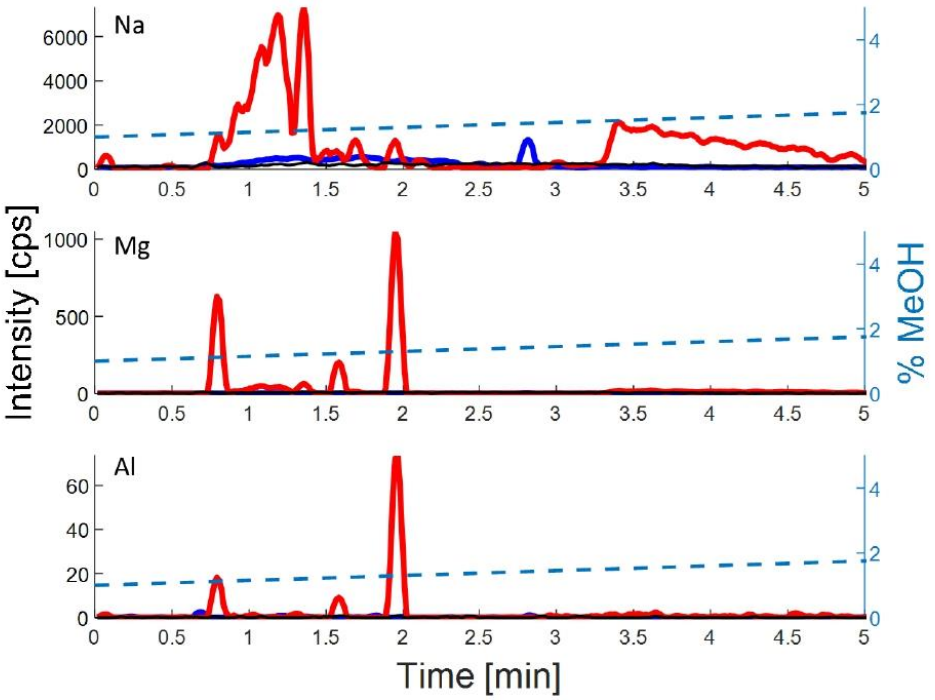

Figure S6. Magnified section of the first 10 minutes of the SFC-ICP-MS SICs for the analysis of pyrolysis oil produced from milorganite fertilizer (blue), coal tar (red) and the corresponding blank (THF).

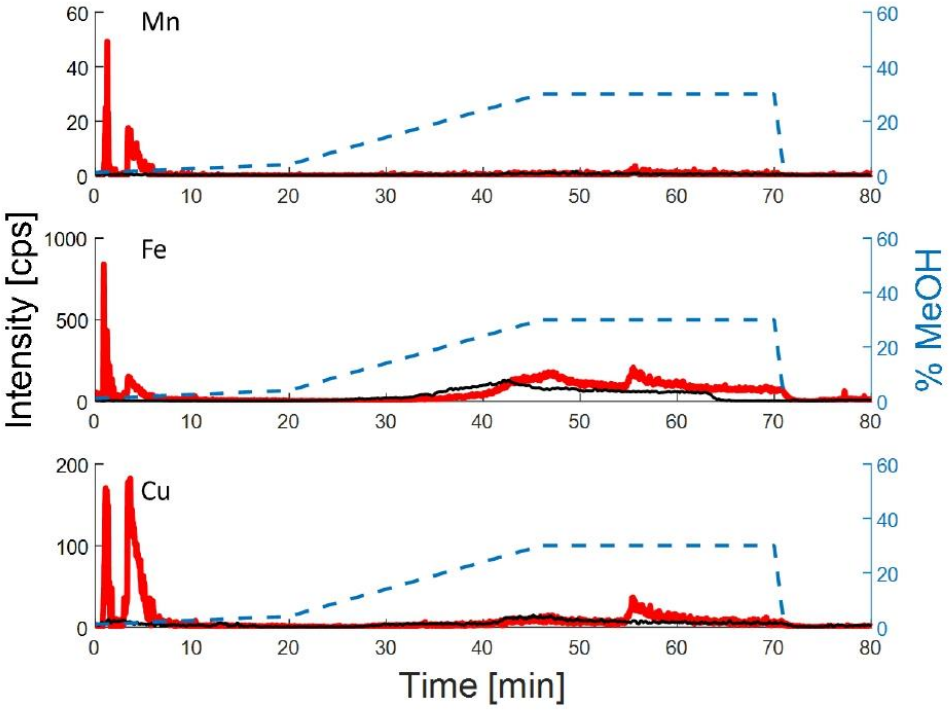

Figure S7. SFC-ICP-MS SICs for Mn, Fe and Cu in a coal tar (red) and the corresponding blank (black).

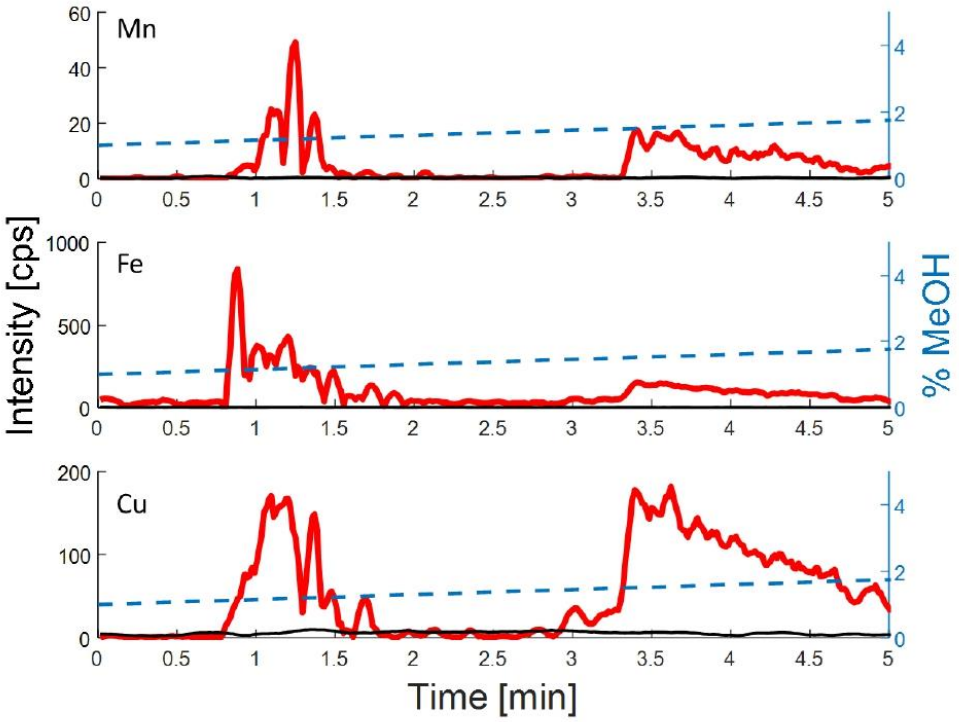

Figure S8. Extended SFC-ICP-MS SICs for Mn, Fe and Cu in a coal tar (red) and the corresponding blank (black).

CHAPTER 5. ETV-ICP-OES FOR THE ANALYSIS OF BIO-OILS

In this chapter, the development of a methodology that allows both the quantitative and speciation analysis in complex samples is detailed. Unfortunately, the research work on this topic could not be finished in time and some hypotheses have not been tested. However, the continuation of this work will be carried out in the near future within the scope of other projects and further analysis will be done by following the methodology explained within this chapter, providing with a better understanding of the behaviour and the composition of some of trace element species present in complex samples, such as the feedstocks that were analysed in this three-year project. Nevertheless, in this work, the basis of a novel methodology that hyphenates ETV and ICP-OES have been stablished, being able to fulfil one of the main sub-objectives of this PhD thesis (**O1c**).

5.1. Introduction

As it was introduced in Chapter 1, the common presence of trace elements in renewable feedstocks becomes an undesirable factor that can affect negatively to the yield of their conversion into hydrocarbon fuels and their quality and environmental properties.

Numerous techniques can determine the presence of these undesirable trace elements in complex samples such as crude oil and biomass products. One of these techniques, ICP-MS, has been used throughout this PhD providing high-quality results. However, other methodologies might be considered to obtain a fingerprint of these trace elements species, like Electrothermal Vaporisation – Inductively Coupled Plasma – Optical Emission Spectroscopy.

With this methodology, quantifying and determining the fingerprint of trace elements based on their pyrolysis or boiling temperatures was possible by using the hyphenation of an Electrothermal Vaporiser Spectral Systems 4000-c with an ICP-OES Spectro Arcos.

An electrothermal vaporiser is an evaporator that can be used as a sample introduction technique for a plasma source spectrometry. As it is shown in Figure 35,Figure 35.

Experimental setup of an electrothermal vaporiser (Adapted from Asfaw et al.[89]). the vaporiser consists of an oven where a graphite boat containing the sample, which can be a liquid or a solid, is placed. The oven is electrically heated to the desired temperatures, normally by following a heating program, and the evaporated sample is carried by an inert gas such as argon that flows towards a detector such as ICP-OES, which is the detection method used in this work.

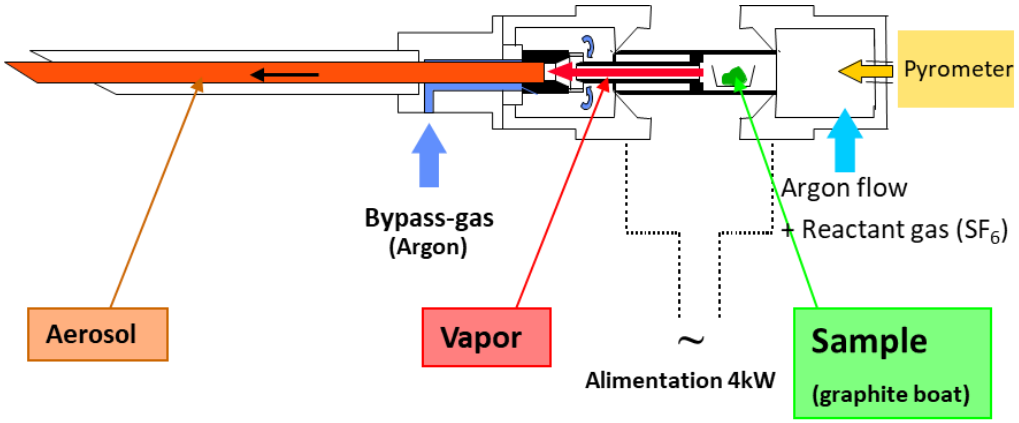

Figure 35. Experimental setup of an electrothermal vaporiser (Adapted from Asfaw et al.[89]).

A reaction gas is used to avoid the formation of carbides from elements such as Cr, Ti and V among others.[90] One of the most common ETV reaction gases is CCl_2F_2, also known as Freon R12, which improves the volatilization efficiency of the inorganic elements by reacting and forming volatile halides. However, due to its damaging effect on the ozone layer, its manufacture and commercialisation have been banned from most of the developed countries, including the US and Europe.[91,92] Hence the need to test and to find a new reaction gas that allows the volatilisation of all the inorganic species in samples such as bio-oils. In this work, SF_6 gas has been used alternatively, since it is cheaper and more environmentally friendly.

One of the main advantages of using this technique is the nonrequirement of sample preparation steps and the low amount of sample required to carry out the analysis, which normally is less than 1 mg. Besides, it consists of a less time-consuming technique with shorter times of analysis (less than 2 minutes) with no dilution needed, which improves significantly the sensitivity, are some of the other advantages that make this technique ideal for the aim this project.

The mode of operation of this instrument can be summarized in four steps:

I. *Deposition of the sample*: A liquid or solid sample is deposited in a graphite boat, which is introduced within the ETV graphite furnace.
II. *Heating*: A temperature programme is designed with temperatures that allow the first step of desolvation of the sample, followed by the ashing of the matrix and finally the vaporisation of the analytes.
III. *Transport towards the detector*: Via a transfer tube which normally is made of Teflon, vaporised analytes are transferred towards a detector, which normally consists of a plasma source.
IV. *Recording of the transient signal in function of time.*

The electrothermal vaporised that has been used in this work consists of a state-of-the-art model. Spectral Systems, which is the provider of this instrument, has been specialised in ETV instrumentation for more than 16 years. [93] The use of ETV-ICP-OES has been mainly focused on the determination of several trace elements in numerous types of samples and rarely used for speciation analysis purposes: The most recent articles that have been published on ETV-ICP-OES analyses show the high efficiency of this methodology for fast analysis in solid samples: Vogt et al.[94] quantified Al, Ba, Ca, Cr, Cu, Fe, K, Mg, Mn, Na, Ni, P, Pb, S, Si, Ti, V and Zn by ETV-ICP-OES in Argonne Premium Coal samples; Santos et al. [95] determined As, Cd, Cr, Cu, Mn, Ni, Pb and Zn in medicinal plants and Silva et al.[96] determined the concentration of 16 rare elements in crude oil. Bauer et al.[97] developed for the first time an ETV-ICP-OES methodology for the speciation of sulfur in coals. This methodology did not require any sample preparation and was validated by analysing a standard reference material.

These recent experiments were carried out by using the same instrument (ETV 4000c purchased from Spectral Systems). However, all these methodologies have used Freon-R12 as reaction gas during the analyses, which, as it has been mentioned before, its use in the European Union has been forbidden.

5.2. Materials and methods

5.2.1. Instrumentation

All the measurements have been carried out in an ETV Spectral Systems 4000-c. During the electrothermal vaporisation, both carrier gas and bypass flows were optimised, and these optimum values were 0.05 and 0.15 L min^{-1} respectively. An SF_6 flow of 0.35 mL min^{-1} was used during the analyses to improve the volatilization efficiency of the compounds that were analysed. The graphite boats and graphite furnaces used during this work have been purchased from Spectral Systems (Germany).

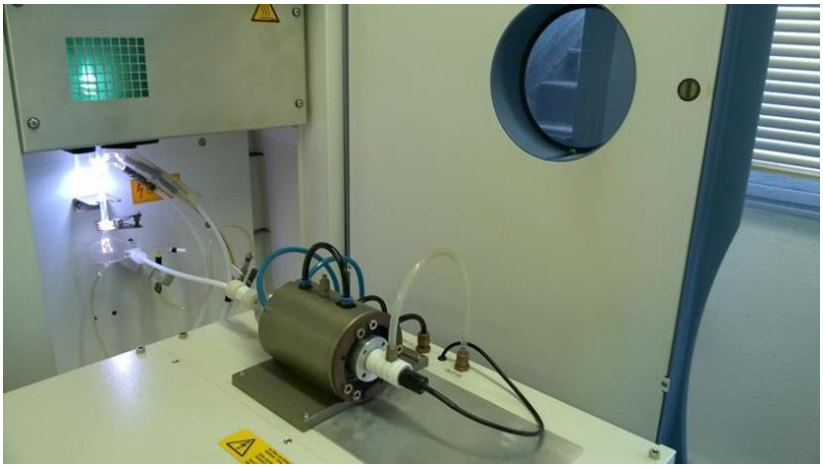

Figure 36. ETV-ICP-OES set up.

A Teflon tube (1/4', 4 mm i.d.) was used to transfer the analytes from the electrothermal vaporised towards the ICP-OES (Spectro Arcos), which was equipped with a spray chamber with double 6 mm nebuliser inlets and with a female ball 12/5 outlet, purchased from Symalab (Pau, France).

A Sea-spray nebuliser was used for the continuous addition of an internal solution containing 5 ppm of Rh. Figure 36 shows a picture containing the typical appearance of this ETV-ICP-OES setup, and Table 2 resumes the main parameters of the ICP-OES.

Table 2. ICP-OES parameters used for all the analysis carried out via ETV-ICP-OES.

ICP/AES (SPECTRO ARCOS)	
Observation plasma	Radial
Power	1650W
Nebuliser	Sea-spray
Plasma Ar flow rate	15L/min
Auxiliary Ar flow rate	1.8L/min
Integration time	10 ms

5.2.2. Samples and reagents

THF, Multisolvent GPC-grade, ACS-grade, and stabilised with 250 ppm of butylated hydroxytoluene (BHT) to prevent the formation of peroxides, purchased from Sharlab (Spain) was used to prepare the corresponding dilution of the samples analysed in this work.

For both method optimisation and quantification purposes, a Conostan S21 containing 50 ppm of Al, B, Ba, Ca, Cd, Cr, Cu, Fe, Mg, Mn, Mo, Na, Ni, P, Pb, Si, Sn, Ti, V and Zn, purchased from SCP science, was employed.

The standard reference material, SRM 1085b, purchased from NIST (National Institute for Standards and Technology, Gaithersburg, MD, USA) containing 300 ppm wear metals in lubricant oils (Al, As, Ba, B, Cd, Ca, Cl, Cr, Cu, Fe, Pb, Mg, Mn, Mo, Ni, P, Si, Ag, Na, Sn, V and Zn) was used for method validation.

Six different fast pyrolysis oil samples have been analysed via ETV-ICP-OES. Two of them (Samples P and T) consist of commercial pyrolysis oils that were obtained from Haldor Topsoe (Lyngby, Denmark) and the other four, whose production will be discussed in Chapter 7, were provided by RTI. The feedstocks employed to produce the fast pyrolysis oils and their respective names in the figures are detailed below:

- Sample A: Pyrolysis oil produced from a 50:50 mixture of milorganite and loblolly pine wood.

- Sample B: Pyrolysis oil produced from a 50:50 mixture of milorganite and red oak wood.
- Sample C: Pyrolysis oil produced from milorganite fertilizer.
- Sample D: Pyrolysis oil produced from red oak wood.
- Sample P: This sample consists of a pyrolysis oil produced from pine wood.
- Sample T: Pyrolysis oil produced from used tyres.

5.2.3. Procedure

A dilution (DF = 10) was carried out to obtain a 5 ppm solution which was used for the optimisation of the gas flows. For each run, 10 μL of this solution were deposited in the graphite boat, after having waited for one minute to let the THF evaporate and then starting the analysis. Dilutions of the S21 and K standards were carried out in order to obtain solutions containing 0, 0.001, 0.01, 0.02, 0.05, 0.1, 0.5, 1, 5, 10 and 20 ppm of the corresponding elements, to perform an external calibration.

The SRM 1085b was diluted 10,000 times in THF. The Conostan multielement solution was diluted in THF and added to aliquots of the diluted SRM 1085 b in order to have five different solutions containing each analyte plus an added concentration of 0, 0.5,1, 2 and 4 ppm. 10 μL of each standard was introduced in the graphite boat and ran by triplicate.

Each of the pyrolysis oils analysed in this work was diluted 10 times with THF to avoid the saturation that a high concentration of some elements might cause in the detector. 20 μL of each diluted sample was injected by triplicate.

The transient signal obtained via the methods used in this work has been corrected with the intensities obtained for the internal standard via the division of their correspondent transients ($S_{analyte}$ / S_{IS}) followed by an integration of the intensities that conform the corresponding peaks observed.

Matlab 2018b and Microsoft Excel were used for the data treatment and graphic design of the results obtained.

5.3. Results and discussion

5.3.1. ETV-ICP-OES Optimisation

To obtain a good sensitivity is a critical step in the acquisition of ETV-ICP-OES data since an inaccurate combination of the three different gas flows that are used in the electrothermal vaporised could drop significantly the sensitivity rates.

To perform this optimisation, a temperature ramp with a very fast increase of the graphite furnace temperature was chosen to obtain the highest transient signal in the shortest possible time for one sample.

Figure 37 shows the temperature ramp that was chosen for these optimisation experiments. It starts with a smooth increase of the temperatures (20 °C s^{-1}) which is held for 5 minutes up to 20 s of analysis. Then, a very fast gradient has been programmed in order to reach a temperature of 2200 °C which will vaporise and send towards the ICP-OES the target analytes. This temperature is held for 20 seconds and then, a second gradient of temperature is programmed to completely pyrolyze and vaporise those potential compounds that might have been retained in the graphite boat. Thus, temperature raises for 10 seconds (40 °C s^{-1}) and finally held at 2600 °C for the last 9 seconds.

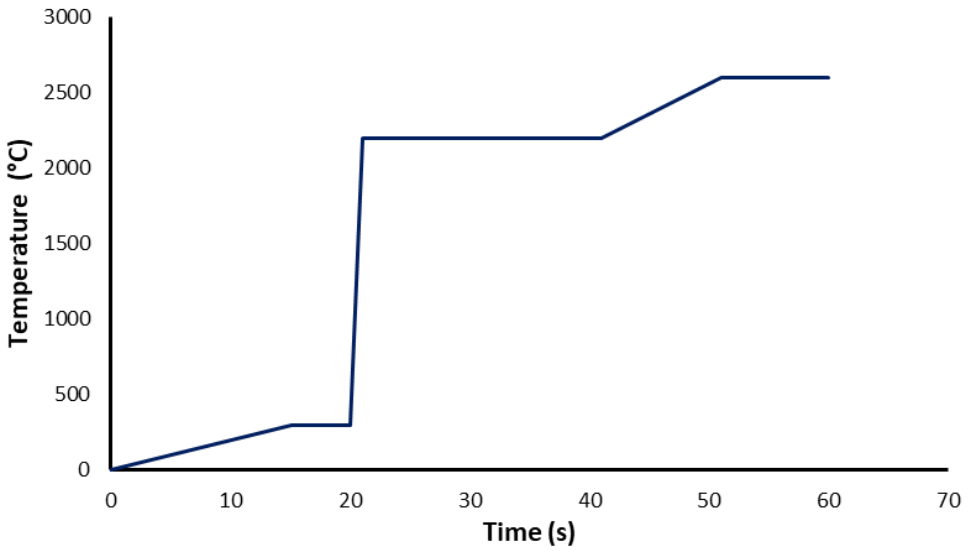

Figure 37. Temperature ramp design for the optimisation of the ETV-ICP-OES parameters.

The fist flow to be optimised was the SF_6 reaction gas. To do so, ETV gas flow rates were set up using the same values that Silva et al. [98] used for determining rare earth elements in crude oil samples. Whereas both the carrier and the bypass flows were set up to 0.4 L min^{-1}, the transient signal generated by the analysis of the same standard solution was fully integrated and corrected with the Rh internal standard transient values.

Figure 38 shows the intensity variations of different wavelengths with the different gas flow values. It is interesting to mention that, for all the elements, with a few exceptions, there are common patterns: (1) the absence of reaction gas reduces the sensitivity of the detection and (2) an excess of reaction gas also reduces the sensitivity of the detection.

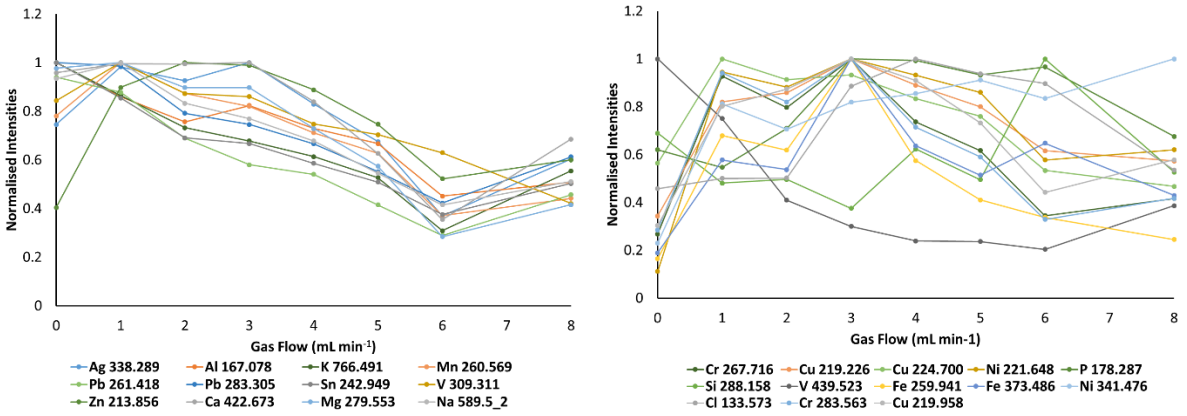

Figure 38. Corrected intensities for each wavelength and normalised vs. reaction gas flow.

In order to choose accurately the optimum reaction gas flow value, the relative standard deviations of each analyte were studied. Figure 39 shows the relative standard deviation of the integrated signals for each measured wavelength. There is a region, between 3 and 5 mL min^{-1} where higher precision is obtained.

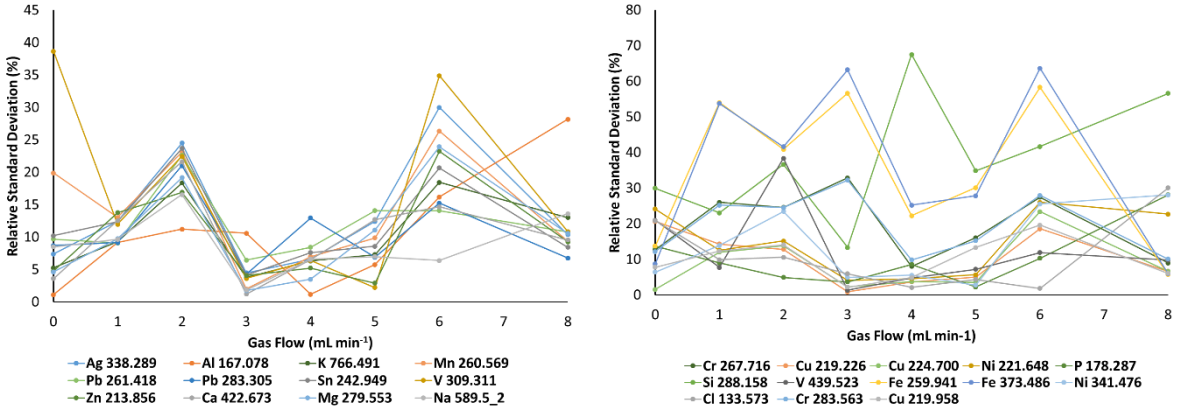

Figure 39. Relative standard deviation (n = 3) of each wavelength vs. reaction gas flow.

Thus, considering the sensitivity values and the precision obtained, a reaction gas flow of 3.5 mL min^{-1} was elected.

The carrier gas flow was optimised once the reaction gas rates were optimal. To perform this optimisation, the gas reaction flow was held at 0.35 mL min^{-1} and the bypass flow was held at 0.5 L min^{-1}. Figure 40 shows the intensity average values obtained for the different

wavelengths analysed. Except for 4 different wavelengths (on the right side of the figure), generally, the sensitivity of the transient signals decreases with higher carrier gas flows. Besides, as it can be observed in Figure 41, the precision increases at low gas flow rates. Taking into account this information and considering that a very low carrier gas flow might not be able to transport all the analytes to the plasma, a compromise was taken and a flow of 0.05 L min^{-1} was chosen.

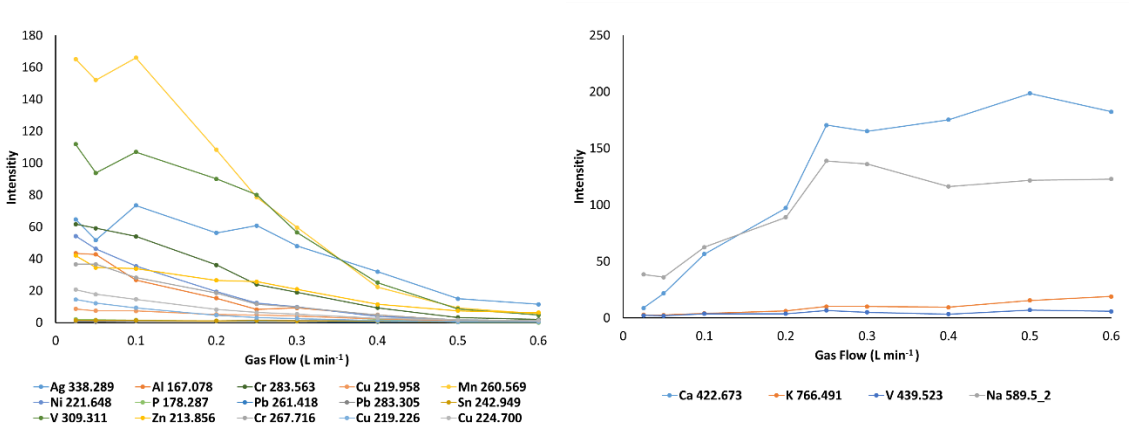

Figure 40. Corrected intensities for each wavelength and normalised vs. carrier gas flow.

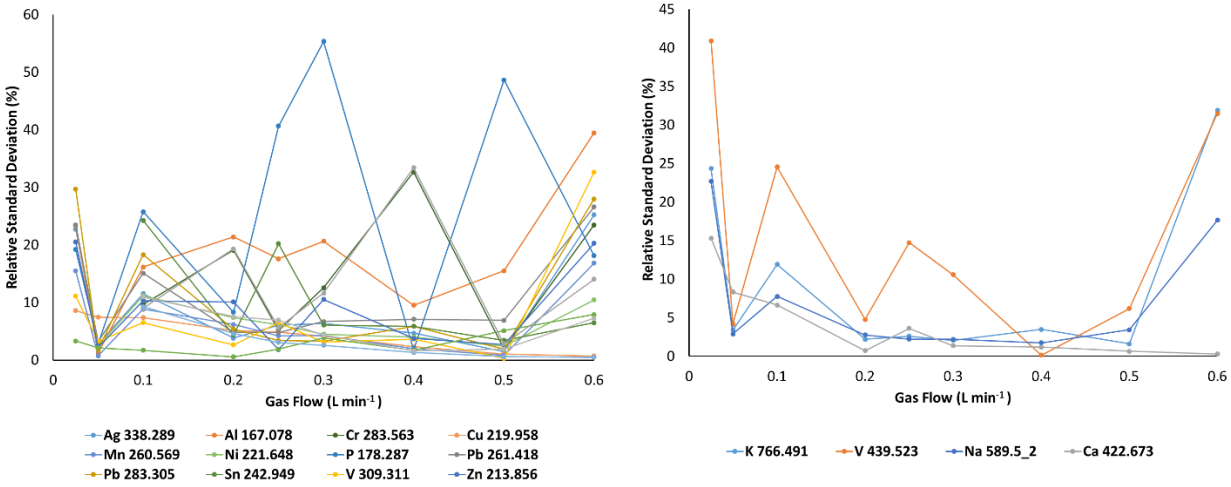

Figure 41. Relative standard deviation (n = 3) of each wavelength vs. carrier gas flow.

Finally, once both reaction and carrier gas flows were set up, the same procedure has been followed to evaluate the sensitivity concerning the different bypass gas rates. Figure 41, Figure 42 and Figure 43 show respectively the different sensitivities and relative standard

deviations obtained for different bypass flow rates. There is a flow rate that provides high intensities with a low relative standard deviation. Since a compromise had to be taken, the gas flow that has been chosen for the argon bypass was 0.15 L min^{-1}.

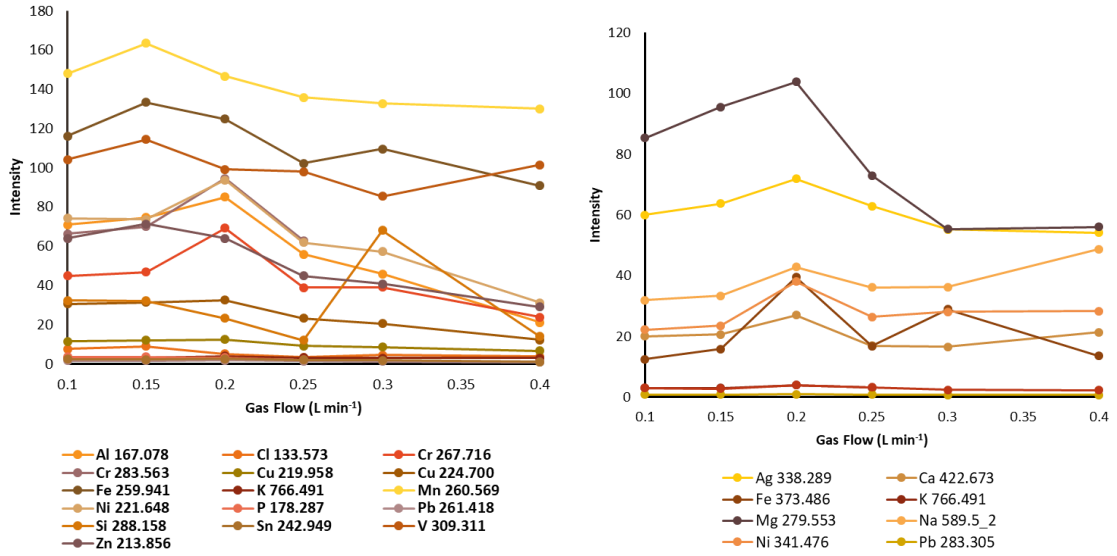

Figure 42. Corrected intensities for each wavelength and normalised vs. bypass gas flow.

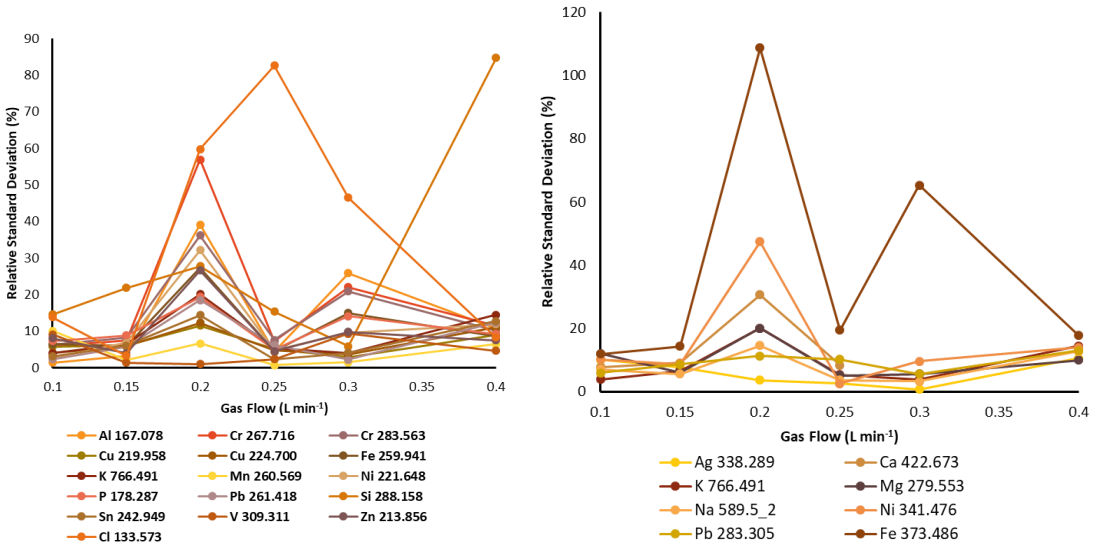

Figure 43. Relative standard deviation (n = 3) of each wavelength vs. bypass gas flow.

Once the three gas flows that control the electrothermal vaporisation process and the transportation of the analytes to the plasma were optimized, a calibration was carried out

to check the linearity of the method and its limit of detection for the different elements that have been analysed. Figure 44 shows the regression curve of three different elements analysed simultaneously in this experiment.

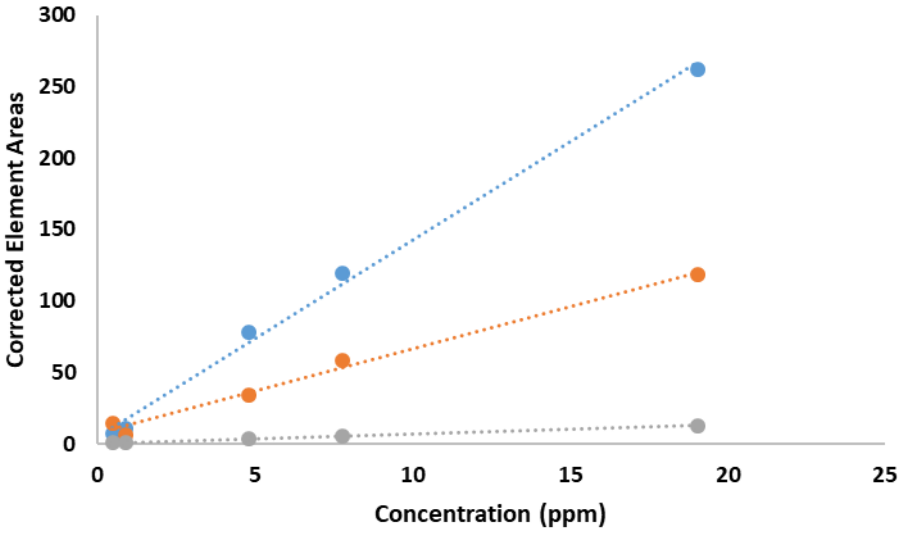

Figure 44. Regression curves obtained for three elements: Ag 338.289 nm (blue), Al 167.078 nm (orange) and K 766.491 (grey).

Table 3. R^2 coefficient for each analysed wavelength.

Element (Wavelength in nm)	R^2	Element (Wavelength in nm)	R^2
Ag (338.289)	0.990	Mn (260.569)	0.860
Al (167.078)	0.990	Na (589.502)	0.944
Ca (422.673)	0.994	Ni (221.648)	0.999
Cr (267.716)	0.997	Ni (341.476)	0.999
Cr (283.563)	0.992	P (178.287)	0.997
Cu (219.226)	0.998	Pb (261.418)	0.999
Cu (219.958)	0.998	Pb (283.305)	0.996
Cu (224.700)	0.998	Si (288.158)	0.493
Fe (259.941)	0.797	Sn (242.949)	0.999
Fe (373.486)	0.850	V (309.311)	0.897
K (766.491)	0.997	V (439.523)	0.969
Mg (279.553)	0.971	Zn (213.856)	0.992

In Table 3, the coefficients of determination for the different transient wavelength are depicted. In general, there is a great correlation between the concentration of each element and the intensities detected. However, certain elements like Fe do not have good linearity, probably due to the high presence of this element within the instrument joints, since the graphite furnace is placed inside of a steel compartment.

5.2.2. Method validation.

The quantitative analysis of a reference sample, SRM 1085b, has been carried out with this configuration with the purpose of validating the ETV-ICP-OES methodology that has been optimised.

The results, detailed in Table 4, show that the methodology that has been employed to carry out the analyses do not possess a very high precision. This fact might be associated with the use of a less-reactive reaction gas due to legislation issues.

However, the accuracy of the method is acceptable for the simultaneous quantification of up to 8 different elements. Considering that this method does not require any sample preparation but the dissolution of the sample in a solvent (in this case THF) and carrying out the standard additions, the results prove that this methodology could be established in the industry since it provides with cheaper and faster alternatives to other methodologies that might be more costly and slower.

Table 4. Concentrations in mg kg^{-1}, R^2 and detection limits in mg kg^{-1} determined for the SRM 1085b via ETV-ICP-OES.

Element	Certified Value	Measured Concentration	R^2	DL
Cr	302.9 ± 2.1	291 ± 55	0.992	0.14
Cu	295.6 ± 8.5	300 ± 111	0.968	0.27
Mg	297.3 ± 4.1	345 ± 34	0.997	0.08
Mn	289	334 ± 87	0.993	0.13
Ni	295.9 ± 7.4	287 ± 69	0.987	0.17
Pb	297.7 ± 6.8	247 ± 53	0.991	0.14
Sn	294	310 ± 85	0.987	0.23
V	297.8 ± 6.8	290 ± 26	0.991	0.14

Other elements, however, did not provide with good results. That is the case for phosphorus, aluminium, calcium, iron and zinc. The only reason why the analysis of these elements has not provided with a good result might be related to the quality of SF_6 as a reaction gas. The standard additions were performed using the Conostan S21 standard solution, which contains 100 ppm of 21 elements. Since these elements are dissolved in the standard matrix as salts, SF_6 may not be reactive enough to achieve the quantitative vaporisation of all the different element salts.

5.3.3. Speciation analysis of fast pyrolysis oils via ETV-ICP-OES

In order to obtain the elemental distribution of some of the trace elements present within different fast pyrolysis oils based on their evaporation/pyrolysis temperatures, the length of the analyses has been increased up to 250 seconds using a different temperature gradient. Figure 45 shows the temperature program that was designed for this experiment.

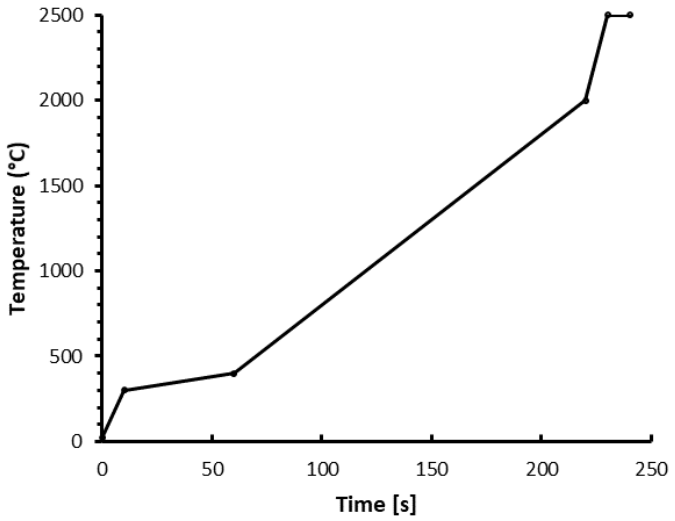

Figure 45. Temperature program for the speciation analysis of trace elements in fast pyrolysis oils via ETV-ICP-OES.

In this method, the temperature was initially increased up to 300 °C during the first 10 seconds of sequence. This temperature was then increased up to 400 °C during the following 50 seconds to eliminate all those volatile compounds that do not provide with useful information to the analysis (solvent, water, etc.). Then, a heating ramp of 10 °C s^{-1} was applied for 160 seconds until it reached 2000 °C. Finally, a last increase of the temperature up to 2500 °C was applied for 10 seconds and held for another 10 seconds to pyrolyze all those potential residual compounds that might have not been removed from the graphite boat, to be able to be reused.

All the samples were diluted (with a dilution factor of 10) in THF and 20 µL of each solution were deposited in the graphite boat by triplicate.

One of the trace elements, Phosphorous, and whose characterisation via GPC-ICP-HRMS was achieved for 4 of the following samples (Samples A, B, C and D), presents the ETV-ICP-OES distribution showed in Figure 46.

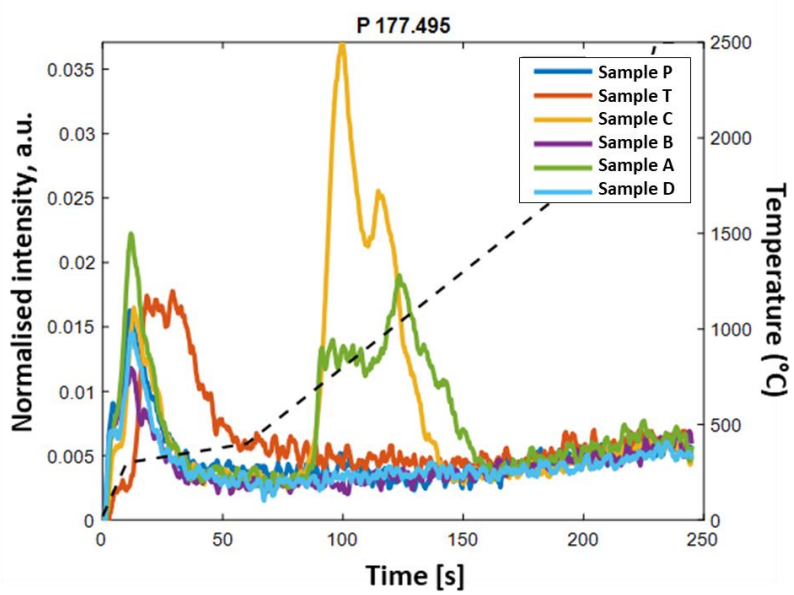

Figure 46. ETV-ICP-OES transient signal for P species in different fast pyrolysis oil samples.

From this distribution of the phosphorus species based on their evaporation temperature, it is possible to conclude that there exist at least two different species with a very different chemical nature. An early peak is observed for all the samples when the temperature has reached 300 °C, which is the temperature where the pyrolysis process takes place. This fact suggests that the phosphorus species could be covalently bonded to an organic compound. However, this peak is much broader in the tyres pyrolysis oil and it is observed at higher temperatures than for the rest of the samples. While the presence of phospholipids is evident in the feedstocks that were employed to produce the corresponding lignocellulosic fast pyrolysis oil, their presence in tyres might be justified since the tyre's thread has been fabricated from rubber and phosphorus compounds, such as orthophosphates, sugar phosphates and phospholipids that have been found in rubber analysis.[99] In order to confirm this hypothesis, a standard containing either phospholipids or other phosphate salts should be analysed with this current method: the temperature when the corresponding peaks are detected will determine whether any similarities are found with respect to the phosphorus peaks found in this sample set.

Concerning the peaks observed for the samples C and A (milorganite and the blend of milorganite and loblolly pine wood fast pyrolysis oils respectively) at a temperature of approximately 600 - 700 °C, they might be linked to the high presence of phosphorus

pentoxide in milorganite.[100] However, although the presence of this compound is expected in the milorganite:red oak blend pyrolysis oil, no peak is observed. Further analysis should be carried out, considering the analysis of P_2O_5 via ETV-ICP-OES to either confirm or reject this hypothesis, since another potential cause of the presence of phosphorus in pyrolysis oils would be inefficient removal of ashes within the sample matrix during the fast pyrolysis process.[35]

In Figure 47, the transient signals obtained via ETV-ICP-OES for Na, Cr, Mn and Ca are shown for the same set of samples.

These four elements present almost the same distribution: only one peak with different widths presented for each sample, which agrees with the hypothesis that these species share the same chemical structure or reactivity with the reaction gas and suggests that the same compound is present on all the samples.

The presence of Na and Ca, which are very important nutrients in plants and essential element in the cell walls, is therefore justified, whereas the presence of Mn and Cr is assumed to be originated from the presence of these elements in soils as salts. Furthermore, these trace elements should be linked to non-volatile compounds: these peaks are detected when the graphite furnace was working at high temperatures (above 1000 °C), which agrees with the hypothesis that suggests that the presence of these trace elements in the pyrolysis oil samples is originated from the salts that are present in the soils.

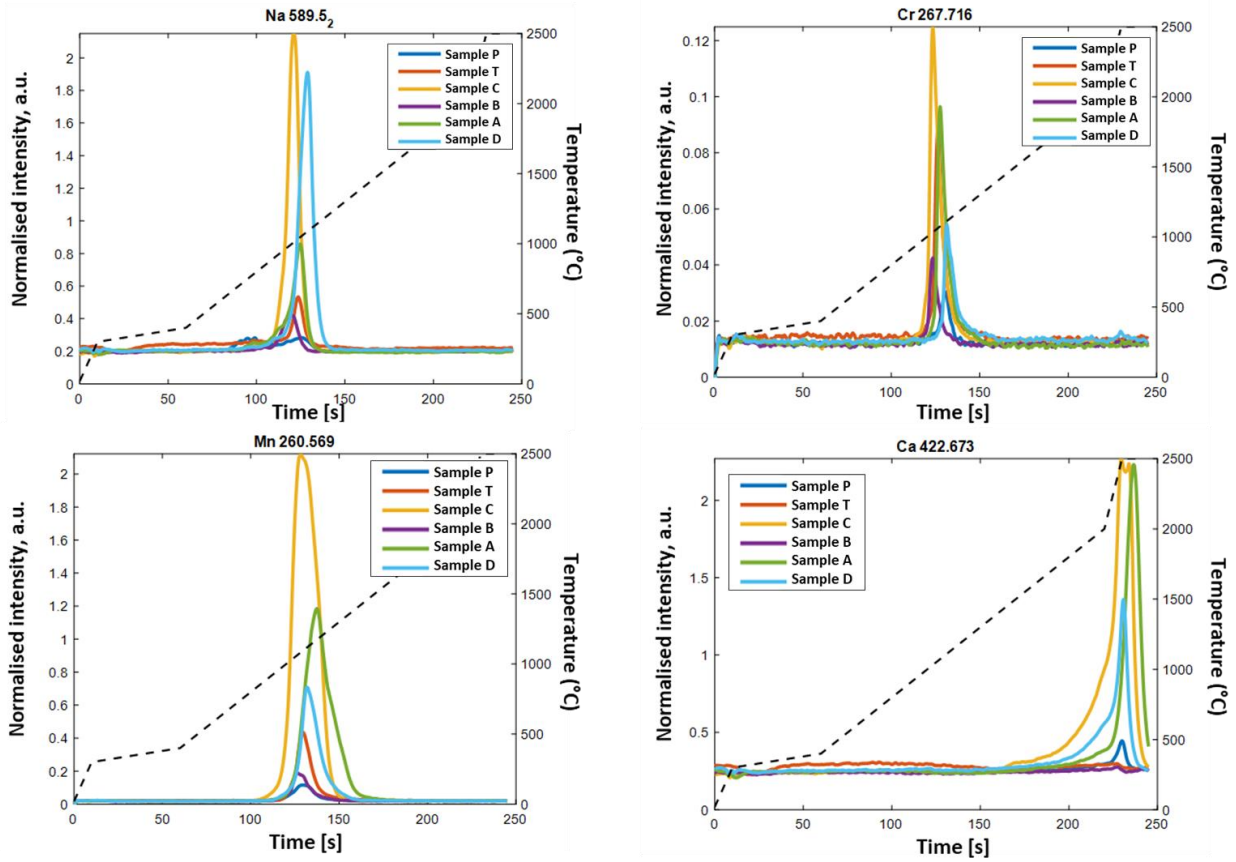

Figure 47. ETV-ICP-OES transient signal for Na, Cr, Mn and Ca species in different fast pyrolysis oil samples.

Not only monomodal distributions are found by ETV-ICP-OES. Figure 48 shows the transient signals measured for the wavelengths corresponding to K, Mg, Al and Zn in the same set of samples.

Concerning the analysis of potassium, a high abundance of this element can be observed in the sample C (milorganite pyrolysis oil). This high abundance was expected since milorganite possesses a high concentration of K_2O, which constitutes an essential nutrient for plants. [100] The analysis of potassium oxide via ETV-ICP-OES would allow the confirmation of this hypothesis. However, since this compound is not expected to be found at high concentrations in other natural materials, such as red oak wood (120D), the presence of a peak within the transient signal for its corresponding pyrolysis oil might indicate a presence of potassium salts in the sample. Magnesium, however, presents peaks that can be observed when very high temperatures are applied. Magnesium is expected to

be found in this type of samples since Mg^{2+} is present within the chemical structure of chlorophyll.

The aluminium ETV-ICP-OES distribution is one of the most interesting. At least four different compounds containing these elements are expected from the distribution of the transient. Temperatures above 500 °C suggest the presence of aluminium as salts, although a bad elimination of ashes from the fast pyrolysis oil would be another cause. Aluminium is a very abundant element in the earth's crust, its higher presence within the lignocellulosic pyrolysis oil than within the tyres pyrolysis oil agrees with the data obtained with this methodology.

Finally, concerning zinc, the data suggests that at least two different species are present within the samples that have been analysed (bimodal distributions). As one of the essential micronutrients within the cell plants, its presence within these samples was expected. However, a monomodal distribution with a high abundance has been found for the tyres fast pyrolysis oil: zinc is highly present within the tyres' pyrolysis ashes. However, with this methodology, it is not possible to confirm the hypothesis of the presence of ashes within the samples without the analysis of a reference ash containing zinc.

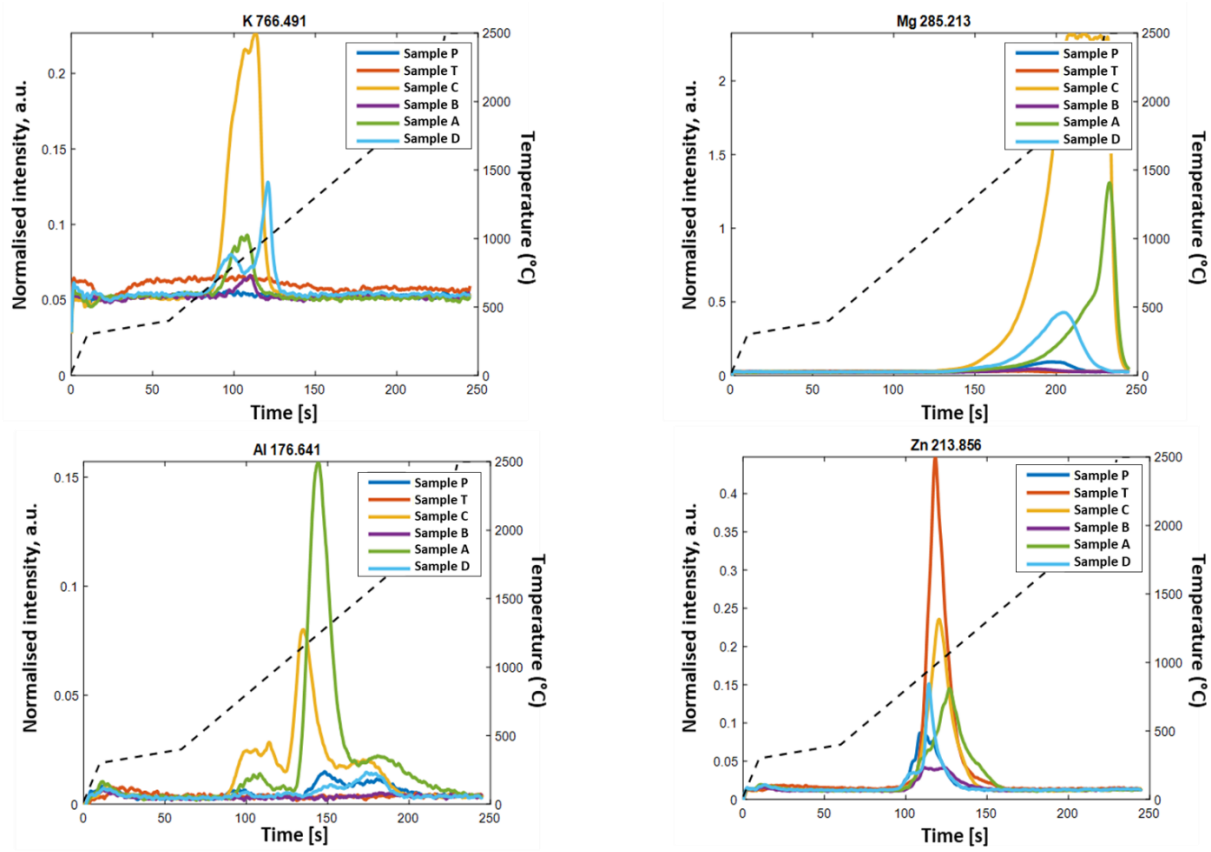

Figure 48. ETV-ICP-OES transient signal K, Mg, Al and Zn species in different fast pyrolysis oil samples.

5.4. Conclusion

The development of a methodology that allows not only the speciation analysis of trace elements via ETV-ICP-OES but as well the quantitative analysis of certain trace elements in complex samples has been achieved and validated for certain elements. This methodology, which uses SF_6 as a reaction gas, has shown a lower efficiency than previous methodologies that used gases with a higher reactivity and whose commercialisation has been forbidden by the public institutions.

By using ETV-ICP-OES, the industry could be benefitted from a very fast methodology that does not require very expensive instrumentation. While the presence of ICP-OES instruments is quite common in this sector, coupling it to an electrothermal vaporiser should be an easy task.

However, further experiments must be carried out to fully determine the speciation of these trace elements present within this set of samples: while the analysis of standards, such as phospholipids and salts, would help with the identification of the peaks that have been obtained with this methodology.

CHAPTER 6: IMPORTANCE OF GPC-ICP-HRMS ON THE SPECIATION ANALYSIS OF COMPLEX MATRICES

This chapter focuses on the great advantages of coupling gel permeation chromatography and inductively coupled plasma mass spectrometry to carry out speciation analysis in complex matrices.

Although the topic of this thesis consists of the speciation analysis of bio-oils, familiarisation with the instrumentation that was going to be used through this PhD project had to be done. Thus, through collaborations with Haldor Topsoe, a Danish company specialised in the production of heterogeneous catalysts and the design of catalytic processes, different samples were received to get a better understanding of their elemental composition through two very important catalytical processes designed to improve the quality of crude oil with the elimination of the different compounds containing V, Ni and S within its matrix: Hydrodemetallization (HDM) and Hydrodesulfurization (HDS). In addition, one of the sub-objectives of this thesis (**O2a**) was fulfilled, confirming the hypothesis that suggested that a different reaction pathway might occur for the different species present in this type of samples.

Performing inorganic speciation analysis of such complex matrices via GPC-ICP-HRMS was a success. Fingerprints of the V, Ni and S aggregates present in atmospheric residue samples, based on their molecular size, have been obtained at different stages of the respective catalytical processes, providing insights into the catalyst behaviour concerning the different hetero-compounds present within such complex samples.

Future analyses should be carried out in order to fully understand the composition of these aggregates. One of the techniques that might provide with this information is the FT-ICR-MS since its high-resolution power will allow the full identification of each of the aggregates that were detected via GPC-ICP-MS.

6.1. Crude oil composition and its derivates

Crude oil, also known as petroleum, is a black liquid that consists of a naturally occurring mixture of hydrocarbons and other complex organic compounds that can be found in several geological formations (also known as petroleum reservoirs) which are located beneath the earth's surface. Crude oil has been the most used source of primary energy in terms of heating, transportation and production of energy. During 2019, the production of crude oil reached an average of 2.2 millions of barrels per day.[101]

As it has been already mentioned, hydrocarbons such as alkanes, cycloalkanes and aromatic hydrocarbons are the main components of crude oil: carbon and hydrogen can represent between 83-87% and 11-14% of its mass composition.[102] These hydrocarbons can be separated through a distillation process that is carried out in the petroleum refineries. Figure 49 shows the typical distillation cuts that are obtained from crude oil.

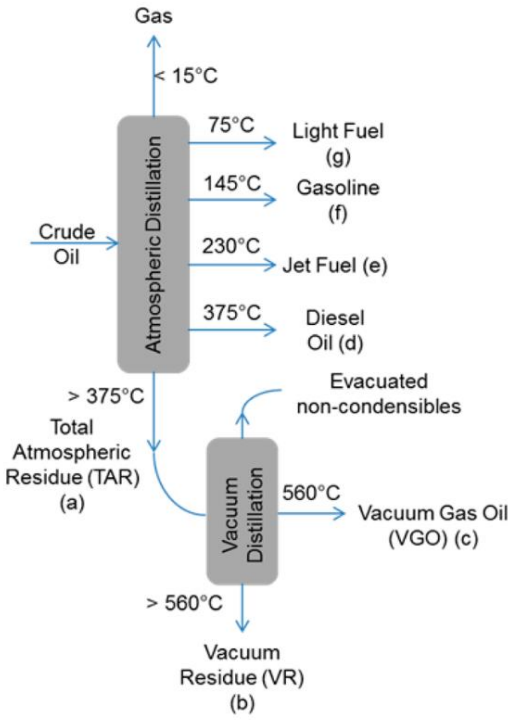

Figure 49. Schematic representation of the crude oil distillation cuts.[73]

Apart from their main composition based on hydrocarbons, crude oils also contain low percentages of hetero-elements such as sulfur (0.04-8%), oxygen, nitrogen and other metals, such as vanadium and nickel, with concentrations that are at the ppm levels. Their presence consists of an issue in terms of corrosion and reduction of the efficiency of the catalysts during the refining process. Besides, their presence can also contribute to the emission of environmental pollutants. [102]

The upcoming shortage of crude oil reserves is accelerating the research on alternative sources of hydrocarbon fuels. One of these alternatives consists of the conversion of the heavy distillation fractions of crude oil into transportation fuels.

Atmospheric residue, which is one of the heavy fractions of crude oil, consists of a mixture of hydrocarbons that have carbon numbers greater than C11 and boiling temperatures above 200 °C.[103] These crude oil cuts have a higher content of hetero-elements, which are pre-concentrated during the distillation process and remain within this residue. Hence the need for carrying out two very important processes that will guarantee that none of these hetero-compounds is present in the products: Hydrodemetallization and Hydrodesulfurization. Both processes will be shortly explained in the publication enclosed in this chapter.

In this chapter, the results on the speciation analysis of V, Ni and S in atmospheric residue is reported through the article (**Article 2**) published in "Fuel Processing Technology" in December 2019: "Understanding the removal of V, Ni and S in crude oil atmospheric residue hydrodemetallization and hydrodesulfurization.

This study has provided with very valuable information related to the size distributions of the S, Ni and V species present in atmospheric residue feedstocks and how their size distributions change during the HDM and HDS processes. One detail that has not been mentioned in the following article is that, in Figures 2 and 4, a little shift can be observed from the feed peak with respect to the product peaks. Further investigations should be carried out in order to clarify whether any type of aggregation process has occurred. The analysis of both feed and products via FT-ICR-MS could provide with useful information about this topic.

6.2. Understanding the removal of V, Ni and S in crude oil atmospheric residue hydrodemetallization and hydrodesulfurization

Fuel Processing Technology 201 (2020) 106341

Contents lists available at ScienceDirect

Fuel Processing Technology

journal homepage: www.elsevier.com/locate/fuproc

Understanding the removal of V, Ni and S in crude oil atmospheric residue hydrodemetallization and hydrodesulfurization

Victor Garcia-Montoto[a,b], Sylvain Verdier[c], Zeina Maroun[c], Rasmus Egeberg[c], Joan L. Tiedje[c], Sara Sandersen[c], Per Zeuthen[c], Brice Bouyssiere[a,*]

[a] Universite de Pau et des Pays de l'Adour, E2S UPPA, CNRS, IPREM, Institut des Sciences Analytiques et de Physico-chimie pour l'Environnement et les Materiaux, UMR5254, Hélioparc, 64053 Pau, France
[b] Department of Plant and Environmental Sciences, University of Copenhagen, Thorvaldsensvej, 40, Frederiksberg C, Denmark
[c] Haldor Topsoe A/S, Haldor Topsøes allé 1, 2800 Kgs. Lyngby, Denmark

ARTICLE INFO

Keywords:
Vanadium
Nickel
Sulfur
Demetallization
Desulfurization
Catalysis
Residue
GPC

ABSTRACT

This study describes the use of gel permeation chromatography inductively coupled plasma high-resolution mass spectrometry (GPC ICP HRMS) to examine and explain two important petroleum industry catalytic processes: hydrodemetallization (HDM) and hydrodesulfurization (HDS).

The sulfur, nickel and vanadium species size distributions in atmospheric residue fractions were studied to track their evolution during both catalytic processes and examine their mechanisms, especially those mechanisms linked to changes in temperature and initial deactivation via coke laydown. Chromatogram shapes as well as peak areas were used to study the V, Ni and S aggregate types and concentrations in the feedstock as well as in the product after varying the operating temperature and residence time at a constant temperature. For the V and Ni compounds, the low and medium molecular weight (LMW and MMW, respectively) aggregates are easily hydrotreated under all conditions, while the high molecular weight (HMW) compounds are more refractory. For the S compounds, a different reactivity pattern was observed whereby the LMW, MMW and HMW aggregates were more similar in their reactivity, showing that the catalyst is less selective towards a certain aggregate size for the S compounds compared to the V or Ni compounds.

1. Introduction

Hydroprocessing atmospheric residues using fixed-bed reactors is a mature technology that has been extensively studied, and close to 100 units are in operation across the globe [1]. Most of these units are located in Asia and the Middle East, and the total catalyst demand is estimated to be approximately 50,000 tons/year. This technology is still relevant for many refineries as it can address key issues faced by the refining industry. For example, environmental specifications are getting stricter for bunker fuels as the revised MARPOL Annex VI will reduce the sulfur cap from 3.5 to 0.5 wt% from 2020 on. Furthermore, heavier crude oils are being processed, and those feedstocks require residue technologies such as atmospheric residue desulfurization (ARDS).

Among the numerous elements present in crude oil, the most abundant and undesirable elements are sulfur, vanadium and nickel [2], which have negative effects, such as catalyst poisoning, fouling and equipment corrosion [3,4]. The presence of sulfur compounds causes environmental and health problems as well, with the emission of toxic S species into the atmosphere [5,6]. With the purpose of reducing these undesirable effects, catalytic removal of these elements is currently carried out in the industry, especially for atmospheric and vacuum residue oils, whose content of these elements is much higher.

The ARDS process will be briefly described below, but various detailed reviews and their respective references can be consulted for further information about the process and its evaluation [1,7,8]. The process consists of downflow trickle bed reactors in series with the following catalyst loading distributed across several reactors [9]: large-pore guard hydrodemetallization (HDM) catalyst (whose function is to trap V, Ni and As), a smaller-pore transition catalyst combining HDM and hydrodesulfurization (HDS) activities and a third catalyst with a higher HDS activity. The deactivation mechanisms of the catalysts in such a service have also been widely studied over the years [10]. The initial step, which is quite rapid, is mostly due to coke formation [11]. This step is followed by a slower deactivation phase during which metals gradually cover the catalyst surface [12]. The last phase is a rapid loss of activity where the metals and coke create pore plugging or

* Corresponding author.
E-mail address: brice.bouyssiere@univ-pau.fr (B. Bouyssiere).

https://doi.org/10.1016/j.fuproc.2020.106341
Received 5 December 2019; Received in revised form 10 January 2020; Accepted 10 January 2020
Available online 25 January 2020
0378-3820/ © 2020 Elsevier B.V. All rights reserved.

restrict access to the pore structure.

Many ARDS units are operated to obtain a fixed sulfur or Conradson carbon residue (CCR) content in the product. However, due to the difficult nature of the feedstock (high amount of metals and coke precursors), many challenges are encountered: short cycle length due to high deactivation rates, pressure-drop issues due to coking, demanding catalyst unloading process, long turnarounds (typically one month), etc. To minimize these issues, it is crucial that the optimal ratio between the HDM, HDM/HDS and HDS catalysts is determined for each specific ARDS unit.

The total amounts of Ni, V or S are an important piece of information here but do not provide any information about the nature of the molecules containing these elements. Therefore, speciation of the metals in the various feedstocks is an asset in regard to understanding the feed reactivity and the influence on the various deactivation mechanisms and ultimately in optimizing the catalyst loading. One option is to use inorganic speciation in crude oil that has been developed by using size exclusion chromatography in an organic solvent linked with a high-resolution mass spectrometer working as the detector. This technique is referred to as gel permeation chromatography (GPC) and employs an organic solvent to perform the analysis, in this case tetrahydrofurane (THF) [4]. In this technique, the compounds are separated according to their hydrodynamic volumes, which in the case of these samples follow the molecular weights of the nanoaggregates and molecules that are present in the sample. By dissolving the sample in THF, it is possible to obtain a fingerprint of the molecular distribution of the species present in the sample and evaluate how the concentrations of each fraction increase or decrease as a function of the industrial process carried out.

Pohl et al. [13] successfully used this method for two crude oils and two residue fractions and managed to map and fingerprint V, Ni, S, Fe, Co, Cr, Zn and Si. The distributions between high molecular weight (HMW) aggregates (possibly asphaltene structures), medium molecular weight (MMW) aggregates and low molecular weight (LMW) compounds (possibly free metal porphyrins and non-porphyrinic complexes) differ significantly between these samples, which will affect the HDM and HDS activities and their relative deactivation rates. Gascon et al. [14] used the same approach on the Saturate, Aromatic, Resin and Asphaltene (SARA) fractions of four crude oils, one atmospheric residue and one vacuum residue. The amount of each type of aggregate (HMW, MMW and LMW) was calculated, and significant variations can be observed among the four crude oils and their residue fractions. However, to understand the significance of these variations in the ARDS process, it is necessary to study not only the feedstock but also the hydrotreated product to understand the reactivity of the various types of aggregates.

With an increasing demand for low-sulfur fuel oil (LSFO), refineries are starting to consider alternative usages for their ARDS units, for example, by coprocessing vacuum residues, which are typically processed in ebullated bed reactors due to the high amount of metals and asphaltenes in this type of feed, which causes an extremely rapid deactivation of the catalyst. A feedstock change often requires changing the operating conditions in the unit (e.g., by lowering the feed rate to lower the liquid hourly space velocity) and redesigning the catalyst loading. The latter is not always straightforward, as it requires a very thorough understanding of the feed and its effect on the catalyst activity throughout the entire cycle to avoid untimely shutdowns. To this end, a better understanding of not only the feed properties (contents of sulfur, nitrogen, asphaltene, etc.) but also the molecular composition is invaluable. Thus, in this paper, two ARDS pilot plant studies are reported. In study A, the temperature was adjusted from 375 to 385 °C to evaluate its influence on the reactivity of the various sulfur, nickel and vanadium species. In study B, the fate of sulfur, nickel and vanadium nanoaggregates was monitored under constant operating conditions to examine the role of the initial coke laydown on the HDM and HDS reactions.

2. Materials and methods

2.1. Instrumentation

A quantitative analysis of all the feedstocks was carried out with the purpose of determining the mass variations of the target elements by using inductively coupled plasma mass spectrometry (ICP-MS). The principle of the method is to determine the total amount of xylene-soluble Ni and V compounds with inductively coupled plasma mass spectrometry (ICP-MS) after suitable dilution of the petroleum/petroleum product sample by weight with xylene. The vanadium and nickel contents are quantified by ICP-MS using a vanadium-isotope mass of 51 and a nickel-isotope mass of 60 through comparison with calibration curves obtained via 500 wt ppm Conostan organometallic V and Ni standards diluted with xylene. Scandium is used as an internal standard to correct for drift and matrix effects. The removal of molecular interferences in the ICP-MS analysis was performed with helium kinetic energy discrimination. EnviroMAT used-oil matrix reference material containing V and Ni was analyzed with each sample batch to monitor the analysis accuracy. The physico-chemical properties of the feeds and products were measured using the following standard methods: Nitrogen (ASTM D5762), Sulfur (ASTM D 4294), Hydrogen (ASTM D 7171 H), asphaltene (ASTM D6560), microcarbon residue (MCR) (ASTM D4530), specific gravity (SG) (ASTM D4052), and simulated distillation (ASTM D7169). Carbon (wt%) content was calculated by difference with 100% with N, S and H content.

All the speciation analyses were carried out with a Thermo Scientific Element XR double focusing sector field ICP-MS (Thermo Fisher, Germany) instrument accessing the spectrally interfered isotopes of ^{32}S, ^{51}V and ^{58}Ni at a resolution of 4000 (medium resolution). The mass spectrometer was equipped with a quartz injector (1.0 mm inner diameter (i.d.)), a Pt sampler cone (1.1 mm orifice diameter) and a Pt skimmer cone (0.8 mm orifice diameter). An O_2 gas flow of 0.08 mL/min was included to avoid carbon deposition. Both the instrument and mass calibration settings were optimized daily at resolutions of 300 (low resolution) and 4000. A medium resolution avoids the spectral interference of O_2 on the ^{32}S isotope. These optimizations were carried out using a tuning solution containing 1.0 ng g-1 of Ag, Al, B, Ba, Ca, Cd, Co, Cr, Cu, Fe, In, K, Li, Mg, Mn, Mo, Na, Ni, P, Pb, Sc, Si, Sn, Ti, V, Zn and Y in tetrahydrofuran (THF). A mass offset was also applied to compensate for the mass drift coming from the sector field magnet [15,16].

The mass spectrometer was equipped with a modified DS-5 microflow total consumption nebulizer (CETAC, Omaha, NE) mounted with a laboratory-made jacketed spray chamber heated to 60 °C by a water/glycol mixture working with a temperature-controller bath circulator Neslab RTE-111 (Thermo Fisher Scientific, Waltham, MA) [17].

The chromatographic separation was carried out using three Waters (Waters Corporation, Milford, MA) styrene-divinylbenzene gel permeation columns (7.8 mm i.d. and 300 mm length). These three columns included an HR4 column (particle size of 5 μm with an exclusion limit of 600,000 Da of polystyrene equivalent), an HR2 column (particle size of 5 μm with an exclusion limit of 20,000 Da) and an HR0.5 column (particle size of 5 μm and an exclusion limit of 1000 Da of polystyrene equivalent). A Dionex high-performance liquid chromatography (HPLC) system fitted with an UltiMate 3000 microflow pump, an UltiMate 3000 autosampler and a low port-to-port dead-volume microinjection valve were used to deliver the carrier solution and mobile phase. To prevent possible damage to the GPC columns, a Styragel guard column (4.6 mm i.d. and 30 mm length) was also fitted between the columns and the pumping system.

2.1.1. Methodology

One feed, which is a blend of 93% of atmospheric residue (ATM) and 7% vacuum residue (VAC), was hydrotreated under different conditions for the purpose of evaluating and understanding the removal of

the target compounds by applying the method optimized by Desprez et al. [16] and Vargas et al. [18]. These researchers studied the size distributions of V, Ni and S and established the integration intervals for HMW, MMW and LMW aggregates in crude oil as follows: 1100–1400 s (18–23 mL of eluted sample) for HMW compounds, 1400–1600 s (23–27 mL) for MMW compounds and above 1600 s (< 27 mL) for LMW compounds. The comparison of the different sizes of species will provide useful information about the removal of target compounds.

In addition, with the purpose of monitoring the stability of the ICP HR MS intensities, analysis of known crude oil samples, whose composition had been studied previously, was periodically carried out.

2.1.2. Reagents, samples and solutions

Tetrahydrofuran, multisolvent GPC grade, ACS, stabilized with 250 ppm of butylated hydroxytoluene (BHT) (Scharlau, Spain) to prevent the formation of peroxides, was used both for sample preparation and for chromatographic elution.

All the atmospheric residue crude oil feeds were provided by Haldor Topsoe (Denmark), and the feeds were analyzed by diluting them in THF at dilution factors of 50 for the 93% ATM/7% VAC feed blend and of 5 for the products.

2.2. Pilot plant testing

The pilot tests were performed in a once-through downflow trickle bed pilot plant located in Haldor Topsoe's R&D facilities. The unit consists of two reactors in series. The product was first separated in a high-pressure separator (HPS). The liquid product from the HPS was sent to a low-pressure separator (LPS) and to a stripper for removal of gases and other noncondensed light hydrocarbons. Nitrogen was used as the stripping agent, and once-through pure hydrogen was used. The catalyst was diluted with an inert material (mesh 60 carborundum) using a 25 vol% SiC/75 vol% catalyst ratio. The operating conditions are given in Table 1 for study A (influence of the temperature) and study B (influence of the initial deactivation). The feed properties are listed in Table 2. The results of study A are summarized in Table 3, and the results of study B are provided in Table 4. Note that the catalysts loaded were commercial catalysts used in residue service developed and produced by Haldor Topsoe A/S.

3. Results and discussion

3.1. Feedstock properties and fingerprints of the metal complexes in the feedstocks

The physico-chemical properties of the atmospheric and vacuum residues as well as those of the blends are listed in Table 2. The properties are in line with those of the typical atmospheric and vacuum residues reported in the literature [1]. It is interesting to note that there is a factor of 2 difference between the two residues with respect to the Ni, V, asphaltene and MCR contents.

When two feeds are blended, it is important to check whether aggregation phenomena occur as these aggregates may influence the asphaltene stability and thereby the residue hydrotreating process. As shown in Fig. 1, the theoretical blend (i.e., the calculated profile based on the analysis of the atmospheric and vacuum residues) and the physical blend show the same distribution, indicating that no nanoaggregation occurs. It should be noted that this finding could be a consequence of the fractions stemming from the same crude oil. Indeed, trimodal size distributions are observed for both the V and Ni compounds present in these feedstocks, while a less pronounced trimodal distribution, much richer in MMW aggregates, is observed for the sulfur compounds.

The size distributions of different crude oils and residues were studied elsewhere [14], showing the presence of HMW, MMW and LMW nanoaggregates, and the HMW compounds were the most abundant in Ni and V, while the MMW nanoaggregates were most abundant in S. The results obtained in this study are consistent with these previous results.

Table 1
Operating conditions of the pilot plant tests.

Inlet pressure hydrogen (barg)	165
H_2/oil (mL/L)	550
Overall liquid hourly space velocity (LHSV) (h^{-1})	0.2

Table 2
Feed properties.

Property	Method	Atmospheric residue (ATM)	Vacuum residue (VAC)	Blend 93 vol% ATM and 7 vol% VAC
Nitrogen, wt ppm	D 5762	2800	4500	3100
Sulfur, wt%	D 4294	3.985	5.00	4.061
Hydrogen, wt%	D 7171H	10.75	(11.18)[a]	10.78
C, wt%	By difference	85.0	83.4	84.8
H/C	–	0.13	0.13	0.13
SG 60/60 °F	D 4052	0.9797	–	0.9847
Density at 40 °C, g/ml	D 4052	0.9621	–	0.9672
Nickel, wt ppm	ICP-MS	21.1	42.4	27.0
Vanadium, wt ppm	ICP-MS	61.1	121	73.0
Carbon Residue, wt%	D 4530	12.02	24.42	12.96
Asphalthenes, wt%	D 6560	5.1	11.0	6.4
Simulated Distilation	D 7169			
0.5 wt% (IBP), °C		221	415	235
5 wt%, °C		341	515	353
10 wt%, °C		378	542	388
30 wt%, °C		454	600	467
50 wt%, °C		535	649	546
70 wt%,°C		614	709	627
80 wt%, °C		665	–	676
85 wt%, °C		698	–	705
90 wt%, °C		736	–	–
95 wt%, °C		–	–	–
99.5 wt% (FBP), °C		–	–	–

[a] H content back-calculated from the properties of the atmospheric residue and of the blend assuming that volume and weight fractions are equivalent as density could not be measured for the vaccum residue.

Table 3
Results of study a (influence of the temperature).

Sample type		Feed	Product	Product	Product
Run time, hours			1003	1101	1337
Temperature of the reactor, °C			375	380	385
Sulfur, wt%	ASTM D4294	4.061	0.446	0.349	0.291
Nickel, wt ppm	ICP-MS	27	5.16	4.12	3.62
Vanadium, wt ppm	ICP-MS	73	8.61	6.65	5.85
Asphaltenes, wt%	ASTM D6560	6.4	1.4	1.2	1.6
Simulated distillation	ASTM D7169				
0.5 wt% (IBP), °C		235	142	142	128
5 wt%, °C		353	258	244	234
10 wt%, °C		388	306	295	285
30 wt%, °C		467	399	391	394
50 wt%, °C		546	466	456	464
70 wt%,°C		627	541	532	542
80 wt%, °C		676	579	572	586
85 wt%, °C		705	603	595	612
90 wt%, °C		–	630	623	641
95 wt%, °C		–	665	658	678
99.5 wt% (FBP), °C		–	721	721	717

Table 4
Results of study B (influence of the initial deactivation due to coke laydown).

Sample type		Feed	Product	Product	Product	Product
Run time, hours			23	52	76	100
Temperature of the reactor, °C			375	375	375	375
Sulfur, wt%	ASTM D4294	4.061	0.098	0.179	0.212	0.282
Nickel, wt ppm	ICP-MS	27	1.18	1.74	2.08	2.89
Vanadium, wt ppm	ICP-MS	73	2.02	2.84	3.25	4.32
Simulated Distillation	ASTM D7169					
0.5 wt% (IBP), °C		235	142	67	142	155
5 wt%, °C		353	249	247	260	272
10 wt%, °C		388	301	300	313	323
30 wt%, °C		467	407	403	415	421
50 wt%, °C		546	482	474	491	497
70 wt%,°C		627	572	553	577	583
80 wt%, °C		676	632	598	632	639
85 wt%, °C		705	675	626	668	676
90 wt%, °C		–	–	659	716	721
95 wt%, °C		–	–	702	–	–
99.5 wt% (FBP), °C		–	–	–	–	–

3.2. Study A – influence of the temperature

3.2.1. Behavior of V and Ni

The evolution of the V and Ni species present in the feed after having been through the hydrotreating process at different temperatures has been studied. The samples were hydrotreated at the three different temperatures previously mentioned: 375 °C, 380 °C and 385 °C.

Fig. 2 shows that, as expected, at higher temperatures, more V, Ni and S species are removed. For V and Ni, the LMW and MMW aggregates are easily hydrotreated even at low temperatures, and as the temperature is increased, only the remaining HMW aggregates are hydrotreated. This phenomenon can be quantitatively observed in Fig. 3, where the concentration of each nanoaggregate size is determined based on the areas of the peaks (details of the integration method are available in the open literature) [15]. The concentration of LMW and MMW aggregates is negligibly small at all temperatures, while the concentration of HMW aggregates shows a linear decrease as a function of the temperature. The correlation coefficient of the slope is better for the regression of the HMW nanoaggregates compared to those of the MMW and LMW nanoaggregates, confirming that the temperature is driving the HMW hydrotreatment. From the slopes of these linear trends, as listed in Table 5, it can be readily observed that the HMW V aggregates are hydrotreated faster than the Ni aggregates. This observation is in agreement with previous results in the open literature [19].

3.2.2. Behavior of S

Interestingly, the fate of the S aggregates differs from that observed for the V and Ni aggregates. Figs. 2 and 3 show that the LMW and MMW S aggregates are not fully hydrotreated at the lowest temperatures. This phenomenon indicates that these LMW and MMW compounds are more refractory compared to the size-similar V and Ni compounds. It is also worth noting that a bimodal HMW-MMW S distribution is observed in the hydrotreated products, while this distribution was not clearly present in the feedstock. It is likely that a trimodal distribution occurs in the feedstock but is hidden due to the high concentration of aggregates eluting in the MMW range. These results show that S compounds/nanoaggregates with molecular weights between HMW and MMW are more easily removed, indicating that the catalyst possesses a higher efficiency for these kinds of nanoaggregates.

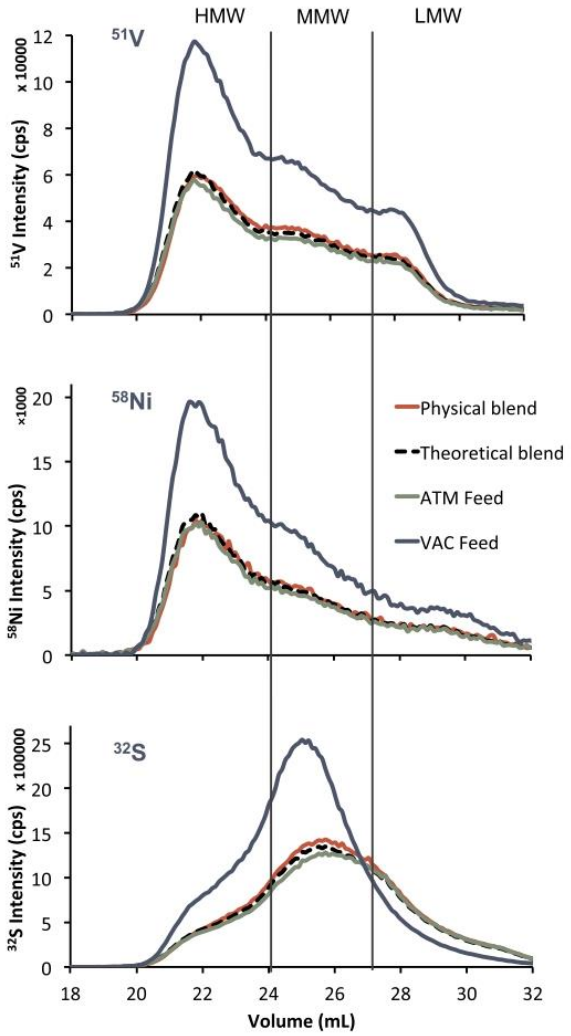

Fig. 1. GPC ICP HR MS chromatograms of the V, Ni and S species in the atmospheric residue feedstock (ATM, green line), vacuum residue (VAC, blue line), blend of 93 vol% ATM and 7% VAC (physical blend, red line) and theoretically reconstructed blend of 93 vol% ATM and 7 vol% VAC (black dashed line) based on individual ATM and VAC chromatograms. (For interpretation of the references to colour in this figure legend, the reader is referred to the web version of this article.)

3.3. Study B - initial deactivation due to coke laydown

The initial and fast deactivation during ARDS tests is due to coking and, more specifically, the strong initial adsorption of polyaromatic compounds, including N-containing molecules onto the surface of the catalyst [11]. In commercial units, the impact of the initial coke laydown on HDS and HDM is not simple to evaluate. For some units, it is clear that the HDM activity is more affected than the HDS activity during the first hundred hours. For other units, the initial deactivations of the HDS and HDM activities are equal, which depends on the catalyst loading, feed properties and operating conditions. Therefore, the goal of this study was to evaluate how the initial deactivation (which is due to coke laydown) affected the hydrotreatment rates of the various aggregates and if certain differences between the initial deactivations of HDM and HDS could be observed, which could be related to the

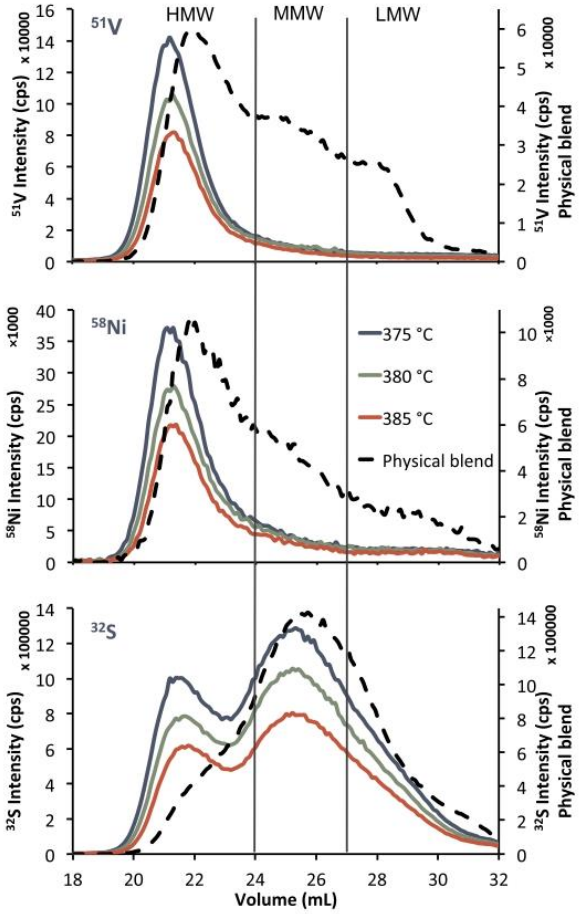

Fig. 2. GPC ICP HR MS chromatograms of the V, Ni and S species in the feed (black dashed line) and the product after having been hydrotreated at different temperatures (the hydrotreatments at 375 °C, 380 °C and 385 °C correspond to the blue, green and red lines, respectively). (For interpretation of the references to colour in this figure legend, the reader is referred to the web version of this article.)

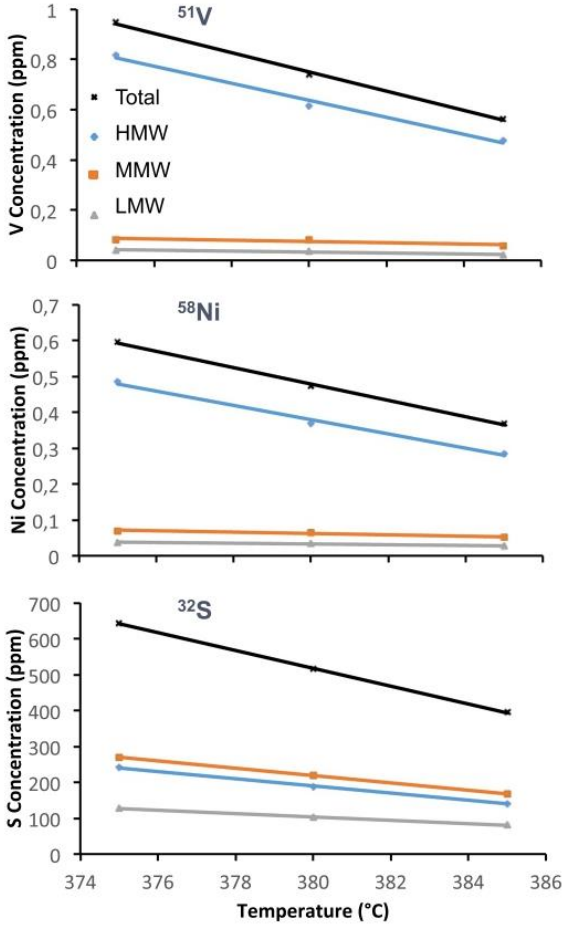

Fig. 3. The concentrations of V, Ni and S (total in black, HMW in blue, MMW in orange and LMW in gray) in the products that were hydrotreated at different temperatures quantified based on the total concentration and the GPC ICP HR MS chromatograms. (For interpretation of the references to colour in this figure legend, the reader is referred to the web version of this article.)

aggregate distribution. For this purpose, the temperature of the process was kept constant at 375 °C to evaluate the changes due to the initial catalyst deactivation (at 23, 52, 76 and 100 run hours).

3.3.1. Behavior of V and Ni

The evolution of the V and Ni species present in the feed after having been through the hydrotreating process at different times has been studied. As shown in Fig. 4, initially, the concentration of V and Ni species is very low, but during the first hours of the test, a steady increase in the total concentration of V and N is observed. Fig. 5 shows the quantitative description of this increase. This increase is almost entirely ascribed to an increase in the HMW fraction. It should be noted that most of the LMW and MMW aggregates are removed throughout the test despite the increasing deactivation (Table 6) of the catalyst, as indicated by the total product Ni and V contents listed in Table 4.

3.3.2. Behavior of S

In Fig. 4, it is observed that the sulfur species follow a different evolution. A bimodal distribution of the HMW and MMW peaks is observed, and its ratio has been calculated, resulting in an almost constant value. As shown more clearly in Fig. 5, the increase in S species is similar for the three groups of hydrodynamic volume distributions, which could indicate either a higher preference of the catalyst for the HMW species (if we compare the behavior of S with the behavior of V and Ni) or a more refractory behavior from the S species with the catalyst.

4. Conclusion

This study has provided innovative and valuable information related to the size distributions of the different species present in atmospheric residue feedstocks and how these distributions vary during HDS and HDM processes. Obtaining fingerprints of the metal aggregates in these feedstocks has provided us with a better understanding of their speciation in S, Ni and V. For the Ni and V aggregates, it was found that the HMW compounds are more refractory compared to the LMW and MMW compounds, which are removed at low temperatures or even after long run hours.

For the S aggregates, a slightly different behavior was observed whereby the LMW and MMW aggregates are not as easily hydrotreated, and in fact, the MMW nanoaggregates/compounds are slightly less easily hydrotreated compared to the HMW aggregates. This

Table 5
Slopes and regression coefficients for the variation in V, Ni and S concentrations vs. temperature.

	Total		HMW		MMW		LMW	
	Slope	r^2	Slope	r^2	Slope	r^2	Slope	r^2
V	−3.82 E-02	0.998	−3.39 E-02	0.988	−0.25 E-02	0.733	−0.19 E-02	0,965
Ni	−2.28 E-02	0.998	−1.98 E-02	0.992	−0.19 E-02	0.957	−0.10 E-02	0,879
S	−24.84	0.999	−9.955	0.997	−10.21	0.999	−4.678	0,999

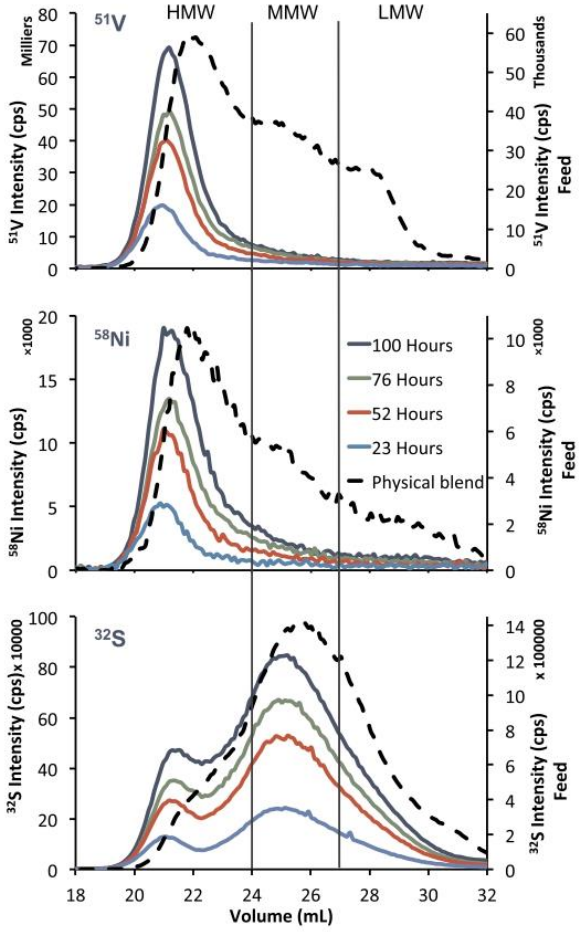

Fig. 4. GPC ICP HR MS chromatograms of the V, Ni and S species in the feed (black dashed line) and the product for different run times after having been hydrotreated at the same temperature (the run times of 23 h, 52 h, 76 h and 100 h correspond to the light blue, red, green and blue lines, respectively). (For interpretation of the references to colour in this figure legend, the reader is referred to the web version of this article.)

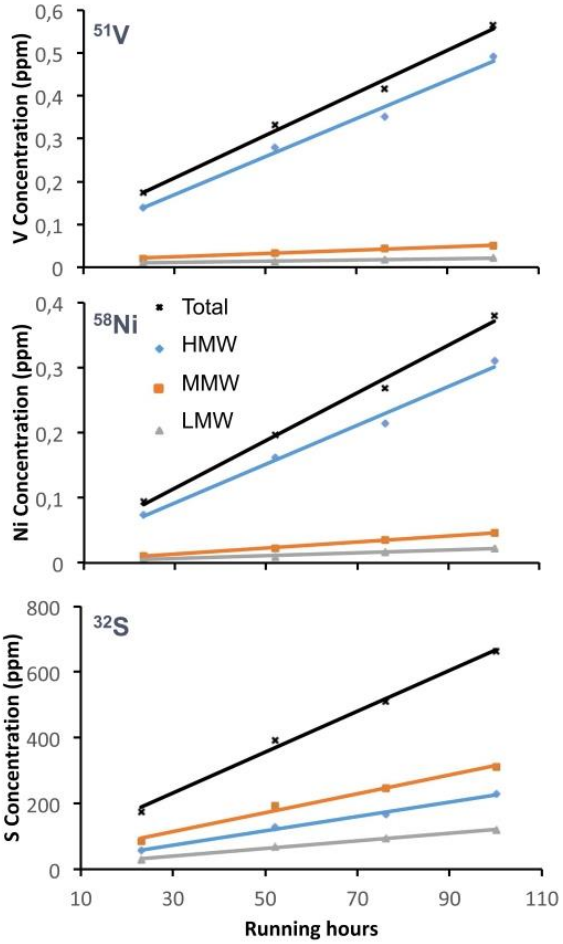

Fig. 5. The concentrations of V, Ni and S (total in black, HMW in blue, MMW in orange and LMW in gray) in the products that were hydrotreated for different run times quantified based on the total concentration and the GPC ICP HR MS chromatograms. (For interpretation of the references to colour in this figure legend, the reader is referred to the web version of this article.)

phenomenon illustrates the inherent difference in chemical composition of the metallo-organic compounds compared to the sulfur-containing compounds and their reactivity. In a previous study [15,20,21] free porphyrinic compounds were easily removed, possibly via easy access of the molecules to the catalyzer. Of the HMW nanoaggregate part, only a small portion can be easily removed, which can be the porphyrins linked at the surface of the nanoaggregates [15], but the Ni and V compounds that are located deeper in the nanoaggregates are more difficult to remove as the shell of the nanoaggregates has to be removed first before the V and Ni compounds can access the catalyst. In regard to the S compounds, the observed behavior seems to me driven more by the types of S compounds than by the aggregation states of the S compounds. Here, the molecular conformation of the S compounds needs to be studied. More in-depth molecular studies have to be conducted.

Nevertheless, this study provides insights into the catalyst preference towards these compounds/nanoaggregates, which is an important factor for future optimization of the balance between the HDM and HDS catalysts for those ARDS units processing different feedstocks with different V, Ni and S nanoaggregate distributions.

Table 6
Slopes and regression coefficients for the variation in V, Ni and S concentration vs. run time (hours).

	Total		HMW		MMW		LMW	
	Slope	r^2	Slope	r^2	Slope	r^2	Slope	r^2
V	4.96 E-03	0.991	4.44 E-03	0.987	0.38 E − 03	0.989	0.14 E − 03	0,997
Ni	3.66 E-03	0.993	2.98 E − 03	0.989	0.46 E − 03	0.997	0.22 E − 03	0,966
S	6,22	0.994	2.19	0.994	2.87	0.990	1.16	0,995

Funding sources

The authors declare no competing financial interest.

CRediT authorship contribution statement

Victor Garcia-Montoto: Investigation, Visualization, Writing - original draft. **Sylvain Verdier:** Supervision, Resources, Writing - original draft. **Zeina Maroun:** Resources, Writing - original draft. **Rasmus Egeberg:** Resources, Writing - original draft. **Joan L. Tiedje:** Resources, Writing - original draft. **Sara Sandersen:** Resources, Writing - original draft. **Per Zeuthen:** Resources, Writing - original draft. **Brice Bouyssiere:** Supervision, Visualization, Writing - original draft, Writing - review & editing.

Declaration of competing interest

The authors declare that they have no known competing financial interests or personal relationships that could have appeared to influence the work reported in this paper.

Acknowledgment

Financial support from the Conseil Régional d'Aquitaine (20071303002PFM) and FEDER (31486/08011464) is acknowledged.

References

[1] P. Raybaud, H. Toulhoat, Catalysis by transition metal sulphides, http://www.editionstechnip.com/fr/catalogue-detail/1176/catalysis-by-transition-metal-sulphides.html , Accessed date: 12 July 2018.
[2] M. Ali, S. Abbas, A review of methods for the demetallization of residual fuel oils, Fuel Process. Technol. 87 (2006) 573–584.
[3] J.G. Reynolds, W.R. Biggs, S.A. Bezman, Reaction sequence of metallopetroporphyrins during heavy residuum upgrading, in: R.H. Filby, J.F. Branthaver (Eds.), Metal Complexes in Fossil Fuels, American Chemical Society, Washington, DC, 1987, pp. 205–219.
[4] G. Caumette, C.-P. Lienemann, I. Merdrignac, B. Bouyssiere, R. Lobinski, Element speciation analysis of petroleum and related materials, J. Anal. At. Spectrom. 24 (3) (2009) 263–276.
[5] O. Yépez, Influence of different sulfur compounds on corrosion due to naphthenic acid, Fuel 84 (1) (2005) 97–104.
[6] N. Vorapalawut, M.M. Labrador, P. Pohl, M. Caetano, J. Chirinos, C. Arnaudguilhem, B. Bouyssiere, J. Shiowatana, R. Lobinski, Application of TLC and LA ICP SF MS for speciation of S, Ni and V in petroleum samples, Talanta 97 (2012) 574–578.
[7] M.S. Rana, V. Sámano, J. Ancheyta, J.A.I. Diaz, A review of recent advances on process technologies for upgrading of heavy oils and residua, Fuel 86 (9) (2007) 1216–1231.
[8] R. Sahu, B.J. Song, J.S. Im, Y.-P. Jeon, C.W. Lee, A review of recent advances in catalytic hydrocracking of heavy residues, J. Ind. Eng. Chem. 27 (2015) 12–24.
[9] J. Bartholdy, B.H. Cooper, Optimizing hydrotreater catalyst loadings for the upgradingof atmospheric residues, in: M. Absi-Halabi, J. Beshara, A. Stanislaus (Eds.), Studies in Surface Science and Catalysis, Elsevier, Amsterdam, 1996, pp. 117–124.
[10] J.Z.P. Bartholdy, B.H. Cooper, The Interplay of Coke and Metals in Resid Deactivation, Atlanta (1994).
[11] P. Zeuthen, J. Bartholdy, P. Wiwel, B.H. Cooper, Formation of coke on hydrotreating catalysts and its effect on activity, in: B. Delmon, G.F. Froment (Eds.), Studies in Surface Science and Catalysis, Elsevier, Amsterdam, 1994, pp. 199–206.
[12] J. Bartholdy, P.N. Hannerup, Hydrodemetallization in resid hydroprocessing, in: C.H. Bartholomew, J.B. Butt (Eds.), Studies in Surface Science and Catalysis, Elsevier, 1991, pp. 273–280.
[13] P. Pohl, J. Dural, N. Vorapalawut, I. Merdrignac, C.P. Lienemann, H. Carrier, B. Grassl, B. Bouyssiere, R. Lobinski, Multielement molecular size fractionation in crude oil and oil residue by size exclusion microchromatography with high resolution inductively coupled plasma mass spectrometric detection (HR ICP MS), J. Anal. At. Spectrom. 25 (12) (2010) 1974–1977.
[14] G. Gascon, V. Vargas, L. Feo, O. Castellano, J. Castillo, P. Giusti, S. Acavedo, C.-P. Lienemann, B. Bouyssiere, Size distributions of sulfur, vanadium, and nickel compounds in crude oils, residues, and their saturate, aromatic, resin, and asphaltene fractions determined by gel permeation chromatography inductively coupled plasma high-resolution mass spectrometry, Energy Fuel 31 (8) (2017) 7783–7788.
[15] S. Gutierrez Sama, A. Desprez, G. Krier, C.-P. Lienemann, J. Barbier, R. Lobinski, C. Barrere-Mangote, P. Giusti, B. Bouyssiere, Study of the aggregation of metal complexes with asphaltenes using gel permeation chromatography inductively coupled plasma high-resolution mass spectrometry, Energy Fuel 30 (9) (2016) 6907–6912.
[16] A. Desprez, B. Bouyssiere, C. Arnaudguilhem, G. Krier, L. Vernex-Loset, P. Giusti, Study of the size distribution of sulfur, vanadium, and nickel compounds in four crude oils and their distillation cuts by gel permeation chromatography inductively ccoupled plasma high-resolution mass spectrometry, Energy Fuel 28 (6) (2014) 3730–3737.
[17] G. Caumette, C.P. Lienemann, I. Merdrignac, H. Paucot, B. Bouyssiere, R. Lobinski, Sensitivity improvement in ICP MS analysis of fuels and light petroleum matrices using a microflow nebulizer and heated spray chamber sample introduction, Talanta 80 (2) (2009) 1039–1043.
[18] V. Vargas, J. Castillo, R.O. Torres, B. Bouyssiere, C.-P. Lienemann, Development of a chromatographic methodology for the separation and quantification of V, Ni and S compounds in petroleum products, Fuel Process. Technol. 162 (2017) 37–44.
[19] A.-Y. Huc, Heavy Crude Oils, IFP Publications, 2011.
[20] G. Gascon, J. Negrin, V. Garcia-Montoto, S. Acevedo, C.-P. Lienemann, B. Bouyssiere, Simplification of heavy matrices by liquid–liquid extraction: part I—how to separate LMW, MMW, and HMW compounds in maltene fractions of V, Ni, and S compounds, Energy Fuel 33 (3) (2019) 1922–1927.
[21] G. Gascon, J. Negrín, V.G. Montoto, S. Acevedo, C.-P. Lienemann, B. Bouyssiere, Simplification of heavy matrices by liquid–solid extraction: part II—how to separate the LMW, MMW, and HMW compounds in asphaltene fractions for V, Ni, and S compounds, Energy Fuel 33 (9) (2019) 8110–8117.

CHAPTER 7: GPC-ICP-MS SPECIATION ANALYSIS IN BIO-OILS

One of the aims of this fifth chapter, together with the sub-aim **O2b** that was presented in the Introduction of this thesis, consists of providing to the reader with a short review of the current methods of analysis of inorganic compounds (trace elements) within the biomass feedstocks, pyrolysis products and other bio-oils that were introduced in Chapter 1, together with a brief overview of the composition of these samples. As it was mentioned, numerous compounds can be found within these matrices. For example, considering the pyrolysis oils as one of the most complex samples analysed in this work, up to 300 different oxygenated compounds have been identified within only one sample.

The second, and most important aim of this chapter, consists of reporting the results that were obtained by studying the speciation of phosphorus in different types of fast pyrolysis oil and fatty acid feedstocks. As it was explained before, phosphorus is one of those elements present within most of the bio-oils feedstocks that would cause serious issues during the catalyst process that transforms these bio-oils into high-quality transportation fuels. Thus, both the phosphorus content and its speciation in three different lignocellulosic fast pyrolysis oils and three fatty acid feedstocks, are under discussion in this chapter.

7.1. Current trends on inorganic speciation and total analysis of bio-oils

7.1.1. Total analysis

As an example of how challenging quantifying inorganic compounds in biomass feedstocks and bio-oils, in 2018, Haldor Topsoe carried out a Round Robin analysis for the determination of different elements in three type of samples which are included in this work. The results of this study agree on the difficulties of achieving good reproducibility among the 12 laboratories that took part in this study. Out of these three samples, one, consisting in a vegetable oil, provided with reproducible results and a very good

performance concerning the quantification of inorganic contaminants (Al, Ca, Fe, K, Na, Mg, P, Si and Zn). However, concerning the other two samples, a pyrolysis oil produced from pine wood and an animal fat (pork tallow), the results show clearly how the large deviations obtained among the different laboratories make the analysis of these samples a highly challenging task.[104] Some of these results have been reported in the Section 5.2.1. of this thesis.

7.1.1.1. Biodiesel, bioethanol and their feedstocks

Acid digestion before ICP-MS analysis is one of the most used analytical techniques for the quantification of metals and other elements in the whole spectrum of bio-oils and their feedstocks. From vegetable oils and animal fats, up to biodiesel samples follow the same guidelines for their total analysis.

In vegetable oil feedstocks, several ICP-MS quantification methods have already been developed. Like many other environmental samples, acid digestion is a good choice of sample preparation before ICP-MS analysis. For example, two research groups, Llorent et al.[105] and Benicasa et al.[106] investigated the detection of trace elements in vegetable oils and developed methods where the samples were microwave digested by using nitric acid prior to ICP-MS analysis. However, this methodology is not the only one for the total analysis of trace elements in vegetable oils. Different authors developed and optimised different sample preparation procedures, such as Jimenez et al.[107] and Castillo et al.[108], who developed a sample preparation procedure where the vegetable oil samples were mixed with Triton-X emulsified and then, directly introduced into the plasma.

The sample introduction method can change to perform total analysis. This is the case of the study that Chaves et al.[109] have carried out by using ETV-ICP-MS for the determination of Co, Cu, Fe, Mn, Ni and V in diesel and biodiesel samples, using a fast gradient for the quantification of the analytes and having performed a sample emulsion preparation before the analyses. Good linear correlations and low LODs and LOQs (at the order of ng g^{-1}) were obtained, suggesting that ETV as a method for sample introduction is trustworthy for the analysis of samples with complex matrices. Figure 50 describes in bar plots the accuracy regarding the concentrations found for different elements by using different techniques, which is practically similar to the figures obtained for GF-AAS.

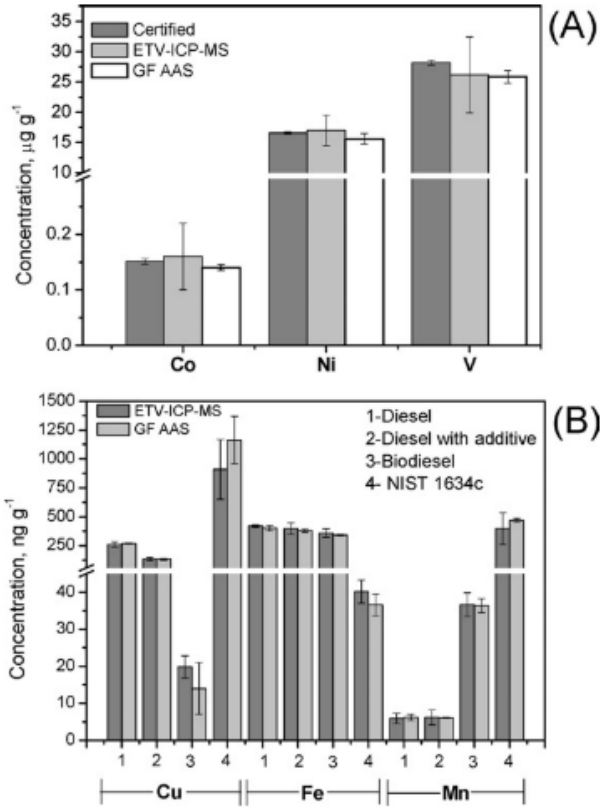

Figure 50. (A) Determination of Co, Ni and V in a certified reference material by three different methods. (B) Determination of Cu, Fe and Mn in four different samples by GF AAS and ETV-ICP-MS[109].

Even so, ICP-MS is not the only method that has been used for the analysis of this type of feedstocks. Nerin et al.[110] analysed the metal content of different waste industrial oils by graphite-furnace atomic absorption spectrometry (GF-AAS), after an acid digestion sample treatment.

Respect to biodiesel samples, since the content of certain trace elements is regulated and standardised, numerous methods for biodiesel total analysis have been developed.[111]

Sanchez et al.[112] reviewed the main techniques employed for the determination of metals and metalloids in biodiesel. They agree on the challenging of working with these complex samples since the target elements are present in very low concentrations and the calibration with organic complex matrices reduces the accuracy of these determinations. In their review, they describe numerous procedures for sample preparation, including

emulsification, micro emulsification, dilution with ethanol to work in aqueous mode and acid digestion amongst others, followed by either ICP-MS or ICP-OES detection.

Regarding the total analysis carried out for the trace elements in bioethanol, there exists numerous publications discussing the topic, but it seems that microwave acid assisted digestion using HNO_3 and posterior analysis by ICP-MS is the optimal method to obtain the highest, as it was reported by Sanchez et al.[112,113], obtaining acceptable LODs and both high short and long term precision within their method.

However, other techniques such as MP-ICP-OES that have been tested for the analysis of Si in complex samples such as diesel and biodiesel might be very useful for the determination of other trace elements in other fatty feedstocks and biodiesel.[114,115]

7.1.1.2. Pyrolysis Oils

The total analysis of trace elements in all types of pyrolysis oils is mainly carried out by ICP techniques once they have been acid-digested. Among all the methods that have been designed for these purposes, different variations on the acid composition or the detection may occur. For example, while acid digestion using H_2O_2 and HNO_3 and ICP-OES detection was the method chosen by Al Chami et al.[116], Chiang et al.[117] performed a more aggressive digestion using a mixture of HNO_3, $HCLO_4$ and HF. Posteriorly, and after a preconcentration, two different methods were chosen to carry out the analyses: an ICP-OES for the analysis of Al, Ca, Fe, K, Mg, Na, S, Co and Zn, and an ICP-MS for the analysis of As, Ba, Cd, Cr, Cu, Mn, Ni, Pb, Sb, Se, Sr, Ag and V concentrations, achieving in both cases detection limits at the ppb level.

However, other techniques have been explored for the quantification of trace elements in these bio-oils, such as the TGA method for the determination of Na, Ca, Mg and K in bioslurry fuels (mixtures of biochar and bio-oil) developed by Zhang et al.[118].

7.1.2. Speciation Analysis

Strictly speaking, “speciation” is considered by the IUPAC as the “distribution of an element amongst defined chemical species in a system”.[119] However, due to the lack of

literature related to the speciation of metalloids and trace elements in some of the samples that are referred in this work, other methods that help to characterize and elucidate species containing certain elements will be discussed in this section.

7.1.2.1. Biodiesel, bioethanol and their feedstocks

As it has been discussed in the previous section, both biodiesel and bioethanol samples possess already established methods of quantification of their trace elements and possible future applications of these methods that might be used for speciation analysis. However, extra information needs to be obtained to understand the presence of these trace elements within the matrices they belong to.

One technique that has been mentioned in this thesis and that was used for the determination of certain trace elements in ethanol fuel, ETV-ICP-MS obtained good calibration figures and LODs by using an isotopic dilution calibration method.[120] The optimised coupling of these two techniques might be used, with a different temperature ramp, for the speciation of these trace elements and obtaining their fingerprint concerning their boiling/pyrolysis temperature.

One interesting method, that helps to understand the behaviour of some trace elements species throughout the production process for bioethanol, was developed by Sanchez et. Al.[121] They quantified and compared several trace elements from samples taken at different phases of the industrial process and, as it is shown in Figure 51, by ICP-MS analysis.

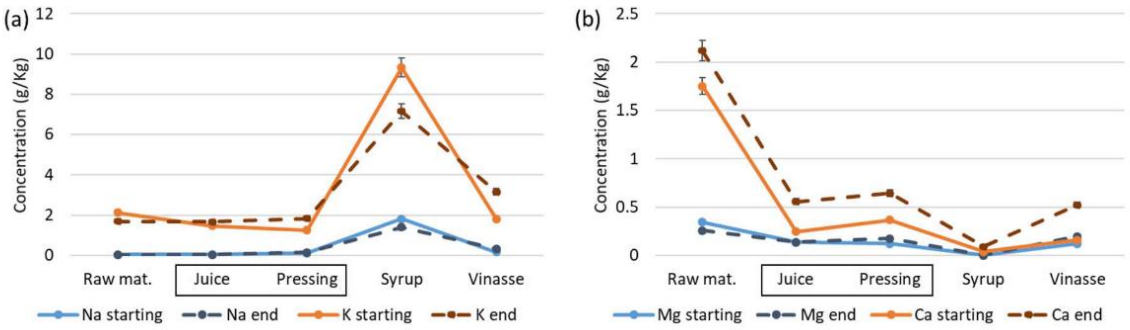

Figure 51. Evolution of the concentration of Na and Mg along the bioethanol production process[121].

The information obtained from both the increase and decrease of Na, K, Ca and Mg respectively within the bioethanol production process can facilitate the determination of the source of these emerging contaminations and study their degradation and elimination. A similar method has been reported for sorghum biomass samples and their metal distribution along the bio-oil process.[122] However, further information might be obtained when coupling HPLC-ICP-MS to each one of the collected samples, in term of obtaining a fingerprint based on their polarity, size, etc., depending on the stationary phase and the solvents used to this end.

7.1.2.2. Pyrolysis Oils

Even though numerous analytical methods for the characterisation of pyrolysis oil samples have been developed, there are not a high abundance of speciation methods focusing on the trace elements present within these samples. A review of some of these methods have been written by Kanaujia et al.[123], and some of the main techniques used for the general speciation analysis are resumed in Table 5.

Table 5. Main techniques used for the speciation analysis of pyrolysis oils.[123]

Technique	Properties measured	Highlights
TGA	Loss of mass	• Content of water, carbon, ash, cellulose, lignin, etc.
FT-IR	Fundamental vibrations	• Functional groups. • Ageing mechanisms.
GC-MS	Ions (m/z)	• Quantification of PAHs, organic acids, ketones, alcohols, etc.
FT-ICR-MS	Ions (m/z)	• Hydrocarbon and small organic molecules characterisation.
NMR	Magnetic properties	• Functional groups, quantification. • Degradation mechanisms.
HPLC-UV **HPLC-RI**	Absorbance	• Polar/apolar species identification. • Size distribution fingerprinting.

Another speciation method for the analysis of heavy metals (Cu, Cr, Pb, Zn, Cd, and Ni) in sewage sludge pyrolysis oil was carried out by Yuan et al.[124]. They carried out an extraction procedure where four fractions were extracted. These four fractions, consisting of (1) exchangeable metals and carbonate-associated fractions, (2) Fe and Mn oxides fraction (3) organic-mater-bonded fraction and (4) the residuals. Then, the total concentration of these elements was obtained by ICP-OES. They found out that these trace elements are present within all the four fractions, being Cu and Cr the most abundant ones within the organic-mater-bonded fraction, demonstrating that these metals can be present as free ions but also bonded to organic compounds within the pyrolysis oil matrices. These results are shown in Figure 52 being F1, F2, F3 and F4 the four fractions described before.

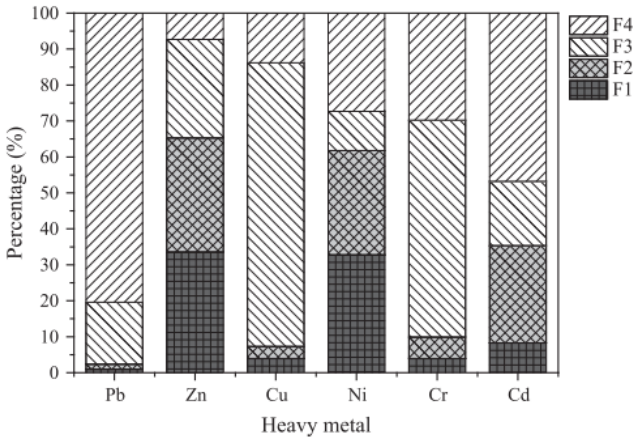

Figure 52. Speciation of heavy metals in pyrolysis oil from sewage sludge

The speciation analysis of P and the transformations that its species have during the hydrothermal treatments of animal manures has been reported in the literature. Huang et al.[125] performed a sequential extraction to consider all the P species by using different solvents, acids and bases among others. They carried out the analyses with three different techniques: X-ray powder diffraction analysis, liquid ^{31}P NMR spectroscopy and X-ray absorption near-edge structure (XANES) analysis and obtained information about the abundance of P species along the hydrotreating process of beef, chicken and dairy manure samples.

However, apart from a few publications where speciation analyses are performed targeting the trace elements present within pyrolysis oils, the rest of the publications focus on the speciation analysis of organic compounds, such as sugars, aldehydes, PAHs, etc, making the work carried out within this project quite novel and contributing a new point of view to the research in pyrolysis oil characterisation. Nonetheless, the following reviews cover these speciation and characterization methods for the main components of pyrolysis oil samples.[126–130]

7.2. Speciation analysis of trace elements in renewable feedstocks via GPC-ICP-HR MS

7.2.1. Samples, methodology and instrumentation

As it was demonstrated in Chapter 4, GPC-ICP-HRMS is a powerful technique that can provide with very useful information about the size distribution of numerous trace elements. Thus, in this chapter, the application of the already developed methodology is carried out in a set of renewable feedstock samples.

Speciation analyses based on their molecular size are carried out for phosphorus, sulfur, sodium, iron and magnesium in five lignocellulosic fast pyrolysis oil samples and three fatty acid feedstocks.

Five lignocellulosic fast pyrolysis oils were provided by Haldor Topsoe (Denmark) and RTI (United States). To elaborate these fast pyrolysis bio-oils, woods from red oak, loblolly pine and pine (commercial sample) were used. Besides, three fatty acid samples, consisting of two types of unprocessed animal fat (pork and tallow) and a soybean oil were also provided by Haldor Topsoe.

The origin of the lignocellulosic fast pyrolysis oils is described below:

- Sample A: Pyrolysis oil produced from a 50:50 mixture of milorganite and loblolly pine wood.
- Sample B: Pyrolysis oil produced from a 50:50 mixture of milorganite and red oak wood.
- Sample C: Pyrolysis oil produced from milorganite fertilizer.
- Sample D: Pyrolysis oil produced from red oak wood.
- Sample P: This sample consists of a commercial pyrolysis oil sample produced from pine wood.

The origin of the fatty acid feedstocks used in this chapter is described below:

- Sample AF: Unprocessed tallow fat.

- Sample VO: Unprocessed soybean oil.
- Sample TRIG.X: Unprocessed pork fat.

Except for the Sample P, all the other pyrolysis oils were produced at the RTI facilities in the United States. A fast pyrolysis process was carried out in a pilot-scale catalytic fast pyrolysis unit with γ-Al2O3 being the catalyst, with a catalyst-to-biomass ratio average equal to 5.

The concentration of the trace elements obtained for some of the samples whose speciation is studied in this chapter is detailed in Table 6.

Table 6. Sample name, type of feedstock and total concentration in ppm of P, S, Na, Fe and Mg.

Sample name	Feedstock	P	S	Na	Fe	Mg
A	50:50 blend of pinewood and milorganite.	150	n.m.	23	220	42
B	50:50 blend of red oak wood and milorganite	34	n.m.	19	690	24
C	Milorganite	260	n.m.	150	320	230
D	Red oak wood	7.3	n.m.	65	1210	27
P	Pinewood (commercial sample)					
TRIG.X	Pork fat	105	20.1	7.87	14.3	15.8

n.m. stands for “not measured”.

The reader might have noticed that the details concerning three of the samples described above are not reflected in Table 6. These samples are the commercial pyrolysis oil sample, the tallow fat and the soybean oil.

In order to determine the concentration of trace elements within these three samples, Haldor Topsoe carried out the round-robin study, described in Section 5.1.1., for the quantification of several trace elements, including P, S, Na, Fe and Mg. [104,131] The results of this round-robin study concerning the trace elements studied in this chapter are detailed in Figure 53.

While the analyses carried out for the quantification of trace elements in the vegetable oil sample are quite precise, the animal fat and pyrolysis oil results indicate how challenging the quantitative analysis becomes by presenting very high deviations among laboratories that followed the same methodology.

Figure 53. Results of the analyses of P, S, Na, Mg and Fe (in ppm) for the different laboratories that participated in the round-robin study directed by Haldor Topsoe. [104,131]

For all the analyses carried out within this section via GPC-ICP-HRMS, the same instrumentation and solvents that are described in the article displayed within the Section 4.3 of this manuscript were used. Each of the samples was diluted with a factor of 5 in THF. Injections of 20 µL were carried out by triplicate.

7.2.2. Methodology and calibration of the columns

With the purpose of having an estimation of the molecular size of the eluting compounds, the chromatographic profile of nine commercial polystyrene standards was obtained via GPC-UV/VIS. ICP-MS detection was not possible for these compounds, since they are composed of carbon and hydrogen, and detecting these elements via this technique is not possible.

These polystyrene standards were dissolved in three different solutions with THF and injected by triplicate. Figure 54 shows the profile obtained for the three different solutions. Solution 1 contains PSs with a MW of 3 152 000, 1 044 000 and 466 300 Da respectively; Solution 2 contains PSs with a MW of 206 000, 67 600 and 27 060 respectively and the Solution 3 contains PSs with a MW of 12 980, 6 660, 1 140 and 162 Da. The peaks are eluted from the highest to the lowest molecular size, which in this case, agrees with their molecular weight.

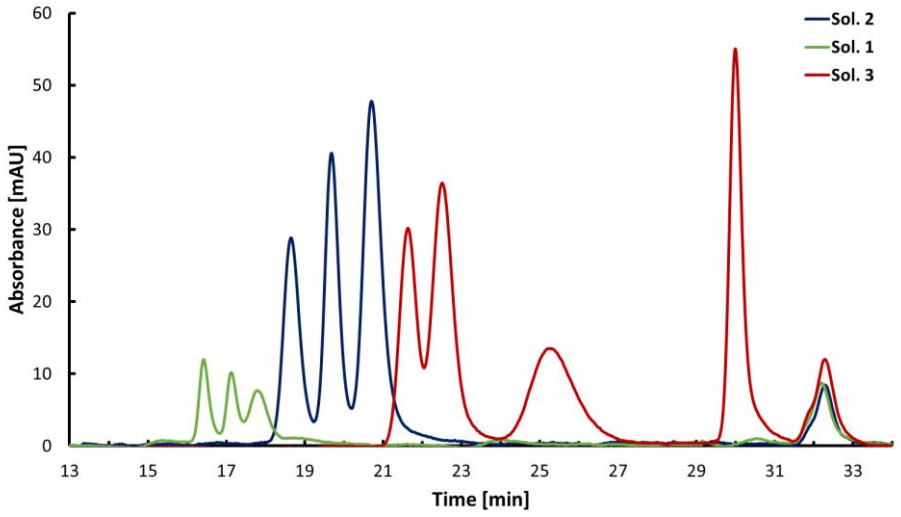

Figure 54. GPC calibration using 10 polystyrene standards dissolved in three different solutions and detected by a UV-VIS detector.

A common peak for the three PS solutions can be observed after approximately 32 min of analysis. This peak, which corresponds to the solvent peak, determines the total permeation volume of the GPC columns. Theoretically, if there are no other interactions between the analytes and the stationary phase (meaning that the separation is based only on the hydrodynamic volume of the analytes), the elution of compounds beyond this point will not occur.

A calibration curve was obtained by plotting the logarithm of the molecular weight of each PS standard versus their corresponding retention times and it is shown in Figure 55.

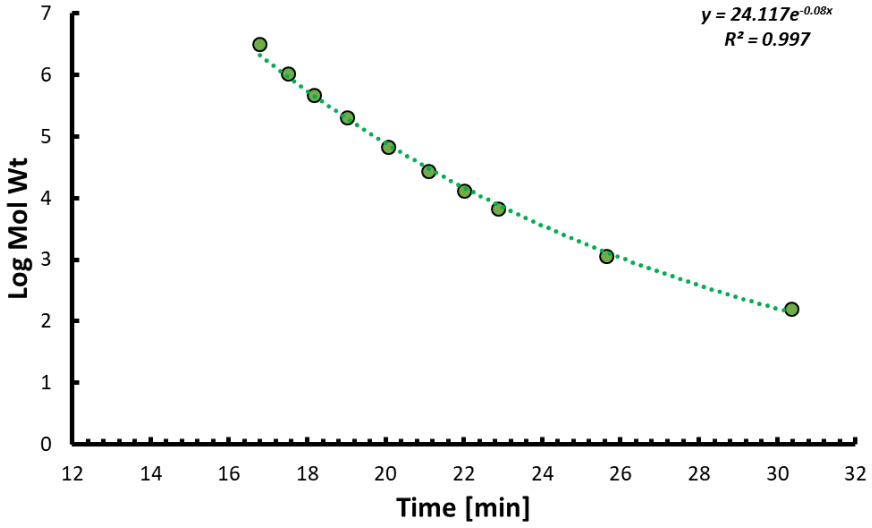

Figure 55. GPC calibration curve.

Since the objective of this mass calibration is to approximately estimate the molecular weight of the eluting peaks via GPC-ICP-MS, a vanadium porphyrin was injected by triplicate and simultaneously analysed with ICP-MS and UV/VIS detections. A difference of 0.36 minutes was found between both detections, and it is caused by the difference of tubing lengths between the split and the respective detectors. Thus, the calibration curve has been drawn considering this time difference, in order to estimate more accurately the mass of the different peaks via GPC-ICP-MS.

7.2.3. Analysis of S, Na, Fe and Mg in fast pyrolysis oils

In order to classify the different peaks in groups based on their molecular weight, which theoretically should be associated approximately to their hydrodynamic volume, a separation between classes has been carried out considering the MW values detailed in Table 7. Four classes have been stablished, resembling to those ones that were defined for crude oil analysis in previous works.[74,132] However, in this case, the retention time and, therefore, the size of each group of species varies with respect to these previous works. High molecular weight (HMW), medium molecular weight (MMW), low molecular weight (LMW) and tailing fractions have been defined for this classification purposes.

Table 7. Definition of the molecular weight interval for the different fractions obtained via GPC-ICP-MS.

Fraction / Class	Molecular Weight
HMW	≥ 3152 – 91 KDa
MMW	91 – 21 KDa
LMW	21 KDa – 318 Da
Tailing	≤ 318 Da

7.2.3.1. Sulfur species.

Figure 56 and Figure 57 show the GPC-ICP-HR MS distribution of sulfur species in six different fast pyrolysis oils. Sulfur's distributions in fast pyrolysis oils are very different from the distributions found in petroleum products. In these renewable feedstocks, the sulfur species possess a slightly lower size (below 30 KDa) and all of them show trimodal profiles of those S-containing species.

Although the same distribution can be observed and the retention time of each of the peaks is common to all the feedstocks used to produce these pyrolysis oils, some differences can be observed:

- Milorganite fast pyrolysis oils show higher intensities than the rest of the samples. This higher presence of sulfur-containing species might be linked with the numerous salts containing sulfur that are present in fertilizers, such as ammonium sulfates or potash sulfates, amongst others, intended to provide to the plants either with very essential nutrients for their growth or with protection against pests and insects.

- The commercial pyrolysis oil sample shows a high intensity for the peak eluting after 32 minutes of analysis. The molecular size of this species might suggest a high concentration of sulfur-containing salts that do not interact with any other compounds within the pyrolysis oil matrix. These salts might have been caused through the rupture of bigger aggregates during the production of this commercial unit. One methodology that might help to confirm this hypothesis could be the injection of a sulfur-containing salt in a low concentration.

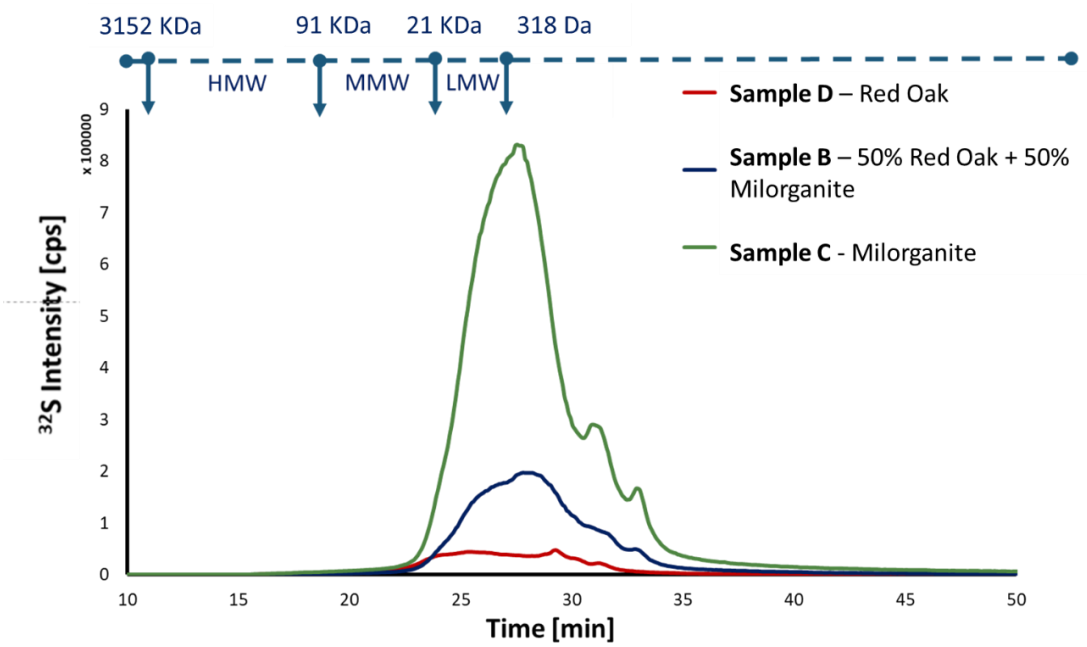

Figure 56. Sulfur (^{32}S) size distribution via GPC-ICP-HRMS for pyrolysis oils produced from red oak, milorganite and a 50:50 blend of both.

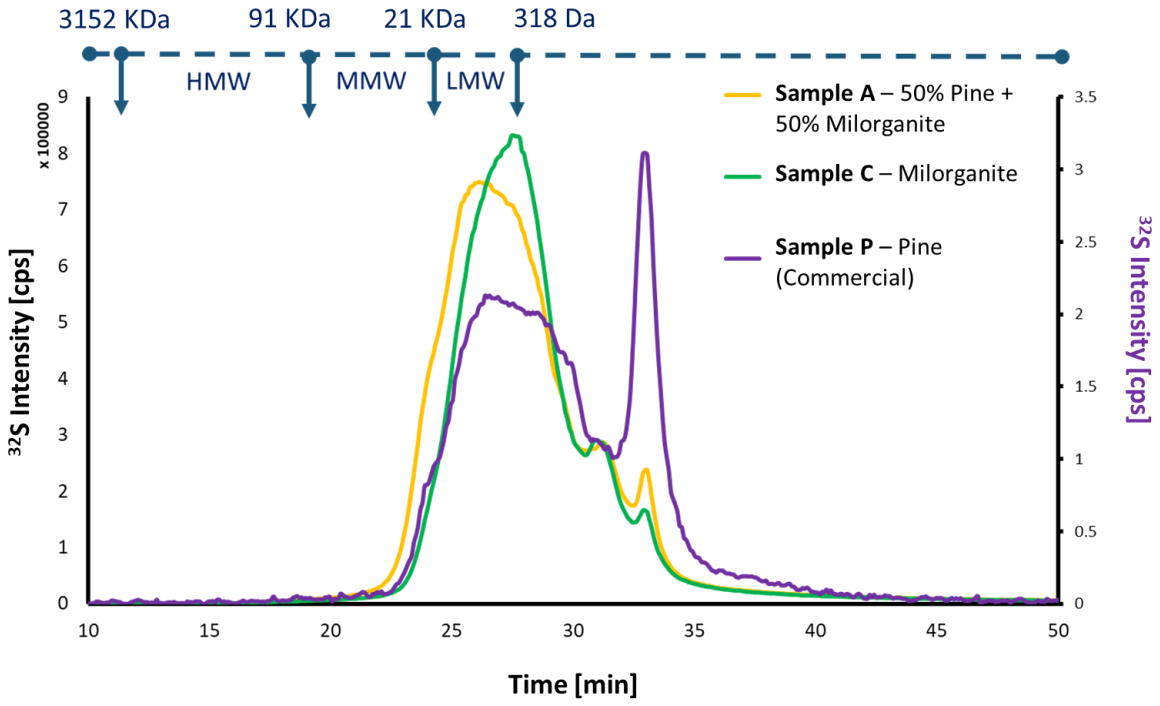

Figure 57. Sulfur (^{32}S) size distribution via GPC-ICP-HRMS for pyrolysis oils produced from milorganite, a blend of milorganite and loblolly pine wood and a commercial fast pyrolysis oil sample.

Besides, the presence of compounds within the MMW and LMW fractions, indicates that either aggregation, complexation or polymerisation reactions have taken place within all the samples. By performing a fractionation via preparative GPC of these samples, further analysis might be carried out to determine the structure of these compounds, such as the use of FT-ICR-MS.

The contribution of each fraction with respect to the total area of the chromatogram was calculated and the results can be observed in Figure 58. A high presence of MMW and LMW compounds is common within all the pyrolysis samples, no matter their feedstocks. However, regarding the commercial pyrolysis oil produced from pine, a change can be noticed, since an increase of the tailing compounds (probably salts) and a reduction of the MMW compounds has taken place.

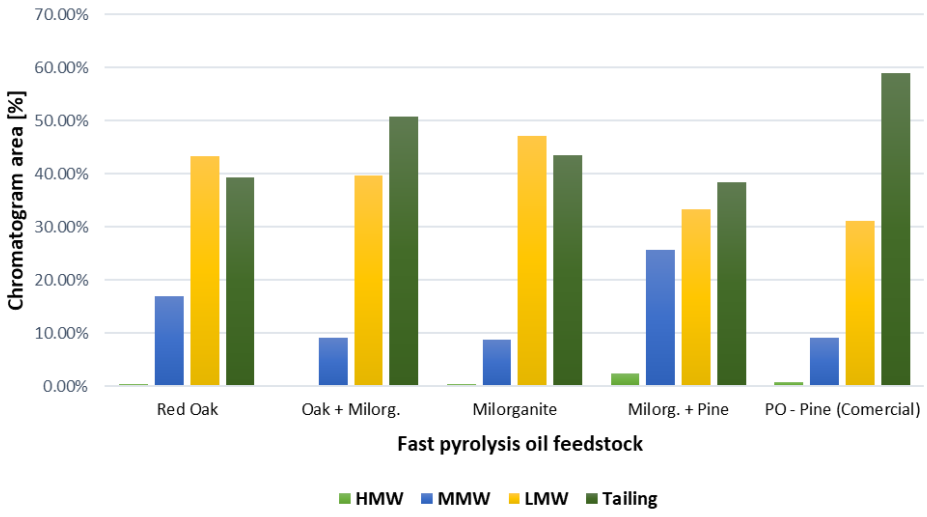

Figure 58. Distribution of the S-containing species for the five samples analysed via GPC-ICP-HRMS.

7.2.3.2. Sodium species

The GPC-ICP-HRMS chromatograms corresponding to the distribution of Na-containing species in the same set of samples are detailed in Figure 59 and Figure 60.

A trimodal distribution is observed as well for all the pyrolysis oils except for red oak pyrolysis oil, which presents a multimodal distribution with, at least, five different non-resolved peaks.

Red oak pyrolysis oil presents some compounds eluting at very early retention times and suggesting that Na-containing compounds with a molecular weight higher than 91 KDa are present within this sample. These compounds, however, do not seem to be present when milorganite is blended to with red oak wood to produce a fast pyrolysis oil.

Another difference that can be observed between the Na-containing and the S-containing compounds is the absence of an intense peak near the permeation volume of the column, where the solvent peak was detected for the PS standards during the mass calibration of the columns. The absence of this peak could suggest that the sodium present within these samples might be strongly linked to other compounds via complexation.

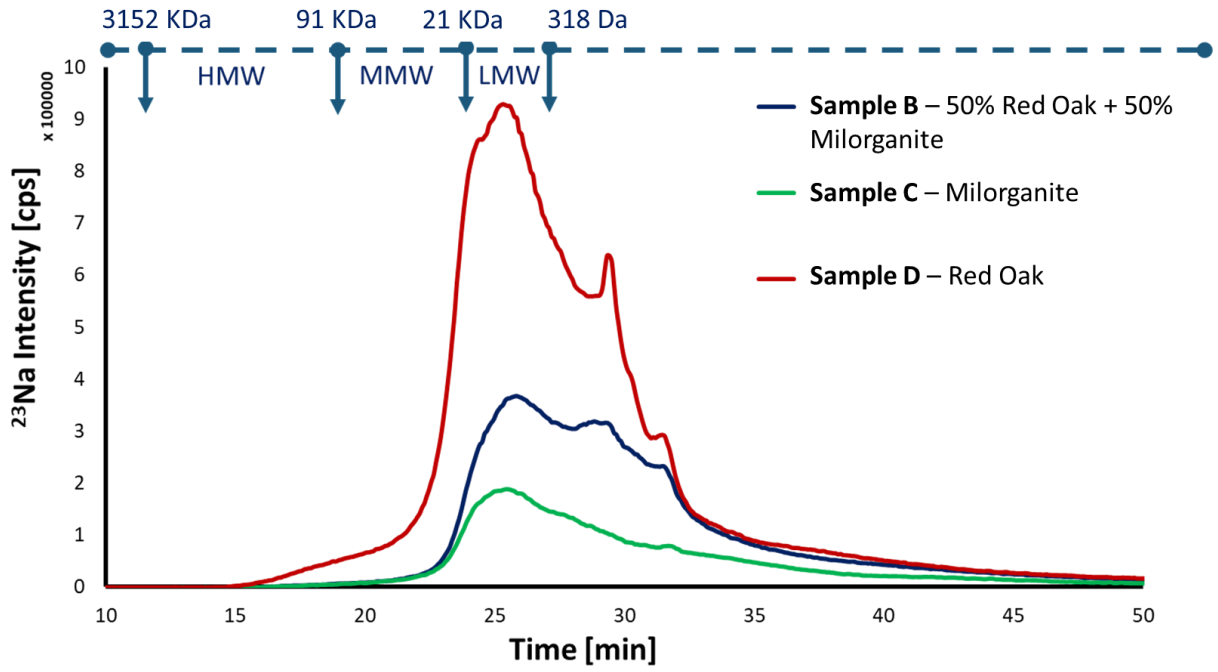

Figure 59. Sodium (^{23}Na) size distribution via GPC-ICP-HRMS for pyrolysis oils produced from red oak, milorganite and a 50:50 blend of both.

The contribution of each fraction with respect to the total area of the chromatogram was also calculated for the Na-containing species that were eluted from the GPC columns. The

results have been plotted in Figure 61. It can be observed how the commercial pyrolysis oil produced from pinewood lacks HMW sodium species within its matrix, whereas, for the rest, the abundance of all the size fractions is observed in decrescent order, from lower to high molecular weight compound.

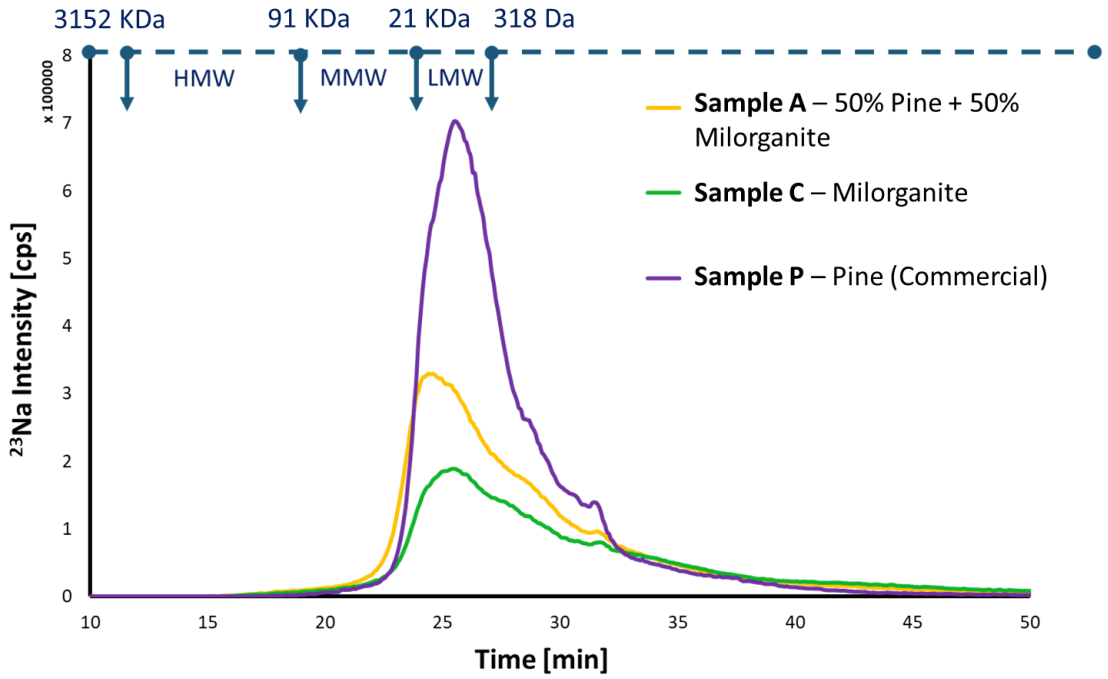

Figure 60. Sodium (^{23}Na) size distribution via GPC-ICP-HRMS for pyrolysis oils produced from milorganite, a blend of milorganite and loblolly pine wood and a commercial fast pyrolysis oil sample.

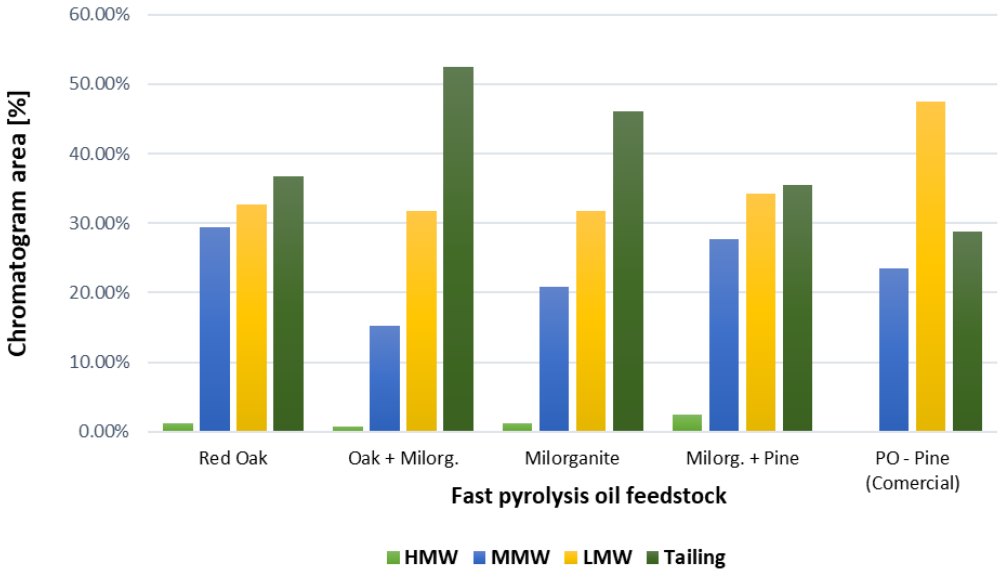

Figure 61. Distribution of the Na-containing species for the five samples analysed via GPC-ICP-HRMS.

7.2.3.3. Iron species

The fingerprints obtained for the Fe-containing species based on their size are shown in Figure 62 and Figure 63 for the same samples, where a common peak can be observed. This peak, which corresponds to a Fe-containing compound with a molecular weight of approximately 21,000 Da is present amongst all the lignocellulosic fast pyrolysis oils that have been analysed.

As it has been mentioned in Chapter 1, iron is one of the most common elements in the earth crust and, therefore, it is present within both vegetable and animal tissues. It is very usual to see natural complex and other organometallic compounds with iron in nature. [133]

Besides, the data suggests that bigger complexes have been formed during the fast pyrolysis process, as the elution of iron species takes place from after 15 minutes of analysis except for the commercial fast pyrolysis oil produced from pinewood.

A very small peak can also be observed after minute 30 of analysis, near the limit of permeation of the columns, which might be caused by the presence of Fe^{2+} and Fe^{3+} ions that are not complexed.

Thus, the data obtained via GPC-ICP-HRMS suggests that a high molecular weight iron-containing complex is formed during the fast pyrolysis of lignocellulosic feedstocks.

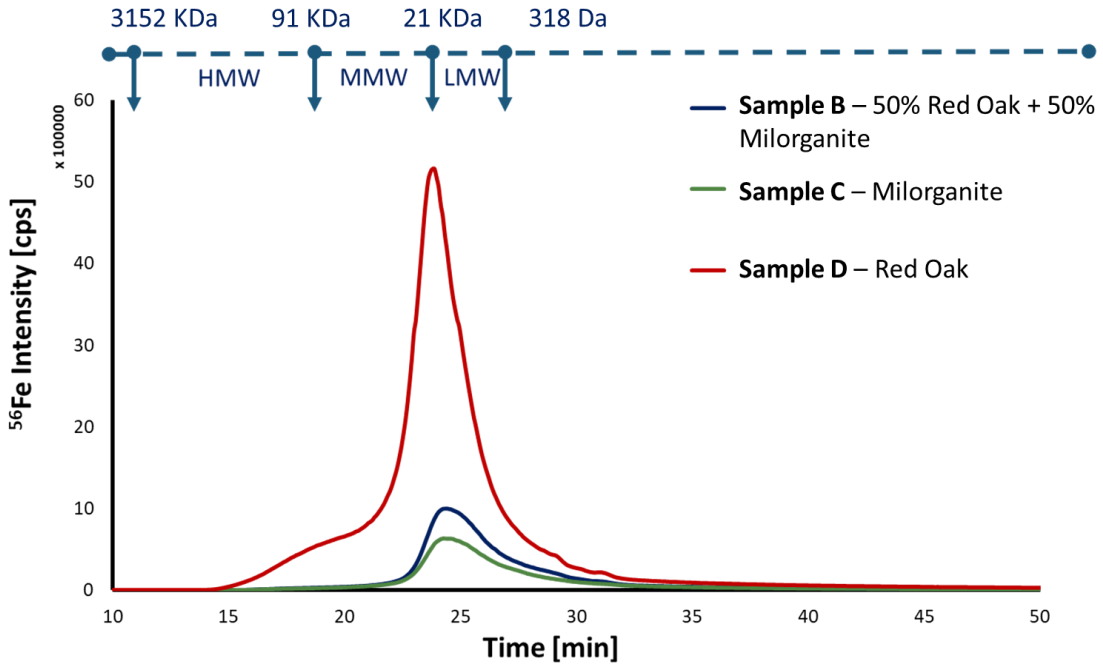

Figure 62. Iron (^{56}Fe) size distribution via GPC-ICP-HRMS for pyrolysis oils produced from red oak, milorganite and a 50:50 blend of both.

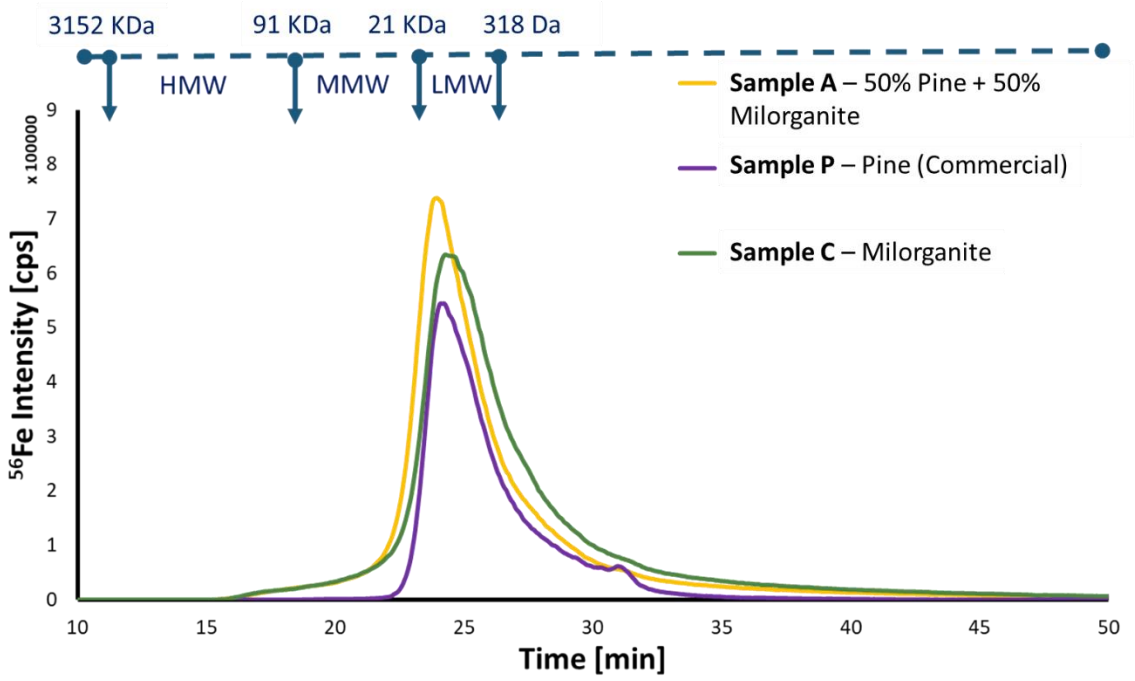

Figure 63. Iron (^{56}Fe) size distribution via GPC-ICP-HRMS for pyrolysis oils produced from milorganite, a blend of milorganite and loblolly pine wood and a commercial fast pyrolysis oil sample.

In Figure 64, the distribution of the different fractions based on their contribution to the total chromatogram area is observed, where the absence of high molecular weight iron species for the commercial pyrolysis oil can be observed clearly. However, the medium molecular weight species are the more abundant ones for all the lignocellulosic fast pyrolysis oils. The fractionation of this samples and posterior analysis with other techniques such as FT-ICR-MS would allow the identification of these species.

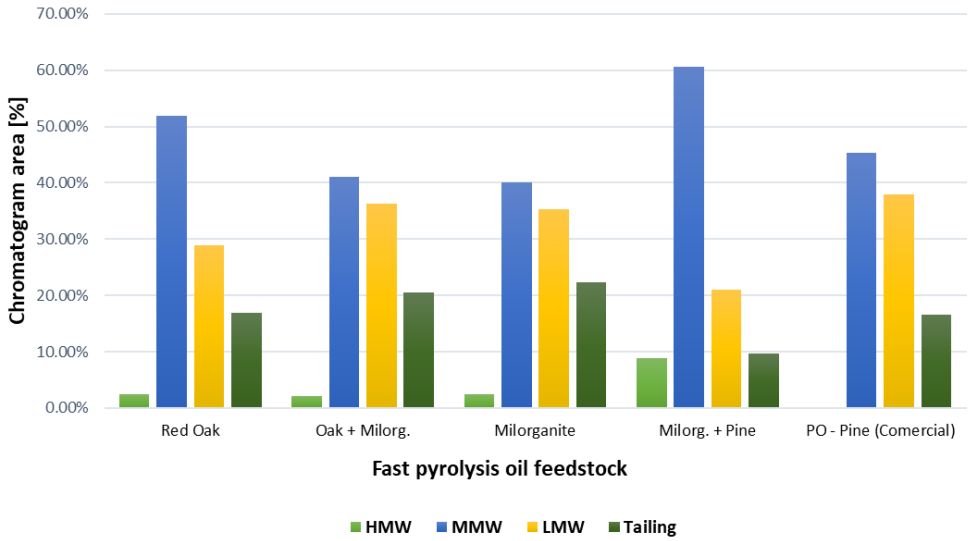

Figure 64. Distribution of the Fe-containing species for the five samples analysed via GPC-ICP-HRMS.

7.2.3.4. Magnesium species

Magnesium-containing species, which are expected in lignocellulosic feedstock due to the presence of chlorophylls in all the vegetable tissues. The weight distribution of these compounds obtained via GPC-ICP-HRMS analyses is detailed in Figure 65 and Figure 66.

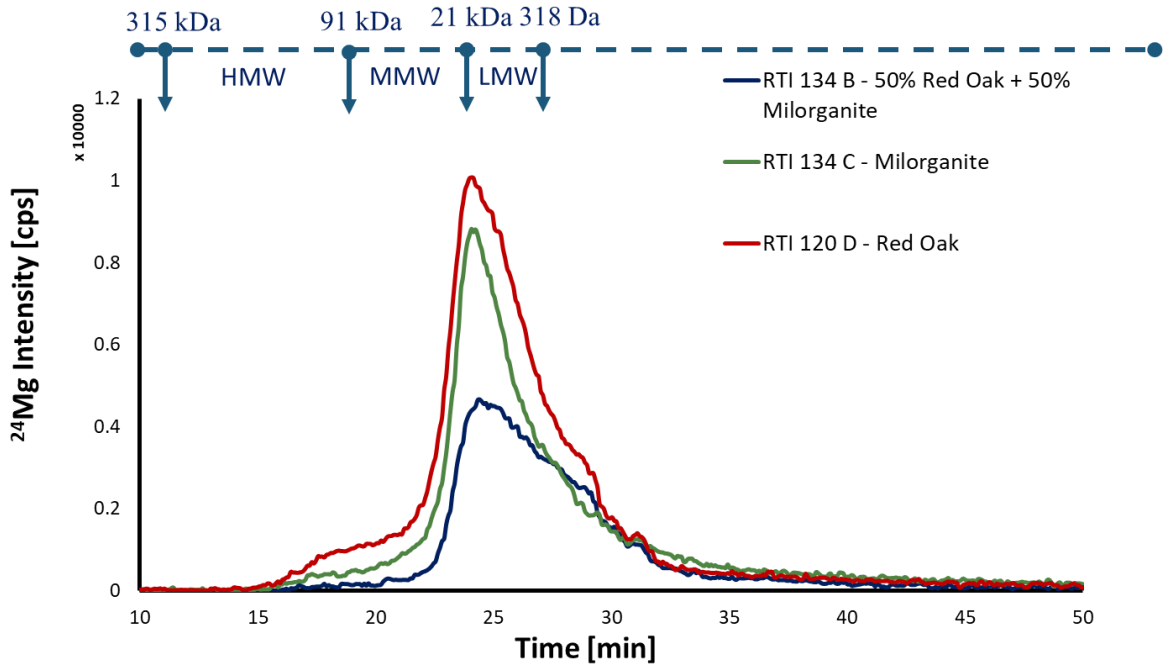

Figure 65. Magnesium (^{24}Mg) size distribution via GPC-ICP-HRMS for pyrolysis oils produced from red oak, milorganite and a 50:50 blend of both.

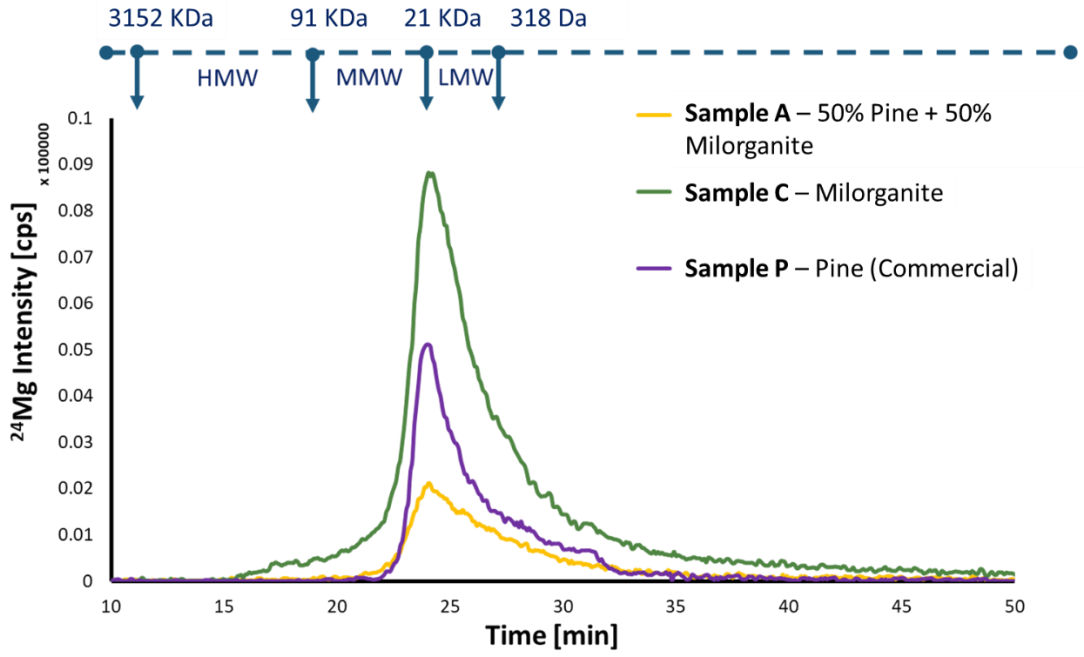

Figure 66. Magnesium (^{24}Mg) size distribution via GPC-ICP-HRMS for pyrolysis oils produced from milorganite, a blend of milorganite and loblolly pine wood and a commercial fast pyrolysis oil sample.

An eluting peak with approximately the same size as the most abundant peak found for the analysis of iron in the same set of samples can be observed. This peak, which corresponds to several compounds with an approximate mass of 21 KDa, is present among all the fast pyrolysis oils. Furthermore, bigger compounds, which start eluting after 15 minutes of analysis can be observed, suggesting that aggregation of Mg-containing compounds occurs during the fast pyrolysis process.

Since a high presence of different chlorophyll high-molecular-weight aggregates in complex matrices was found under different matrices and temperature conditions, [134–136] the data obtained via GPC-ICP-HRMS analyses suggest that aggregation reactions have occurred either during the fast pyrolysis process or the storage of the sample.

A GPC-ICP-HRMS analysis of chlorophyll should be carried out in the near future to study the size distribution of Mg. Although chlorophyll is an expensive reagent, with a TLC plate and a similar methodology to the one that Tswett carried out with vegetal pigments (mentioned at the beginning of the Chapter 2 of this PhD thesis), the extraction of chlorophyll from spinach could be achieved. The TLC spot where the chlorophyll is eluted could be extracted and collected in order to be injected via GPC-ICP-HRMS.

Figure 67 shows the bar plot corresponding to the different size fractions based on their relative area with respect to the total chromatogram area. Same abundances are observed for all the samples, with exception of the 50:50 red oak wood and milorganite fast pyrolysis oil, where the low molecular weight compounds are the most abundant ones. In addition, as it happens for all the trace elements concerning the commercial pyrolysis oil sample, a lower number of high-molecular-weight compounds has been found as well in this sample.

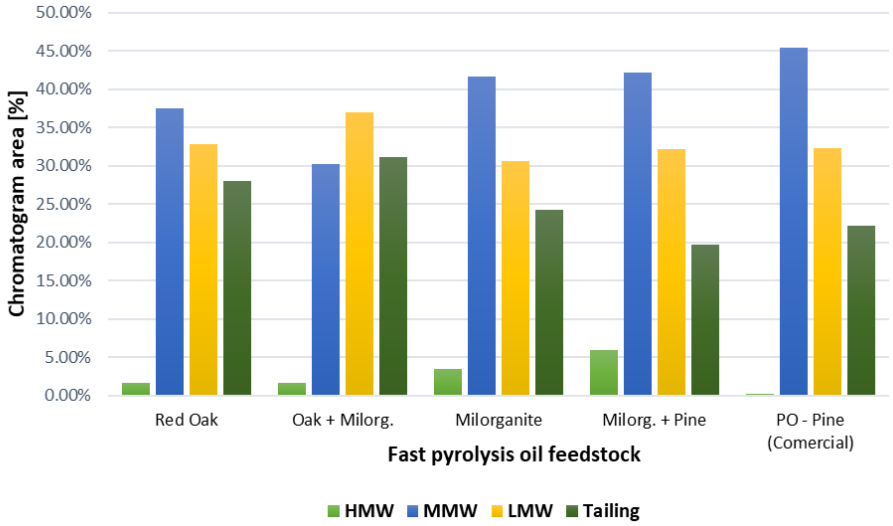

Figure 67. Distribution of the Fe-containing species for the five samples analysed via GPC-ICP-HRMS.

7.2.4. Phosphorus speciation analysis of fatty-acid based feedstocks and fast pyrolysis biocrudes via gel permeation chromatography inductively coupled plasma high resolution mass spectrometry.

The results that concern the analysis of the phosphorus-containing compounds in fast pyrolysis oils and fatty acid feedstocks have been summarised in the **Manuscript 1** that is attached below. This manuscript is not in its final version. Further changes will be considered before its submission in the RSC Green Chemistry journal.

To be submitted to RSC Green Chemistry

Phosphorus speciation analysis of fatty-acid based feedstocks and fast pyrolysis biocrudes via gel permeation chromatography inductively coupled plasma high resolution mass spectrometry.

Victor Garcia-Montoto, Sylvain Verdier, David Dayton, Ofei Mante, Carine Arnauldguilhem, Jan H. Christensen, Brice Bouyssiere.

ABSTRACT:

Renewable feedstocks, such as lignocelulosic fast pyrolysis oils and both vegetal and animal oils and fats are becoming an alternative to fossil fuels to produce high-quality transportation fuels. However, several problems occur when these feedstocks are being treated: the presence of phosphorus-contaning compounds is causing pressure drops and catalyst poisoning during the hydrotreating processes that transform these renewable feedstocks into hydrocarbons. In this work, the use of gel permeation chromatography (GPC) hyphenated with inductively coupled plasma high-resolution mass spectrometry (ICP-HRMS) has been applied to the analysis of such complex samples.

Aggregation of phosphorus-containing compounds has been observed for different fatty acid feedstocks, suggesting that high-hydrodinamic volume micelles or liposomes might have been formed among the phospholipids contained in these samples.

With respect to the lignocellulosic fast pyrolysis oil samples, either aggregation or polimerisation reactions might have occurred during the pyrolysis process: phosphorus-containing compounds with a hydrodynamic volume equivalent to a PS with a molecular weight above 91000 KDa have been found.

1. Introduction

The use of renewable feedstocks, such as fatty acid or lignocellulosic materials, destined to obtain transportation fuels is increasing to mainstream the use of renewable energy in the transport sector. The RED II legislation (Renewable Energy Directive for 2021–2030 in the EU) has set an obligation on fuel suppliers that ensures that the share of renewable energy supplied for final consumption in the transport sector is at least 14% by 2030 and at least 3.5% of transportation fuels have to be produced from renewable feedstocks. Furthermore, the overall EU target for Renewable Energy Sources consumption by 2030 has been raised to 32%.[1,2]

Fatty acid feedstocks, such as virgin oils, used cooking oils and animal fats, are the most employed feedstocks to produce either biodiesel or renewable diesel. Biodiesel is produced through a transesterification process, where the fatty acids present within the feedstocks are transformed into fatty acid methyl esters (FAMEs) when they are mixed in a reactor with an alcohol, generally methanol, and a catalyst. In addition, the fatty acid present within this type of feedstocks can also react under hydroprocessing conditions to form n-alkanes (n-C_{15}, n-C_{16}, n-C_{17} and n-C_{18}). This mixture of n-alkanes, once purified, is known as renewable diesel or hydrotreated vegetable oil (HVO).[3–6]

Lignocellulosic fast pyrolysis biocrudes are mostly used to produce renewable transportation fuels. Lignocellulosic-derived feedstocks such as red oak and pine woods are heated at temperatures between 450 and 600 °C in absence of oxygen to decompose their organic matter into char, gas and organic vapours that are posteriorly condensed, thus obtaining a liquid that is known as fast pyrolysis oil.[7–9] These pyrolysis oils can be used as feedstocks to produce, through a hydrotreating process, hydrocarbon fuels with a high heating value and low content of impurities.

Both fatty acid and lignocellulosic-derived feedstocks possess a high amount of phosphorus compounds, most of them coming from the phospholipids present within the cell walls in both animal and vegetal cells that are present within their matrices, such as those that belong to tissues, bones, etc. for the animal fat feedstocks and the vegetable cells for the vegetable oils and lignocellulosic feedstocks.

Although some studies have shown the high efficiency during catalysis on model phospholipids, [10] the other phosphorus compounds that are present within these samples can affect negatively the

upgrading processes that transform these feedstocks in high-energy-value hydrocarbon fuels. When they approach the catalyst, in the absence of alkalis, these compounds are decomposed into phosphoric acid that acts as an oligomerization/polymerization catalyst. That makes the high-molecular-weight oligomers to deposit on the catalyst surface causing, therefore, carbon deposits and ultimately causing catalyst deactivation. Furthermore, when charged alkalis are present, the deactivation is also partially caused by the deposition of the phosphates on the catalyst bed, leading to the formation of deposits and reducing the activity of the catalysts. [11] The formation of these deposits may indeed cause serious issues in industrial units such as pressure drops and high deactivation.[12]

The structure of these phospholipids is already well known for fatty acid feedstocks and they can be divided into two groups regarding their behaviour while interacting with water: non-hydratable phospholipids (NHPLs) and hydratable phospholipids (HPLs). Within the NHPLs, phosphatidic acid (PA) and phosphatidylethanolamine (PE) are the most representative ones and they tend to form salts with Ca and Mg ions. The second group, HPLs, are represented by phosphatidylcholine (PC), phosphatidylinositol (PI) and phosphatidylserine (PS) which are easily removed from the feedstock matrix with water due to the formation of insoluble hydrates. The structure of these phospholipids is detailed in Figure 1. Structure of the principal NHPLs and HPLs.

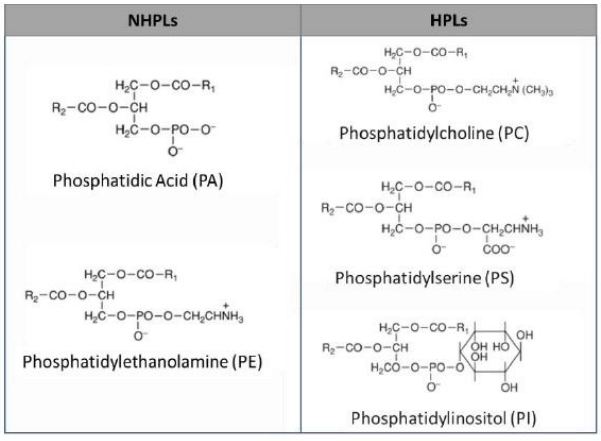

Figure 1. Structure of the principal NHPLs and HPLs.

The elimination of these phosphorus species is known as “degumming” and this treatment is carried out through different processes that reduce the content of phosphorus in these feedstocks

77 up to less than 1 ppm. Water degumming, acid degumming and absorption are some of the most
78 used methods to pre-treat feedstocks and to remove phosphorus and other contaminants. [13,14]
79 However, regarding the lignocellulosic pyrolysis oils, the elimination of these phosphorus species
80 cannot be carried out with standard techniques and the search for an alternative that guarantees the
81 elimination of the phosphorus-containing compounds has to be done.

82 Nevertheless, these phospholipids, depending on the matrix they belong to, might follow different
83 structure patterns. They can form micelles, consisting of spherical phospholipid aggregates that
84 formed when the hydrophilic part of the phospholipids (the phosphate group) interact amongst
85 themselves while sequestering the hydrophobic part of the phospholipids (the fatty acid chains).

86 However, some processes such as hydroxylation, which is one type of structural change that some
87 phospholipids might suffer, increases the number of hydroxyl groups within their fatty acid chains
88 and might avoid the formation of micelles due to their presence within the fatty acid chains: they
89 are introduced through the double bonds present in the fatty acid chains and change completely
90 the polarity of the whole molecule, affecting thus to their aggregation behaviour. [15]

91 The phosphorus present within other type of samples such as lignocellulosic feedstocks or
92 fertilizers can also have a phospholipidic origin, since these compounds are present in all the cell
93 membranes that conform the different vegetable cells organelles such as chloroplasts and nucleus,
94 among others. These phospholipids might follow different reaction paths during the pyrolysis
95 processes consisting on the first step in order to be converted into hydrocarbon fuels.
96 Understanding their structure would be very useful in order to adjust the feedstock pre-treatment
97 process conditions and improve the efficiency of the corresponding hydrotreating processes (e.g.
98 by developing an efficient catalyst that facilitates and increases the conversion of these bio-oils to
99 biodiesel or renewable transportation fuel hydrocarbons).

100 The use of GPC for the analysis of pyrolysis oils has already been used as a complementary
101 technique to obtain an overview of the general composition of these samples and some of their
102 fractions by using either UV-VIS or RI detectors[16–19]. However, the coupling of this technique with
103 element detection has not been widely used for this type of samples.

104 One method that might help to understand the composition of these phosphorous species could be
105 the hyphenation of gel permeation chromatography (GPC) with inductively coupled plasma high-

resolution mass spectrometry (GPC-ICP-HRMS) to obtain a size distribution fingerprint of those species that contain phosphorus within their structure.

These techniques have been used already for the speciation analysis of different elements in complex matrix samples, such as petroleum[20–23] atmospheric resid oils[24] and asphaltene samples.[25,26]

By obtaining the fingerprint of phosphorus species related to their hydrodynamic volume in fatty acid feedstocks, whose phosphorus composition is already known, might help to find out similarities or differences in the nature of the corresponding species in those lignocellulosic feedstocks like the biocrudes that have been analysed in this work. By comparing the information obtained for both of them with could lead to obtaining useful information that might help the understanding of these species and facilitate their posterior elimination in order to achieve a highly efficient method of conversion into high-quality transportation fuels.

2. Materials and methods

2.1. Instrumentation

Quantitative analyses

A Round Robin study for the quantitative analysis of trace elements in renewable feedstocks has been carried out by Haldor Topsoe with the participation of twelve analytical laboratories that used certified methods to carry out the analyses. Although all the laboratories carried out the analyses via ICP-OES, laboratories 1, 2, 3, 9 and 10 used mineralisation with nitric acid; laboratories 4 and 12 followed the UOP 389-proc A methodology; laboratory 5 and 6 ICP-OES through dissolution in kerosene and laboratories 7 and 8 followed the ISO 118855 method. Related information was been reported by Verdier et al. [12,27]

Speciation analyses

The speciation analyses were carried out with a Thermo Scientific Element XR double focusing sector field ICP-MS (Thermo Fischer, Germany) instrument, used as a element selective detector, accessing the spectrally interfered isotopes of ^{31}P at a resolution of 4000, which avoids the spectral interferences caused by species such as $^{14}N^{16}O^{1}H^{+}$ and $^{12}C^{18}O^{1}H$, amongst others.[28] The instrument was equipped with a quartz injector (1.0 mm of orifice internal diameter), a Pt sampler cone (1.1 mm of orifice diameter) and a Pt skimmer cone (0.8 mm of orifice diameter) purchased from Thermo Fischer (Germany). In order to avoid carbon deposition on the cones surface, a flow of 0.08 mL min^{-1} of O_2 was added into the ICP-HRMS carrier gas, consisting of Ar.

The instrument was equipped with a modified DS-5 microflow total consumption nebulizer (CETAC, Omaha, NE) mounted with a laboratory-made spray chamber heated up to 65 °C by a water/glycol mixture in a temperature-controller bath circulator Neslab RTE-111 (Thermo Fisher Scientific, Waltham, MA).

The mass spectrometer was optimized and mass-calibrated daily at resolutions of 300 and 4000 by injecting a tune solution containing 1.0 ng g^{-1} of Ag, Al, B, Ba, Ca, Cd, Co, Cr, Cu, Fe, In, K, Li, Mg, Mn, Mo, Na, Ni, P, Pb, Sc, Si, Sn, Ti, V, Zn and Y in tetrahydrofuran (THF). A mass offset was applied as well to compensate for the mass drift coming from the sector field magnet.[24,29]

The chromatographic instrumentation was consisted of a Dionex high-performance liquid chromatography (HPLC) system fitter with an UltiMate 3000 microflow pum, an UltiMate 300 autosampler and a low port-to-port dead-volume microinjection valve. The separation was carried out via three Waters (Waters Corporation, Mildford, MA) styrene-divinylbenzene gel permeation columns (7.8 mm i.d. and 300 mm length). More specifically, the columns consisted of an HR4 column (particle size of 5 μm and exclusion limit of 600,000 Da of polystyrene equivalent), an HR2 column (particle size of 5 μm and exclusion limit of 20,000 Da) and an HR0.5 column (particle size of 5 μm and exclusion limit of 1000 Da of polystyrene equivalent). In order to prevent from any damages to the columns, a Styragel guard column (4.6 mm i.d. and 30 mm length) was fitted between the columns and the HPLC instrument.

2.2. Reagents, samples and solutions

Three samples with different origins: a soybean unprocessed vegetable oil and two samples of animal fat, one from tallow and the other one from pork, were provided by Haldor Topsoe.

The hydroxylation of the vegetable oil has been carried out following a method developed by Casper et al. [30] Into a 500 mL glass flask, where 20 g of this sample were added together with 40 mL of glacial acetic acid (analytical grade) and 10.71 mL of hydrogen peroxide (35% w/w), both of them purchased from Sharlau (Spain). The mixture has been heated to reflux for 1 hour and then the organic layer was washed with saturated solutions of sodium bisulphite (ACS reagent), sodium bicarbonate (ACS reagent, ≥99.7%) and sodium chloride (ACS reagent), which were purchased from Sigma-Aldrich (Germany). Then, the product was dried over anhydrous magnesium sulphate (≥99.5%), purchased from Sigma-Aldrich (Germany), and the presence of any other solvent was eliminated using a rotavapor.

Pure red oak and milorganite were the lignocellulosic feedstocks used in this work. They were processed separately and, afterwards, 50% blends of both were also processed to determine the influence of biosolids such as milorganite in the biocrude composition respect to the pure red oak biocrudes. The pyrolysis process was carried out in a pilot-scale catalytic fast pyrolysis unit with γ-Al_2O_3 being the catalyst, with a catalyst-to-biomass ratio average equal to 5. Asolectin from soybean (mixture of phospholipids) was purchased from Sigma.

3. Results and discussion

3.1. Quantitative Results

While an outlier has been found for the quantification of P in vegetable oil, the animal fat presented several deviations for the P concentrations, indicating how complex quantifying this analyte becomes in this type of samples. Figure 2 shows the concentration of phosphorus for the different laboratories that participated in the Round Robin study.

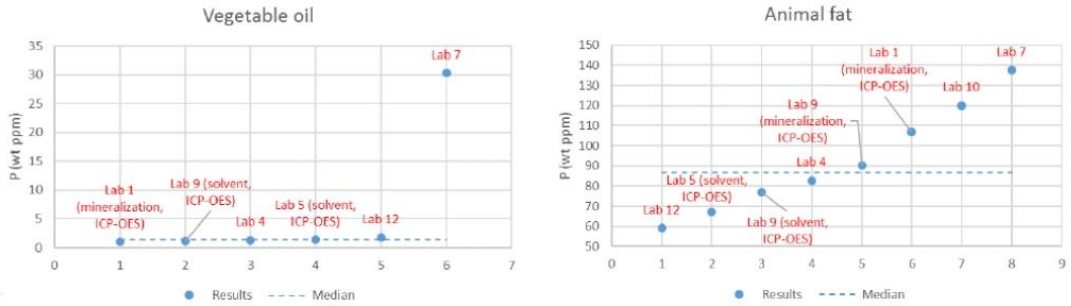

Figure 2. Concentration in ppm of phosphorus found by the different laboratories that participated in the Round Robin study-analysis of renewable feedstocks. [12]

Table 1 presents the phosphorus determined concentration, considering the median concentration values for the two samples that participated in the Round Robin study.

Table 1. Phosphorus concentrations (ppm) found for the samples that are under study in this work.

Sample Name	Abbreviation	Method	P Concentration (ppm)
Soybean Vegetable Oil	V.O.	ICP-OES*	~2
Tallow Animal Fat	A.F.T.	ICP-OES*	~87
Pork Animal Fat	A.F.P.	ICP-MS	105
Milorganite Pyr. Oil	P.O.M.	ICP-OES	260
Milorganite & Red Oak Pyr. Oil	P.O.MRO.	ICP-OES	34
Red Oak Pyrolysis OIl	P.O.RO.	ICP-OES	7.3

*Different methodologies carried out by 12 independent analytical laboratories.

3.2. GPC-ICP-MS analysis of fatty acid feedstocks

Figure 3 shows the chromatogram corresponding to the GPC-ICP-HRMS analysis of phosphorus in three different fatty acid feedstocks where different fingerprints corresponding to the phosphorus molecular weight species have been obtained. Whereas for the vegetable oil there is a wide peak at a very early retention time, the behaviour of the two animal fats is quite different amongst them. The phosphorus species present in these two animal fat samples possess one common peak at t_R = 27 min, which approximately corresponds to a compound with a molecular weight lower than 600 g mol^{-1}, indicating that these species might correspond to a free phospholipidic structure. In addition, the latest peaks might also correspond to the phosphate group which has been separated from the glyceryl group ($POOR^-$, being R= Ethanolamine, Choline, Serine or Inositol) and whose molecular weight is approximately 240 Da, depending on the radical group. However, with respect to the earlier peaks, considering their width and retention times, they indicate that a potential aggregation of the different phosphorus species possibly due to either the formation of micelles or any other polymerization process might have occurred within this type of samples. This aggregation could also explain the big width of the chromatographic peaks, since not all the micelles can have the same size, hence the large variety of sizes that increase the width of the gaussian peak.

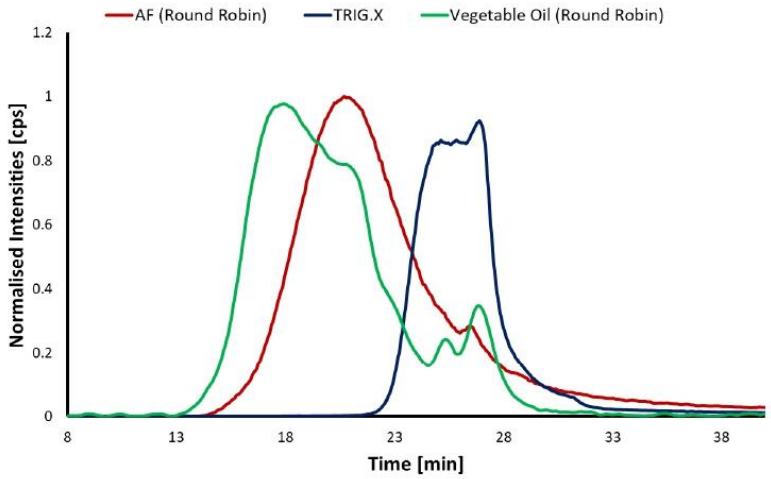

Figure 3.GPC-ICP-HRMS chromatogram corresponding to the analysis of P in three fatty acid feedstocks: A soybean vegetable oil (green) and two animal fats (red and blue).

224

225 In order to test this hypothesis, the hydroxylation of the vegetable oil was carried out by adding
226 hydroxy groups within the fatty acid chains, which can cause the loss of hydrophobicity of the
227 phospholipid fatty acid chains, avoiding the formation of micelles. Figure 4 shows the
228 chromatograms corresponding to the phosphorus species weight distribution for the vegetable oil
229 sample and its product after (1) hydroxylation and (2) being washed with water in a basic pH.

230 The phosphorus molecular weight distribution in the hydroxylated vegetable oil possesses a
231 completely different fingerprint in comparison to the vegetable oil. In this case, the presence of a
232 high amount of high-molecular-weight (HMW) species has been drastically reduced, confirming
233 that the fact of introducing a hydroxy group within the phospholipid fatty acid chains will reduce
234 their aggregation. In fact, introducing a polar group within the hydrophobic part of the
235 phospholipid will complicate the formation of micelles in the presence of a polar solvent since
236 these hydroxy groups will interact with the solvent via hydrogen bonds.

237 By analysing the washing step products of the vegetable oil, it is possible to observe a reduction
238 on the HMW species that should be caused by the elimination of some those hydratable
239 phospholipids present in the sample. These eliminated species might be aggregated forming
240 micelles, hence the reduction of the high molecular weight peak areas with respect to the other
241 species.

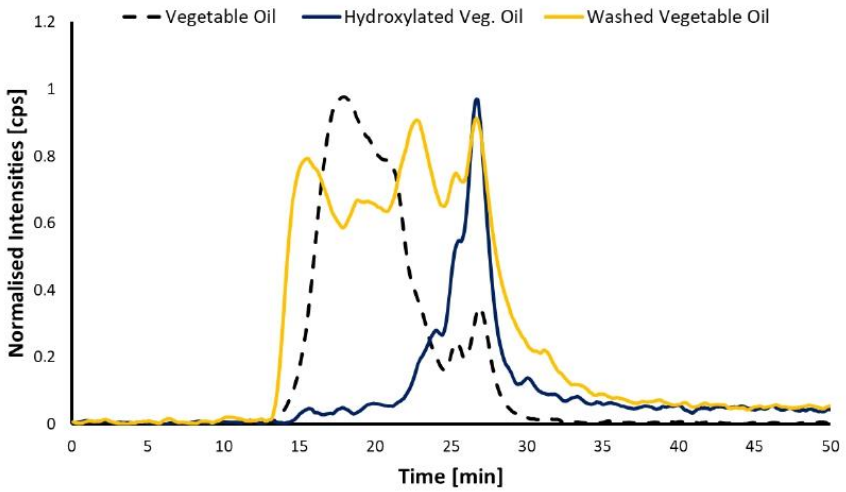

Figure 4. GPC-ICP-MS chromatogram of the vegetable oil, washed vegetable oil and hydroxylated vegetable oil samples.

3.3. GPC-ICP-MS analysis of soy asolectin.

Figure 5 shows the chromatograms corresponding to the analysis of a standard containing soybean asolectin, which consists of a mixture of lecithin (643 g mol^{-1}), cephalin (347 g mol^{-1}) and phosphatidylinositol (887 g mol^{-1}) before and after having been hydroxylated. While the asolectin chromatogram shows that the majority of the detected species are located within the medium- and low-molecular weight regions, which is almost a 3 % of the total chromatogram area that is eluted before t_R=20, for the hydroxylated asolectin, this region is reduced to 0.5 % of the total chromatogram area. As it can be seen in Figure 4, the early retention time of both peaks indicate that either aggregation or micellization processes have occurred, since this retention time is not corresponded to the actual molecular weights of the asolectin components.

One of the main changes that the hydroxylation has produced on the asolectin sample can observed in the chromatogram as a retention time swift of 1.08 min. This variation of the time supposes a difference of approximately an average of 8503 Da between the phosphorus species before and after the hydroxylation process. Such size can indicate that the phospholipids present in both

samples are forming micelles. Thus, the lower presence of HMW compounds in the hydroxylated asolectin and the reduction of the molecular size of the phosphorus species added to the fact that the species possess a lower size, might indicate that the micelles that are formed in the hydroxylated vegetable oil are smaller in hydrodynamic volume and therefore, a smaller molecular mass might be expected, which agrees with the hypothesis of the hydroxyl group avoiding the formation of the micelles: In this case, these micelles would be smaller, since there are a lower availability of "micellable" phospholipids.

In addition, asolectin can be considered as a typical gum that is formed within the vegetable oil, since lecithin is one of the typical examples of gums. [31] Thus, these results indicate that further aggregation is occurring in the vegetable oil matrices. Micelle formation or complexation with other species that are present in the matrix are the hypothesis that can be extracted from these results.

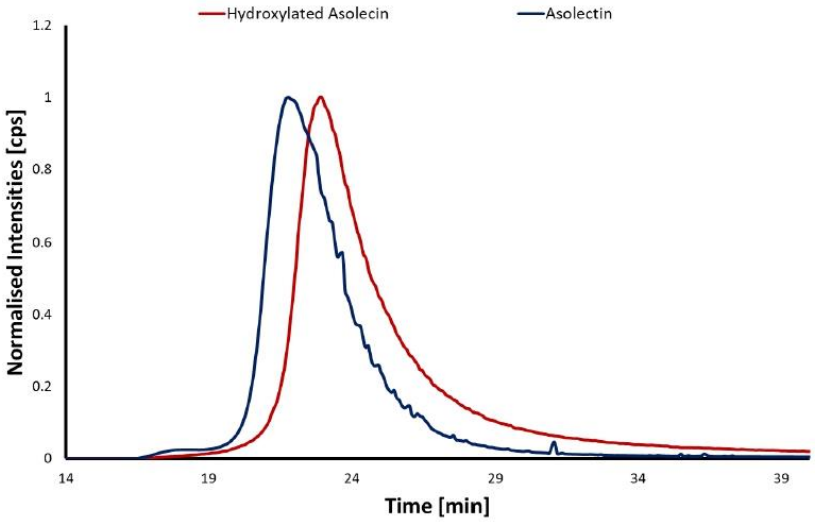

Figure 5. GPC-ICP-MS chromatograms corresponding to the asolectin standard (blue) and the hydroxylated azolectin standard (red).

3.4. GPC-ICP-MS analysis of fast pyrolysis feedstocks.

3.4.1. Xylene soluble extract (XSE).

The upper chromatogram depicted in Figure 6 shows the molecular weight distribution of the phosphorus species present within the organic extract (in xylene) of two different biocrudes and the mixture of both of them. Even though the distribution is different for each of the biocrudes, there are two main similarities amongst them: (1) The same species might be shared among the three biocrudes, such as the first eluting peak, corresponding to a molecular weight that is approximately about 784 Da (t_R=26.5 min), whose intensities vary for each feedstock and (2) an increasing among of species varying from the Red Oak, where no peak is seen, and reaching the maximum when the Milorganite was used as a feedstock. The retention time of this peak might indicate a molecular weight of around 235 Da, similar to the peaks observed for the vegetable oil and animal fat samples, which could perfectly correspond to the rupture of the phospholipids by the loss of the two fatty acid chains. This theory fits the reality, since milorganite consists of an already processed feedstock before the pyrolysis process. These earlier processing might have caused the rupture of the phospholipids within its matrix, causing the peak that it is observed at t_R=29 min. In addition, these results agree with the fact that the phospholipids do not suffer any rupture or decomposition during the pyrolysis process.

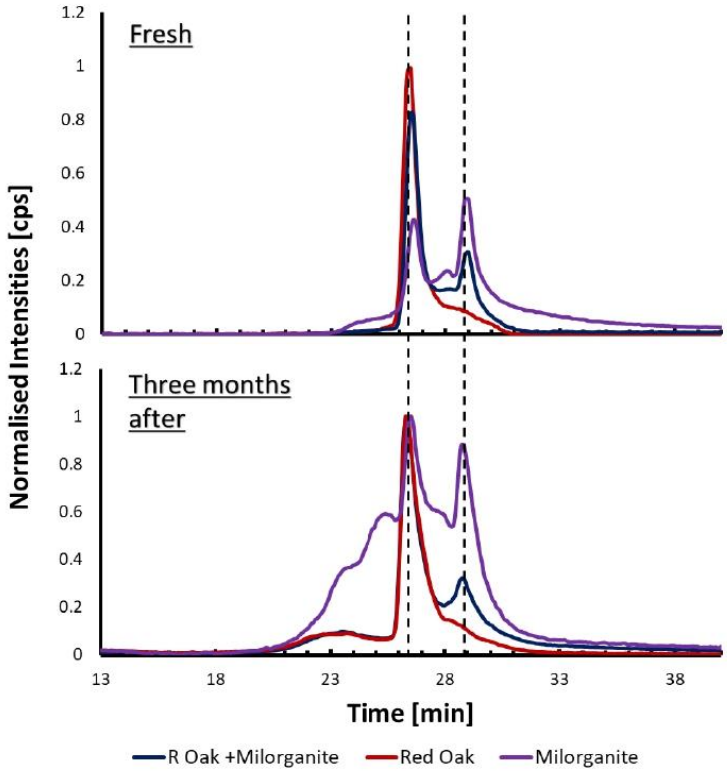

Figure 6. GPC-ICP-HRMS chromatogram corresponding to the analysis of P in the two extracts of three lignocellulosic feedstocks: Red Oak (red), Milorganite (purple) and a 50:50 mixture of Red Oak and Milorganite (blue).

The bottom chromatogram in Figure 6 shows the GPC-ICP-MS chromatogram of the same xylene extract after being stored for three months. While the presence of the same peaks remains constant, there is a great increase of the high molecular weight species areas. To be more precise, they have reached up to almost 20 % of the chromatogram total area, whereas when they were extracted, the same region of the chromatogram was lower than 5 % of the total area. This fact means that some aging and other aggregation processes, such as the polymerization of the phospholipids or their fatty acids, that might have taken place during this period. This hypothesis agrees with other observations found in the literature.[32]

312 **3.4.1. Xylene insoluble extract (XIE).**

313

314 An aliquot of the XIE obtained during the phase separation was injected and the chromatogram is
315 shown in the top Figure 7. Earlier peaks are observed for the three samples but those corresponding
316 to the samples containing milorganite fertilizer as their feedstocks possess wider peaks which a
317 longer tail. As it is observed in Figure 7, Red Oak biocrudes tend to have phosphorus species with
318 a higher hydrodynamic volume rather than milorganite and related biocrudes. This difference
319 might be caused by the previous treatments that milorganite had been through with respect to the
320 Red Oak wood. In addition, the bigger signal-to-ratio corresponding to the Red Oak peaks confirm
321 the hypothesis of the preference for these species to aggregate themselves via the hydrogen bonds
322 that a possible hydroxylation might generate within the phospholipid of this feedstock.

323 Following the same procedure as with the pyrolysis oil xylene extracts, the bottom graph in Figure
324 7 shows the chromatogram of the XIE sample where very significant changes in the size of the
325 phosphorus species can be appreciated.

326 In general, an increase of the chromatogram area of those species within the HMW region can be
327 noticed, especially for the sample that consists of a 50:50 mixture of milorganite and read oak.
328 This fact could be due to the formation of micelles or liposomes within the sample matrix. Since
329 the pyrolysis oils contain water and a lot of polar compounds, they might still be present in the
330 matrix.

331 In this extract, a high presence of salts is also expected. The formation of macro-complexes within
332 the matrix might be another reason that could explain the high presence of HMW species, that vary
333 from 35 to 67% of the total areas in these xylene insoluble extracts.

334

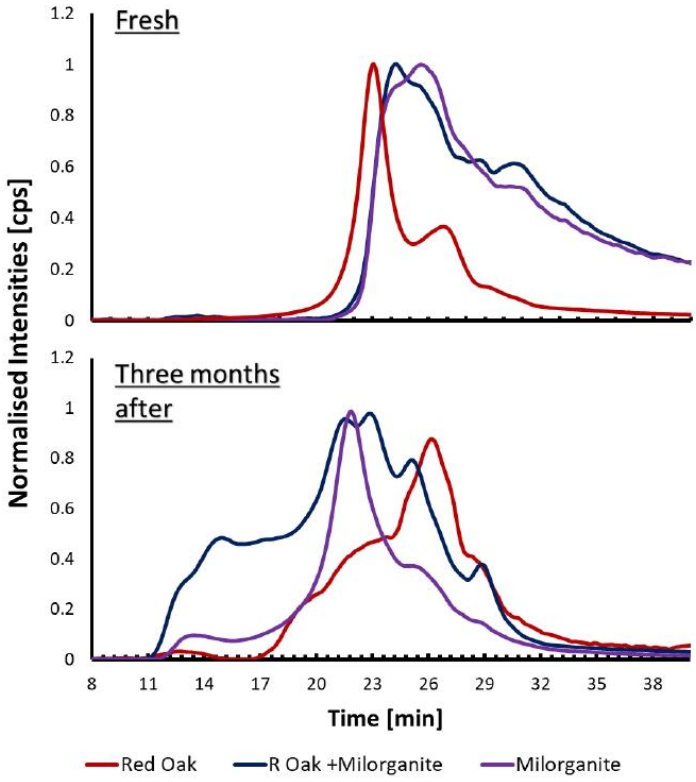

Figure 7. GPC-ICP-HRMS chromatograms corresponding to the analysis of P in the two extracts of three lignocellulosic feedstocks: Red Oak (red), Milorganite (purple) and a 50:50 mixture of Red Oak and Milorganite (blue).

4. Conclusion

GPC-ICP-MS analyses have proven the presence of complex phosphorus species in renewable and feedstocks that differ significatively from phospholipids due to their higher molecular weight. These aggregates are the cause of catalyst poisoning during the hydrotreating process that transform these feedstocks into renewable transportation fuels and cause pressure drop issues.

Whereas in vegetable oils the formation the presence of high molecular weight compounds is an indicator of gum or micelles formation, the hydroxylation of the vegetable oil has pointed out that these structures are not compatible with the presence of hydroxyl groups within the hydrophobic part of the phospholipids. Thus, aggregation processes like the formation of micelles or liposomes may be occurring while storing these fatty acid feedstocks.

With respect to the phosphorus species within the fast pyrolysis oils, they possess a different chemical structure when they are separated in terms of polarity: While those species soluble in xylene possess a smaller size that is in agreement with the size of free phospholipids or their fragments, those polar species that will not be solubilised in xylene tend to be much greater in size, suggesting that formation of big aggregates, such as macro-complex, micelles or liposomes might be occurring.

Notes

The authors declare no competing financial interest.

REFERENCES

1 H. D. C. HAMJE, H. HASS, L. LONZA, H. MAAS, A. REID, K. D.ROSE and T. VENDERBOSCH, *EU renewable energy targets in 2020: Revised analysis of scenarios for transport fuels. Luxembourg: Publications Office of the European Union*, 2014.

2 European Commission, *Official Journal of the European Union*, 2018, **61**, 1–230.

3 S. N. Naik, V. v Goud, P. K. Rout and A. K. Dalai, *Renewable and Sustainable Energy Reviews*, 2010, **14**, 578–597.

4 J. van Gerpen, *Fuel Processing Technology*, 2005, **86**, 1097–1107.

5 R. G. Egeberg, N. H. Michaelsen and L. Skyum, 2010, 21.

6 G. W. Huber, P. O'Connor and A. Corma, *Applied Catalysis A: General*, 2007, **329**, 120–129.

7 A. v. Bridgwater, *Biomass and Bioenergy*, 2012, **38**, 68–94.

8 T. Bridgwater, S. Czernik and A. v Bridgwater, 2016, 590–598.

9 V. Dhyani and T. Bhaskar, *Renewable Energy*, 2018, **129**, 695–716.

10 E. D. Revellame, W. E. Holmes, T. J. Benson, A. L. Forks, W. T. French and R. Hernandez, in *Topics in Catalysis*, Springer, 2012, vol. 55, pp. 185–195.

11 D. Kubička and J. Horáček, *Applied Catalysis A: General*, 2011, **394**, 9–17.

12 S. Verdier, O. F. Alkilde, R. Chopra, J. Gabrielsen and M. Grubb, .

13 G. Sengar, P. Kaushal, H. K. Sharma and M. Kaur, *Reviews in Chemical Engineering*, 2014, **30**, 183–198.

14 Y. C. Sharma, M. Yadav and S. N. Upadhyay, *Biofuels, Bioproducts and Biorefining*, 2019, **13**, 174–191.

15 O. Ekholm, S. Jaikishan, M. Lönnfors, T. K. M. Nyholm and J. P. Slotte, *Biochimica et Biophysica Acta - Biomembranes*, 2011, **1808**, 727–732.

16 M. Garcia-Perez, A. Chaala, H. Pakdel, D. Kretschmer and C. Roy, *Biomass and Bioenergy*, 2007, **31**, 222–242.

17 C. A. Mullen and A. A. Boateng, *Journal of Analytical and Applied Pyrolysis*, 2011, **90**, 197–203.

18 Y. S. Choi, P. A. Johnston, R. C. Brown, B. H. Shanks and K. H. Lee, *Journal of Analytical and Applied Pyrolysis*, 2014, **110**, 147–154.

19 B. Scholze, C. Hanser and D. Meier, *Journal of Analytical and Applied Pyrolysis*, 2001, **58–59**, 387–400.

20 G. Caumette, C.-P. Lienemann, I. Merdrignac, B. Bouyssiere and R. Lobinski, *Journal of Analytical Atomic Spectrometry*, 2009, **24**, 263–276.

21 G. Caumette, C. P. Lienemann, I. Merdrignac, B. Bouyssiere and R. Lobinski, *Journal of Analytical Atomic Spectrometry*, 2010, **25**, 1123–1129.

22 G. Gascon, V. Vargas, L. Feo, O. Castellano, J. Castillo, P. Giusti, S. Acavedo, C.-P. Lienemann and B. Bouyssiere, *Energy & Fuels*, 2017, **31**, 7783–7788.

23 V. Vargas, J. Castillo, R. Ocampo Torres, B. Bouyssiere and C. P. Lienemann, *Fuel Processing Technology*, 2017, **162**, 37–44.

24 V. Garcia-Montoto, S. Verdier, Z. Maroun, R. Egeberg, J. L. Tiedje, S. Sandersen, P. Zeuthen and B. Bouyssiere, *Fuel Processing Technology*, 2020, **201**, 106341.

25 G. Gascon, J. Negrín, V. G. Montoto, S. Acevedo, C.-P. Lienemann and B. Bouyssiere, *Energy & Fuels*, 2019, **33**, 8110–8117.

26 G. Gascon, J. Negrin, V. Garcia-Montoto, S. Acevedo, C. P. Lienemann and B. Bouyssiere, *Energy and Fuels*, 2019, **33**, 1922–1927.

27 S. Verdier, P. Wiwel, J. Gabrielsen and L. F. Østergaard, .

28 S. H. Tan and G. Horlick, *Applied Spectroscopy*, 1986, **40**, 445–460.

29 A. Desprez, B. Bouyssiere, C. Arnaudguilhem, G. Krier, L. Vernex-Loset and P. Giusti, *Energy & Fuels*, 2014, **28**, 3730–3737.

30 2006, 1, US 20060041156 A1.

31 D. R. Erickson, in *Practical Handbook of Soybean Processing and Utilization*, Elsevier, 1995, pp. 174–183.

32 S. W. Banks, D. J. Nowakowski and A. v Bridgwater, *Energy & Fuels*, 2016, **30**, 8009–8018.

CONCLUDING REMARKS AND PERSPECTIVES

The main objectives of this thesis project were to provide with novel alternatives for the speciation analysis in bio-oils and other petroleum heavy oil fractions and to achieve a better knowledge and understanding on the behaviour of the hetero-atomic species present in these samples. Through combining different modern separation techniques with the elemental detection that the ICP provides, different solutions have been proposed in order to understand the behaviour of some of the trace elements present in such complex samples.

The first main objective of this thesis, which consisted of introducing, developing and validating novel analytical tools for the speciation analysis of bio-oils and renewable feedstocks, has been partially fulfilled.

For the first time, in order to fulfil the sub-objective **O1a**, a 3D-printed total consumption nebuliser has been developed and optimised for speciation analysis purposes. 3D-printing technology has proven its usefulness in the analytical chemistry field, being able to provide with cheap and high-quality consumables. Furthermore, the use of PEEK tubing within this 3D-printed total consumption nebuliser will avoid the potential interferences that other species might have with the former silica capillary present in previous total consumption nebulisers.

Further analysis will be carried out in the near future with this consumable for the speciation analysis of both crude oil products and renewable feedstocks. In addition, the development of a complemental heating device, designed to increase the temperature of the spray chamber that links the nebuliser with the ICP torch, has already started. Through the combination of these two novel consumables, a higher sensitivity on the ICP-MS analysis will reduce the DL of this technique and improve the quality of the GPC-ICP-HRMS chromatograms, specially of those elements that require a higher resolution, such as K and Si.

Besides, with the purpose of fulfilling the objectives **O1b** and **O1c**, the use of two alternative techniques has been studied and a methodology has been established for the analysis of unconventional oils for each of them: SFC-ICP-MS and ETV-ICP-OES. Further

experiments must be carried out in order to improve the quality of the information that these methodologies can provide.

Although the results obtained with the use of 2-Picolylamine as stationary phase in the hyphenation of SFC and ICP-MS did not provide with broad information about the speciation of the trace elements studied in the correspondent section of this thesis, the objective **O1b** has been partially achieved, since a proof-of-concept that comprises a novel interface that allows the hyphenation of modern supercritical fluid chromatographs with ICP-MS has been validated, allowing the use of two co-eluents (CO_2 and MeOH) during the separation process. Further experiments, considering the evaluation of different stationary phases should be carried out.

With regard to the objective **O1c**, the development of a new speciation technique has been achieved. ETV-ICP-OES analyses of fast pyrolysis oil samples have been carried out with an alternative reaction gas, less reactive but more environmentally friendly than the former gases that were commercialised (Freon-R12). However, further experiments need to be carried out to understand the speciation of these trace elements in renewable feedstocks. The analysis of standards that resemble those analytes of interest might provide with useful information about the vaporisation temperatures of different chemical structures and families.

Concerning the second main objective of this thesis, which consisted of obtaining a better understanding of the trace element composition of petroleum heavy oil fractions and renewable feedstocks, significative advances have been achieved during this three-year project.

In Chapter 6, alongside a familiarisation with the state-of-the-art GPC-ICP-HRMS technique that allows the study of the trace elements in petroleum compounds, a better understanding of how V, Ni and S compounds during the hydrodemetallization and hydrodesulfurization process of crude oil atmospheric residue has been achieved, together with the fulfilment of the objective **O2a**. In addition, this study has provided with insights into the preference that the catalysts possess towards some of the compounds and nanoaggregates that are present in crude oil atmospheric residues.

The results obtained in the Chapter 6 of this thesis might be very useful for further analyses carried out with other analytical techniques, since the elucidation of the structure of such aggregates would be useful for the industry, as better catalysts could be designed to avoid this undesirable reduction of their activity during the hydrothermal processes. For this purpose, FT-ICR-MS would be one of the best candidates to achieve this goal in future projects. By knowing the structure of these compounds, a novel generation of longer-life catalysts might be designed, providing to the petroleum industry with important economic savings and a faster production process of high-quality transportation fuels.

This familiarisation with the GPC-ICP-MS technique has eased the optimisation of a method, which allowed the analysis of other trace elements in fast pyrolysis oils and fatty acid feedstocks, and which has been described in the Chapter 7 of this PhD thesis, fulfilling the sub-objective **O2b**. A better understanding of the behaviour of the phosphorus compounds present in this type of samples has been achieved through the obtention of their corresponding GPC profiles: phosphorus compounds form high molecular weight compounds, potentially micelles, liposomes or long polymers, when they are present in these feedstocks. Furthermore, an aggregation/polymerisation phenomenon of these compounds has been confirmed by analysing the same samples over a period of three months. These resulting big aggregates might have a great contribution to the catalyst poisoning and the pressure drops that occur during the processes that transform these feedstocks into high-quality transportation fuels.

By performing a fractionation of these different compounds based on their molecular size, added to the use of complementary techniques such as FT-ICR-MS it will be possible to achieve a new insight into the structure and reactivity of these compounds, which would allow the synthesis of novel and more refractory catalysts towards these compounds.

Furthermore, for the first time, a fingerprint based on the molecular size of the sulfur-, sodium-, iron- and magnesium-containing compounds in pyrolysis oil feedstocks has been obtained via GPC-ICP-HRMS analysis. The early retention times that have been obtained for the different pyrolysis oil feedstocks that have been analysed, concerning these four elements, suggest that they are present as complexes or high molecular weight compounds within the pyrolysis oil matrices. In addition, the different distributions that have been

observed in the GPC-ICP-HRMS chromatograms suggest that each of the detected elements form different species on each of the analysed feedstocks. As mentioned before, the size fractionation of these samples and their posterior analysis with a technique such as FT-ICR-MS might help for the elucidation of the structures of these species. The hypothesis that suggests that the presence of chlorophyll derivates and iron and sodium complexes would be confirmed.

This technique has showed a great performance on the obtention of molecular fingerprints. By using the novel 3D-printed nebuliser that was designed and developed during this work, the speciation analysis of more elements such as Si and K could be carried out. In addition, a sampling approach, similar to the one that is detailed in Article 2, of hydrotreating pyrolysis oil products would provide with insights on the behaviour of such hetero-atom-containing species during the hydrodeoxygenation process, through their analysis via GPC-ICP-HRMS.

BIBLIOGRAPHY

(1) Wermuth, C. G.; Ganellin, C. R.; Lindberg, P.; Mitscher, L. a. Glossary for Chemists of Terms Used in Medicinal Chemistry. *Pure Appl. Chem.* **1998**, *70* (5), 1129–1143. https://doi.org/10.1351/pac197951081725.

(2) European Parliament. *Directive 2009/28/EC of the European Parliament and of the Council of 23 April 2009 on the Promotion of the Use of Energy from Renewable Sources and Amending and Subsequently Repealing Directives 2001/77/EC and 2003/30/EC*; 2009; Vol. OJ L, pp 16–62. https://doi.org/10.3000/17252555.L_2009.140.eng.

(3) Demirbaş, A. Current Technologies for the Thermo-Conversion of Biomass into Fuels and Chemicals. *Energy Sources* **2004**, *26* (8), 715–730. https://doi.org/10.1080/00908310490445562.

(4) U.S. Energy Information Administration. *Monthly Energy Review October 2018*; 2018; Vol. 0035.

(5) Chen, D.; Zhou, J.; Zhang, Q.; Zhu, X. Evaluation Methods and Research Progresses in Bio-Oil Storage Stability. *Renew. Sustain. Energy Rev.* **2014**, *40*, 69–79. https://doi.org/10.1016/j.rser.2014.07.159.

(6) Vassilev, S. V.; Baxter, D.; Andersen, L. K.; Vassileva, C. G. An Overview of the Chemical Composition of Biomass. *Fuel* **2010**, *89* (5), 913–933. https://doi.org/10.1016/j.fuel.2009.10.022.

(7) Nigam, P. S.; Singh, A. Production of Liquid Biofuels from Renewable Resources. *Prog. Energy Combust. Sci.* **2011**, *37* (1), 52–68. https://doi.org/10.1016/j.pecs.2010.01.003.

(8) Chisti, Y. Biodiesel from Microalgae. *Biotechnol. Adv.* **2007**, *25* (3), 294–306. https://doi.org/10.1016/j.biotechadv.2007.02.001.

(9) Shuba, E. S.; Kifle, D. Microalgae to Biofuels: 'Promising' Alternative and Renewable Energy, Review. *Renew. Sustain. Energy Rev.* **2018**, *81*, 743–755. https://doi.org/10.1016/j.rser.2017.08.042.

(10) Brennan, L.; Owende, P. Biofuels from Microalgae—A Review of Technologies for Production, Processing, and Extractions of Biofuels and Co-Products. *Renew. Sustain. Energy Rev.* **2010**, *14* (2), 557–577. https://doi.org/10.1016/j.rser.2009.10.009.

(11) Powell, R. W.; Elton, C.; Prestidge, R.; Belanger, H. Biobased Chemicals and Polymers. In *Plant Biomass Conversion*; Hood, E. E., Nelson, P., Powell, R., Eds.; John Wiley & Sons, Inc.: Hoboken, NJ, USA, 2011; pp 275–309.

(12) Tolbert, A.; Akinosho, H.; Khunsupat, R.; Naskar, A. K.; Ragauskas, A. J. Characterization and Analysis of the Molecular Weight of Lignin for Biorefining Studies. *Biofuels, Bioprod. Biorefining* **2014**, *8* (6), 836–856. https://doi.org/10.1002/bbb.1500.

(13) Sakagami, H.; Kushida, T.; Oizumi, T.; Nakashima, H.; Makino, T. Distribution of Lignin-Carbohydrate Complex in Plant Kingdom and Its Functionality as Alternative Medicine. *Pharmacol. Ther.* **2010**, *128* (1), 91–105. https://doi.org/10.1016/j.pharmthera.2010.05.004.

(14) Wang, S.; Dai, G.; Yang, H.; Luo, Z. Lignocellulosic Biomass Pyrolysis Mechanism: A State-of-the-Art Review. *Prog. Energy Combust. Sci.* **2017**, *62*, 33–86. https://doi.org/10.1016/j.pecs.2017.05.004.

(15) Stryer, L. *Biochemistry*; San Francisco : W. H. Freeman, 1975.

(16) Kordulis, C.; Bourikas, K.; Gousi, M.; Kordouli, E.; Lycourghiotis, A. Development of Nickel Based Catalysts for the Transformation of Natural Triglycerides and Related Compounds into Green Diesel: A Critical Review. *Appl. Catal. B Environ.* **2016**, *181*, 156–196. https://doi.org/10.1016/J.APCATB.2015.07.042.

(17) Doshi, V. A.; Vuthaluru, H. B.; Bastow, T. Investigations into the Control of Odour

and Viscosity of Biomass Oil Derived from Pyrolysis of Sewage Sludge. *Fuel Process. Technol.* **2005**, *86* (8), 885–897. https://doi.org/10.1016/j.fuproc.2004.10.001.

(18) Mastral, A. M.; Murillo, R.; Callén, M. S.; García, T.; Snape, C. E. Influence of Process Variables on Oils from Tire Pyrolysis and Hydropyrolysis in a Swept Fixed Bed Reactor. *Energy & Fuels* **2000**, *14* (4), 739–744. https://doi.org/10.1021/ef990183e.

(19) Dhyani, V.; Bhaskar, T. A Comprehensive Review on the Pyrolysis of Lignocellulosic Biomass. *Renew. Energy* **2018**, *129*, 695–716. https://doi.org/10.1016/j.renene.2017.04.035.

(20) Bridgwater, A. V. Review of Fast Pyrolysis of Biomass and Product Upgrading. *Biomass and Bioenergy* **2012**, *38*, 68–94. https://doi.org/10.1016/j.biombioe.2011.01.048.

(21) Bridgwater, T.; Czernik, S.; Bridgwater, A. V. Overview of Applications of Biomass Fast Pyrolysis Oil Overview of Applications of Biomass Fast Pyrolysis Oil. **2016**, No. MARCH 2004, 590–598. https://doi.org/10.1021/ef034067u.

(22) Van de Velden, M.; Baeyens, J.; Brems, A.; Janssens, B.; Dewil, R. Fundamentals, Kinetics and Endothermicity of the Biomass Pyrolysis Reaction. *Renew. Energy* **2010**, *35* (1), 232–242. https://doi.org/10.1016/j.renene.2009.04.019.

(23) Bridgwater, A. V. Renewable Fuels and Chemicals by Thermal Processing of Biomass. *Chem. Eng. J.* **2003**, *91* (2), 87–102. https://doi.org/10.1016/S1385-8947(02)00142-0.

(24) Zhang, S.; Yan, Y.; Li, T.; Ren, Z. Upgrading of Liquid Fuel from the Pyrolysis of Biomass. *Bioresour. Technol.* **2005**, *96* (5), 545–550. https://doi.org/10.1016/j.biortech.2004.06.015.

(25) Mohan, D.; Pittman, C. U.; Steele, P. H. Pyrolysis of Wood/Biomass for Bio-Oil: A Critical Review. *Energy and Fuels* **2006**, *20* (3), 848–889. https://doi.org/10.1021/ef0502397.

(26) Agblevor, F. A.; Besler, S. Inorganic Compounds in Biomass Feedstocks. 1. Effect on the Quality of Fast Pyrolysis Oils. *Energy & Fuels* **1996**, *10* (2), 293–298. https://doi.org/10.1021/ef950202u.

(27) Vitolo, S.; Seggiani, M.; Frediani, P.; Ambrosini, G.; Politi, L. Catalytic Upgrading of Pyrolytic Oils to Fuel over Different Zeolites. *Fuel* **1999**, *78* (10), 1147–1159. https://doi.org/10.1016/S0016-2361(99)00045-9.

(28) Czernik, S.; Johnson, D. K.; Black, S. Stability of Wood Fast Pyrolysis Oil. *Biomass and Bioenergy* **1994**, *7* (1–6), 187–192. https://doi.org/10.1016/0961-9534(94)00058-2.

(29) Nowakowski, D. J.; Jones, J. M.; Brydson, R. M. D.; Ross, A. B. Potassium Catalysis in the Pyrolysis Behaviour of Short Rotation Willow Coppice. *Fuel* **2007**, *86* (15), 2389–2402. https://doi.org/10.1016/j.fuel.2007.01.026.

(30) Nowakowski, D. J.; Jones, J. M. Uncatalysed and Potassium-Catalysed Pyrolysis of the Cell-Wall Constituents of Biomass and Their Model Compounds. *J. Anal. Appl. Pyrolysis* **2008**, *83* (1), 12–25. https://doi.org/10.1016/j.jaap.2008.05.007.

(31) Moses, C. A.; Bernstein, H. January 1994 • NRELffP-430-6085. **1994**, No. January.

(32) Knudsen, J. N.; Jensen, P. A.; Lin, W.; Frandsen, F. J.; Dam-Johansen, K. Sulfur Transformations during Thermal Conversion of Herbaceous Biomass. *Energy & Fuels* **2004**, *18* (3), 810–819. https://doi.org/10.1021/ef034085b.

(33) Williams, P. T.; Bottrill, P. Sulfur-Polycyclic Tyre Pyrolysis Oil. *Fuel* **1995**, *74* (5), 736–742.

(34) Banks, S. W.; Nowakowski, D. J.; Bridgwater, A. V. Impact of Potassium and Phosphorus in Biomass on the Properties of Fast Pyrolysis Bio-Oil. *Energy & Fuels* **2016**, *30* (10), 8009–8018. https://doi.org/10.1021/acs.energyfuels.6b01044.

(35) Tan, Z.; Lagerkvist, A. Phosphorus Recovery from the Biomass Ash: A Review. *Renew. Sustain. Energy Rev.* **2011**, *15* (8), 3588–3602.

https://doi.org/10.1016/j.rser.2011.05.016.

(36) Naik, S. N.; Goud, V. V; Rout, P. K.; Dalai, A. K. Production of First and Second Generation Biofuels: A Comprehensive Review. *Renew. Sustain. Energy Rev.* **2010**, *14* (2), 578–597. https://doi.org/10.1016/j.rser.2009.10.003.

(37) Knothe, G.; Krahl, J.; Van Gerpen, J. H. *The Biodiesel Handbook*; AOCS Press, 2010.

(38) Hoekman, S. K.; Broch, A.; Robbins, C.; Ceniceros, E.; Natarajan, M. Review of Biodiesel Composition, Properties, and Specifications. *Renew. Sustain. Energy Rev.* **2012**, *16* (1), 143–169. https://doi.org/10.1016/j.rser.2011.07.143.

(39) Egeberg, R. G.; Michaelsen, N. H.; Skyum, L. Novel Hydrotreating Technology for Production of Green Diesel. **2010**, 21.

(40) Huber, G. W.; O'Connor, P.; Corma, A. Processing Biomass in Conventional Oil Refineries: Production of High Quality Diesel by Hydrotreating Vegetable Oils in Heavy Vacuum Oil Mixtures. *Appl. Catal. A Gen.* **2007**, *329*, 120–129. https://doi.org/10.1016/J.APCATA.2007.07.002.

(41) Gerpen, J. Van. Biodiesel Processing and Production. *Fuel Process. Technol.* **2005**, *86* (10), 1097–1107. https://doi.org/10.1016/j.fuproc.2004.11.005.

(42) Caballero, B. Encyclopedia of Food Sciences and Nutrition. *Encycl. food Sci. Nutr.* **2003**, *1* (9), 1689–1699. https://doi.org/10.1017/CBO9781107415324.004.

(43) Sengar, G.; Kaushal, P.; Sharma, H. K.; Kaur, M. Degumming of Rice Bran Oil. *Rev. Chem. Eng.* **2014**, *30* (2), 183–198. https://doi.org/10.1515/revce-2013-0030.

(44) Sharma, Y. C.; Yadav, M.; Upadhyay, S. N. Latest Advances in Degumming Feedstock Oils for Large-Scale Biodiesel Production. *Biofuels, Bioprod. Biorefining* **2019**, *13* (1), 174–191. https://doi.org/10.1002/bbb.1937.

(45) Mohammad, M.; Kandaramath Hari, T.; Yaakob, Z.; Chandra Sharma, Y.; Sopian, K. Overview on the Production of Paraffin Based-Biofuels via Catalytic

Hydrodeoxygenation. *Renew. Sustain. Energy Rev.* **2013**, *22*, 121–132. https://doi.org/10.1016/j.rser.2013.01.026.

(46) de Oliveira, L. C. C.; Vieira, M. A.; Ribeiro, A. S.; Lisboa, M. T.; Gonçalves, R. A.; de Campos, R. C. Determination of Silicon in Vegetable Oil and Biodiesel by High-Resolution Continuum Source Flame Atomic Absorption Spectrometry Using Sample Dilution with Xylene. *Energy & Fuels* **2012**, *26* (11), 7041–7044. https://doi.org/10.1021/ef3012867.

(47) Vakh, C. S.; Bulatov, A. V.; Shishov, A. Y.; Zabrodin, A. V.; Moskvin, L. N. Determination of Silicon, Phosphorus, Iron and Aluminum in Biodiesel by Multicommutated Stepwise Injection Analysis with Classical Least Squares Method. *Fuel* **2014**, *135*, 198–204. https://doi.org/10.1016/j.fuel.2014.06.059.

(48) Bridgwater, A. V; Peacocke, G. V. C. Fast Pyrolysis Processes for Biomass. *Renew. Sustain. Energy Rev.* **2000**, *4* (1), 1–73. https://doi.org/10.1016/S1364-0321(99)00007-6.

(49) Khosravanipour Mostafazadeh, A.; Solomatnikova, O.; Drogui, P.; Tyagi, R. D. A Review of Recent Research and Developments in Fast Pyrolysis and Bio-Oil Upgrading. *Biomass Convers. Biorefinery* **2018**, *8* (3), 739–773. https://doi.org/10.1007/s13399-018-0320-z.

(50) Dabros, T. M. H.; Stummann, M. Z.; Høj, M.; Jensen, P. A.; Grunwaldt, J. D.; Gabrielsen, J.; Mortensen, P. M.; Jensen, A. D. Transportation Fuels from Biomass Fast Pyrolysis, Catalytic Hydrodeoxygenation, and Catalytic Fast Hydropyrolysis. *Prog. Energy Combust. Sci.* **2018**, *68*, 268–309. https://doi.org/10.1016/j.pecs.2018.05.002.

(51) Sepúlveda, C.; Escalona, N.; García, R.; Laurenti, D.; Vrinat, M. Hydrodeoxygenation and Hydrodesulfurization Co-Processing over ReS 2 Supported Catalysts. *Catal. Today* **2012**, *195* (1), 101–105. https://doi.org/10.1016/j.cattod.2012.05.047.

(52) Nolte, M. W.; Zhang, J.; Shanks, B. H. Ex Situ Hydrodeoxygenation in Biomass Pyrolysis Using Molybdenum Oxide and Low Pressure Hydrogen. *Green Chem.* **2015**, *18* (1), 134–138. https://doi.org/10.1039/c5gc01614b.

(53) Bartholomew, C. H. Mechanisms of Catalyst Deactivation. *Appl. Catal. A Gen.* **2001**, *212* (1–2), 17–60. https://doi.org/10.1016/S0926-860X(00)00843-7.

(54) Laurent, E.; Delmon, B. Influence of Water in the Deactivation of a Sulfided NiMoγ-Al2O3 Catalyst during Hydrodeoxygenation. *J. Catal.* **1994**, *146* (1), 281–291. https://doi.org/10.1016/0021-9517(94)90032-9.

(55) Mortensen, P. M.; Gardini, D.; Damsgaard, C. D.; Grunwaldt, J.-D.; Jensen, P. A.; Wagner, J. B.; Jensen, A. D. Deactivation of Ni-MoS2 by Bio-Oil Impurities during Hydrodeoxygenation of Phenol and Octanol. *Appl. Catal. A Gen.* **2016**, *523*, 159–170. https://doi.org/10.1016/J.APCATA.2016.06.002.

(56) Kubička, D.; Horáček, J. Deactivation of HDS Catalysts in Deoxygenation of Vegetable Oils. *Appl. Catal. A Gen.* **2011**, *394* (1–2), 9–17. https://doi.org/10.1016/j.apcata.2010.10.034.

(57) Skoog, D. A.; Crouch, S. R.; Holler, F. J. *Instrumental Analysis Principles*, 7th Editio.; Cengage Learning, 2016.

(58) Snyder, L. R.; Kirkland, J. J.; Dolan, J. W. *Introduction to Modern Liquid Chromatography*, 3rd ed.; Wiley, 2010.

(59) Eddy Diffusion (Multipath) Broadening in Chromatography - Chemistry LibreTexts https://chem.libretexts.org/Bookshelves/Analytical_Chemistry/Supplemental_Modules_(Analytical_Chemistry)/Analytical_Sciences_Digital_Library/JASDL/Courseware/Separation_Science/02_Text/03_Broadening_of_Chromatographic_Peaks/02_Eddy_Diffusion_(Multipath)_B (accessed Jul 9, 2019).

(60) Striegel, A. M.; Yau, W. W.; Kirkland, J. J.; Bly, D. D. *Modern Size-Exclusion Liquid Chromatography*; John Wiley & Sons, Inc.: Hoboken, NJ, USA, 2009. https://doi.org/10.1002/9780470442876.

(61) Held, D. Tips & Tricks GPC/ SEC: What Are the Differences Between GPC, SEC, and GFC, and How Do You Get Started with the Technique? *The Column* **2018**, *14* (10), 2–8.

(62) Laboureur, L.; Ollero, M.; Touboul, D. Lipidomics by Supercritical Fluid Chromatography. *Int. J. Mol. Sci.* **2015**, *16* (12), 13868–13884. https://doi.org/10.3390/ijms160613868.

(63) Lesellier, E.; West, C. The Many Faces of Packed Column Supercritical Fluid Chromatography – A Critical Review. *J. Chromatogr. A* **2015**, *1382*, 2–46. https://doi.org/10.1016/J.CHROMA.2014.12.083.

(64) Beginner's Guide to Convergence Chromatography 3 : Waters https://www.waters.com/waters/en_US/Beginner%27s-Guide-to-Convergence-Chromatography-3/nav.htm?cid=134941694&locale=en_US (accessed Jul 18, 2019).

(65) Gere, D. Supercritical Fluid Chromatography. *Science (80-.).* **1983**, *222* (4621), 253–259.

(66) Skoog, D. A.; Holler, F. J.; Crouch, S. R. *Principles of Instrumental Analysis*.

(67) Schaumlöffel, D.; Encinar, J. R.; Łobiński, R. Development of a Sheathless Interface between Reversed-Phase Capillary HPLC and ICPMS via a Microflow Total Consumption Nebulizer for Selenopeptide Mapping. *Anal. Chem.* **2003**, *75* (24), 6837–6842. https://doi.org/10.1021/ac034819h.

(68) Pröfrock, D.; Leonhard, P.; Ruck, W.; Prange, A. Development and Characterisation of a New Interface for Coupling Capillary LC with Collision-Cell ICP-MS and Its Application for Phosphorylation Profiling of Tryptic Protein Digests. *Anal. Bioanal. Chem.* **2005**, *381* (1), 194–204. https://doi.org/10.1007/s00216-004-2930-5.

(69) Schaumlöffel, D.; Giusti, P.; Zoriy, M. V.; Pickhardt, C.; Szpunar, J.; Łobiński, R.; Becker, J. S. Ultratrace Determination of Uranium and Plutonium by Nano-Volume Flow Injection Double-Focusing Sector Field Inductively Coupled Plasma Mass Spectrometry (NFI-ICP-SFMS). *J. Anal. At. Spectrom.* **2005**, *20* (1), 17–21.

https://doi.org/10.1039/b411567h.

(70) Giusti, P.; Schaumlöffel, D.; Encinar, J. R.; Szpunar, J. Interfacing Reversed-Phase NanoHPLC with ICP-MS and on-Line Isotope Dilution Analysis for the Accurate Quantification of Selenium-Containing Peptides in Protein Tryptic Digests. *J. Anal. At. Spectrom.* **2005**, *20* (10), 1101–1107. https://doi.org/10.1039/b506620d.

(71) Bustos, A. R. M. The Role of ICP-MS in Separation Science. *Chromatographia*. Springer February 1, 2020, pp 145–147. https://doi.org/10.1007/s10337-019-03846-2.

(72) Giusti, P.; Nuevo Ordonez, Y.; Philippe Lienemann, C.; Schaumlffel, D.; Bouyssiere, B.; Lobinski, R. UFlow-Injection-ICP Collision Cell MS Determination of Molybdenum, Nickel and Vanadium in Petroleum Samples Using a Modified Total Consumption Micronebulizer. *J. Anal. At. Spectrom.* **2007**, *22* (1), 88. https://doi.org/10.1039/b611542j.

(73) Desprez, A.; Bouyssiere, B.; Arnaudguilhem, C.; Krier, G.; Vernex-Loset, L.; Giusti, P. Study of the Size Distribution of Sulfur, Vanadium, and Nickel Compounds in Four Crude Oils and Their Distillation Cuts by Gel Permeation Chromatography Inductively Coupled Plasma High-Resolution Mass Spectrometry. *Energy & Fuels* **2014**, *28* (6), 3730–3737. https://doi.org/10.1021/ef500571f.

(74) Vargas, V.; Castillo, J.; Ocampo Torres, R.; Bouyssiere, B.; Lienemann, C. P. Development of a Chromatographic Methodology for the Separation and Quantification of V, Ni and S Compounds in Petroleum Products. *Fuel Process. Technol.* **2017**, *162*, 37–44. https://doi.org/10.1016/j.fuproc.2017.03.027.

(75) Caumette, G.; Lienemann, C. P.; Merdrignac, I.; Bouyssiere, B.; Lobinski, R. Fractionation and Speciation of Nickel and Vanadium in Crude Oils by Size Exclusion Chromatography-ICP MS and Normal Phase HPLC-ICP MS. *J. Anal. At. Spectrom.* **2010**, *25* (7), 1123–1129. https://doi.org/10.1039/c003455j.

(76) Caumette, G.; Lienemann, C. P.; Merdrignac, I.; Paucot, H.; Bouyssiere, B.; Lobinski,

R. Sensitivity Improvement in ICP MS Analysis of Fuels and Light Petroleum Matrices Using a Microflow Nebulizer and Heated Spray Chamber Sample Introduction. *Talanta* **2009**, *80* (2), 1039–1043. https://doi.org/10.1016/j.talanta.2009.08.017.

(77) Bernardin, M.; Bessueille-Barbier, F.; Le Masle, A.; Lienemann, C. P.; Heinisch, S. Suitable Interface for Coupling Liquid Chromatography to Inductively Coupled Plasma-Mass Spectrometry for the Analysis of Organic Matrices. 1 Theoretical and Experimental Considerations on Solute Dispersion. *J. Chromatogr. A* **2018**, *1565*, 68–80. https://doi.org/10.1016/j.chroma.2018.06.024.

(78) Shen, L.; Sun, J.; Cheng, H.; Liu, J.; Xu, Z.; Mu, J. A Demountable Nanoflow Nebulizer for Sheathless Interfacing Nano-High Performance Liquid Chromatography with Inductively Coupled Plasma Mass Spectrometry. *J. Anal. At. Spectrom.* **2015**, *30* (9), 1927–1934. https://doi.org/10.1039/c5ja00198f.

(79) Hoffmann, E. de; Stroobant, V. *Mass Spectrometry: Principles and Applications*, Third Edit.; Wiley, 2008.

(80) Introduction to mass analyzers : SHIMADZU (Shimadzu Corporation) https://www.shimadzu.com/an/lcms/support/fundamental/mass_analyzers.html (accessed Jul 18, 2019).

(81) Inductively Coupled Plasma Mass Spectrometry Information: ICP-MS Systems and Technologies https://www.thermofisher.com/dk/en/home/industrial/spectroscopy-elemental-isotope-analysis/spectroscopy-elemental-isotope-analysis-learning-center/trace-elemental-analysis-tea-information/inductively-coupled-plasma-mass-spectrometry-icp-ms-information/icp (accessed Jul 18, 2019).

(82) Gutierrez-Sama, S. Molecular Identification of Heteroatomic and Metal Species Related to Hydrometallation and Hydroconversion, University of Pau and Adour Countries, 2017.

(83) Caumette, G.; Lienemann, C.-P.; Merdrignac, I.; Bouyssiere, B.; Lobinski, R.

Element Speciation Analysis of Petroleum and Related Materials. *J. Anal. At. Spectrom.* **2009**, *24* (3), 263–276. https://doi.org/10.1039/B817888G.

(84) Garcia-Montoto, V.; Verdier, S.; Maroun, Z.; Egeberg, R.; Tiedje, J. L.; Sandersen, S.; Zeuthen, P.; Bouyssiere, B. Understanding the Removal of V, Ni and S in Crude Oil Atmospheric Residue Hydrodemetallization and Hydrodesulfurization. *Fuel Process. Technol.* **2020**, *201*, 106341. https://doi.org/10.1016/j.fuproc.2020.106341.

(85) Pohl, P.; Vorapalawut, N.; Bouyssiere, B.; Carrier, H.; Lobinski, R. Direct Multi-Element Analysis of Crude Oils and Gas Condensates by Double-Focusing Sector Field Inductively Coupled Plasma Mass Spectrometry (ICP MS). *J. Anal. At. Spectrom.* **2010**, *25* (5), 704–709. https://doi.org/10.1039/C000658K.

(86) Goussard, J.; Roulet, B. Free Expansion for Real Gases. *Am. J. Phys.* **1993**, *61* (9), 845–848. https://doi.org/10.1119/1.17417.

(87) Carey, J. M.; Vela, N. P.; Caruso, J. A. Multi-Element Detection for Supercritical Fluid Chromatography by Inductively Coupled Plasma Mass Spectrometry. *J. Anal. At. Spectrom.* **1992**, *7* (8), 1173. https://doi.org/10.1039/ja9920701173.

(88) Vela, N. P.; Caruso, J. A. Element Selective Detection for Supercritical-Fluid Chromatography. *J. Biochem. Biophys. Methods* **2000**, *43* (1), 45–58. https://doi.org/10.1016/S0165-022X(00)00091-9.

(89) Asfaw, A.; Wibetoe, G.; Beauchemin, D. Solid Sampling Electrothermal Vaporization Inductively Coupled Plasma Optical Emission Spectrometry for Discrimination of Automotive Paint Samples in Forensic Analysis. *J. Anal. At. Spectrom.* **2012**, *27* (11), 1928. https://doi.org/10.1039/c2ja30193h.

(90) Detcheva, A.; Barth, P.; Hassler, J. Calibration Possibilities and Modifier Use in ETV ICP OES Determination of Trace and Minor Elements in Plant Materials. *Anal. Bioanal. Chem.* **2009**, *394* (5), 1485–1495. https://doi.org/10.1007/s00216-009-2835-4.

(91) EU legislation to control F-gases | Climate Action

https://ec.europa.eu/clima/policies/f-gas/legislation_en (accessed Jul 13, 2019).

(92) United States Environmental Protection Agency (US EPA). Refrigerant Transition & Environmental Impacts https://www.epa.gov/mvac/refrigerant-transition-environmental-impacts (accessed Jul 13, 2019).

(93) Spectral Systems. ETV. http://www.spectral-systems.de/english/prod01.htm (accessed Jun 30, 2020).

(94) Vogt, T.; Bauer, D.; Neuroth, M.; Otto, M. Quantitative Multi-Element Analysis of Argonne Premium Coal Samples by ETV-ICP OES – A Highly Efficient Direct Analytical Technique for Inorganics in Coal. *Fuel* **2015**, *152*, 96–102. https://doi.org/10.1016/j.fuel.2014.12.057.

(95) Santos, C. M. M.; Nunes, M. a. G.; Costa, A. B.; Pozebon, D.; Duarte, F. A.; Dressler, V. L. Multielement Determination in Medicinal Plants Using Electrothermal Vaporization Coupled to ICP OES. *Anal. Methods* **2017**, *9* (23), 3497–3504. https://doi.org/10.1039/C7AY01021D.

(96) Silva, J. S.; Schneider Henn, A.; Dressler, V. L.; Mello, P. A.; Flores, E. M. M. Feasibility of Rare Earth Element Determination in Low Concentration in Crude Oil: Direct Sampling Electrothermal Vaporization-Inductively Coupled Plasma Mass Spectrometry. *Anal. Chem.* **2018**, *90* (11), 7064–7071. https://doi.org/10.1021/acs.analchem.8b01460.

(97) Bauer, D.; Vogt, T.; Klinger, M.; Masset, P. J.; Otto, M. Direct Determination of Sulfur Species in Coals from the Argonne Premium Sample Program by Solid Sampling Electrothermal Vaporization Inductively Coupled Plasma Optical Emission Spectrometry. *Anal. Chem.* **2014**, *86* (20), 10380–10388. https://doi.org/10.1021/ac502823e.

(98) Silva, J. S.; Schneider Henn, A.; Dressler, V. L.; Mello, P. A.; Flores, E. M. M. Feasibility of Rare Earth Element Determination in Low Concentration in Crude Oil: Direct Sampling Electrothermal Vaporization-Inductively Coupled Plasma

Mass Spectrometry. *Anal. Chem.* **2018**, *90* (11), 7064–7071. https://doi.org/10.1021/acs.analchem.8b01460.

(99) Loadman, M. J. R.; Loadman, M. J. R. Inorganic Fillers and Trace Metal Analysis. In *Analysis of Rubber and Rubber-like Polymers*; Springer Netherlands, 1998; pp 243–264. https://doi.org/10.1007/978-94-011-4435-3_10.

(100) Fertilizer Facts | Milorganite https://www.milorganite.com/blog/garden-landscape/fertilization-numbers (accessed Jul 6, 2020).

(101) BP. *BP Statistical Review of World Energy 2019.*; 2019. https://doi.org/10.1001/jama.1973.03220300055017.

(102) Gutiérrez Sama, S.; Barrère-Mangote, C.; Bouyssière, B.; Giusti, P.; Lobinski, R. Recent Trends in Element Speciation Analysis of Crude Oils and Heavy Petroleum Fractions. *TrAC - Trends in Analytical Chemistry*. Elsevier B.V. July 1, 2018, pp 69–76. https://doi.org/10.1016/j.trac.2017.10.014.

(103) Residues (petroleum), atmospheric - Substance Information - ECHA https://echa.europa.eu/substance-information/-/substanceinfo/100.063.414 (accessed Jun 18, 2020).

(104) Verdier, S.; Wiwel, P.; Gabrielsen, J.; Østergaard, L. F. Renewable Feedstock Analyses : Critical Need for Reproducibility Improvements.

(105) Llorent-Martínez, E. J.; Ortega-Barrales, P.; Fernández-De Córdova, M. L.; Domínguez-Vidal, A.; Ruiz-Medina, A. Investigation by ICP-MS of Trace Element Levels in Vegetable Edible Oils Produced in Spain. *Food Chem.* **2011**, *127* (3), 1257–1262. https://doi.org/10.1016/j.foodchem.2011.01.064.

(106) Benincasa, C.; Lewis, J.; Perri, E.; Sindona, G.; Tagarelli, A. Determination of Trace Element in Italian Virgin Olive Oils and Their Characterization According to Geographical Origin by Statistical Analysis. *Anal. Chim. Acta* **2007**, *585* (2), 366–370. https://doi.org/10.1016/j.aca.2006.12.040.

(107) Jiménez, M. S.; Velarte, R.; Castillo, J. R. On-Line Emulsions of Olive Oil Samples and ICP-MS Multi-Elemental Determination. *J. Anal. At. Spectrom.* **2003**, *18* (9), 1154–1162. https://doi.org/10.1039/b303131d.

(108) Castillo, J. R.; Jiménez, M. S.; Ebdon, L. Semiquantitative Simultaneous Determination of Metals in Olive Oil Using Direct Emulsion Nebulization. *J. Anal. At. Spectrom.* **1999**, *14* (9), 1515–1518. https://doi.org/10.1039/a900754g.

(109) Chaves, E. S.; Lepri, F. G.; Silva, J. S. A.; de Quadros, D. P. C.; Saint'Pierre, T. D.; Curtius, A. J. Determination of Co, Cu, Fe, Mn, Ni and V in Diesel and Biodiesel Samples by ETV-ICP-MS. *J. Environ. Monit.* **2008**, *10* (10), 1211. https://doi.org/10.1039/b809501a.

(110) Nerín, C.; Domeño, C.; Moliner, R.; Lázaro, M. J.; Suelves, I.; Valderrama, J. Behaviour of Different Industrial Waste Oils in a Pyrolysis Process: Metals Distribution and Valuable Products. *J. Anal. Appl. Pyrolysis* **2000**, *55* (2), 171–183. https://doi.org/10.1016/S0165-2370(99)00097-2.

(111) ASTM D6751 - 20 Standard Specification for Biodiesel Fuel Blend Stock (B100) for Middle Distillate Fuels https://www.astm.org/Standards/D6751.htm (accessed Apr 1, 2020).

(112) Sánchez, R.; Sánchez, C.; Lienemann, C. P.; Todolí, J. L. Metal and Metalloid Determination in Biodiesel and Bioethanol. *J. Anal. At. Spectrom.* **2015**, *30* (1), 64–101. https://doi.org/10.1039/c4ja00202d.

(113) Sánchez, C.; Lienemann, C.-P.; Todolí, J.-L. Analysis of Bioethanol Samples through Inductively Coupled Plasma Mass Spectrometry with a Total Sample Consumption System. *Spectrochim. Acta Part B At. Spectrosc.* **2016**, *124*, 99–108. https://doi.org/10.1016/j.sab.2016.08.018.

(114) Amais, R. S.; Donati, G. L.; Schiavo, D.; Nóbrega, J. A. A Simple Dilute-and-Shoot Procedure for Si Determination in Diesel and Biodiesel by Microwave-Induced Plasma Optical Emission Spectrometry. *Microchem. J.* **2013**, *106*, 318–322.

https://doi.org/10.1016/j.microc.2012.09.001.

(115) Amais, R. S.; Donati, G. L.; Schiavo, D.; Nóbrega, J. A. Determination of Silicon in Diesel and Biodiesel by Microwave Plasma-Atomic Emission Spectrometry (Application Note 5991-0490EN). *Agil. Technol.* **2012**, 1–6.

(116) Al Chami, Z.; Amer, N.; Smets, K.; Yperman, J.; Carleer, R.; Dumontet, S.; Vangronsveld, J. Evaluation of Flash and Slow Pyrolysis Applied on Heavy Metal Contaminated Sorghum Bicolor Shoots Resulting from Phytoremediation. *Biomass and Bioenergy* **2014**, *63*, 268–279. https://doi.org/10.1016/j.biombioe.2014.02.027.

(117) Chiang, H. L.; Lin, K. H.; Lai, N.; Shieh, Z. X. Element and PAH Constituents in the Residues and Liquid Oil from Biosludge Pyrolysis in an Electrical Thermal Furnace. *Sci. Total Environ.* **2014**, *481* (1), 533–541. https://doi.org/10.1016/j.scitotenv.2014.02.083.

(118) Zhang, M.; Gao, X.; Wu, H. A Method for the Quantification of Alkali and Alkaline Earth Metallic Species in Bioslurry Fuels. *Energy and Fuels* **2013**, *27* (11), 6823–6830. https://doi.org/10.1021/ef401632h.

(119) IUPAC. *Compendium of Chemical Terminology, 2nd Ed. (the "Gold Book"). Compiled by A. D. McNaught and A. Wilkinson*; Blackwell Scientific Publications, Oxford, 1997. https://doi.org/https://doi.org/10.1351/goldbook.

(120) Saint'Pierre, T. D.; Frescura, V. L. A.; Curtius, A. J. The Development of a Method for the Determination of Trace Elements in Fuel Alcohol by ETV-ICP-MS Using Isotope Dilution Calibration. *Talanta* **2006**, *68* (3), 957–962. https://doi.org/10.1016/j.talanta.2005.06.047.

(121) Sánchez, C.; Vidal, J. P.; Lienemann, C. P.; Todolí, J. L. Evolution of the Metal and Metalloid Content along the Bioethanol Production Process. *Fuel Process. Technol.* **2018**, *173* (January), 1–10. https://doi.org/10.1016/j.fuproc.2018.01.001.

(122) Vintila, T.; Negrea, A.; Barbu, H.; Sumalan, R.; Kovacs, K. Metal Distribution in the Process of Lignocellulosic Ethanol Production from Heavy Metal Contaminated

Sorghum Biomass. *J. Chem. Technol. Biotechnol.* **2016**, *91* (6), 1607–1614. https://doi.org/10.1002/jctb.4902.

(123) Kanaujia, P. K.; Sharma, Y. K.; Agrawal, U. C.; Garg, M. O. Analytical Approaches to Characterizing Pyrolysis Oil from Biomass. *TrAC - Trends Anal. Chem.* **2013**, *42*, 125–136. https://doi.org/10.1016/j.trac.2012.09.009.

(124) Yuan, X.; Leng, L.; Huang, H.; Chen, X.; Wang, H.; Xiao, Z.; Zhai, Y.; Chen, H.; Zeng, G. Speciation and Environmental Risk Assessment of Heavy Metal in Bio-Oil from Liquefaction/Pyrolysis of Sewage Sludge. *Chemosphere* **2015**, *120*, 645–652. https://doi.org/10.1016/j.chemosphere.2014.10.010.

(125) Huang, R.; Fang, C.; Zhang, B.; Tang, Y. Transformations of Phosphorus Speciation during (Hydro)Thermal Treatments of Animal Manures. *Environ. Sci. Technol.* **2018**, *52* (5), 3016–3026. https://doi.org/10.1021/acs.est.7b05203.

(126) Staš, M.; Chudoba, J.; Auersvald, M.; Kubička, D.; Conrad, S.; Schulzke, T.; Pospíšil, M. Application of Orbitrap Mass Spectrometry for Analysis of Model Bio-Oil Compounds and Fast Pyrolysis Bio-Oils from Different Biomass Sources. *J. Anal. Appl. Pyrolysis* **2017**, *124*, 230–238. https://doi.org/10.1016/j.jaap.2017.02.002.

(127) Scholze, B.; Meier, D. Characterization of the Water-Insoluble Fraction from Pyrolysis Oil (Pyrolytic Lignin). Part I. PY–GC/MS, FTIR, and Functional Groups. *J. Anal. Appl. Pyrolysis* **2001**, *60* (1), 41–54. https://doi.org/10.1016/S0165-2370(00)00110-8.

(128) Mythili, R.; Venkatachalam, P.; Subramanian, P.; Uma, D. Characterization of Bioresidues for Biooil Production through Pyrolysis. *Bioresour. Technol.* **2013**, *138*, 71–78. https://doi.org/10.1016/j.biortech.2013.03.161.

(129) Michailof, C. M.; Kalogiannis, K. G.; Sfetsas, T.; Patiaka, D. T.; Lappas, A. A. Advanced Analytical Techniques for Bio-Oil Characterization. *Wiley Interdiscip. Rev. Energy Environ.* **2016**, *5* (6), 614–639. https://doi.org/10.1002/wene.208.

(130) Garcia-Perez, M.; Chaala, A.; Pakdel, H.; Kretschmer, D.; Roy, C. Characterization

of Bio-Oils in Chemical Families. *Biomass and Bioenergy* **2007**, *31* (4), 222–242. https://doi.org/10.1016/j.biombioe.2006.02.006.

(131) Verdier, S.; Alkilde, O. F.; Chopra, R.; Gabrielsen, J.; Grubb, M. Hydroprocessing of Renewable Feedstocks - Challenges and Solutions. **2019**.

(132) Gascon, G.; Vargas, V.; Feo, L.; Castellano, O.; Castillo, J.; Giusti, P.; Acavedo, S.; Lienemann, C.-P.; Bouyssiere, B. Size Distributions of Sulfur, Vanadium, and Nickel Compounds in Crude Oils, Residues, and Their Saturate, Aromatic, Resin, and Asphaltene Fractions Determined by Gel Permeation Chromatography Inductively Coupled Plasma High-Resolution Mass Spectrometry. *Energy & Fuels* **2017**, *31* (8), 7783–7788. https://doi.org/10.1021/acs.energyfuels.7b00527.

(133) Greenwood, N. N.; Earnshaw, A. Iron, Ruthenium and Osmium. In *Chemistry of the Elements*; Elsevier, 1997; pp 1070–1112. https://doi.org/10.1016/b978-0-7506-3365-9.50031-6.

(134) Uehara, K.; Mimuro, M.; Fujita, Y.; Tanaka, M. SPECTRAL ANALYSIS OF CHLOROPHYLL a AGGREGATES IN THE PRESENCE OF WATER-SOLUBLE MACROMOLECULES. *Photochem. Photobiol.* **1988**, *48* (6), 725–732. https://doi.org/10.1111/j.1751-1097.1988.tb02887.x.

(135) Helenius, V. M.; Hynninen, P. H.; Korppi-Tommola, J. E. I. CHLOROPHYLL a AGGREGATES IN HYDROCARBON SOLUTION, A PICOSECOND SPECTROSCOPY AND MOLECULAR MODELING STUDY. *Photochem. Photobiol.* **1993**, *58* (6), 867–873. https://doi.org/10.1111/j.1751-1097.1993.tb04985.x.

(136) Zandvoort, M. A. M. J. van; Wróbel, D.; Lettinga, P.; Ginkel, G. van; Levine, Y. K. CHLOROPHYLLS IN POLYMERS. I. STATE OF CHLOROPHYLL a IN UNSTRETCHED POLYMER SYSTEMS. *Photochem. Photobiol.* **1995**, *62* (2), 279–289. https://doi.org/10.1111/j.1751-1097.1995.tb05270.x.

ANNEXES

Poster presented at the 48th International Symposium on High-Performance Liquid Phase Separations and Related Techniques

This poster has been presented at the *48th International Symposium on High-Performance Liquid Phase Separations and Related Techniques* in Milan, Italy, on June 2019. This poster collects the original idea of hyphenating SFC simultaneously with ESI-MS and ICP-MS. However, due to technical issues, this simultaneous coupling could not have been completed.

Inorganic speciation of bio-oils and their feedstocks with GPC ICP MS / ESI MS & SFC ESI MS / ICP MS

Victor Garcia-Montoto, Pablo Denti, Linus Malmquist, Giorgio Tomasi, Sylvain Verdier, Jan H. Christensen, Brice Bouyssiere

As part of a PhD project under the name "Speciation Analysis in Bio-oils" this poster comprises the experiments taking place currently at the University of Copenhagen (Denmark) since last February. In this work, the on-line combination of two chromatographic techniques hyphenated with elementary and molecular detection techniques (ICP MS and ESI MS) is carried out with the purpose of elucidating the different inorganic species present in these considerably complex matrices. A first step consisted of determining the size distributions of the different inorganic species in the bio-oil samples by GPC ICP MS. Then, fraction collection is carried out and each fraction will be analysed by SFC ICP MS and SFC ESI MS in order to obtain both elemental and molecular information.
This poster resumes the analyses carried out so far, focusing on the characterisation of pyrolysis oils, whose complex matrix and low solubility determine the challenges during analysis.

GPC ICP HRMS

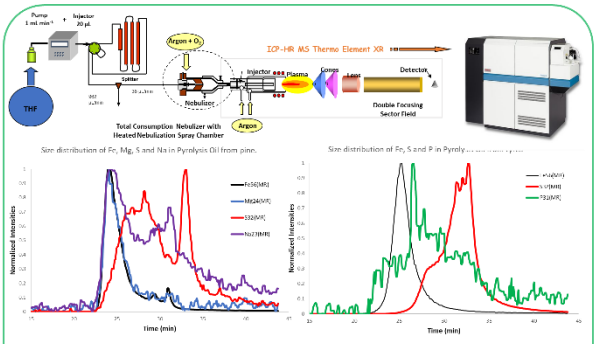

- ✓ Diverse size distributions have been found for different elements, indicating a different nature of the species. Metals tend to be linked to higher molecular weight compounds.
- ✓ The use of HR MS provides higher resolution, being thus able to determine the distributions of Sulphur and P species.

GPC ICP MS

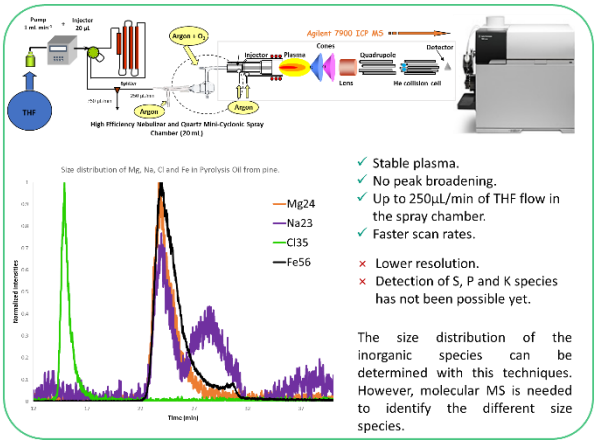

- ✓ Stable plasma.
- ✓ No peak broadening.
- ✓ Up to 250µL/min of THF flow in the spray chamber.
- ✓ Faster scan rates.
- × Lower resolution.
- × Detection of S, P and K species has not been possible yet.

The size distribution of the inorganic species can be determined with this techniques. However, molecular MS is needed to identify the different size species.

Preparative GPC

Waters Styragel GPC Columns x 3	
ID (mm)	7.8
Length (mm)	300
Stationary phase	PS/DVB
Exclusion limit (Da)	1000-600000
Pore size	HR 4, HR 2 and HR 0.5
Particle size (µm)	5

- ✓ The same three Gel Permeation Chromatography columns used for the previous analyses are also used for sample fractionation.
- ✓ 10 injections are needed for each sample in order to collect enough fractions to be analysed by SFC ICP MS.

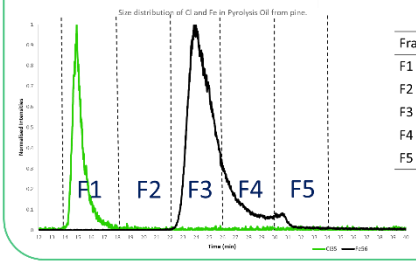

Fraction	Time (min)
F1	14 – 18
F2	18 – 22
F3	22 – 26
F4	26 - 30
F5	30 - 34

SFC ESI MS

- ✓ Two of the less complex samples were analysed by SFC ESI MS in order to select the ideal column and check the resolution without causing any damage.
- ✓ Tallow Fat and Soybean Oil samples were diluted up to 100 times in THF and then injected into a Torus 2-picolylamine (2-PIC, 3.0 × 100 mm, 1.7 µm, Waters, USA).
- ✓ Methanol was used as make-up solvent.
- ✓ Identification of the naturally occurring fatty acids within these samples was achieved.

Parameter	Value
Mobile phase	CO_2:EtOH
Flow rate	1.5 mL/min
Run time	40 min
Gradient (A:B)	0 min; 99:1
	10.0 min; 96:4
	23.0 min; 70:30
	35.0 min; 70:30
	35.1 min; 99:1
Injection vol.	1 µL
Column temperature	40 °C
ABPR	170 bar

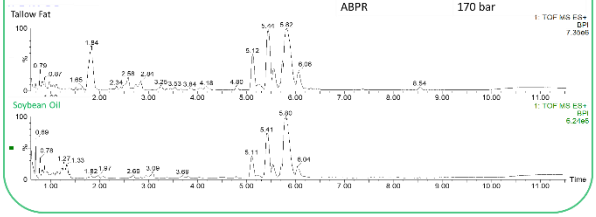

SFC ICP MS

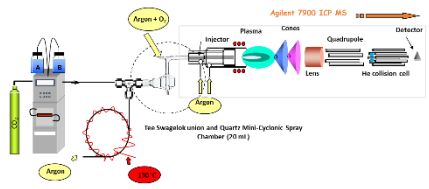

Mobile Phase (A:B): CO_2:EtOH (0.1% FA)
Flow Rate: 0.8 mL/min

- ✓ Heating tapes provide enough energy to avoid the cooling of CO_2 due to its expansion.
- ✓ Up to 30% of EtOH in the mobile phase has been reached.
- ✓ Peek tubing is used to connect the SFC with the ICP via tee union.
- ✓ A spray is formed at the end of the peek tube due to the expansion of the mobile phase.
- ✓ Plasma loss of energy is minimized: The use of a mini spray chamber allows only the finest droplets of mobile phase towards the plasma.
- × The use of a split at the end of the SFC is required.
- × Higher percentages of EtOH cause condensation in the spray chamber.
- × Optimisation in process.

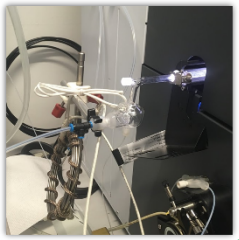

Simplification of heavy matrices by liquid-liquid extraction: Part I – How to separate LMW, MMW and HMW compounds in maltene fractions of V, Ni and S compounds.

energy&fuels
Article
Cite This: Energy Fuels 2019, 33, 1922−1927
pubs.acs.org/EF

Simplification of Heavy Matrices by Liquid−Liquid Extraction: Part I—How to Separate LMW, MMW, and HMW Compounds in Maltene Fractions of V, Ni, and S Compounds

German Gascon,[†,‡,§] Juan Negrin,[†] Victor Garcia-Montoto,[‡] Socrates Acevedo,[§] Charles-Philippe Lienemann,[∥] and Brice Bouyssiere*[,‡]

[†]PDVSA Intevep, Apartado 76343, Caracas 1070-A, Venezuela
[‡]CNRS/Univ pau & pays ADOUR/ E2S UPPA, Institut des Sciences Analytiques et de Physico- Chimie Pour L'environnement et les Materiaux, UMR5254, Helioparc- 2 Avenue du Président Angot, Pau 64000, France
[§]UCV, Facultad de Ciencias, Escuela de Química, Caracas 1053, Venezuela
[∥]IFP Energies Nouvelles, Rond-point de l'échangeur de Solaize, BP 3, Solaize 69360, France

ABSTRACT: A method using liquid−liquid extractions has been developed for matrix simplification and evaluated by gel permeation chromatography coupled with inductively coupled plasma and mass spectrometry. In this method, maltenes were dissolved in *n*-heptane and extractions with methanol (MeOH), acetonitrile (ACN), and dimethylformamide (DMF) were performed. The extraction with ACN is more efficient than that with MeOH for the removal of compounds with low-molecular weights (LMW) containing V (our reference element) and more selective than that with DMF (with this solvent, compounds with LMW and medium-molecular weights (MMW) are extracted). Thus, a sequential extraction was performed by applying ACN to selectively remove LMW compounds, followed by extractions with DMF of the resulting maltene to separate the MMW compounds from the high-molecular weights (HMW) compounds remaining in the final remnant maltene. The results show, for the first time in the literature, that it is possible to separate the three V and Ni species of compounds present in maltenes based on their molecular weights (HMW, MMW, and LMW).

INTRODUCTION

V and Ni are the most abundant metals that are naturally present in petroleum.[1] The high stabilities of these metals in crude oils, asphalts, and bitumens suggest that they mainly occur as tetrapyrrole complex-type metalloporphyrins. The predominance of Ni and V compounds compared to that of other organic metallocompounds is a consequence of the greater stability of nitrogen−vanadium or nickel bonds and their favorable electron configurations, among other factors.[2,3] A study performed using X-ray absorption fine structure spectroscopy showed that the coordination shells of all compounds of V and Ni present in petroleum are very similar to those of vanadyl and nickel porphyrins.[4,5] In terms of their distribution in the products of petroleum, these compounds are almost all concentrated in the atmospheric or vacuum residue based on their boiling points,[6] and they are present in asphaltenes and resins[7−9] when petroleum or the residue is separated in their SARA fractions. Recently, three distinct families coexisting in the crude fraction of petroleum have been identified based on their molecular weights. These have been identified as compounds with high-, medium-, and low-molecular weights (HMW, MMW, and LMW).[6,9,10] Regarding these compound families, we believe that compounds with LMW correspond to simple metalloporphyrins (MPs), whereas compounds with MMW and HMW correspond to MPs trapped or linked in nanoaggregates[9,11] due to the high capacities of some crude oil compounds to trap different compounds.[12,13] This idea is not new; since 1970, it has been accepted that some MPs behave as a single unit of the aromatic sheet in the generalized macrostructure of asphaltenes, as proposed by Dickie and Yen.[14,15] Other authors have proposed that these V or Ni compounds may be assimilated as subunits in these aggregates.[16−18] The physical separations of the different classes of compounds (HMW, MMW, and LMW) have not yet been reached, but this approach is relatively recent[6,9,10] and is due to the improvements made in their possible detection with inductively coupled plasma and mass spectrometry (ICP MS). It has long been believed that in petroleum there are two types of metallocompounds, one porphyrinic and a second that is bound,[14,19] giving rise to Ni and V compounds with high-molecular weights.[20] Over time, this classification was widely supported by the difference between the early direct determinations of metalloporphyrins by UV−vis and the total contents of Ni and V obtained by atomic spectrometric techniques.[19,21] The part that do not absorb in the UV−vis region (based on total determination using UV−vis detection) was then defined as nonporphyrinic compounds.[19] However, no compound different than metalloporphyrins has yet been reported, even through the use of high-resolution techniques in the direct analysis of crude oil or asphaltenes.[21−23] On the other hand, it has been reported that the low contents of metalloporphyrins determined by UV−vis detection are due to the limitations of the technique (UV−vis), the association between the asphaltene molecules and MPs,

Received: November 15, 2018
Revised: January 31, 2019
Published: February 12, 2019

ACS Publications © 2019 American Chemical Society

DOI: 10.1021/acs.energyfuels.8b03974
Energy Fuels 2019, 33, 1922−1927

Downloaded via UNIV OF PAU AND PAYS DE L'ADOUR on June 18, 2020 at 11:38:28 (UTC).
See https://pubs.acs.org/sharingguidelines for options on how to legitimately share published articles.

and the poor efficiency of the extraction methods employed.[24] With respect to this observation, diverse methods have been developed using either Soxhlet extractions or chromatography[25−29] separations with a packed column. However, we believe that these methods are not appropriate for the correct separation of the different compounds with HMW, MMW, and LMW containing V, Ni, and S present in crude oil, as they require a strongly related adsorbent/sample to obtain regular to poor separation.[30] Additionally, it is known that asphaltenes are strongly adsorbed by the adsorbents used with these methods and this adsorption may change the separation phenomena of the adsorbent. For all of these reasons, we have decided to develop a new strategy of separation. Specifically, we have decided to develop a method by liquid−liquid extraction of maltenes and a method by liquid−solid extraction of asphaltenes. These methods are proposed to avoid the use of adsorbents and, therefore, the possible adsorption of compounds containing V, Ni, and S. In this context, the separation of maltenes in three subtractions is presented in this work (the separation of asphaltenes will be presented in a second part). In the first part of this work, we present the results of the extraction performed with different solvents, and in the second part, we present the optimization of the method. The types of compounds obtained according to their MWs with this procedure were evaluated by gel permeation chromatography (GPC) ICP MS.

■ EXPERIMENTAL SECTION

Instrumentation. A high-performance liquid chromatograph (HPLC) (UltiMate 3000, Dionex, Amsterdam, The Netherlands) was used for separation by gel permeation chromatography and was coupled with ICP MS. The detailed conditions for ICP MS detection have previously been reported[9] and are summarized here. A high-resolution ICP MS instrument (Element XR, Thermo Scientific) operated at a resolution of 4000 was used. The ICP HRMS was equipped with an interface based on a microflow total consumption nebulizer without a drain maintained at 60 °C to minimize the signal suppression and increase the sensitivity by a factor of 3−4.[31] An oxygen flow of 0.08 mL/min was continuously added to the nebulizer gas flow (Ar) to avoid the deposition of carbon on the cones.

Samples, Reagents, and Materials. In this work, a Venezuelan crude oil was used (8°API). This was provided by PDVSA Intevep. *n*-heptane, methanol (MeOH), acetonitrile (ACN), and dimethylformamide (DMF) grade HPLC (Sigma-Aldrich) were used for the liquid−liquid extractions, and tetrahydrofuran (THF)-grade HPLC (Sigma-Aldrich) was used for the dilution of the samples and GPC experiments. The GPC separations were carried out using a guard column (4.6 × 30 mm^2) and three styrene-divinylbenzene gel permeation columns (Styragel) connected in series (7.8 × 300 mm^2) in the following order: HR4, HR2, and HR0.5. The characteristics of these columns were already described elsewhere.[6,9]

Obtaining Maltenes. Initially, 20 g of crude oil was placed in an oven at 80 °C for 24 h to eliminate the presence of volatile compounds that could interfere in the mass balance calculations. Later, the crude oil was mixed with *n*-heptane at a heptane/crude ratio of 60:1. To assure the complete precipitation of asphaltenes, this mixture was placed in ultrasound for 10 min, followed by 1 h of agitation (with a magnetic stirrer) at 60 °C. To obtain the maltenes, the mixture was filtered twice with No. 42 filter paper (with a pore size of 2.5 μm, Whatman) and the solvent (of the filtered mixture plus the washes of the asphaltenes) was rotaevaporated.

Part 1. Solvent Evaluations. Five grams of maltenes was weighed and mixed with 25 mL of heptane in a beaker until it was completely dissolved. Later, this mixture was transferred to a decanting funnel with a capacity of 150 mL and another 25 mL of heptane was added to maintain a heptane/maltene ratio of 5:1. In the funnel, the volume occupied by the total mixture was marked to replace the volume of heptane lost by evaporation or partial dissolution during each extraction by MeOH, ACN, and DMF. The extractions were made separately with each solvent, resulting in a total of six extractions of 50 mL each. Between each extraction, the complete separation of both phases was achieved. For each solvent, all extracts were combined. The mass extraction percentage was calculated by evaporating the solvent.

Part II. Sequential Liquid−Liquid Extraction. To achieve a sequential extraction, this experiment was performed in triplicate. As in the previous step, 5 g of maltenes was dissolved and transferred to the decanting funnel. A total of eight extractions with 50 mL of ACN were performed initially; then, extractions were performed with the DMF in the remnant maltene. For the first two replicates, each extract was collected separately; in the third replicate, the extracts obtained with each solvent were combined.

Size-Exclusion Chromatography ICP MS Detection. All samples were diluted 100 times with THF. For the GPC ICP MS detection, 20 μL of sample was injected and isocratically eluted with a THF flow rate of 1 mL/min for 120 min. A postcolumn splitter was used to obtain a low-flow outlet (50 μL/min) to feed the ICP MS. A homemade Microsoft Excel program was used to deconvolute the chromatograms by summing the Gaussian curves.

■ RESULTS AND DISCUSSION

Part I. Direct Extraction. *Extraction Efficiencies of MeOH, ACN, and DMF.* The total mass percentage extracted with each solvent is shown in Table 1. The solvent with the greatest extraction efficiency in terms of mass was MeOH (31%), followed by DMF (27%) and ACN (16%). However, by specificity, the DMF presented better extraction efficiency for compounds containing V, Ni, and S in comparison to those of the other solvents. As it can be observed, the particular

Table 1. Percentages (Total and by Element) of the Masses Extracted with Methanol, Acetonitrile, and Dimethlylformamide

solvent	% mass removed	element	% element extracted
methanol	31	S	36
		V	22
		Ni	12
acetonitrile	16	S	24
		V	30
		Ni	13
dimethylformamide	27	S	46
		V	61
		Ni	48

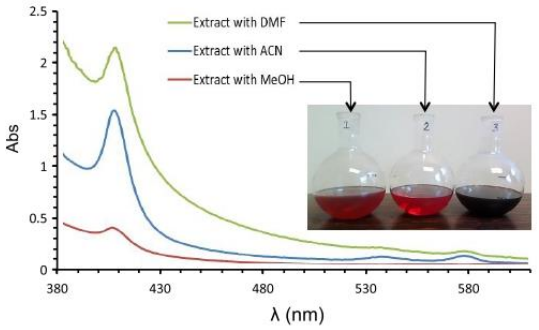

Figure 1. Absorption in the UV−vis region obtained for the MeOH, ACN, and DMF extracts.

DOI: 10.1021/acs.energyfuels.8b03974
Energy Fuels 2019, 33, 1922−1927

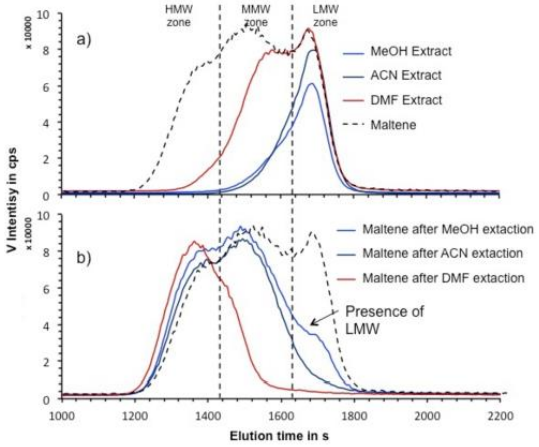

Figure 2. Vanadium GPC ICP MS chromatograms obtained for the MeOH, ACN, and DMF extracts (a) and for the maltene after extraction (b).

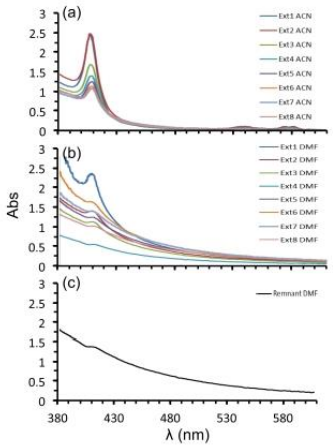

Figure 4. Absorption in the UV−vis region obtained for the sequential extractions with ACN (a), DMF (b), and remnant maltene after extraction with ACN and DMF (c).

distribution of the different compounds of V and Ni principally between the maltene dissolved in heptane and the solvents used as extractant (MeOH, ACN, and DMF) is very difficult to explain in terms of polarity (very similar among the three solvents used (MeOH, ε = 33; ACN, ε = 37; and DMF, ε = 38)), suggesting that certain specific interactions between the solvents and the MPs play a fundamental role. However, no correlation between the intensity of the Soret band (Figure 1) and the percentages of V and Ni compounds extracted suggest that the interactions between the nonpolar parts of the MPs (or aggregates that contain them) and the solvent are more important than a possible metal−solvent interaction due to the fact that other compounds seem to be extracted and do not have this interaction (HC compounds). In this case, the results of Table 1 and Figure 1 show a higher interaction with the DMF.

Size Distribution of Compounds Containing V in Extracts and Remnant Maltenes after Extraction with MeOH, ACN, and DMF. To simplify the discussion, we studied only the V profile obtained after extraction with MeOH, ACN, and DMF,

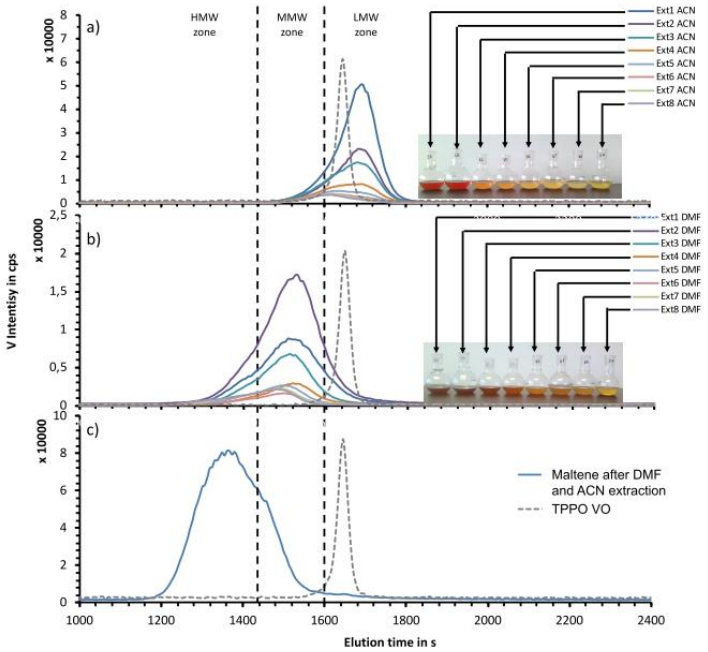

Figure 3. Vanadium GPC ICP MS chromatograms obtained for the ACN extract (a), DMF extract (b), and maltene after extraction (c).

DOI: 10.1021/acs.energyfuels.8b03974
Energy Fuels 2019, 33, 1922−1927

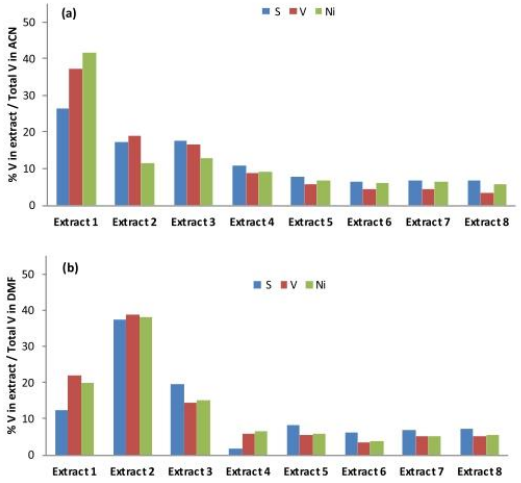

Figure 5. Extraction percentage of V, Ni, and S with ACN extract (a) and DMF extract (b).

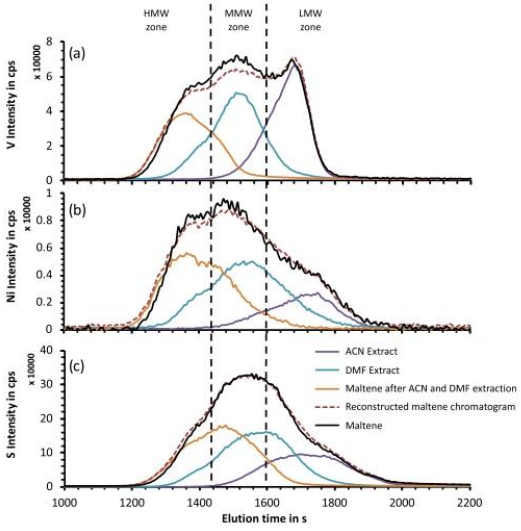

Figure 6. GPC ICP MS chromatograms of V (a), Ni (b), and (S) obtained for the ACN extract, DMF extract, and maltene after extraction.

and to obtain a clear comparison between the different chromatograms, the intensities of each sample were multiplied by its given mass balance. Figure 2a shows the GPC ICP MS chromatograms obtained for all extracts, which are compared to that of the original maltene. As it can be seen, this reveals a particular extraction depending on the solvent used (this is not observed with the data in Table 1). Thus, only compounds in the LMW region are observed in the ACN and MeOH extracts and a bimodal distribution is observed in the DMF extract. This is in good agreement with the high removal efficiency achieved with these solvents (Table 1). In terms of the remnant maltenes (Figure 2b), it can be observed that the size distributions of the V compounds complete the information obtained in Figure 2a. Typically, V compounds with LMW are present in the remnant maltene after their extraction with MeOH. This demonstrates that this solvent does not remove all V compounds with LMW. In contrast, only compounds with MMW and HMW are observed in the remnant maltene obtained after extraction with ACN, whereas most compounds with HMW are observed after extraction with DMF. Again, the differences observed are due to the specific interaction between the solvent and the MPs or with the nanoaggregates that contain or chelate them, being these widely significant when the DMF is used, specifically with the MMW compounds.

Part II. Sequential Extraction. *Optimization of Extraction.* Based on the fact that MeOH extracts the same LMW compounds but with a lower efficiency than ACN (Figure 2b and Table 1), a sequential extraction with ACN was applied to the maltene solutions to extract all of the LMW compounds. This was then followed by extraction with DMF to extract MMW compounds (Figure 2). Figure 3a shows the results obtained for each sequential extraction using ACN. The color of the extract changes from red to yellow with a decrease in the intensity of the peak obtained in the LMW part of the chromatogram. As can be observed, by comparing the signal of the vanadyl tetra-phenylporphyrin (TPPO VO) at 1646 s with the position of the maximum observed for each extract at 1695 s (to extraction with ACN), at 1519 s (to extraction with DMF), and at 1367 s (to remnant maletenes), all of the compounds extracted with ACN have MW values that are very similar to or less than those of the TPPO VO (Figure 3a). On the contrary, all DMF extracts with colors changing from dark red to yellow present compounds in the MMW region (Figure 3b) and the remnant maltene solution (after all of these ACN and DMF extractions) with dark color show compounds in the HMW region (Figure 3c). With regard to the absorption in the UV−vis region of these extracts, it can be observed how the Soret Band is present in all of the extracts obtained with ACN (Figure 4a) and initially in the extracts obtained with DMF until its complete disappearance (Figure 4b) in the remnant maltenes after extraction with ACN and DMF (Figure 4c). These results confirm that large parts of V and Ni compounds do not absorb in the UV−vis region, even when these compounds can be separated by their MWs as is shown here.

About the removal percentage obtained in each extraction, Figure 5a,b shows the percentage of V in the extract versus the total V in the extractant (sum of eight extractions) for ACN and DMF. Concerning ACN extraction, the percentages of V, Ni, and S decrease with each extraction but with different behaviors among elements. This might be due to the difference in molecular forms of the extracted molecules containing V, Ni, and S. Concerning ACN extraction, the behavior is more erratic, showing that after a first extraction of 10−20% the second extraction is near 40%. This might be due to the fact that before extracting S, Ni, and V compounds other compounds have to be extracted (HC compounds).

Size Distribution of V, Ni, and S Compounds Obtained by Sequential Maltene Extractions. A sequential extraction was applied to the maltene fraction, and all of the ACN and DMF extracts were pooled in two groups (ACN and DMF extracts) and evaporated. The size distributions of the compounds containing V, Ni, and S are shown in Figure 6a−c, respectively. As it can be observed, the method of sequential liquid−liquid extraction in maltenes using eight sequential extractions with ACN followed by eight extractions with DMF allows for the separation of the three V, Ni, and S compound families

DOI: 10.1021/acs.energyfuels.8b03974
Energy Fuels 2019, 33, 1922−1927

(HMW, MMW, and LMW) originally present in the maltenes, which were previously identified.[9] The reconstructed chromatogram shows very good agreement with the original maltene chromatogram, indicating that there is minor loss during the extraction procedure. This agreement between the reconstructed and actual chromatograms of the maltene also demonstrates that no modification of the V, Ni, and S species occurs during this extraction.

■ CONCLUSIONS

It has been demonstrated that through liquid−liquid extractions with ACN, followed by extractions with DMF of the maltenes dissolved in heptane, it is possible to very effectively achieve the quantitative separation of V, Ni, and S compounds in maltenes based on their hydrodynamic volumes (LMW, MMW, and HMW). Specifically, it has been made possible to directly extract the LMW compounds with ACN and to extract the MMW compounds with DMF, leaving the HMW in the matrices. These results show for the first time in the literature that it is possible, by extraction, to separate the trimodal distribution of V, Ni, and S compounds. This extraction of LMW, MMW, and HMW species is of great importance for future petrointeractomic studies.[32]

■ AUTHOR INFORMATION

Corresponding Author
*E-mail: Brice.bouyssiere@univ-pau.fr.
ORCID
Brice Bouyssiere: 0000-0001-5878-6067

Notes
The authors declare no competing financial interest.

■ ACKNOWLEDGMENTS

The financial support of the Conseil Régional d'Aquitaine (20071303002PFM) and FEDER (31486/08011464) is acknowledged. This work is a collaboration between the University of Pau (UPPA), Total, IFP Energies Nouvelles, PDVSA INTEVEP, and the Central University of Venezuela (UCV) on behalf of the PCP project "Metalopetroleomic" financially supported by the MAE.

■ REFERENCES

(1) Speight, J. G. *The Chemistry and Technology of Petroleum*; Taylor & Francis: Boca Raton, FL, 1999.
(2) Lewan, M. D. Factors Controlling the Proportionality of Vanadium to Nickel in Crude Oils. *Geochim. Cosmochim. Acta* **1984**, *48*, 2231−2238.
(3) Quirke, J. M. E. Rationalization for the Predominance of Nickel and Vanadium Porphyrins in the Geosphere. In *Metal Complexes in Fossil Fuels: Geochemistry, Characterization, and Processing*; Filby, R. H.; Branthaver, J. F., Eds.; American Chemical Society: New York, NY, 1987; pp 74−83.
(4) Goulon, J.; Retournard, A.; Friant, P.; Goulon-Ginet, C.; Berthe, C.; Muller, J. F.; Poncet, J. L.; Guilard, R.; Escalier, J. C.; Neff, B. Structural Characterization by X-Ray Absorption Spectroscopy (Exafs/Xanes) of the Vanadium Chemical Environment in Boscan Asphaltenes. *J. Chem. Soc., Dalton Trans.* **1984**, 1095−1103.
(5) Miller, J. T.; Fisher, R. B.; Van Der Eerden, A. M. J.; Koningsberger, D. C. Structural Determination by XAFS Spectroscopy of Non-Porphyrin Nickel and Vanadium in Maya Residuum, Hydrocracked Residuum, and Toluene-Insoluble Solid. *Energy Fuels* **1999**, *13*, 719−727.
(6) Desprez, A.; Bouyssiere, B.; Arnaudguilhem, C.; Krier, G.; Vernex-Loset, L.; Giusti, P. Study of the Size Distribution of Sulfur, Vanadium, and Nickel Compounds in Four Crude Oils and Their Distillation Cuts by Gel Permeation Chromatography Inductively Coupled Plasma High-Resolution Mass Spectrometry. *Energy Fuels* **2014**, *28*, 3730−3737.
(7) Reynolds, J. G.; Biggs, W. R. Effects of Asphaltene Precipitation and a Modified D 2007 Separation on the Molecular Size of Vanadium-and Nickel-Containing Compounds in Heavy Residua. *Fuel Sci. Technol. Int.* **1986**, *4*, 749−777.
(8) Park, J. I.; Al-Mutairi, A.; Marafie, A. M. J.; Yoon, S. H.; Mochida, I.; Ma, X. The Characterization of Metal Complexes in Typical Kuwait Atmospheric Residues Using Both GPC Coupled with ICP−Ms and Ht Gc−AED. *J. Ind. Eng. Chem.* **2016**, *34*, 204−212.
(9) Gascon, G.; Vargas, V.; Feo, L.; Castellano, O.; Castillo, J.; Giusti, P.; Acavedo, S.; Lienemann, C. P.; Bouyssiere, B. Size Distributions of Sulfur, Vanadium, and Nickel Compounds in Crude Oils, Residues, and Their Saturate, Aromatic, Resin, and Asphaltene Fractions Determined by Gel Permeation Chromatography Inductively Coupled Plasma High-Resolution Mass Spectrometry. *Energy Fuels* **2017**, *31*, 7783−7788.
(10) Caumette, G.; Lienemann, C. P.; Merdrignac, I.; Bouyssiere, B.; Lobinski, R. Fractionation and Speciation of Nickel and Vanadium in Crude Oils by Size Exclusion Chromatography-ICP Ms and Normal Phase HPLC-ICP Ms. *J. Anal. At. Spectrom.* **2010**, *25*, 1123−1129.
(11) Acevedo, S.; Guzmán, K.; Labrador, H.; Carrier, H.; Bouyssiere, B.; Lobinski, R. Trapping of Metallic Porphyrins by Asphaltene Aggregates: A Size Exclusion Microchromatography with High-Resolution Inductively Coupled Plasma Mass Spectrometric Detection Study. *Energy Fuels* **2012**, *26*, 4968−4977.
(12) Derakhshesh, M.; Bergmann, A.; Gray, M. R. Occlusion of Polyaromatic Compounds in Asphaltene Precipitates Suggests Porous Nanoaggregates. *Energy Fuels* **2013**, *27*, 1748−1751.
(13) Acevedo, S. C.; Cordero T, J. M.; Carrier, H.; Bouyssiere, B.; Lobinski, R. Trapping of Paraffin and Other Compounds by Asphaltenes Detected by Laser Desorption Ionization−Time of Flight Mass Spectrometry (LDI−TOF Ms): Role of A1 and A2 Asphaltene Fractions in This Trapping. *Energy Fuels* **2009**, *23*, 842−848.
(14) Vaughan, G. B.; Tynan, E. C.; Yen, T. F. Vanadium Complexes and Porphyrins in Asphaltene, 2. The Nature of Highly Aromatic Substituted Porphins and Their Vanadyl Chelates. *Chem. Geol.* **1970**, *6*, 203−219.
(15) Dickie, J. P.; Yen, T. F. Macrostructures of the Asphaltic Fractions by Various Instrumental Methods. *Anal. Chem.* **1967**, *39*, 1847−1852.
(16) Gray, M. R.; Tykwinski, R. R.; Stryker, J. M.; Tan, X. Supramolecular Assembly Model for Aggregation of Petroleum Asphaltenes. *Energy Fuels* **2011**, *25*, 3125−3134.
(17) Strausz, O. P.; Mojelsky, T. W.; Lown, E. M. The Molecular Structure of Asphaltene: An Unfolding Story. *Fuel* **1992**, *71*, 1355−1363.
(18) Murgich, J.; Abanero, J. A.; Strausz, O. P. Molecular Recognition in Aggregates Formed by Asphaltene and Resin Molecules from the Athabasca Oil Sand. *Energy Fuels* **1999**, *13*, 278−286.
(19) Yen, T. F. *The Role of Trace Metals in Petroleum*; Ann Arbor Science Publishers: Michigan, 1975.
(20) Biggs, W. R.; Fetzer, J. C.; Brown, R. J.; Reynolds, J. G. Characterization of Vanadium Compounds in Selected Crudes I. Porphyrin and Non-Porphyrin Separation. *Liq. Fuels Technol.* **1985**, *3*, 397−421.
(21) Qian, K.; Mennito, A. S.; Edwards, K. E.; Ferrughelli, D. T. Observation of Vanadyl Porphyrins and Sulfur-Containing Vanadyl Porphyrins in a Petroleum Asphaltene by Atmospheric Pressure Photonionization Fourier Transform Ion Cyclotron Resonance Mass Spectrometry. *Rapid Commun. Mass Spectrom.* **2008**, *22*, 2153−2160.
(22) Mckenna, A. M.; Purcell, J. M.; Rodgers, R. P.; Marshall, A. G. Identification of Vanadyl Porphyrins in a Heavy Crude Oil and Raw Asphaltene by Atmospheric Pressure Photoionization Fourier Transform Ion Cyclotron Resonance (Ft-ICR) Mass Spectrometry. *Energy Fuels* **2009**, *23*, 2122−2128.

DOI: 10.1021/acs.energyfuels.8b03974
Energy Fuels 2019, 33, 1922−1927

(23) Mckenna, A. M.; Williams, J. T.; Putman, J. C.; Aeppli, C.; Reddy, C. M.; Valentine, D. L.; Lemkau, K. L.; Kellermann, M. Y.; Savory, J. J.; Kaiser, N. K.; Marshall, A. G.; Rodgers, R. P. Unprecedented Ultrahigh Resolution Ft-Icr Mass Spectrometry and Parts-Per-Billion Mass Accuracy Enable Direct Characterization of Nickel and Vanadyl Porphyrins in Petroleum from Natural Seeps. *Energy Fuels* **2014**, *28*, 2454−2464.
(24) Dechaine, G. P.; Gray, M. R. Chemistry and Association of Vanadium Compounds in Heavy Oil and Bitumen, and Implications for Their Selective Removal. *Energy Fuels* **2010**, *24*, 2795−2808.
(25) Márquez, N.; Ysambertt, F.; De La Cruz, C. Three Analytical Methods to Isolate and Characterize Vanadium and Nickel Porphyrins from Heavy Crude Oil. *Anal. Chim. Acta* **1999**, *395*, 343−349.
(26) Ali, M. F.; Perzanowski, H.; Bukhari, A.; Al-Haji, A. A. Nickel and Vanadyl Porphyrins in Saudi Arabian Crude Oils. *Energy Fuels* **1993**, *7*, 179−184.
(27) Xu, H.; Yu, D.; Que, G. Characterization of Petroporphyrins in Gudao Residue by Ultraviolet?Visible Spectrophotometry and Laser Desorption Ionization-Time of Flight Mass Spectrometry. *Fuel* **2005**, *84*, 647−652.
(28) Zhao, X.; Liu, Y.; Xu, C.; Yan, Y.; Zhang, Y.; Zhang, Q.; Zhao, S.; Chung, K.; Gray, M. R.; Shi, Q. Separation and Characterization of Vanadyl Porphyrins in Venezuela Orinoco Heavy Crude Oil. *Energy Fuels* **2013**, *27*, 2874−2882.
(29) Liu, T.; Lu, J.; Zhao, X.; Zhou, Y.; Wei, Q.; Xu, C.; Zhang, Y.; Ding, S.; Zhang, T.; Tao, X.; Ju, L.; Shi, Q. Distribution of Vanadium Compounds in Petroleum Vacuum Residuum and Their Transformations in Hydrodemetallization. *Energy Fuels* **2015**, *29*, 2089−2096.
(30) Vargas, V.; Castillo, J.; Torres, R. O.; Bouyssiere, B.; Lienemann, C. P. Development of a Chromatographic Methodology for the Separation and Quantification of V, Ni and S Compounds in Petroleum Products. *Fuel Process. Technol.* **2017**, *162*, 37−44.
(31) Caumette, G.; Lienemann, C. P.; Merdrignac, I.; Paucot, H.; Bouyssiere, B.; Lobinski, R. Sensitivity Improvement in ICP Ms Analysis of Fuels and Light Petroleum Matrices Using a Microflow Nebulizer and Heated Spray Chamber Sample Introduction. *Talanta* **2009**, *80*, 1039−1043.
(32) Gutiérrez, S. S.; Farenc, M.; Barrère-Mangote, C.; Lobinski, R.; Afonso, C.; Bouyssière, B.; Giusti, P. Molecular Fingerprints and Speciation of Crude Oils and Heavy Fractions Revealed by Molecular and Elemental Mass Spectrometry: Keystone between Petroleomics, Metallopetroleomics, and Petrointeractomics. *Energy Fuels* **2018**, *32*, 4593−4605.

■ NOTE ADDED AFTER ASAP PUBLICATION

This article published March 4, 2019 with errors in Figures 2 and 3. The corrected figures published March 5, 2019.

DOI: 10.1021/acs.energyfuels.8b03974
Energy Fuels 2019, 33, 1922−1927

Simplification of heavy matrices by liquid-solid extraction: Part II – How to separate LMW, MMW and HMW compounds in asphaltene fractions for V, Ni and S compounds.

energy&fuels
Article
Cite This: Energy Fuels 2019, 33, 8110−8117
pubs.acs.org/EF

Simplification of Heavy Matrices by Liquid−Solid Extraction: Part II—How to Separate the LMW, MMW, and HMW Compounds in Asphaltene Fractions for V, Ni, and S Compounds

German Gascon,[†,‡,§] Juan Negrín,[†] Victor G. Montoto,[‡] Socrates Acevedo,[§] Charles-Philippe Lienemann,[∥] and Brice Bouyssiere*[,‡]

[†]PDVSA Intevep, Apartado 76343, Caracas 1070-A, Venezuela
[‡]CNRS/Univ Pau & Pays ADOUR/E2S UPPA, Institut des Sciences Analytiques et de Physico- Chimie Pour L'environnement et les Materiaux, UMR 5254, Helioparc-2 Avenue du Président Angot, Pau 64000, France
[§]UCV, Facultad de Ciencias, Escuela de Química, Caracas 1053, Venezuela
[∥]IFP Energies Nouvelles, Rond-point de l'échangeur de Solaize, BP 3, Solaize 69360, France

Downloaded via UNIV OF PAU AND PAYS DE L'ADOUR on June 18, 2020 at 12:07:30 (UTC).
See https://pubs.acs.org/sharingguidelines for options on how to legitimately share published articles.

ABSTRACT: A method of sequential liquid−solid extraction (leaching) has been developed to extract the V, Ni, and S compounds present in asphaltenes (n-C_7) according to their molecular weight distribution. For the high-molecular-weight (HMW) compounds, two new families of compounds were extracted, labeled as HMW1 and HMW2, where the latter was smaller than HMW1, and together represented approximately 85% of the asphaltene mass according to the mass balance obtained after the extractions. The compounds associated with HMW1 were asphaltenes that were insoluble in hot dimethylformamide (DMF), while the compounds associated with HMW2 were soluble in DMF but insoluble in the second leaching step based on hot acetone. The third family of obtained compounds was the medium-molecular-weight (MMW) compounds, which were soluble in hot acetone but insoluble in acetonitrile (ACN). The last fraction to be obtained was the low-molecular-weight compounds, which were soluble in ACN. The results reported here represent a new method that allows the extraction of different types of aggregated asphaltenes according to their molecular weights. With respect to the temperature and number of extraction steps, it was observed that an increase in both parameters increased the extraction efficiency.

INTRODUCTION

As it is well known, the term asphaltene covers a wide variety of substances with different structures but similar properties (polarity, size, molecular weight, etc.)[1] that exist in crude oil and tend to precipitate when a light nonpolar solvent is added in excess. Mitchell and Speight[2] determined the relationship between the percentage of asphaltenes (AS) that precipitate and the solubility parameters of the paraffinic, iso-paraffinic, and olefinic solvents that were used. The molecular state of these substances in crude oil was initially thought to be soluble or dispersed due to the peptization achieved by the resins (less polarity substances), which acted as surfactants.[3−5] However, due to the reversibility of the precipitation−dissolution process, which is not characteristic of colloidal particles stabilized by surfactants,[6] the behavior in solution, and the high molecular weights observed by various techniques (vapor presure osmometry, gel permeation chromtography (GPC), etc.),[7] this model has been discarded and replaced by the model proposed by Dickie and Yen[7,8] (later modified by Mullins[9,10]). Recently, Gray et al.[11] proposed a model with a macrostructure or supramolecular assembly (nanoaggregates) where asphaltenes are kept in solution due to the different configurations that these substances can adopt. Regarding the size of these nanoaggregates, some studies have mentioned proper colloidal particle sizes (>1 nm) with average sizes between 5 and 10 nm but less than 20 nm, even in dilute solutions,[12,13] although different critical nanoaggregation concentrations have been reported,[14−18] possibly due to solvent effects.

Presence and Distribution of V and Ni in Crude Oil. Ni and V are by far the most abundant metals in crude oil.[19] The predominance of Ni and V compounds compared to other organometallic compounds is a consequence of their highly stable N−V or N−Ni bonds and their favorable electron configurations, among other factors.[20,21] Studies by X-ray absorption fine structure spectroscopy have shown that Ni and V form coordination compounds with tetrapyrrolic ring-type porphyrins.[22,23] Because of their high boiling points, these compounds are concentrated in vacuum residues (99%),[24] and due to their solubilities, they are principle components in resins and asphaltenes (99%).[25−27] Additionally, different studies by gel permeation chromatography with inductively coupled plasma mass spectrometry (GPC-ICP MS)[24−27] have shown on many different heavy fractions and since more than 10 years that these compounds have a wide molecular weight distribution and typically contain high-molecular-weight (HMW/>10 000 Da) and medium-molecular-weight (MMW/1000−10 000 Da) compounds. The mass of these fractions is expressed as weight in Da according to polystyrene standard calibration.

Received: May 13, 2019
Revised: July 31, 2019
Published: August 12, 2019

ACS Publications © 2019 American Chemical Society

DOI: 10.1021/acs.energyfuels.9b01511
Energy Fuels 2019, 33, 8110−8117

Table 1. Mass Percentages of the Soluble Asphaltenes (AS) and Insoluble Asphaltenes (AI) Fractions and Several Physical Characteristics of the Solvents That Were Evaluated

solvent	% AS	% AI	boiling point (°C)	dielectric constant (ε)	Hansen's solubility parameter δ $(MPa)^{1/2}$
methanol (MeOH)	<0.5	99.5	65.0	32.7	29.6
acetic acid	2	98	118.1	6.15	21.4
acetonitrile (ACN)	2	98	82.0	37.5	24.4
1-propanol	2	98	97.0	20.7	24.6
acetone	3	97	56.0	21.5	19.9
methyl-*tert*-butyl-ether (MTBE)	5	95	55.3	2.6	16.2
ethyl acetate (EA)	12	88	77.1	6.0	18.1
acetylacetone	36	64	140.0	23.0	19.9
dimethylformamide (DMF)	38	62	153.0	36.7	24.9
diethylamine	60	40	55.5	3.6	16.61

However, mass spectrometry (MS)[28−31] has identified mainly low-molecular-weight (LMW/<1000 Da) compounds[24,27] in comparison with MMW and HMW compounds that are observed by GPC-ICP MS and this can be explained with the difficulty in ionizing molecules trapped in aggregates by molecular MS.[32] Recently, Ramírez-Pradilla et al.[33] described the identification of more than 300 petroporphyrins in acetonitrile (ACN) extracts of crude oil. According to this study, the ACN extracts corresponded to less than 10% of the V present in crude oil, reflecting the work that remains for a complete identification of petroporphyrins by molecular mass spectrometry (MS).

Association of V and Ni Compounds with Asphaltenes. Because a high percentage of the V and Ni compounds that are present in crude oil, resins, and asphaltenes do not absorb in the UV−vis range, a hypothesis was formulated that a portion of the V and Ni compounds is metalloporphyrins joined via coordination bonds with atoms that have unshared electron pairs, such as the N, O, and S heteroatoms present in asphaltenes with large nanoaggregate structures.[11,34] Another possibility could be that the V and Ni compounds are trapped in asphaltene macrostructures or nanoaggregates without specific metal−heteroatom interactions.[7,35,36] In both cases, these configurations would not exhibit absorption in the UV−vis range, which would explain the MMW and HMW compound distribution observed by GPC-ICP MS for these types of compounds.[24,27]

Role of GPC-ICP MS. Due to the limitations of molecular MS for the direct and quantitative identification of crude oil compounds with HMW- and MMW-type nanoaggregates or macrostructures, GPC-ICP MS constitutes, from our point of view, an interesting tool for studying the S, V, and Ni compounds present in these samples. Despite the criticisms to which the GPC technique is subjected,[37,38] coupling GPC with ICP MS enables the identification of the relative sizes associated with the various V, Ni, and S compounds present in either crude oil or some of its products (distillates,[24] residues,[24] and SARA fractions[27]). In fact, the data obtained by GPC-ICP MS, especially for MMW and HMW compounds, which are difficult to identify by molecular MS due to their poor ionization efficiencies,[39] have been broadly supported by theoretical models regarding the molecular state of asphaltenes in crude oil or solution.[8−11,32]

Separation of V and Ni Compounds according to Their Size or Molecular Weight. Various methods have been developed using either Soxhlet extraction or chromatography with a packed column to separate the different V and Ni compounds in crude oil (not necessarily by separation into different MW fractions).[40−45] However, due to the strong adsorption of asphaltenes onto commonly used adsorbents (alumina, silica gel, etc.), these methods regularly exhibit poor separation.[46] A liquid−liquid extraction method for the separation of HMW, MMW, and LMW compounds in maltenes (including S-, V- and Ni-containing compounds) was previously developed and had excellent results.[47] Based on this method, a similar approach focused on asphaltene is proposed in this work. Specifically, a liquid−solid extraction method for the separation of V and Ni compounds present in asphaltenes is developed based on the Galimov separation of petroporphyrines[48] with the advantage of obtaining GPC-ICP MS profiles to evaluate the efficiency of such fractionation.

■ EXPERIMENTAL SECTION

Instrumentation. A high-performance liquid chromatograph (HPLC) (UltiMate 3000, Dionex, Amsterdam, The Netherlands) was used for the GPC separation and was coupled with an ICP high-resolution MS (HR-MS). The detailed conditions for ICP-HR-MS detection have been previously reported[27] and are summarized here. An ICP-HR-MS instrument (Element XR, Thermo Scientific, Bremen, Germany) operating at a resolution of 4000 was used. The ICP-HR-MS was equipped with an interface based on a microflow total-consumption nebulizer without a drain and was thermoregulated at 60 °C to minimize signal suppression and increase the sensitivity by a factor of 3−4.[49] An oxygen flow of 0.08 mL/min was continuously added to the nebulizer gas flow (Ar) to avoid the deposition of carbon onto the cones.

Samples, Reagents, and Materials. For this work, an 8° API Venezuelan crude oil sample provided by PDVSA Intevep was used. *n*-Heptane was used for asphaltene precipitation, and methanol (MeOH), ACN, 1-propanol, acetone, methyl-*tert*-butyl-ether (MTBE), ethyl acetate (EA), acetylacetone, dimethylformamide (DMF), and diethylamine were used for the liquid−solid extractions. Tetrahydrofuran (THF) was used to dilute the samples and for the GPC experiments.

The separations were carried out using a guard column (4.6 × 30 mm) and three Waters (Waters Corporation, Milford, MA) styrene−divinylbenzene gel permeation columns (7.8 mm inner diameter × 300 mm length, Styragel) connected in series in the following order: HR4, HR2, and HR0.5. The mass obtained is expressed as weight in Da according to polystyrene standard calibration. This calibration is also checked daily with commercial porphyrins with known mass.[27] All solvents were of HPLC grade with a 95% or greater purity and were obtained from Sigma-Aldrich.

Obtaining Asphaltenes. Initially, 50 g of crude oil was heated at 80 °C in an oven for 24 h to eliminate the presence of volatile compounds that could interfere with the mass balances. The crude oil was then mixed with *n*-heptane in a ratio of 60:1 heptane/crude oil to assure complete asphaltene precipitation. This mixture was placed in an ultrasonic bath for 10 min, followed by 1 h of agitation with a magnetic stirrer at 60 °C. To obtain the asphaltenes, the mixture was

DOI: 10.1021/acs.energyfuels.9b01511
Energy Fuels 2019, 33, 8110−8117

filtered twice with a new filter paper each time (pore size 2.5 μm, Whatman) and washed with hot heptane.

Solvent Extraction. First, 0.50 ± 0.01 g of the asphaltenes was weighed, placed in a flask with 150 mL of solvent to maintain a ratio of 300:1 solvent/asphaltene, and heated to reflux for 1 h with agitation using a magnetic stirrer. The resulting mixture was filtered and separated into soluble asphaltenes (AS) and insoluble asphaltenes (AI) by filtration with a filter paper (pore size 2.5 μm, Whatman). The same procedure was repeated for all of the solvents that were evaluated.

GPC-ICP MS Detection. Each sample was diluted 200-fold with THF for GPC-ICP-HR-MS detection. A 20 μL sample was injected and isocratically eluted with a THF flow rate of 1 mL/min for 120 min. A splitter was used after the columns to obtain a low-flow outlet (50 μL/min) to feed the ICP-HR-MS. A custom-made Microsoft Excel spreadsheet was used to deconvolute the chromatograms by summing the Gaussian curves.

■ RESULTS AND DISCUSSION

Part I: Solvent Extraction. The amounts of AS and AI obtained with each solvent are expressed as a percentage of the total asphaltenes in Table 1, along with the values of several physical characteristics for each solvent used. No correlation was found between the parameters proposed in Table 1 and the percentages of the AS and AI extractions, which shows the complexity of the asphaltene solubility phenomenon. It is interesting to observe the GPC-ICP-HR-MS profile of the V compounds (Ni and S compounds are not shown here) for each solvent, shown in Figures 1 and 2, as this allows to

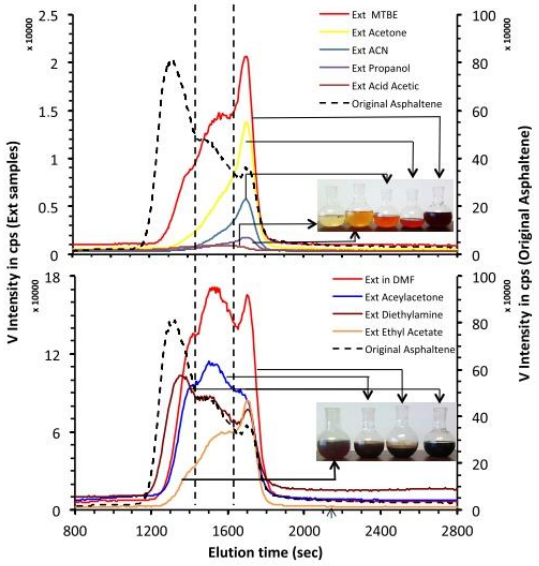

Figure 1. GPC-ICP-HR-MS profiles of the V compounds in the asphaltene extracts obtained with different solvents and with heating.

distinguish the type of V compounds (HMW, MMW, or LMW) extracted by each solvent. As can be seen in both figures, some specific solvents are particularly efficient at extracting only LMW compounds with different yields in the following order: acetone > CAN > 1-propanol > acetic acid (see Figure 1). Similarly, there are solvents for which the extraction of a larger but less specific portion of the asphaltene fraction can be observed, primarily for the MMW compounds

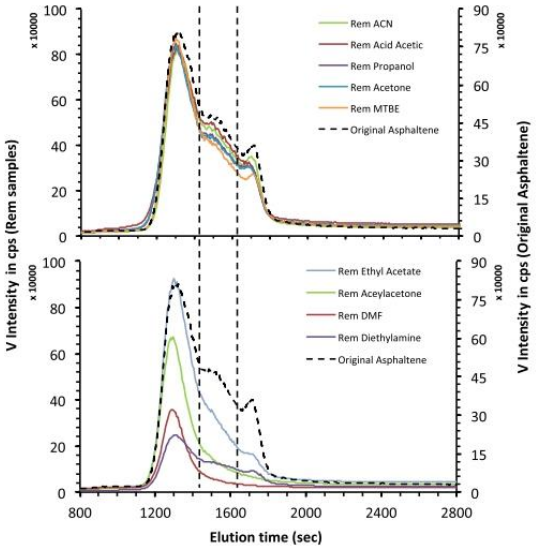

Figure 2. GPC-ICP-HR-MS profiles of the remanent V compounds in asphaltenes obtained with different solvents and with heating.

and, to a lesser extent, the HMW compounds in the following yield order: DMF > acetylacetone > EA > MTBE. Finally, diethylamine dissolved a large proportion of the HMW compounds (see Figure 2).

Effects of Temperature and Number of Extractions. To evaluate the influence of temperature, an extraction with DMF at room temperature was performed and compared with an extraction with hot DMF (lightly below the boiling point: 153 °C). As can be seen in Figure 3, the temperature has a very

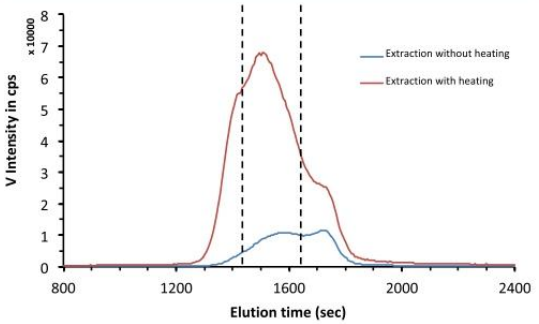

Figure 3. Comparison of the GPC-ICP-HRMS profiles for DMF extractions with and without heating of the asphaltenes.

noticeable effect on the solubilization of asphaltenes; it is highlighted when the solvent is "bad" or "poor" in terms of solubility in comparison with other "good" solvents (THF, dichloromethane, benzene, toluene, xylene, etc.). Thus, the asphaltenes solubility increase when heat is applied. This behavior has been previously reported by Galimov.[48] On the other hand, the effect of four successive extractions was studied. The results are shown in Figure 4. As expected, with an increasing number of extractions, a decrease in the amount of extracted V and Ni compounds is observed (55, 28, 12, and 5%). This decrease is more rapid for the MMW and LMW

DOI: 10.1021/acs.energyfuels.9b01511
Energy Fuels 2019, 33, 8110−8117

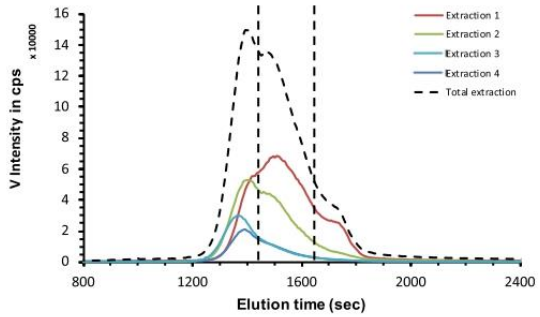

Figure 4. GPC-ICP-HR-MS profiles of the V compounds after four successive extractions of the asphaltenes with DMF.

compounds in comparison to the HMW compounds (Figure 4). Subsequently, in extractions 3 and 4, the profile changes show that only HMW compounds are removed, showing a complete solubility of the compounds with the MMW and LMW compounds in the first two extractions when additionally the DMF is heated.

Part II: Sequential Extraction. *Optimization of the Extraction.* Considering the results shown in Figures 1 and 2, various sequential separation schemes were evaluated. According to these tests, the key results for separating different classes of molecular weight compounds are presented in Figure 5. Here, the total results of three successive extractions for the V compounds (Ni and S compounds are not shown here) are shown, allowing the separation of four different portions of asphaltene. The scheme begins with the whole asphaltene mixture (Figure 5a). Then, the use of hot DMF as the first

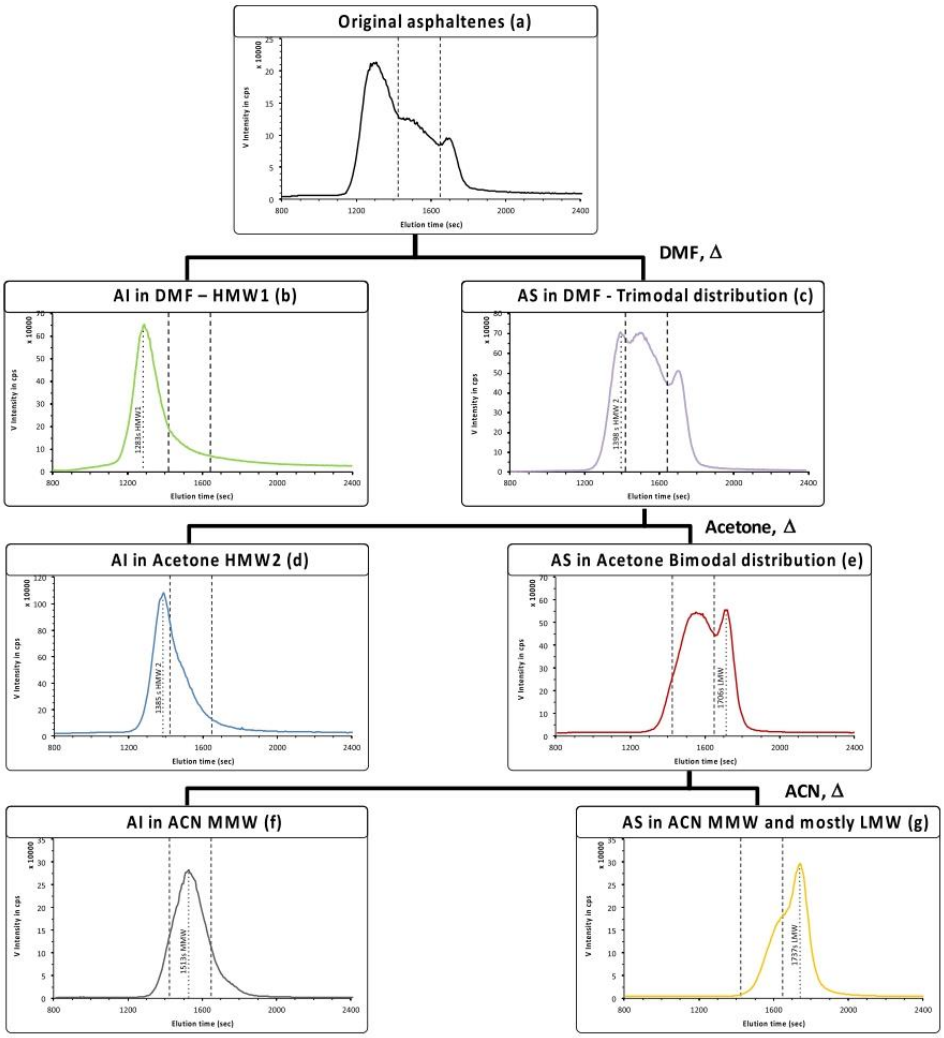

Figure 5. GPC-ICP-HR-MS profiles of the V compounds obtained with the optimum extraction scheme for (a) original asphaltenes, (b) AI in DMF, (c) AS in DMF, (d) AI in acetone, (e) AS in acetone, (f) AI in ACN, and (g) AS in ACN.

DOI: 10.1021/acs.energyfuels.9b01511
Energy Fuels 2019, 33, 8110−8117

extractant allows the separation of an insoluble monomodal HMW fraction of asphaltenes (Figure 5b), labeled as HMW1. The resulting soluble fraction (Figure 5c) clearly shows a trimodal distribution of the molecular weights, suggesting that another family of HMW compounds requires further extraction. From this soluble fraction, it was then possible to separate the remaining HMW compounds (referred to herein as HMW2), which have lower molecular weights than those of HMW1, as can be discerned from the retention time, as a monomodal fraction by using hot acetone (Figure 5d), in which HMW2 is insoluble. In the resulting soluble fraction obtained from this second extraction (Figure 5e), the HMW compounds are gone and a bimodal profile comprising mainly the MMW and LMW compounds remains. These two families of compounds can be separated by hot ACN to obtain an insoluble fraction composed entirely of MMW compounds (Figure 5f). The residual soluble fraction in ACN (Figure 5g) still has a bimodal distribution with a small percentage of MMW compounds and a large percentage of LMW compounds being found in this asphaltene fraction. The scheme of the extraction proposed in this article can separate the initial asphaltene fraction into four individual fractions with specific molecular weights as monitored by GPC-ICP-HR-MS.

The total results from monitoring the complete set of V, Ni, and S compounds of the extraction strategy presented above applied to asphaltene from a Venezuelan extra-heavy crude oil sample are shown in Figure 6. The separation of the V, Ni, and

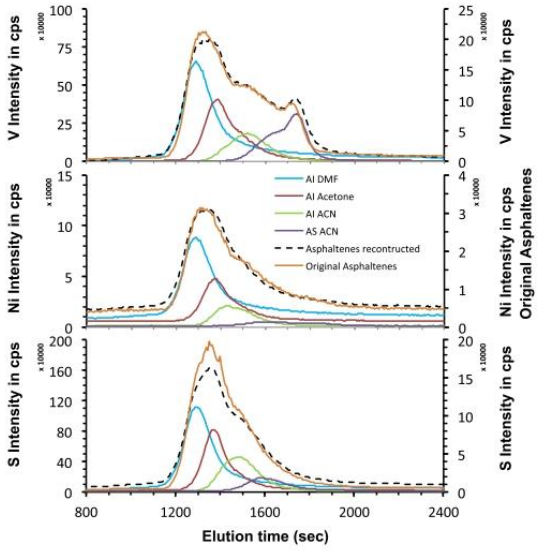

Figure 6. GPC-ICP-HRMS profiles of the V, Ni, and S compounds obtained for all asphaltene extracts.

S compounds present in asphaltene fractions according to their molecular weights is achieved, which has not been previously reported. The mass balance shows that approximately 70−80% of the V and Ni compounds are present in the HMW fractions (Figure 7), which can be interpreted as V and Ni compounds being integrated into the macrostructure of the asphaltenes and thereby eluting in the HMW region of the GPC chromatogram. This behavior can be explained by the tendency of asphaltenes to trap compounds[35,36] or the probability of

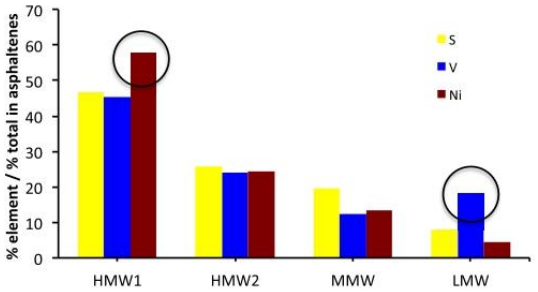

Figure 7. Percentage distributions of the V, Ni, and S compounds in the separated fractions of the asphaltenes.

forming coordination bonds between the metals and electron donor atoms (S, N, and O) of the asphaltenes.[11,34]

Regarding the nature of the specific separation observed, the separation cannot be simply explained in terms of the solvent polarity as solvents with similar dipolar moments (MeOH, ε = 33; ACN, ε = 37; and DMF, ε = 38) show different removal percentages. More likely, the temperature and other generic conditions, as well as the interactions between the solvent and the whole macrostructure or nanoaggregate, have a larger impact than any specific interaction between individual compounds, such as solvent−metal interactions, as previously suggested.[47] This explains the reconstruction of the initial total asphaltene GPC chromatogram from the information obtained from each fraction (Figure 5). As was previously shown[39] for reinjection of the HMW and MMW GPC fractions, we can demonstrate that this extraction scheme extracts nanoaggregates (mainly HMW1 and HMW2) that are stable rather than individual compounds.

Complete Fractionation Method. According to a previous paper[47] that presented a fractionation step for maltenes, Figure 8 shows the mass balance of the complete fractionation protocol for maltene (previous study[47]) and asphaltene (this study) extraction. According to all of the different steps of the extraction procedure, a mass balance of between 95 and 97% obtained for the Ni, V, and S compounds shows that almost all of the Ni, V, and S compounds can be extracted with this protocol. Sulfur has a completely different behavior compared to that of V and Ni, showing that sulfur is not mainly driving the aggregation/sequestration of V and Ni. Regarding Ni and V, similar behavior is obtained except for their LMW extracts, for which the Ni compounds consistently have a lower percentage than that of the V compounds. This can explain why, in most molecular MS studies,[33] V petroporphyrins have primarily been identified because the Ni and V compounds in nanoaggregates associated with the HMW fraction are more difficult to ionize.[39]

CONCLUSIONS

The use of liquid−solid extraction as an adequate methodology for the separation of the V, Ni, and S compounds present in asphaltenes based on their molecular weights is reported for the first time. An optimized extraction procedure establishing a sequence based on the choice of solvent, temperature, and methodology is proposed for the separation of these compounds. For example, an increase in temperature was found to improve the extraction of asphaltenes for a given solvent due to the complex endothermic process of

DOI: 10.1021/acs.energyfuels.9b01511
Energy Fuels 2019, 33, 8110−8117

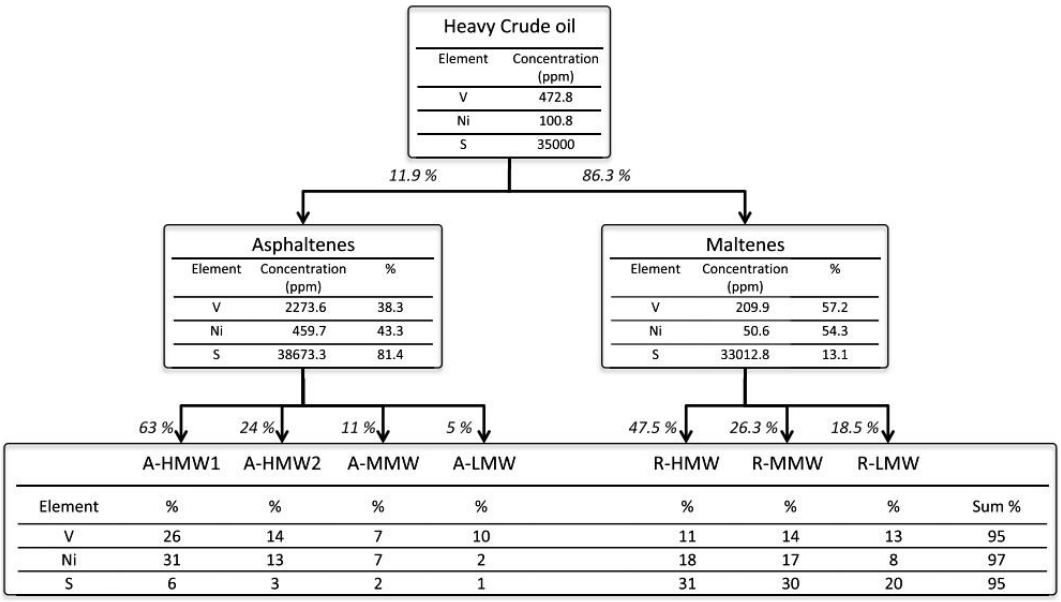

Figure 8. Complete fractionation process according to this study and a previous paper.[47]

solubilization. Additionally, the effectiveness of the overall extraction is determined by the number of extraction steps. With respect to the methodology, sequential extractions were the most successful for the proposed goal. As a result, it was found that at least 70−80% of the V, Ni, and S compounds present in asphaltenes are associated with the HMW fraction, typically containing nanoaggregates or macrostructures. This result seems to be in agreement with the results of previous techniques in which 90% of the asphaltenes form aggregates.[17] Likewise, the results suggest that the solvent−nanoaggregate interactions and the temperature play the most important roles in the separation process. These results also demonstrate that the use of a GPC-ICP-HR-MS technique is a very effective tool for monitoring separation methods, especially for V, Ni, and S compounds.

This new methodology, combined with the results of our previous work,[47] will allow the fractionation of complex petroleum samples into different families of compounds or nanoaggregates based on their solubilities.

AUTHOR INFORMATION

Corresponding Author

*E-mail: Brice.bouyssiere@univ-pau.fr.

ORCID

Brice Bouyssiere: 0000-0001-5878-6067

Notes

The authors declare no competing financial interest.

ACKNOWLEDGMENTS

The financial support of the Conseil Régional d'Aquitaine (20071303002PFM) and FEDER (31486/08011464) is acknowledged. This work is a collaboration among the University of Pau (UPPA), Total, IFP Energies Nouvelles, PDVSA INTEVEP, and the Central University of Venezuela (UCV) on behalf of the PCP project "Metalopetroleomic" financially supported by the MAE.

REFERENCES

(1) Linton, L. A. On the technical analysis of asphaltum. *J. Am. Chem. Soc.* **1894**, *16*, 809−822.
(2) Mitchell, D. L.; Speight, J. G. The solubility of asphaltenes in hydrocarbon solvents. *Fuel* **1973**, *52*, 149−152.
(3) Nellensteyn, F. I. The Colloidal Structure of Bitumens. In *The Science of Petroleum*; Dunstan, A. E., Ed.; Oxford University Press: London, U.K., 1938; pp 1−4.
(4) Pfeiffer, J. P.; Saal, R. N. J. Asphaltic bitumen as colloid system. *J. Phys. Chem. A* **1940**, *44*, 139−149.
(5) Swanson, J. M. A contribution to the physical chemistry of the asphalts. *J. Phys. Chem. A* **1942**, *46*, 141−150.
(6) Porte, G.; Zhou, H.; Lazzeri, V. Reversible description of asphaltene colloidal association and precipitation. *Langmuir* **2003**, *19*, 40−47.
(7) Dickie, J. P.; Yen, T. F. Macrostructures of the asphaltic fractions by various instrumental methods. *Anal. Chem.* **1967**, *39*, 1847−1852.
(8) Yen, T. F.; Erdman, J. G.; Pollack, S. S. Investigation of the structure of petroleum asphaltenes by X-ray diffraction. *Anal. Chem.* **1961**, *33*, 1587−1594.
(9) Mullins, O. C. The modified yen model. *Energy Fuels* **2010**, *24*, 2179−2207.
(10) Dutta Majumbar, R.; Bake, K. D.; Ratna, Y.; Pomerantz, A. E.; Mullins, O. C.; Gerken, M.; Hazendonk, P. Single-Core PAHs in Petroleum- and Coal-Derived Asphaltenes: Size and distribution from Solid-State NMR Spectroscopy and Optical Absorption Measurements. *Energy Fuels* **2016**, *30*, 6892−6906.
(11) Gray, M. R.; Tykwinski, R. R.; Stryker, J. M.; Tan, X. Supramolecular assembly model for aggregation of petroleum asphaltenes. *Energy Fuels* **2011**, *25*, 3125−3134.
(12) Yarranton, H. W.; Ortiz, D. P.; Barrera, D. M.; Baydak, E. N.; Barré, L.; Frot, D.; Eyssautier, J.; Zeng, H.; Xu, Z.; Dechaine, G.; Becerra, M.; Shaw, J. M.; McKenna, A. M.; Mapolelo, M. M.; Bohne, C.; Yang, Z.; Oake, J. On the size distribution of self-associated asphaltenes. *Energy Fuels* **2013**, *27*, 5083−5106.

DOI: 10.1021/acs.energyfuels.9b01511
Energy Fuels 2019, 33, 8110−8117

(13) Eyssautier, J.; Frot, D.; Barré, L. Structure and dynamic properties of colloidal asphaltene aggregates. *Langmuir* **2012**, *28*, 11997−2004.
(14) Evdokimov, I. N.; Eliseev, N. Y.; Akhmetov, B. R. Assembly of asphaltene molecular aggregates as studied by near-UV/visible spectroscopy. *J. Pet. Sci. Eng.* **2003**, *37*, 145−152.
(15) Andreatta, G.; Bostrom, N.; Mullins, O. C. High-Q ultrasonic determination of the critical nanoaggregate concentration of asphaltenes and the critical micelle concentration of standard surfactants. *Langmuir* **2005**, *21*, 2728−2736.
(16) Andersen, S. I.; Speight, J. G. Observations on the critical micelle concentration of asphaltenes. *Fuel* **1993**, *72*, 1343−1344.
(17) Yarranton, H. W.; Alboudwarej, H.; Jakher, R. Investigation of asphaltene association with vapor pressure osmometry and interfacial tension measurements. *Ind. Eng. Chem. Res.* **2000**, *39*, 2916−2924.
(18) Acevedo, S.; Ranaudo, M. A.; Pereira, J. C.; Castillo, J.; Fernández, A.; Pérez, P.; Caetano, M. Thermo-optical studies of asphaltene solutions: evidence for solvent−solute aggregate formation. *Fuel* **1999**, *78*, 997−1003.
(19) Speight, J. G. *The Chemistry and Technology of Petroleum*; CRC Press: Boca Raton, FL, 1999.
(20) Lewan, M. D.; Maynard, J. B. Factors controlling enrichment of vanadium and nickel in the bitumen of organic sedimentary rocks. *Geochim. Cosmochim. Acta* **1982**, *46*, 2547−2560.
(21) Quirke, J. M. E. Rationalization for the Predominance of Nickel and Vanadium Porphyrins in the Geosphere. In *Metal Complexes in Fossil Fuels. Geochemistry, Characterization and Processing*; Filby, R. H., Branthaver, J. F., Eds.; American Chemical Society: Washington, DC, 1987; pp 74−83.
(22) Goulon, J.; Retournard, A.; Friant, P.; Goulon-Ginet, C.; Berthe, C.; Muller, J.-F.; Poncet, J.-L.; Guilard, R.; Escalier, J.-C.; Neff, B. Structural characterization by X-ray absorption spectroscopy (EXAFS/XANES) of the vanadium chemical environment in Boscan asphaltenes. *J. Chem. Soc., Dalton Trans.* **1984**, *6*, 1095−1103.
(23) Miller, J. T.; Fisher, R. B.; van der Eerden, A. M. J.; Koningsberger, D. C. Structural determination by XAFS spectroscopy of non-porphyrin nickel and vanadium in maya residuum, hydrocracked residuum, and toluene-insoluble solid. *Energy Fuels* **1999**, *13*, 719−727.
(24) Desprez, A.; Bouyssiere, B.; Arnaudguilhem, C.; Krier, G.; Vernex-Loset, L.; Giusti, P. Study of the size distribution of sulfur, vanadium, and nickel compounds in four crude oils and their distillation cuts by gel permeation chromatography inductively coupled plasma high-resolution mass spectrometry. *Energy Fuels* **2014**, *28*, 3730−3737.
(25) Biggs, W. R.; Fetzer, J. C.; Brown, R. J.; Reynolds, J. G. Characterization of vanadium compounds in selected crudes I. Porphyrin and non-porphyrin separation. *Liq. Fuels Technol.* **1985**, *3*, 397−421.
(26) Park, J.-I.; Al-Mutairi, A.; Marafie, A. M. J.; Yoon, S.-H.; Mochida, I.; Ma, X. The characterization of metal complexes in typical Kuwait atmospheric residues using both GPC coupled with ICP−MS and HT GC−AED. *J. Ind. Eng. Chem.* **2016**, *34*, 204−212.
(27) Gascon, G.; Vargas, V.; Feo, L.; Castellano, O.; Castillo, J.; Giusti, P.; Acavedo, S.; Lienemann, C.-P.; Bouyssiere, B. Size distributions of sulfur, vanadium, and nickel compounds in crude oils, residues, and their saturate, aromatic, resin, and asphaltene fractions determined by gel permeation chromatography inductively coupled plasma high-resolution mass spectrometry. *Energy Fuels* **2017**, *31*, 7783−7788.
(28) McKenna, A. M.; Purcell, J. M.; Rodgers, R. P.; Marshall, A. G. Identification of vanadyl porphyrins in a heavy crude oil and raw asphaltene by atmospheric pressure photoionization Fourier transform ion cyclotron resonance (FT-ICR) mass spectrometry. *Energy Fuels* **2009**, *23*, 2122−2128.
(29) Qian, K.; Mennito, A. S.; Edwards, K. E.; Ferrughelli, D. T. Observation of vanadyl porphyrins and sulfur-containing vanadyl porphyrins in a petroleum asphaltene by atmospheric pressure photonionization Fourier transform ion cyclotron resonance mass spectrometry. *Rapid Commun. Mass Spectrom.* **2008**, *22*, 2153−2160.
(30) Rodgers, R. P.; Hendrickson, C. L.; Emmett, M. R.; Marshall, A. G.; Greaney, M.; Qian, K. Molecular characterization of petroporphyrins in crude oil by electrospray ionization Fourier transform ion cyclotron resonance mass spectrometry. *Can. J. Chem.* **2001**, *79*, 546−551.
(31) McKenna, A. M.; Williams, J. T.; Putman, J. C.; Aeppli, C.; Reddy, C. M.; Valentine, D. L.; Lemkau, K. L.; Kellermann, M. Y.; Savory, J. J.; Kaiser, N. K.; Marshall, A. G.; Rodgers, R. P. Unprecedented ultrahigh resolution FT-ICR mass spectrometry and parts-per-billion mass accuracy enable direct characterization of nickel and vanadyl porphyrins in petroleum from natural seeps. *Energy Fuels* **2014**, *28*, 2454−2464.
(32) Santos Silva, H.; Alfarra, A.; Vallverdu, G.; Bégué, D.; Bouyssiere, B.; Baraille, I. Impact of H-bonds and porphyrins on asphaltene aggregation as revealed by molecular dynamics simulations. *Energy Fuels* **2018**, *32*, 11153−11164.
(33) Ramírez-Pradilla, J. S.; Blanco-Tirado, C.; Hubert-Roux, M.; Giusti, P.; Afonso, C.; Combariza, M. Y. Comprehensive petroporphyrin identification in crude oils using highly selective electron transfer reactions in MALDI-FTICR-MS. *Energy Fuels* **2019**, *33*, 3899−3907.
(34) Dechaine, G. P.; Gray, M. R. Chemistry and association of vanadium compounds in heavy oil and bitumen, and implications for their selective removal. *Energy Fuels* **2010**, *24*, 2795−2808.
(35) Acevedo, S.; Guzmán, K.; Labrador, H.; Carrier, H.; Bouyssiere, B.; Lobinski, R. Trapping of metallic porphyrins by asphaltene aggregates: a size exclusion microchromatography with high-resolution inductively coupled plasma mass spectrometric detection study. *Energy Fuels* **2012**, *26*, 4968−4977.
(36) Acevedo, S.; Cordero T, J. M.; Carrier, H.; Bouyssiere, B.; Lobinski, R. Trapping of paraffin and other compounds by asphaltenes detected by laser desorption ionization-time of flight mass spectrometry (LDI-TOF MS): role of A1 and A2 asphaltene fractions in this trapping. *Energy Fuels* **2009**, *23*, 842−848.
(37) Behrouzi, M.; Luckham, P. F. Limitations of size-exclusion chromatography in analyzing petroleum asphaltenes: a proof by atomic force microscopy. *Energy Fuels* **2008**, *22*, 1792−1798.
(38) Mullins, O. C.; Martínez-Haya, B.; Marshall, A. G. Contrasting perspective on asphaltene molecular weight. This comment vs the overview of A. A. Herod, K. D. bartle, and R. Kandiyoti. *Energy Fuels* **2008**, *22*, 1765−1773.
(39) Putman, J. C.; Sama, S. G.; Barrère-Mangote, C.; Rodgers, R. P.; Lobinski, R.; Marshall, A. G.; Bouyssière, B.; Giusti, P. Analysis of petroleum products by gel permeation chromatography coupled online with inductively coupled plasma mass spectrometry and offline with fourier transform ion cyclotron resonance mass spectrometry. *Energy Fuels* **2018**, *32*, 12198−12204.
(40) Ysambertt, F.; Marquez, N.; Rangel, B.; Bauza, R.; De La Cruz, C. Isolation and characterization of metalloporphyrins from a heavy crude oil by soxhlet adsorption chromatography and HPLC-SEC. *Sep. Sci. Technol.* **1995**, *30*, 2539−2550.
(41) Márquez, N.; Ysambertt, F.; De La Cruz, C. Three analytical methods to isolate and characterize vanadium and nickel porphyrins from heavy crude oil. *Anal. Chim. Acta* **1999**, *395*, 343−349.
(42) Xu, H.; Yu, D.; Que, G. Characterization of petroporphyrins in Gudao residue by ultraviolet/visible spectrophotometry and laser desorption ionization-time of flight mass spectrometry. *Fuel* **2005**, *84*, 647−652.
(43) Gao, Y. Y.; Shen, B. X.; Liu, J. C. The structure identification of vanadium porphyrins in venezuela crude oil. *Energy Sources, Part A* **2012**, *34*, 2260−2267.
(44) Zhao, X.; Liu, Y.; Xu, C.; Yan, Y.; Zhang, Y.; Zhang, Q.; Zhao, S.; Chung, K.; Gray, M. R.; Shi, Q. Separation and characterization of vanadyl porphyrins in venezuela orinoco heavy crude oil. *Energy Fuels* **2013**, *27*, 2874−2882.
(45) Liu, T.; Lu, J.; Zhao, X.; Zhou, Y.; Wei, Q.; Xu, C.; Zhang, Y.; Ding, S.; Zhang, T.; Tao, X.; Ju, L.; Shi, Q. Distribution of vanadium

DOI: 10.1021/acs.energyfuels.9b01511
Energy Fuels 2019, 33, 8110−8117

compounds in petroleum vacuum residue and their transformations in hydrodemetallization. *Energy Fuels* **2015**, *29*, 2089−2096.
(46) Vargas, V.; Castillo, J.; Torres, R. O.; Bouyssiere, B.; Lienemann, C.-P. Development of a chromatographic methodology for the separation and quantification of V, Ni and S compounds in petroleum products. *Fuel Process. Technol.* **2017**, *162*, 37−44.
(47) Gascon, G.; Negrin, J.; Garcia-Montoto, V.; Acevedo, S.; Lienemann, C.-P.; Bouyssiere, B. Simplification of heavy matrices by liquid−liquid extraction: part I—how to separate LMW, MMW, and HMW compounds in maltene fractions of V, Ni, and S compounds. *Energy Fuels* **2019**, *33*, 1922−1927.
(48) Galimov, R. A.; Krivonozhkina, L. B.; Abushaeva, V. V.; Romanov, G. V. Extraction of vanadylporphyrins from petroleum asphaltenes. *Pet. Chem.* **1993**, *33*, 539−543.
(49) Caumette, G.; Lienemann, C.-P.; Merdrignac, I.; Paucot, H.; Bouyssiere, B.; Lobinski, R. Sensitivity improvement in ICP MS analysis of fuels and light petroleum matrices using a microflow nebulizer and heated spray chamber sample introduction. *Talanta* **2009**, *80*, 1039−1043.

DOI: 10.1021/acs.energyfuels.9b01511
Energy Fuels 2019, 33, 8110−8117

Spatial and temporal trends of Polycyclic Aromatic Hydrocarbon (PAH) contamination in sediments from different locations in western Greenland.

Spatial and temporal trends of Polycyclic Aromatic Hydrocarbon (PAH) contamination in sediments from different locations in western Greenland.

Victor Garcia Montoto[a,b], Thomas Stehrer[a], Yuan Xu[a], Nikoline Juul Nielsen [a], Peter Christensen [a], Jan H. Christensen [a].

[a]Department of Plant and Environmental Sciences, University of Copenhagen, Thorvaldsensvej 40, 1871 Frederiksberg, Denmark.

[b]Energy and Environment Solutions E2S / University of Pau & Pays Adour, Institut des Sciences Analytiques et de Physico-chimie pour l'Environnement et les Matériaux (IPREM), UMR5254, 64000, Pau, France.

Abstract

The augmenting presence of persistent organic pollutants (POPs) in pristine environments such as the Arctic Sea due to the increase of marine traffic, oil spills and human activity among other factors is becoming a concern worldwide. To investigate this hypothesis, sediment samples have been collected in harbours from two Greenlandic settlements: Ilulissat, the third-largest city in Greenland where fishery and tourism are the main economy sources and Qeqertarsuaq, a small and remote town on Disko Island. In this paper, a modified QuEChERS extraction method was adapted for on-site analysis of 18 individual PAHs and 14 groups of alkylated PAHs in arctic wet sediments with gas chromatography (GC) coupled with mass spectrometry (MS). This method involves a two-step addition of organic solvent and the water phase to facilitate a better extraction of the organic compounds applied to wet samples. Recovery

rates ranging from 50 - 85 % and LODs ranging from 0.07 – 331.48 µg/kg of wet sediments were obtained. Spatial ΣPAH concentrations have been shown to be higher in the harbour of Qeqertarsuaq compared to Ilulissat. Concentrations decreased with increasing distance to the peer in Qeqertarsuaq and further decreased at a reference site 10 km outside of Qeqertarsuaq. This is confirming harbours as a local pollution source in that area. In addition, analyses of core sediments from Ilulissat exhibit a higher ΣPAH concentrations in the upper layers of sediments, indicating the influence of increased human activity over the past centuries.

Keywords (max 6 keywords)

Sediment, QuEChERS, PAHs, Greenland, temporal and spatial trends

1. Introduction

The Arctic is an isolated and very sparsely populated region and is amongst the least polluted environments on our planet. However, over the last decades, due to increased human activity such as fishery, industry, and tourism as well as long-range transport of pollutants to the Arctic, increased levels of pollutants were observed (Hung et al., 2005). Fishery, industry and tourism have been accompanied by an overall increase in marine ship traffic and increased activity in harbours. This increased the risk of oil seeps or larger spills from ships and subsequent local pollution of the biotic and abiotic environment including sediments (Cooper, 2001; Vergeynst et al., 2018).

Due to the ongoing climate warming, new shipping routes will be opened through the Arctic Sea (AMAP, 2010) with and accompanied risk of increased concentrations of pollutants in water and sediments. Therefore, it is crucial to establish and optimize new methods to analyse pollutants such as PAHs that allow for accurate and fast quantification to monitor and assure the conservation of these remote areas.

Although polycyclic aromatic hydrocarbons (PAHs) consist of a group of compounds originated from natural processes, their high presence in the atmosphere and oceans is mainly due to anthropogenic emissions originating from incomplete combustion of organic matter such as fossil fuels or oil spills amongst others. Different studies proved the carcinogenic and teratogenic effects that exposure to these compounds can cause in humans (Ravindra et al., 2001).

Anthropogenic PAHs can be classified in two groups: petrogenic and pyrogenic. While petrogenic PAHs are one of the main group of compounds present in fossil fuels, they consist of compounds with a low number of aromatic rings and are typically alkylated to a high degree (Sporstol et al., 1983). However, pyrogenic PAHs are formed during the combustion of fossil fuels or biomass. They are pyrolyzed, leading to the formation of unstable and reactive radicals. These radicals react among other pyrolyzed fragments causing more stable and mainly non-alkylated PAHs with a higher number of rings (4-6) (Hwang et al., 2003). To identify if PAH pollution is derived mainly from pyrogenic or petrogenic sources, diagnostic ratios of isomers based on their molecular weight can be applied. Several, indicator

compounds are described to be associated with a specific type of source. Derived from that, several diagnostic ratios were identified to distinguish between petrogenic and pyrogenic sources in general or other, more specific sources (Ravindra et al., 2008; Tobiszewski and Namieśnik, 2012).

The presence of petrogenic PAHs in sediments is caused by the accumulation of the compounds originating from oil spills and municipal treatment discharges into the seawater amongst others. Furthermore, the presence of organic particles or gases containing PAHs in the atmosphere can lead to a deposition of mainly pyrogenic PAHs in the marine sediment (Tsapakis et al., 2003). PAHs will remain in the sediments until they are degraded by bacteria. However, the lower temperature conditions in arctic waters may cause lower biodegradation rates (Brakstad and Bonaunet, 2006), entailing a long-term presence of these pollutants within the arctic sediments in contrast to warmer environments.

With the current study, spatial and temporal trends of PAH pollution in sediments from Qeqertarsuaq and Ilulissat harbours, Greenland, were analysed. Sediments represent a sink of maritime pollution and are therefore a good indicator for anthropogenic impacts (Ma et al., 2015). Higher pollution is generally found close to areas with higher anthropogenic activity and closer to point sources. Therefore, we expect higher concentrations of PAHs in Ilulissat harbour compared to Qeqertarsuaq with a decrease in PAH concentrations further away from the interior of the harbour. This reflects the number of inhabitants of around 4500 in Ilulissat compared to just under 900 in Qeqertarsuaq. Furthermore, Ilulissat is the most popular tourist destination in Greenland, leading to further increased car and ship traffic. Additionally, upper sediment layers from core samples were expected to have higher overall PAH load due to increasing anthropogenic impact. To investigate these factors, sediment samples in both harbours were taken and analysed for PAH content.

To analyse a high number of samples in field conditions a rapid, precise and accurate extraction and analysis method is required. There are numerous techniques that are used for the extraction of PAHs from sediments, such as Soxhlet extraction or pressurized liquid extraction (Boll et al., 2008; Fang et al., 2003). They entail the use of large and complex equipment and consume large amounts of solvent. Thus, a simpler and less solvent consuming method was designed for in-situ analyses in Greenland. Multiple extraction methods were tested to detect and quantify the different PAHs present in sediments. Cvetkovic et al. (2016) optimized a QuEChERS extraction method for the determination of PAHs. In this work, a modification of this method so that it was applicable to wet sediment samples was tested to improve the time of analyses and ensure sufficient recoveries. The ease and agility of this method will allow its implementation for similar field analyses. Gallotta and Christensen (2012) developed a GC-MS method suitable for analysis of a wide range of PAHs including alkylated PAHs. This method was optimized to achieve shorter runtimes.

105 # 2. Material and Methods
106
107 ## 2.1 Chemicals
108
109 Hexane (Rathburn Chemicals) of HPLC-grade was used as extraction solvent. C18 (Phenomenex) and
110 $MgSO_4$ (Sigma Aldrich) were used for clean-up and phase separation during the QuEChERS extraction.
111 Acid-activated copper was prepared from copper powder (99 % purity, Sigma Aldrich) by addition of
112 excess of concentrated hydrochloric acid followed by filtration and washing with MilliQ water, acetone
113 and pentane. A 10-point calibration curve containing 32 PAH standards with concentrations from 3 to
114 1500 ng/ml (Table S1 and Table S2 in supp. information) prepared in isooctane (HPLC grade, Rathburn
115 Chemicals) was used for quantification. Alkylated standards were used as surrogates to determine the
116 concentration of the entire group. Deuterated compounds were added as internal and recovery
117 standards (Table S3 in supp. information) and were also prepared in isooctane.
118
119 ## 2.2 Sampling
120
121 Sediments were collected in harbours from 2 different environments: Ilulissat and Qeqertarsuaq. A
122 remote site about 10 km west of Qeqertarsuaq was chosen as a reference site. 17 samples from both
123 harbours were taken with increasing spatial distance from suspected point sources such as gas stations
124 or peers with docked boats. Exact sample locations are summarized in Table S4. One core sample was
125 taken in both harbours. Core samples were divided in 3 times 5 cm thick increments. A Van-Veen grab
126 was used for composite samples and a KC Kajak sediment core sampler for core samples. Samples were
127 stored in rilsan bags and kept cooled and in dark till analysis.
128
129 ### 2.2.1 Dry weight/Organic carbon content
130
131 Samples were transported after chemical analysis to Copenhagen for determination of dry weight and
132 organic matter content. Dry weight was analysed by heating 10 g of each sample at 105° C for 48 hours
133 in an oven and weighing prior and after the procedure (n=3). Dried samples were burnt in a muffle
134 furnace at 500° C to determine organic carbon content based on loss on ignition.
135
136 ## 2.3 Sample preparation and PAH extraction
137
138 A modified QuEChERS extraction based on previous research (Ben Salem et al., 2016; Cvetkovic et al.,
139 2016; Miossec et al., 2018) was tested prior to the expedition to Greenland. To shorten the overall
140 extraction procedure, no drying step was considered and therefore, 10 g of wet sediment sample was

placed in 30 ml amber vials and spiked with 200 µl of the internal standard solution. To ensure sufficient contact of solvent and sediment a first addition of 10 mL of hexane was done followed by vortex (1 min) and ultrasonication (15 min). Afterwards, 5 mL of ultrapure water was added followed by vortex and ultrasonication. 4 g $MgSO_4$ and 1 g NaCl were added to the vial and then vortexed and centrifuged for 5 minutes at 1000 G. 3 mL of the upper organic phase were transferred to a new 30 mL amber glass vial. For clean-up and to dry the transferred solution, 150 mg $MgSO_4$ and 50 mg C18 particles were added. In order to remove elemental sulphur (Guo et al., 2014; Rogowska et al., 2016), 300 mg acid activated copper was added in this step and shaken vigorously for 5 minutes. Finally, after centrifuging (5 minutes, 800 G), 1 ml of extract was transferred to a GC vial and spiked with 40 µl recovery standard prior to injection.

2.4 Chemical Analysis

GC-MS was used to quantify 18 different parent PAHs (including the 16 US-EPA PAHs) and 14 groups of alkylated PAHs. The method was based on a previously established method by Gallotta and Christensen (2012) and adapted to achieve a shorter runtime of 19.8 minutes plus approximately 10 minutes cooldown by using a shorter column. An Agilent 7890A GC system was equipped with a 30 m HP-5 capillary column (Agilent Technologies, 5 % phenyl methyl siloxane, 250 µm x 0.25 um) and a 5975C inert XL MSD detector (Agilent Technologies). The temperature program started with a 2-minute hold temperature at 55 °C followed by an increase to 100 °C with an increase of 35 °C per minute. The temperature was finally raised to 315 °C, at a rate of 20 °C per minute. The injection volume was set to 1 µl in pulsed splitless mode at an injection temperature of 300 °C. Helium was used as carrier gas at 1.1 ml per minute. Ion source temperature and quadrupole temperature were set to 230 and 150 °C respectively and an electron ionization energy of 70 eV was used. The instrument was operated in SIM mode with 8 periods of grouped analytes and a dwell time of 15 ms per m/z ratio.

2.5 Analysis of Source materials

To correlate possible sources with pollution patterns in analyzed sediments, fuel, oil and creosote samples in Qeqertarsuaq were collected. The fuel and oil samples were diluted with DCM, 0.5 mg/ml for gasoline and the engine oil and 1 mg/ml for diesel. The solid creosote sample was dissolved at a concentration of 1mg/ml in DCM before injection. Analysis was performed using the same method as described in section 2.4 above.

2.6 Data Analysis

Linear regression models were applied for data analysis using Excel 2013. Calibration curve, recovery, LOD/LOQ and concentrations of analytes were obtained to assess feasibility of the sampling and

extraction method described above. The concentration of PAHs at different sites/depths was calculated to investigate the spatial and temporal trends of contamination. Principal component analysis of the data collected in this work has been carried out by using Matlab 2018b and PLS_Toolbox (Eigenvector).

3. Results and Discussion

3.1 Method validation and quality parameters

The accuracy of this method was validated with the analysis of a NIST reference material containing the PAHs analysed in this method. However, the NIST 1941b consists of a sediment whose characteristics differ significantly with the characteristics of the samples collected for this work and the method employed, such as its low organic matter content and dryness among other factors. An analysis of this sample with this method, designed for wet sediment analysis, proved to be not accurate.

Table 1 lists the average recovery percentages corresponding to the samples collected in Ilulissat and Qeqertarsuaq (n=31) obtained during the extraction of PAHs. Low molecular weight PAHs such as Naphthalene present higher recoveries than higher molecular weight PAHs, probably due to a lower solubility of these in n-hexane. Recoveries from individual samples of Ilulissat and Qeqertarsuaq are shown in Figure S1 and Figure S2 in the supplementary information.

Table 1. Recoveries (%) corresponding to the Internal Standards used in this method for wet sediment analysis.

Internal standards	***Average (%)***	***S. Dev.***
Naphthalene-d8	83.59	12.06
Dibenzothiophene-d8	80.91	11.28
Acenaphthene-d10	85.84	10.73
Phenanthrene-d10	82.72	11.19
Pyrene-d10	83.86	11.35
Fluorene-d10	77.19	12.19
Chrysene-d12	66.20	14.69
Benzo(k)fluoranthene-d12	63.00	17.57
Benzo(g,h,i)perylene-d18	50.37	18.37

Multiple extraction was used to determine the suitability of using spike experiments for determination of the recovery. As seen in Figure 1, concentrations normalized to the first extract are only 4 to 15 % higher for analytes compared to their corresponding internal standards.

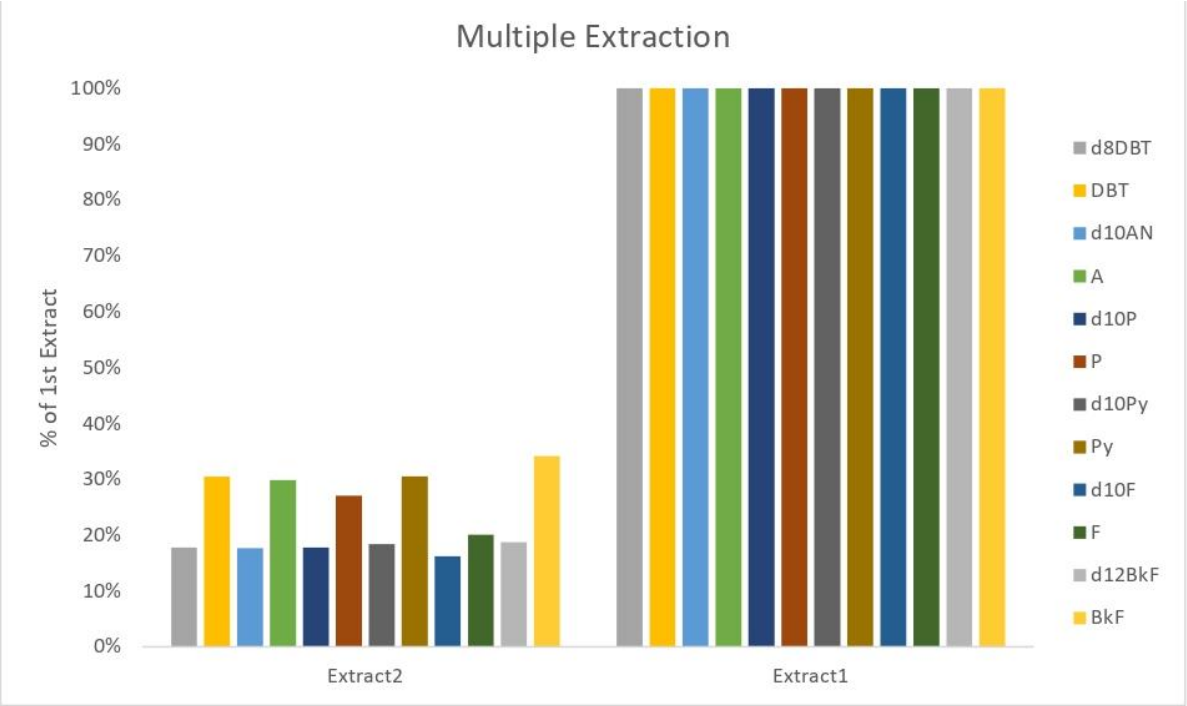

Figure 1. Second extraction recoveries compared to the first extraction. Internal Standards are extracted easier than the corresponding analytes. 4 to 15 % higher extraction efficiencies of internal standards compared with analytes normalized to the first extraction.

The LOD and LOQ obtained are determined as method detection and quantification limits and are listed in Table 2. LODs ranging from 0.07 µg/kg (dry sediment) for C1-Pyrenes up to 331.48 µg/kg for dibenzothiophene. The reference sample from Qeqertarsuaq was used to compute these limits using mean concentration of the analyte in the reference sample plus 3- and 10-times standard deviation respectively divided by the slope of the calibration curve.

Table 2. LOD and LOQ values for the target PAHs and Alkylated PAHs.

Analyte/Group	LOD	LOQ	Group	LOD	LOQ
N	2.77	9.24	C1N	1.39	4.64
DBT	331.48	979.06	C2N	0.12	0.40
A	1.37	2.07	C3N	0.14	0.48
P	3.07	6.65	C1F	15.57	50.07
Fh	2.20	4.15	C2F	0.13	0.42
Chr	2.93	9.75	C1P	230.16	767.20
Py	3.15	6.08	C2P	15.57	50.07
Ba	3.40	6.74	C3P	0.13	0.42
BaP	3.20	7.78	C4P	0.13	0.42
Bper	1.59	5.31	C1Pyr	0.07	0.24
BFh	1.99	3.98	C1Chr	0.33	1.09

DBA	5.26	13.03	C2Chr	0.30	0.99
F	1.34	1.54	C3Chr	1.13	3.75
BeP	1.10	1.59			
Ac	1.73	3.11			
An	1.00	2.01			
Bf	2.76	4.29			
Ind	1.50	4.44			

3.2 Spatial trends.

Sediments from different locations around the harbours of Ilulissat and Qeqertarsuaq have been analysed and the Σ16PAHs concentrations are plotted in **Error! Reference source not found.**2. Together with the histogram of Figure 3, it clearly shows the higher concentration of PAHs within the harbours over the open sea and the sites where no traffic nor activity is present. Due to higher possibility of oil spills and agglomeration of embarkations within the harbours, sediments from these areas show higher concentrations of PAHs than in remote areas with less ship traffic. Hence the high correlation between marine activity and PAHs in sediments.

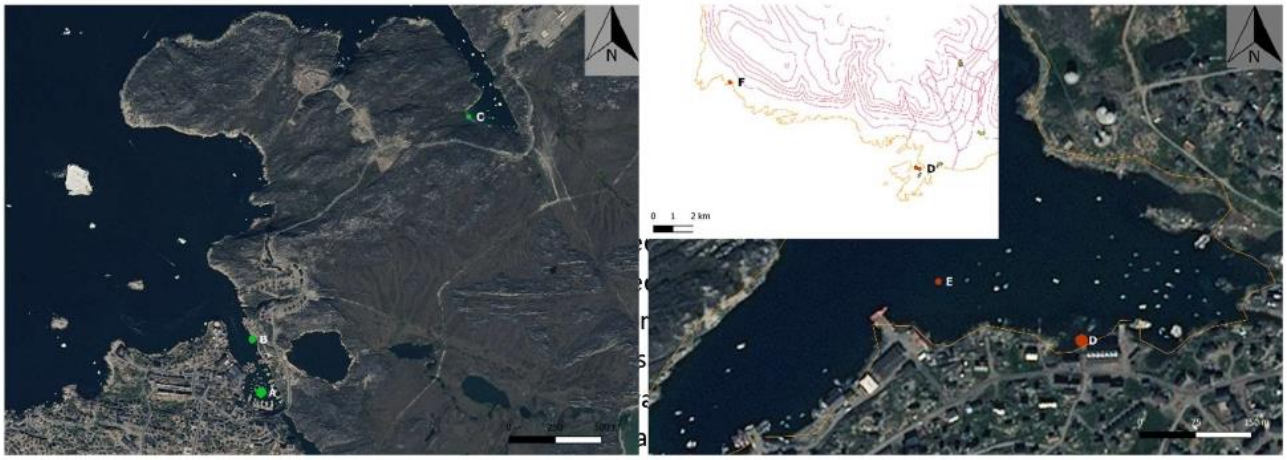

Figure 2: Sampling locations in Ilulissat and Qeqertarsuaq (A: Ilulissat harbour, B: Ilulissat harbour entrance, C: Ilulissat, remote fjord, D: Qeqertarsuaq harbour, E: Qeqertarsuaq bay, F: Disko Island reference site). Size of dots is proportional to the sum of of 16 PAHs. Points A and D are combinations of 3 and 2 sampling sites respectively.

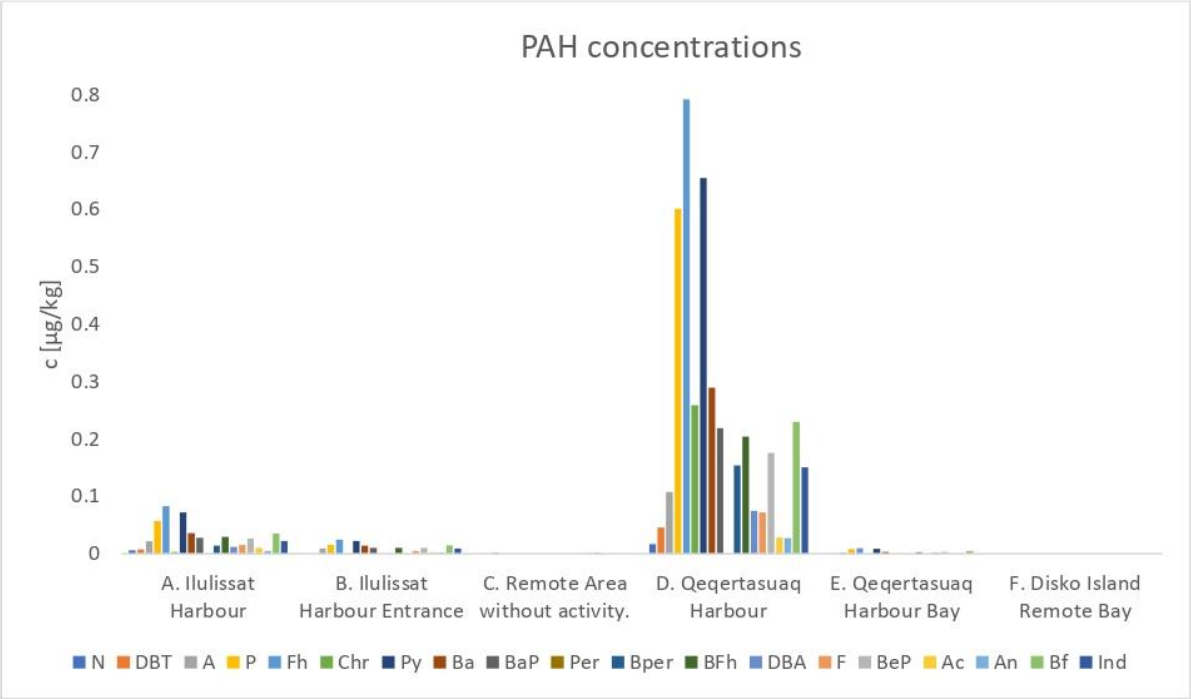

Figure 3. PAHs concentrations in sediments from different sites in Ilulissat and Qeqertarsuaq

Regarding the presence of alkylated PAHs, a similar trend is observed compared to non-alkylated compounds. Concentrations are depicted below in Figure 4.

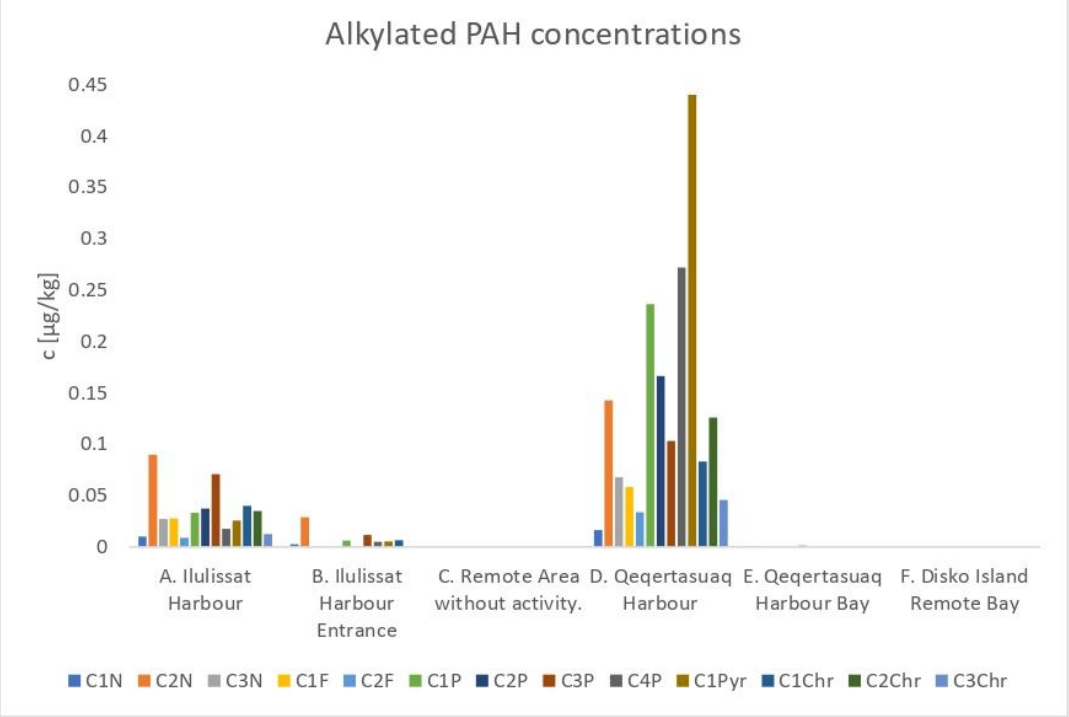

Figure 4: Concentrations of alkylated PAH from different sites in Ilulissat and Qeqertarsuaq.

3.3 Temporal Trends

PAH concentrations corresponding to the core samples from both Ilulissat and Qeqertarsuaq harbours are presented in Figure 5. As dating the sediment was not considered in this work, the division has been carried out by taking core samples from different points in the harbour and separation into 5 cm layers. A difference can be observed between the distributions of both sites. Whereas in Ilulissat harbour PAHs are decreasing with depth, in Qeqertarsuaq harbour the concentrations are highest in the deepest layer of sediments, which would confirm increasing pollution in more recent time only for Ilulissat harbour. Correlation of PAH levels with the organic matter content in individual layers (Figure S3) combined with a positive correlation of all samples with organic matter content, could explain this opposing trend. Anoxic conditions in deeper sediment layers can also contribute to lower degradation rates and therefore lead to higher concentrations in deeper layers. Furthermore, more replicates would be needed to confirm if this trend is consistent for the entire area.

To further distinguish between recent and pollution dating further back, ratios between high and low molecular weight can be used, whereby LMW PAHs are expected to be only present after recent pollution due to their faster biodegradation compared to HMW PAHs (Agarwal et al., 2009). Computed ratios (not shown) for the core samples could not give a clear indication about the pollution history.

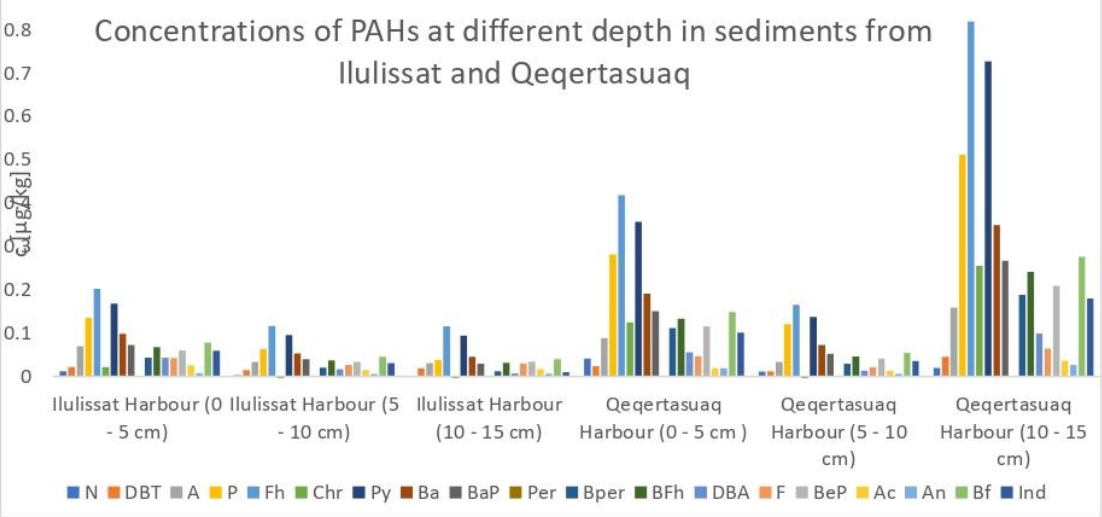

Figure 5. Concentrations of PAHs at different depth in sediments from Ilulissat and Qeqertarsuaq.

3.4 Source Identification

In Table 3, calculated diagnostic ratios for differentiation between petrogenic and pyrogenic pollution are summarized. A/(A+P) values smaller than 0.1 (Pies et al., 2008), and values below 0.4 of F/(F+Py) (Edokpayi et al., 2016) indicate petrogenic sources. A ratio of LMW/HMW PAHs above one is another indicator of petrogenic pollution sources (Edokpayi et al., 2016). Predominance of methyl phenanthrene compared to non-alkylated phenanthrene indicates diesel combustion as the main source compared to petrol combustion (Callén et al., 2011). Originally proposed by Boehm and Farrington (1984), the fossil fuel pollution index (FFPI) relates fossil-fuel derived PAHs (C_0 to C_4 naphthalenes, C_0 to C_4 dibenzothiophenes and C_0 to C_4 phenanthrenes) to the sum of PAHs. The closer the resulting value is to one, the higher is the contribution of petrogenic sources to the overall pollution.

Table 3. Average diagnostic ratios

	LMW[a]/HMW[b]	A/(A+P)	MeP/P	FFPI[c]	F/(F+Py)
Ilulissat harbour	1.04	0.27	3.53	0.37	0.18
Ilulissat harbour entrance	0.76	0.40	1.59	0.28	0.17
Qeqertarsuaq harbour	0.90	0.18	2.28	0.20	0.10
Qeqertarsuaq bay	1.72	0.20	0.15	0.12	0.17

[a]Low molecular weight PAHs (Na, A, F, Ac, An, P)
[b]High molecular weight PAHS (BaP, Bper, Bfh, DBA, Ind, Bf)
[c]Fossil fuel pollution index ($\Sigma N(C_0\text{-}C_4) + \Sigma DBT(C_0\text{-}C_3) + 0.5*\Sigma P(C_0\text{-}C_1) + \Sigma P(C_2\text{-}C_4) / \Sigma PAH$)

Results of above stated ratios represent a snapshot of the analysed samples and can give an indication of their pollution source. Many factors such as different fuel and oil products, sampling uncertainties and others, though contribute to a big variation, limiting the validity of these ratios. A/(A+P) and F/(F+Py) show contradictory trends with the first indicating pyrogenic pollution, whereas the latter would suggest petrogenic sources for PAH pollution. The FFPI are highest for samples from Ilulissat with values from 0.28 to 0.37 indicating a below 40 % contribution of petrogenic pollution to the overall PAH levels.

3.4.1 Source Patterns

The chemical analysis of potential pollution sources did not reveal a clear overlap in PAH composition of source material and analysed sediments. Patterns of parent and alkylated PAHs are shown in Figure 6 and Figure 7 below. Therefore, clear attribution to a single source is not possible. High concentrations of fluorene, pyrene and phenanthrene in diesel could cause their high abundance in samples collected in Qeqertarsuaq harbour. Benzo[e]pyrone in the same samples might origin from creosote used for preserving bilge containing a significant portion of B[e]P.

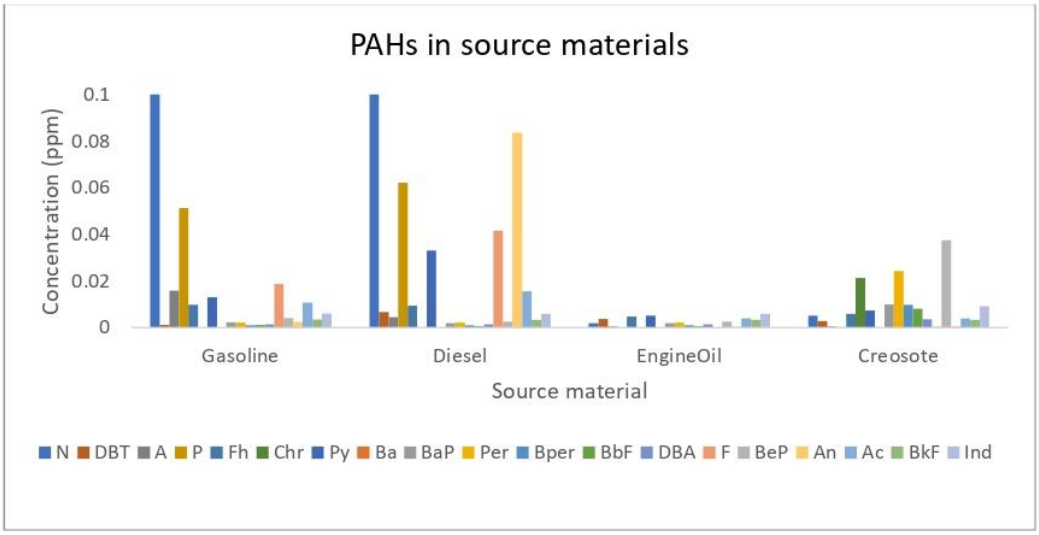

Figure 6. PAH distribution in different source materials. Quantification of PAH fuel, oil and creosote samples. Concentration of Naphthalene as high as 2.2 and 1.6 ppm for gasoline and diesel respectively not shown.

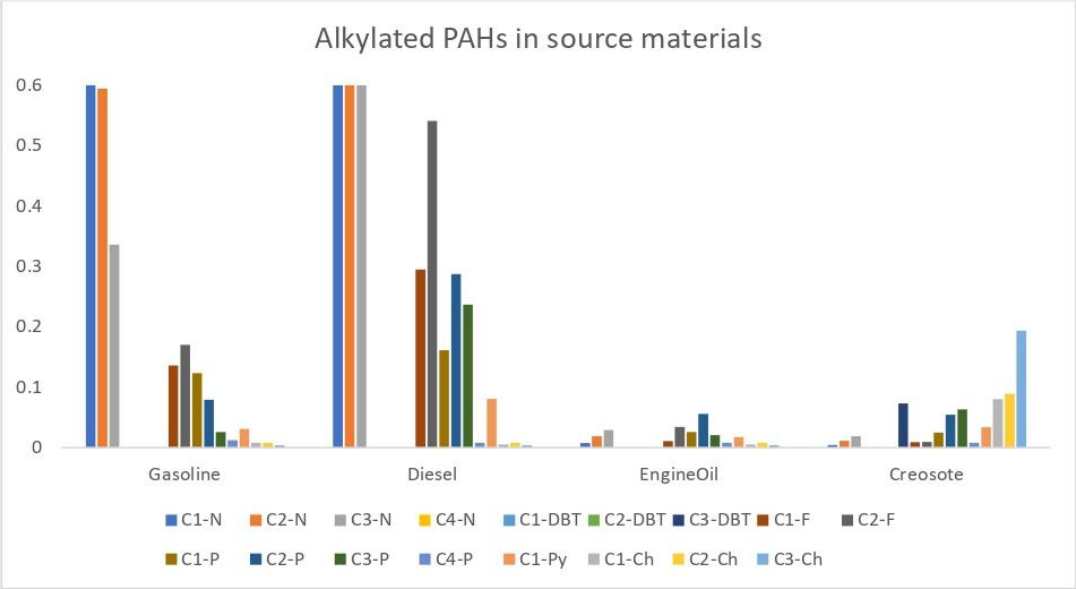

Figure 7. Quantification of alkylated PAHs from fuel, oil and creosote. Alkylated naphthalenes ranging from 10 to 20 ppb in creosote up to 2.9 ppm in diesel fuel not shown int the graph

3.5 Correlations to organic matter and water content

PAHs are mainly linked to organic matter in sediments, whereby interactions with the aromatic fraction of the organic matter compounds are most likely to be predominant (Chiou et al., 1998). Therefore, a positive correlation of PAH concentrations in sediments with increasing TOC content is widely observed (Wang, Xu-Chen et al., 2001). This correlation is strongest where similar types and amounts of pollution are present. Water content shows a huge fluctuation from 22% to 75%, so correlation between water content and PAHs concentration and recovery is also studied to check if water influences the extraction procedure. Correlation between Σ16PAH concentrations of all sites and organic matter and water content are presented in Figure S4 and Figure S5 Pearson correlation coefficient (r) is calculated to quantify the linear correlation between two variables.

Total organic matter content (TOC) was ranging from 0.7 % to 21 %. A strong positive correlation (r>=0.70, Figure S4) is found between TOC to PAHs concentration. Most analytes show a comparable high correlation, which clearly shows PAHs' strong affinity to organic matter in sediment. But for C_1 and C_2 phenanthrene, there is an exclusively high correlation (r>0.82), which indicates a stronger association with sediment. This also explains the observed predominance of alkylated phenanthrene over non--alkylated phenanthrene.

A moderate positive correlation (r>=0.50, Figure S5) is found between water and PAHs concentration. But no significant correlation between water and recovery of internal standards is observed. This may be explained by the physical properties of sediment samples. Water content has also a rather strong

correlation (r=0.90) with organic matter content. A dense sample with small particle size tends to keep both water and organic matter, while a sandy sample with large particle size has a low affinity for water and organic matter.

3.6 Principal component analysis.

The data collected in this work, including both water and organic matter contents and the concentrations of the parent and alkylated PAHs have been treated mathematically in order to perform a principal component analysis (PCA). The dataset has been autoscaled, and a two principal components model has been built, as a higher number of components would not provide with extra information. These two principal components explain 84.7 % of the data.

The different nature of the samples collected can be observed in Figure 8A, where the scores corresponding to PC2 and PC1 have been plotted. Figure 9 shows the different loadings for this model, corresponding the red dot to the water content and the green dot to the organic matter content. The rest of the loadings correspond to the different analytes, and most of their variation is explained with only 7.79% of the data.

While the samples collected in Qeqertarsuaq, which are lower in water content and higher in PAHs, are plotted in the positive values for PC1, the samples collected in Ilulissat are plotted towards more negative values.

A third group of samples can be observed in Figure 8A. This area of the plot has been zoomed and shown in Figure 8B. Three samples from Qeqertarsuaq possess the same score values as the reference samples. Both group of samples, which are low in PAHs and both water and organic content, due to absence of traffic and the depth of the sediments in these areas have the same properties and cannot be distinguished with the properties quantified in this work.

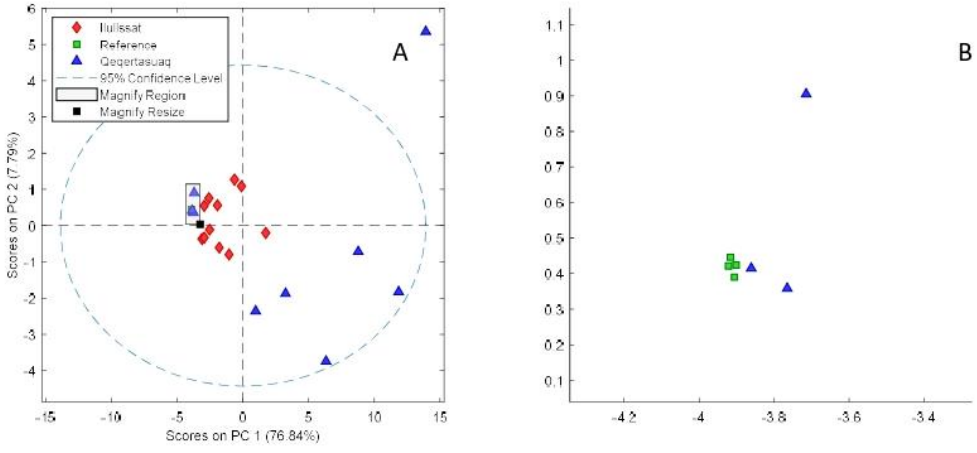

Figure 8. Principal Component Analysis of the dataset collected in this work. Figure 9A shows the PC2 vs. PC1 score values, and Figure 9B corresponds to the magnified region in Figure 9A.

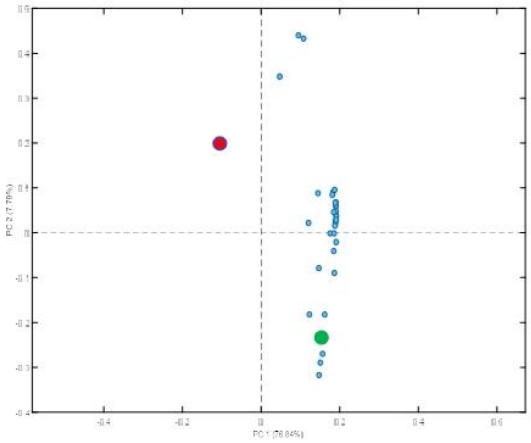

Figure 9. PC2 vs. PC1 loading values plot. The blue loadings correspond to the different PAHs values. The green dot corresponds to the Total Organic Content and the red loading corresponds to the water content.

4. Conclusion

A new method for the analysis of PAHs in sediments designed to be carried out on-site has been used in this work. Acceptable recoveries have been obtained, showing better extraction efficiency for lower molecular weight PAHs with n-hexane. These recoveries based on spiking experiments with internal standards have been validated by carrying out a multiple extraction of the method's quality control sample replicates. This confirmed, that internal standards were slightly better extracted then corresponding analytes, but within an acceptable range of 4 to 15 % lower values normalized to the first extract. When correlated to organic matter and water content, no positive association with recoveries could be detected. This indicates, wet extraction to be a feasible method for quantification of PAHs in marine sediments.

Multiple PAHs including alkylated PAHs have been found in different sites in Western Greenland: Ilulissat, the third biggest town in Greenland, and Qeqertarsuaq, a more remote settlement in the Disko Island. Analysis of sediments at different locations within these places have shown a tendency of having a high concentration of PAHs where the boats are docked. Concentrations decrease considerably in the sediments within a few meters from the harbor, indicating that the pollution is locally confined to small areas by local sources.

Principal component analysis of the data collected in this dataset shows the different nature of the sediments collected in both sites and it has proven to be a powerful tool for the classification of samples originated in different locations.

Furthermore, a temporal analysis of the PAHs concentration in sediments has been carried out. Layers at different depths show very different concentrations of PAHs, which may indicate the increasing or decreasing activities within the harbor. The concentration of 16 EPA PAHs is decreasing in samples taken in Ilulissat harbor with increasing depth, following an expected trend. This would support the hypothesis, that increased human activity over the last few decades led to the deposition of an

increased amount of PAHs in harbor sediments. Contrary, the core sample from Qeqertarsuaq shows highest values for 16 EPA PAHs in the deepest layer. This may be caused by different local conditions. Validity of these findings is limited due to the small number of samples and the lack of an exact dating of the age of the individual sediments.

Acknowledgments

We would like to thank Nikoline, Jan and Peter for their tremendous support throughout the course and for realizing this project. We would also like to Jette for all her work behind in supporting this work. Many thanks also to everybody else at the department of Plant and Environmental Science involved in this course. We would also like to thank everybody involved in providing such great research infrastructure in Greenland and the local communities in Qeqertarsuaq and Ilulissat.

391 References
392

393 Agarwal, T., Khillare, P.S., Shridhar, V., Ray, S., 2009. Pattern, sources and toxic potential of PAHs in the
394 agricultural soils of Delhi, India. Journal of Hazardous Materials 163, 1033–1039.
395 https://doi.org/10.1016/j.jhazmat.2008.07.058
396 Ben Salem, F., Ben Said, O., Duran, R., Monperrus, M., 2016. Validation of an Adapted QuEChERS
397 Method for the Simultaneous Analysis of Polycyclic Aromatic Hydrocarbons, Polychlorinated
398 Biphenyls and Organochlorine Pesticides in Sediment by Gas Chromatography–Mass
399 Spectrometry. Bull Environ Contam Toxicol 96, 678–684. https://doi.org/10.1007/s00128-016-
400 1770-2
401 Boehm, P.D., Farrington, John W., 1984. Aspects of the Polycyclic Aromatic Hydrocarbon Geochemistry
402 of Recent Sediments in the Georges Bank Region. Environmental Science and Technology 18,
403 840–845.
404 Boll, E.S., Christensen, J.H., Holm, P.E., 2008. Quantification and source identification of polycyclic
405 aromatic hydrocarbons in sediment, soil, and water spinach from Hanoi, Vietnam. J. Environ.
406 Monit. 10, 261–269. https://doi.org/10.1039/B712809F
407 Brakstad, O.G., Bonaunet, K., 2006. Biodegradation of Petroleum Hydrocarbons in Seawater at Low
408 Temperatures (0–5 °C) and Bacterial Communities Associated with Degradation. Biodegradation
409 17, 71–82. https://doi.org/10.1007/s10532-005-3342-8
410 Callén, M.S., de la Cruz, M.T., López, J.M., Mastral, A.M., 2011. PAH in airborne particulate matter. Fuel
411 Processing Technology 92, 176–182. https://doi.org/10.1016/j.fuproc.2010.05.019
412 Chiou, C.T., McGroddy, S.E., Kile, D.E., 1998. Partition Characteristics of Polycyclic Aromatic
413 Hydrocarbons on Soils and Sediments. Environ. Sci. Technol. 32, 264–269.
414 https://doi.org/10.1021/es970614c
415 Cooper, D.A., 2001. Exhaust emissions from high speed passenger ferries. Atmospheric Environment 35,
416 4189–4200. https://doi.org/10.1016/S1352-2310(01)00192-3
417 Cvetkovic, J.S., Mitic, V.D., Stankov Jovanovic, V.P., Dimitrijevic, M.V., Petrovic, G.M., Nikolic-Mandic,
418 S.D., Stojanovic, G.S., 2016. Optimization of the QuEChERS extraction procedure for the
419 determination of polycyclic aromatic hydrocarbons in soil by gas chromatography-mass
420 spectrometry. Anal. Methods 8, 1711–1720. https://doi.org/10.1039/C5AY03248B
421 Edokpayi, J.N., Odiyo, J.O., Popoola, O.E., Msagati, T.A.M., 2016. Determination and Distribution of
422 Polycyclic Aromatic Hydrocarbons in Rivers, Sediments and Wastewater Effluents in Vhembe
423 District, South Africa. Int J Environ Res Public Health 13.
424 https://doi.org/10.3390/ijerph13040387
425 Fang, M.-D., Lee, C.-L., Yu, C.-S., 2003. Distribution and source recognition of polycyclic aromatic
426 hydrocarbons in the sediments of Hsin-ta Harbour and adjacent coastal areas, Taiwan. Marine
427 Pollution Bulletin 46, 941–953. https://doi.org/10.1016/S0025-326X(03)00099-7
428 Gallotta, F.D.C., Christensen, J.H., 2012. Source identification of petroleum hydrocarbons in soil and
429 sediments from Iguaçu River Watershed, Paraná, Brazil using the CHEMSIC method
430 (CHEMometric analysis of Selected Ion Chromatograms). Journal of Chromatography A 1235,
431 149–158. https://doi.org/10.1016/j.chroma.2012.02.041
432 Guo, J., Li, Z., Sandy, A.L., Li, A., 2014. Method development for simultaneous analyses of multiple legacy
433 and emerging organic chemicals in sediments. Journal of Chromatography A 1370, 1–8.
434 https://doi.org/10.1016/j.chroma.2014.10.031
435 Hung, H., Blanchard, P., Halsall, C.J., Bidleman, T.F., Stern, G.A., Fellin, P., Muir, D.C.G., Barrie, L.A.,
436 Jantunen, L.M., Helm, P.A., Ma, J., Konoplev, A., 2005. Temporal and spatial variabilities of
437 atmospheric polychlorinated biphenyls (PCBs), organochlorine (OC) pesticides and polycyclic

438 aromatic hydrocarbons (PAHs) in the Canadian Arctic: Results from a decade of monitoring.
439 Science of The Total Environment 342, 119–144.
440 https://doi.org/10.1016/j.scitotenv.2004.12.058
441 Hwang, H.-M., Wade, T.L., Sericano, J.L., 2003. Concentrations and source characterization of polycyclic
442 aromatic hydrocarbons in pine needles from Korea, Mexico, and United States. Atmospheric
443 Environment 37, 2259–2267. https://doi.org/10.1016/S1352-2310(03)00090-6
444 Ma, Y., Halsall, C.J., Crosse, J.D., Graf, C., Cai, M., He, J., Gao, G., Jones, K., 2015. Persistent organic
445 pollutants in ocean sediments from the North Pacific to the Arctic Ocean: POPs in sediment of
446 the Arctic Ocean. J. Geophys. Res. Oceans 120, 2723–2735.
447 https://doi.org/10.1002/2014JC010651
448 Miossec, C., Lanceleur, L., Monperrus, M., 2018. Adaptation and validation of QuEChERS method for the
449 simultaneous analysis of priority and emerging pollutants in sediments by gas
450 chromatography—mass spectrometry. International Journal of Environmental Analytical
451 Chemistry 98, 695–708. https://doi.org/10.1080/03067319.2018.1496245
452 Pies, C., Hoffmann, B., Petrowsky, J., Yang, Y., Ternes, T.A., Hofmann, T., 2008. Characterization and
453 source identification of polycyclic aromatic hydrocarbons (PAHs) in river bank soils.
454 Chemosphere 72, 1594–1601. https://doi.org/10.1016/j.chemosphere.2008.04.021
455 Programme (AMAP), A.M. and A., 2010. Assessment 2007: Oil and Gas Activities in the Arctic - Effects
456 and Potential Effects. Volume 1. Arctic Monitoring and Assessment Programme (AMAP).
457 Ravindra, K., Sokhi, R., Vangrieken, R., 2008. Atmospheric polycyclic aromatic hydrocarbons: Source
458 attribution, emission factors and regulation. Atmospheric Environment 42, 2895–2921.
459 https://doi.org/10.1016/j.atmosenv.2007.12.010
460 Ravindra, Mittal, A.K., Van Grieken, R., 2001. Health Risk Assessment of Urban Suspended Particulate
461 Matter with Special Reference to Polycyclic Aromatic Hydrocarbons: A Review. Reviews on
462 Environmental Health 16. https://doi.org/10.1515/REVEH.2001.16.3.169
463 Rogowska, J., Sychowska, J., Cieszynska-Semenowicz, M., Wolska, L., 2016. Elemental sulfur in
464 sediments: analytical problems. Environ Sci Pollut Res 23, 24871–24879.
465 https://doi.org/10.1007/s11356-016-7739-1
466 Sporstol, Sigve., Gjos, Nina., Lichtenthaler, R.G., Gustavsen, K.O., Urdal, Kjell., Oreld, Froydis., Skei, Jens.,
467 1983. Source identification of aromatic hydrocarbons in sediments using GC/MS. Environ. Sci.
468 Technol. 17, 282–286. https://doi.org/10.1021/es00111a008
469 Tobiszewski, M., Namieśnik, J., 2012. PAH diagnostic ratios for the identification of pollution emission
470 sources. Environmental Pollution 162, 110–119. https://doi.org/10.1016/j.envpol.2011.10.025
471 Tsapakis, M., Stephanou, E.G., Karakassis, I., 2003. Evaluation of atmospheric transport as a nonpoint
472 source of polycyclic aromatic hydrocarbons in marine sediments of the Eastern Mediterranean.
473 Marine Chemistry 80, 283–298. https://doi.org/10.1016/S0304-4203(02)00132-9
474 Vergeynst, L., Wegeberg, S., Aamand, J., Lassen, P., Gosewinkel, U., Fritt-Rasmussen, J., Gustavson, K.,
475 Mosbech, A., 2018. Biodegradation of marine oil spills in the Arctic with a Greenland
476 perspective. Science of The Total Environment 626, 1243–1258.
477 https://doi.org/10.1016/j.scitotenv.2018.01.173
478 Wang, Xu-Chen, Zhang, Yi-Xian, Chen, Robert F., 2001. wangetal.pdf. Marine Pollution Bulletin 42, 1139–
479 1149.
480
481
482

483

488 *Table S3: Deuterated internal and recovery standards used.*

Internal standards	Recovery standards
Naphthalene-d8	Acenaphthylene-d8
Dibenzothiophene-d8	Anthracene-d10
Acenaphthene-d10	Fluoranthene-d10
Phenanthrene-d10	Benz(a)anthracene-d12
Pyrene-d10	Benzo(a)pyrene-d12
Fluorene-d10	Indeno(1,2,3-c,d)pyrene-d12
Chrysene-d12	
Benzo(k)fluoranthene-d12	
Benzo(g,h,i)perylene-d12	

489

490

491

492 *Table S4: Sample locations*

Label	Location	Longitude [°]	Latitude [°]	Notes
VV1	Ilulissat, inner harbour	-51.089821	69.220229	
VV2	Ilulissat, inner harbour	-51.093864	69.22086	
VV3	Ilulissat, inner harbour	-51.089951	69.221161	
VV4.1 – 4.3	Ilulissat, outer harbour	-51.093767	69.223162	3 sample replicates
VV5.1 – 5.3	Ilulissat, small fjord next to airport	-51.070954	69.235707	3 sample replicates
Q1.1 – 1.3	Qeqertarsuaq harbour, 30 m offshore	-53.544778	69.247828	3 sample replicates
Q2	Qeqertarsuaq harbour	-53.547872	69.247141	
Q3.1 to 3.3	Qeqertarsuaq harbour	-53.538047	69.248005	3 sample replicates
QRef1 - 3	10 km west of Qeqertarsuaq	-53.803808	69.265147	3 sample replicates
QC	Mix of all Ilulissat samples			used as quality control sample

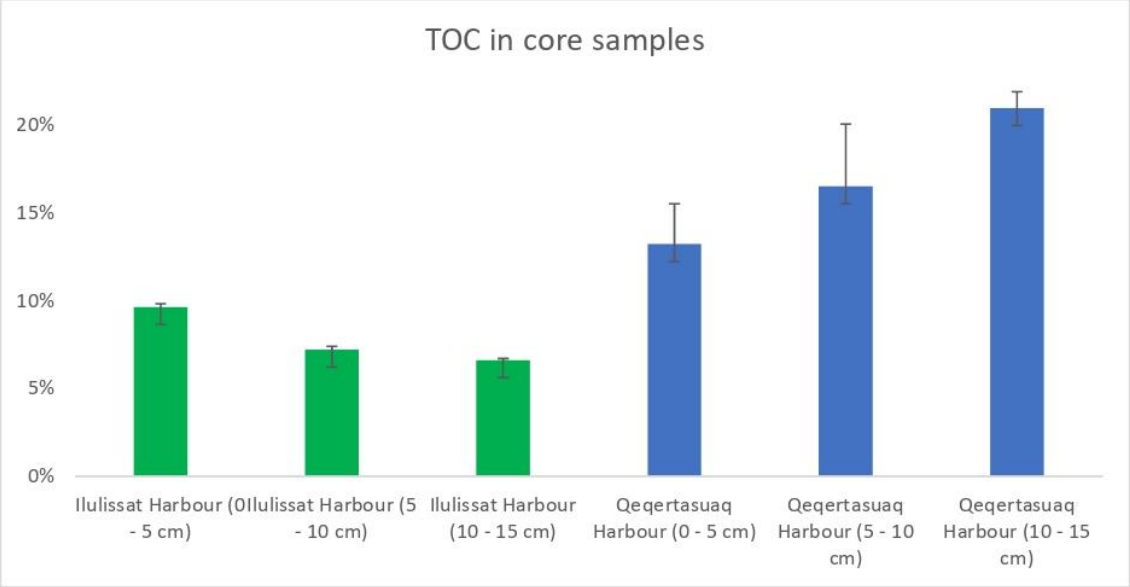

498

499 *Figure S3: Total Organic Carbon (TOC) corresponding to samples at different depths.*

500

501

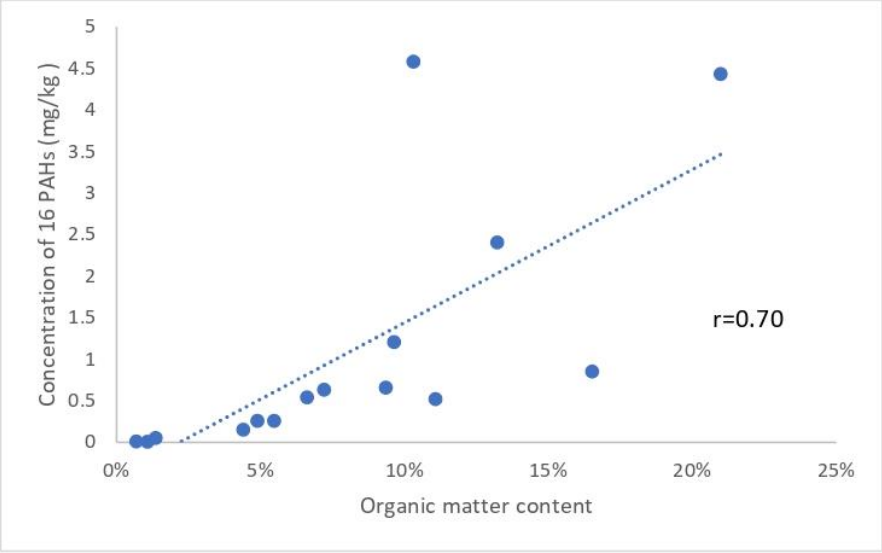

502

503 *Figure S4: Plot between the organic matter content vs. the PAHs concentration for each of the samples.*

504

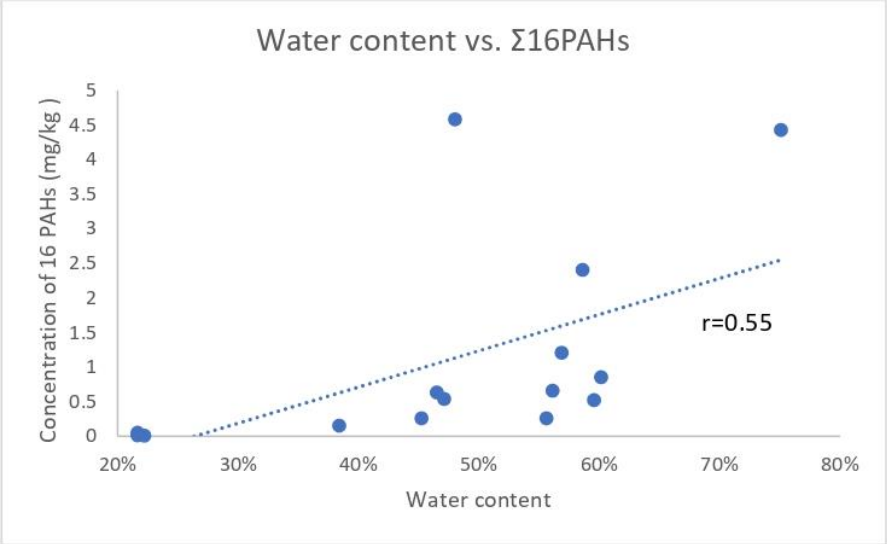

505

506 *Figure S5: Plot between the water content vs. the PAHs concentration for each of the samples.*

ECOLE DOCTORALE :
Sciences Exactes et leurs Applications

LABORATOIRE :
UMR 5254 IPREM, Université de Pau et des Pays de l'Adour
RAACE, PLEN, University of Copenhagen

Victor GARCIA MONTOTO
victormontoto@gmail.com